POWER SYSTEM TRANSIENT INSTABILITY PREDICTION AND MITIGATION USING SYNCHROPHASORS

BY

MUHAMMAD WAQAR AHMED

A Thesis Presented to the

DEANSHIP OF GRADUATE STUDIES

KING FAHD UNIVERSITY OF PETROLEUM & MINERALS

DHAHRAN, SAUDI ARABIA

In Partial Fulfillment of the
Requirements for the Degree of

MASTER OF SCIENCE

In

ELECTRICAL ENGINEERING
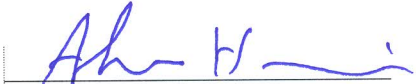
MAY 2014

بِسْمِ اللهِ الرَّحْمٰنِ الرَّحِيمِ

This Thesis is dedicated to

My Dear Parents

Beloved wife

Sisters

And

Brother

ACKNOWLEDGMENTS

**In the name of Allah, the Most Gracious, the Most Merciful
All praise and thanks to Almighty Allah for His countless blessings**

TABLE OF CONTENTS

LIST OF TABLES

LIST OF FIGURES

NOMENCLATURE

3PC	:	Triple Processor Card
AC	:	ACcelerating Parameter
AE	:	Asynchronous kinetic Energy
AEP	:	American Electric Power
ANN	:	Artificial Neural Network
AVR	:	Automatic Voltage Regulator
B&B	:	Branch and Bound
BPA	:	Bonneville Power Administration
BPSO	:	Binary Particle Swarm Optimization
BSA	:	Binary Search Algorithm
CCT	:	Critical Clearing Time
COI	:	Center of Inertia
DE	:	Differential Evolution
DEA	:	Differential Evolution Algorithm
DFT	:	Discrete Fourier Transform
DSA	:	Dynamic Stability Assessment

DSP	:	Digital Signal Processor
EAC	:	Equal Area Criterion
EEAC	:	Extended Equal Area Criterion
ELM	:	Extreme Learning Machine
EMF	:	Electro-Motive Force
EPRI	:	Electric Power Research Institute
FACTS	:	Flexible Alternative Current Transmission System
GA	:	Genetic Algorithm
GPC	:	Giga Processor Card
GPS	:	Global Positioning System
GPS	:	Global Positioning System
GTO	:	Gate Turn-Off Thyristor
GTWIF	:	Giga Transceiver Workstation Interface
HVDC	:	High Voltage Direct Current
ICGT	:	Insulated Gate-Commuted Thyristor
IGBT	:	Insulated Gate Bipolar Transistor
ILP	:	Integer Linear Programming

IPFC	:	Interline Power Flow Controller
IQP	:	Integer Quadratic Programming
IRC	:	Inter Rack Communication
KCL	:	Kirchov's Current Law
KE	:	Kinetic Energy
MSE	:	Mean Square Error
ODE	:	Ordinary Differential Equation
OPF	:	Optimal Power Flow
ORI	:	Observability Redundancy Index
PEBS	:	Potential Energy Boundary Surface
PHIL	:	Power Hardware In Loop
PMU	:	Phasor Measurement Unit
PWM	:	Pulse Width Modulation
RAS	:	Remedial Action Scheme
RCGA	:	Real Coded Genetic Algorithm
RISC	:	Reduced Instruction Set Computer
RTDS	:	Real Time Digital Simulator

SCDR	:	Symmetrical Component Distance Relay
SEP	:	Stable Equilibrium Point
SIME	:	SIngle Machine Equivalent
SMES	:	Superconducting Magnetic Energy Storage
SPEA	:	Strength Pareto Evolutionary Algorithm
SSI	:	Synchronism Status Index
SSSC	:	Static Synchronous Series Compensator
STATCOM	:	STATic synchronous COMpensator
SVC	:	Static Var Compensator
SVM	:	Support Vector Machine
TCPS	:	Thyristor Controlled Phase Shifters
TCSC	:	Thyristor Controlled Series Capacitor
TDS	:	Time Domain Simulations
TEF	:	Transient Energy Function
TMAR	:	Transmission power MARgin
TSCOPF	:	Transient Stability Constrained Optimal Power Flow
TSOPF	:	Transient Stable Optimal Power Flow

TSSC	:	Thyristor Switched Series Capacitor
UEP	:	Unstable Equilibrium Point
UFLS	:	Under Frequency Load Shedding
UPFC	:	Unified Power Flow Controller
UTC	:	Coordinated Universal Time
VSC	:	Voltage Source Converter
VSI	:	Voltage Source Inverter
WAMS	:	Wide Area Measurement System
WSCC	:	Western System Coordinating Council

ABSTRACT

Full Name   : Muhammad Waqar Ahmed

Thesis Title   : Power System Instability Prediction and Mitigation Using Synchrophasors.

Major Field   : Electrical Engineering

Date of Degree : May 2014

With the never ending growing needs for the human beings, the usage of electricity which is now essentially the backbone for every need, is growing. This growth in the demand of energy requires the expansion or new installations of current power reserves. Rather than achieving any of the fore mentioned tasks i.e. of expanding or installing new reserves for power, power system operators tend to push the existing power systems to the operating limits because of the cost constraint. This on one hand saves the cost but on other hand exposes whole of the power system to risk i.e. to operate the power system efficiently without a collapse or destabilizing the system. This makes the stability study of the power system critical. One of the vital outcome of this study is to detect the conditions that will make the system unstable and apply counter measures to mitigate it. In addition, the outcome of these studies are also used in designing and operating the power system to ensure stable operation under different probable contingencies.

This thesis focuses on presenting a complete package for improving power system transient stability, starting from planning and designing phase till operational phase. From the design and planning perspective, a multi objective PMU placement technique to achieve maximum system observability with minimum cost is presented, along with this a new Kinetic Energy (KE) based Flexible Alternating Current Transmission System (FACTS) placement using Differential Evolution Algorithm (DEA) in order to improve transient stability of the power system; from the operational point of view, a novel strategy for operating the power system economically and feasibly along with the improvement in transient stability of the system. Moreover to this an Artificial Neural Network (ANN) based power system instability detector is designed to serve as an input to the PMU based Remedial Action System (RAS) namely braking resistor and Under Frequency Load Shedding (UFLS), which will take measures against the detected instability. The proposed algorithms and techniques have been simulated using MATLAB and SIMULINK and practically implemented using Real Time Digital Simulator (RTDS) with Power Hardware in Loop (PHIL) configuration. Simulation results revealed that the developed algorithms and techniques produce reliable and high-quality solutions.

<div align="center">

Master of Science Degree
King Fahd University of Petroleum and Minerals
Dhahran, Saudi Arabia
May 2014

</div>

ملخص الرسالة

الاسم الكامل: محمد وقار احمد

عنوان الرسالة: تنبؤ و تقليل عدم استقرار نظام الطاقة الكهربائية باستخدام اجهزة قياسات الزاوية المتزامنة

التخصص: الهندسة الكهربائية

تاريخ الدرجة العلمية: مايو 2014

مع الاحتياجات المتزايدة للبشرية التي لا تنتهي أبدا ، واستخدام الكهرباء التي تعتبر الآن أساسا العمود الفقري لكل حاجة بشكل متزايد. يتطلب هذا النمو في الطلب على الطاقة في التوسع في احتياطيات الطاقة الحالية أو انشاء منشآت جديدة . و لكن بدلا من تحقيق أي من المهام المذكورة الصدارة أي توسيع أو تثبيت احتياطيات جديدة للطاقة ، يميل مشغلو نظام الطاقة إلى دفع أنظمة الطاقة القائمة على حدود التشغيل بسبب قيد التكلفة. هذا من ناحية يوفر تكلفة ولكن على الجانب الآخر يعرض كامل نظام الطاقة للخطر مما يعني أهمية تشغيل نظام الطاقة بكفاءة دون حدوث انهيار أو زعزعة استقرار النظام. هذا السبب يوضح أهمية دراسة استقرار نظام الطاقة. واحدة من النتائج الحيوية من هذه الدراسة هي الكشف عن الظروف التي من شأنها أن تجعل النظام غير مستقر وتطبيق تدابير مضادة لتخفيف ذلك. بالإضافة إلى ذلك، يتم استخدام نتائج هذه الدراسات أيضا في تصميم وتشغيل نظام الطاقة لضمان تشغيل مستقر في ظـــــــــــــــــــــــل حــــــــــــــــــــالات الطـــــــــــــــــــوارئ المحتمــــــــــــــــــــــــة مختلفـــــــــــــــــــة.

وتركز هذه الأطروحة على تقديم مجموعة كاملة لتحسين استقرار نظام الطاقة، بدءا من التخطيط و حتى مرحلة تصميم المرحلة التشغيلية . من ناحية التصميم والتخطيط ، تم طرح تقنية متعددة الاهداف لوضع اجهزة PMU لتحقيق أقصى قدر من قابلية الملاحظة النظام بأقل تكلفة ، بالاضافة الى تقنية الطاقة الحركية (KE) الجديدة لوضع نظام نقل التيار المتردد المرن (FACTS) باستخدام خوازمية التطور التفريقي (DEA) من أجل تحسين استقرار نظام الطاقة اللحظي . من وجهة النظر التشغيلية ، تم وضع استراتيجية جديدة لتشغيل نظام الطاقة اقتصاديا و عمليا تعمل أيضا على تحسين استقرار النظام اللحظي. وعلاوة على ذلك فقد تم تصميم نظام كاشف لعدم الاستقرار في النظام باستخدام الشبكة العصبية الاصطناعية (ANN) و الذي سيكون بمثابة مُدخل لانظمة علاج النظام (RAS) الموجودة في أجهزة PMU التي هي عبارة عن مقاومات كابحة و قطع لتيار في حياة انخفاض التردد (UFLS) و التي ستقوم باتخاد اجراءات من شأنها معالجة حالة عدم الاستقرار. تم محاكاة خوارزميات وتقنيات المقترحة باستخدام MATLAB و SIMULINK وتنفيذها عمليا باستخدام محاكاة الوقت الحقيقي الرقمية (RTDS) مع اعدادات (PHIL). كشفت نتائج المحاكاة أن الخوارزميات والتقنيات المتقدمة قامت بانتاج حلول ذات جودة عالية يمكن الاعتماد عليها

درجة الماجستير في العلوم
جامعة الملك فهد للبترول والمعادن
الظهران ـ المملكة العربية السعودية
مايو 2014

CHAPTER 1

INTRODUCTION

1.1   Overview

The electrical grids are amongst the most complex systems worldwide. The power system planners and operators work hard to operate the system in a reliable manner to provide the safe and satisfied electric power to the customers. With the introduction of free marketing and deregulation of the power system, the economic factors are added to the power system operation, leading to new uncertainties and challenges to large interconnected power system. Power systems continue to be stressed as they are operated in many instances at or near their full capacities. In such a situation, power system protection and control becomes an important safeguard of power system and also the key enabler to meet the challenges of the electrical grid in the 21st century.[1]

The technological advancement in this millennia has made us more dependent on electrical power than ever. Due to this dependency power systems are growing in size

and complexity which makes it more prone to failure as they are pushed to their limits by power system operators. Theses failures can prove to be disastrous and can lead to unamendable losses and system black outs. To know which failures will lead to make the system instable, power system stability studies are carried during the design, planning and even in the operational phase of the power system to figure out the actions to mitigate or avoid instability and time required to take these actions. These facts highlight the importance of the stability study of the power system. To add to these facts Table 1.1 [2] shows some history of blackouts in different parts of the world due to instability occurrence and failure to take action against it. To accurately identify the scenarios which will make the power system instable is still a challenging task even after such technological advancement in fields of measurement, protection and computation. Although it has been almost 80 years since the power systems came into being, stability is still a scorching topic for researchers.

The lessons learned from several recent major blackouts revealed that current protection systems were not always sufficient to stop an uncontrolled cascading failure of the power system and, therefore, the application of existing protection system should be revisited. Phasor measurement units (PMUs) using synchronization signals from the satellite global positioning system (GPS) have recently evolved into mature tools with the potential to revolutionize the way electric power systems are monitored and controlled. Since PMUs were introduced into power system thirty years ago, their values have been proved by their extensive applications in power system operation and planning. In recent years, varieties of PMU application areas, including the area of power system stability, have been studied, proposed and implemented with their significant benefits.

2

TABLE 1.1: BLACKOUT HISTORY IN DIFFERENT PARTS OF WORLD

Country	Date of blackout	Estimated time of blackout	People affected	Loss in USD
New Zealand	20.02.1998	4 weeks	70,000	Not reported
Brazil (70% of the territory)	11.03.1999	5 hours	97,000,000	Not reported
India	02.01.2001	12 hours	226,000,000	110 million
U.S.A (North-East) + Canada (Central)	14.08.2003	4 days	50,000,000	6 billion
Italy	28.09.2003	18 hours	56,000,000 (4 deaths)	Not reported
Indonesia	18.08.2005	7 hours	100,000,000	Not reported
Spain	29.11.2004	5 blackouts in 10 days	2,000,000	Not reported
South West Europe	04.11.2006	2 hours	15,000,000	Not reported

At present, a large number of PMUs have been installed and the wide area measurement system (WAMS) that gathers real-time phasor measurements by PMUs across broad geographical areas has been gradually implemented.[1]

Flexible AC Transmission Systems (FACTS) is another worth specifying tool for power system enhancement. The emergence of facts some 20 years ago has changed the complete picture of power system operation. They have opened a new world in power system control. They have made power systems operations more flexible and secure.

3

They have ability to control, in fast and effective manner the three key players in power flow. These are circuit impedance, voltage magnitude and phase angle. This gain in flexibility in power flow is not a small achievement at all. The great economic and technical benefits of this to the power systems have been well proven.

1.2   Thesis Motivation

Due to the increasing importance, power system stability research studies have attracted widespread attention among researchers in power system technology. Accurate identification, detection and mitigation of instability in power network can reduce the risk of blackouts, speed up power restoration and thus enhancing the reliability and availability of power systems. A number of different areas for improving the power system stability are reconnoitered which are given as follows:

1.2.1   PMU-based Instability detection and mitigation

At present, PMUs have come out of their academic infancy with commercial viability. There are now about 24 commercial manufacturers of PMUs and pertinent industry standards have made possible the interoperability of units from different manufacturers [3], [4].A PMU has the potential to revolutionize the monitoring and control of electric power systems. This device has the ability to measure current, voltage, and calculate the angle between the two. Phase angles from buses around the system can then be calculated in real time. This is possible because of two important advantages over traditional measurement; time stamping and synchronization. With the satellite GPS availability, digital measurements at different part of power system can be performed synchronously to the accuracy of one micro-second. The ability of GPS to

provide a time reference signal, synchronized at widely separated locations has been widely recognized as having many applications in power-systems including the application for power system stability detection, monitoring and control. PMU-based instability detection and control algorithms are highly accurate and, therefore, needed to cope with the modern power system requirements. Being in very initial and crude stages these algorithms to identify and control power system instability are just simulated rather than being tested on real hardware. One of the biggest stimulus of this thesis is to develop and test such algorithm through real time simulations with real hardware in loop.

1.2.2 Optimal Placement of FACTS Devices

Another crucial player in the area of power system stability enhancement is FACTS devices. Installing FACTS devices in any power system is an investment issue. It offer flexibility in power flow at the expense of the cost. Therefore, it is necessary for any new installation of FACTS to be very well justified [5]–[9]. Most of the published literature on FACTS devices focuses on improving the small signal stability or voltage stability of the power system. There are rather very few papers being published on improving the transient stability of the power system. Being an under explored area, the ability of FACTS devices in the area of transient stability is still grim. This thesis aims to discover the ability of FACTS devices for improving power system transient stability and presents a new formulation for FACTS devices placement in power system for improving the transient stability.

1.2.3 Transient Stable Optimal Power Flow

In the past decade or so, the focus of the research has been to improve the transient stability of the power system without extra investment on the infrastructure of the power

system. Power system operators and researchers are continuously striving to achieve better transient performance of the system by altering the available control parameters of the system. This led to the formulation of Transient Stability Constrained Optimal Power Flow (TSCOPF). As from the literature this problem has been formulated as a single objective constrained optimization problem with targeted or selected faults. This kind of approach can improve the transient performance for the selected faults but for the faults other than the considered one, we cannot say anything about them. So, still we need an approach that can improve the global transient performance of the system. This thesis aims to present a novel true multi-objective formulation of the Optimal Power Flow, that will not only ensure that the system is operating economically, but will also improve the global transient performance of the system under consideration.

1.3   Thesis Objectives

With the motivations laid in the previous sub-section, the objective of this thesis are listed as follows:

1. Proposing a novel approach for optimal placement of shunt FACTS device that is STATic synchronous COMpensator (STATCOM) in electrical network and solving it using population based technique and testing the placement for two control modes that are voltage control mode and reactive power control mode.

2. Development of multi objective formulation for optimal PMU placement (OPP) problem and solving it using heuristic multi objective optimization algorithm.

3. Proposing a novel true multi objective optimal power flow in order to improve the transient stability of the power system with minimum cost and solving it using heuristic multi objective optimization algorithm.

4. Development of PMU and Artificial Neural Network based transient instability predictor.

5. Algorithm and prototype development of PMU based transient instability mitigation schemes namely braking resistor scheme and under frequency load shedding scheme (UFLS).

1.4   Contributions:

The main contributions of the work carried out under this thesis can be summarized as follows:

- Proposal of novel kinetic energy and hybrid synchronism classifier based formulation for optimally placing shunt type FACTS devices in power system in order to improve the transient stability.

- Development of optimal placement of shunt type FACTS device problem solver based on Differential Evolution Algorithm (DEA) to achieve maximum improvement in stability of the system with minimum number of FACTS devices.

- Development of multi objective OPP problem solver based on Strength Pareto Evolutionary Algorithm (SPEA) to achieve full network observability with minimum PMU installation cost with maximizing PMU measurement redundancy.

- Proposal of novel multi objective Transient Stable Optimal Power Flow (TSOPF) based on kinetic energy and hybrid synchronism classifier to improve the transient stability of the system with minimum possible cost.

- Development of multi objective TSOPF solver based on SPEA for maximizing transient stability and minimizing cost.

- Implementation of real time hardware in loop schemes using RTDS and real time PMUs for transient instability mitigation. The said schemes will help to reduce the risk of blackouts and enhance power system's availability and reliability.

1.5   Thesis Organization

The material of this thesis is organized in seven chapters. It starts, after this introductory chapter, with a literature survey addressing different problems that are under consideration in this work in Chapter 2. Chapter 3 is dedicated to the formulation of OPP problem formulation, SPEA Algorithm and its implementation on OPP problem. Chapter 4 presents the formulation for STATCOM placement in the system and the Differential Evolution (DE) application for solving the STATCOM placement problem. Chapter 5 present the formulation of Transiently Stable Optimal Power Flow and SPEA application for solution of the presented problem. Chapter 6 presents some overview of PMU technology and then PMU based transient instability detection and mitigation schemes are presented. Finally, Chapter 7 concludes the work with some highlights of the work and future pathways for the work are proposed.

CHAPTER 2

LITERATURE REVIEW

2.1   Transient Stability of Power System

As per CIGRE Study Committee 38 and the IEEE Power System Dynamic Performance Committee [10] power system stability can be defined as follows:

"Power system stability is the ability of an electric power system, for a given initial operating condition, to regain a state of operating equilibrium after being subjected to a physical disturbance, with most system variables bounded so that practically the entire system remains intact."

From the fore mentioned power system stability definition it is evident that for the preservance of integrity of most of the power system's components should be in-service or intact other than those which has been isolated or tripped intentionally so as to counter the disturbance and to keep the system in operation. The ever changing loading conditions on the power system are considered small disturbance and the system is

capable enough to cope up with these small disturbances via load frequency control. The instantaneous tripping of significant portion of load or generation or a fault are considered as large disturbance and are referred as transient disturbance. In the post-transient period the system reaches a new state of equilibrium provided if it is stable and usually human intervention or automatic controls are required to bring the system back to its original state (pre-disturbance period).

Depending on the nature, the size of disturbance and the time span considered instability can take various forms. To device the method for countering the instability it is essential to identify the contributing factors, the categorization of stability greatly serves this purpose. Figure 2.1 [10] depicts the classification of power system stability in general and sub-classes.
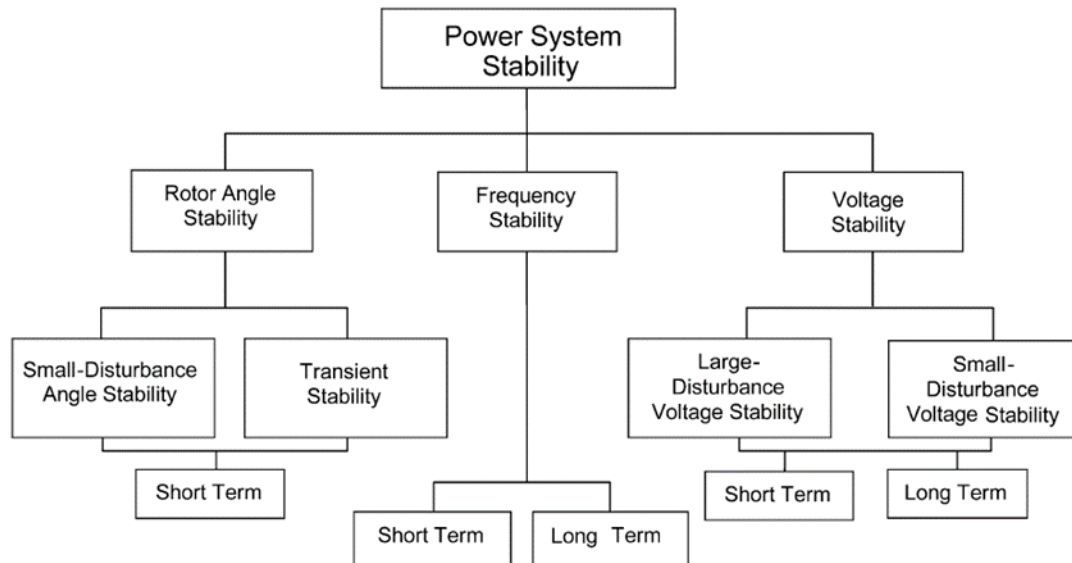
Figure 2.1:   Classification of Power system stability [10].

Historically the terms steady-state stability and dynamic stability has been used to refer different kind of stabilities, however IEEE and CIGRE [10], in order to avoid

confusion, merged the two fore mentioned terms as small disturbance stability. This survey emphasizes solely on the rotor angle stability analysis which is often regarded as transient stability analysis.

IEEE and CIGRE [10] defines *Rotor angle stability* or *Transient Stability* as the ability of the interconnected system to remain in synchronism after being subjected to a severe disturbances. As a response to the disturbances the generator's rotor angle experiences large excursions with an embedded nonlinear relationship between generator power and rotor angle. This kind of stability not only depends on the pre-fault conditions of the power system but also on the severity of disturbance.

For modern power systems that are heavily interconnected by complex transmission network and large-scale with tens of synchronous machines, transient stability assessment or analysis is more suitably carried out by computer aided tools or simulations. For a particular system and specific disturbance the combination of differential and algebraic equations are solved iteratively. The dynamics governing the synchronous machine is represented by second order differential equation called as swing equation (2.1) and the network behavior i.e. power flow is represented by non-linear algebraic equation(2.2).

$$M_i \frac{d^2\delta_i}{dt^2} = P_{m_i} - P_{max_i} Sin\delta_i = P_{m_i} - P_{e_i} \tag{2.1}$$

and

$$P_{e_i} = E_i \sum_{j=1}^{N_G} E_j \left(G_{ij} \; . \; Cos(\delta_i - \delta_j) + B_{ij} \; . Sin\left(\delta_i - \delta_j\right) \right) \tag{2.2}$$

11

P_{e_i} = Electrical power output of generator i.

P_{m_i} = Mechanical Power input of generator i.

δ_i = Rotor angle generator i.

E_i = EMF behind transient reactance.

M_i = Inertia constant of generator i.

G_{ij} = Transfer conductance between branch i and j.

B_{ij} = Transfer suseptance of branch i and j.

N_G = number of generators in the network.

2.2 Numerical Simulation method

2.2.1 Numerical Integration Method

These methods are based on solving the swing equation via numerical integration where the exact solution to the transient stability problem can be obtained. Many techniques exist for solving non-linear ordinary differential equations (ODE's). The widely used techniques in power system stability studies are Euler's method, trapezoidal method, and Runge-Kutta method. These algorithms employ step-by-step solving method. For solving swing equation by these methods it is decomposed into two single order differential equations as (2.3) and (2.4)

$$\frac{d\delta_i}{dt} = \omega_i - \omega_b \qquad (2.3)$$

$$\frac{d\omega_i}{dt} = \frac{1}{M_i}\left(P_{m_i} - P_{e_i}\right) \qquad (2.4)$$

where,

ω_i = Speed of ith generator.

ω_b = Synchronous Speed.

It is evident that for a system with 'N_G' generators '2 N_G' equations must be solved. The following disadvantages are evident for these methods.

1. For accuracy the time step should be as small as possible. This increases the computational time for assessing transient stability.

2. Each of the fault must be dealt separately.

3. CCT obtained by separate trials.

These short comings make these method ill-fit for real time transient stability assessment. The usage of "Extended Equal Area Criterion (EEAC)" has shown promising results in this regards. Developed [12], [13] as a tool for online transient stability assessment. It employs the replacement of multi-machine by two machine equivalent and further amenable to single machine infinite bus turning the problem solely into algebraic equations. Ref. [14] has successfully demonstrated the effectiveness of EEAC algorithm by assessing the stability of islanded power system and developed a priori transient stability indicator for the islanded power systems. Yang *et al.* [15] has presented a case study of Anhui power grid applying EEAC to assess the power system stability for a permanent 3 phase fault to ground at two terminal line of 500kV demonstrating the power

of generalization of EEAC algorithm. Li *et al* [16] shows the effectiveness of EEAC in real time based on wide area measurements and proposes an emergency EEAC to predict, analyze and to measure the degree of instability. Another real time application of EEAC can be found in [17] which determines the transient stability margin based on measurements from Wide Area Measurement System (WAMS). Ferreira *et al* [18] have shown the robustness of the algorithm by presenting the effects of topological changes like generator or line tripping etc. and assessing the transient stability using EEAC. Authors in [19] expose the speed of the algorithm and justifying its use in the online or dynamic stability assessment. Aside from all the advantages that EEAC provides, the aggregation of multi-machine into equivalent machine is not a simple task and also introduces numerical inaccuracies which may serve as a disadvantage in some studies to use EEAC.

2.2.2 Direct/Lyapnov or Transient Energy Function Based Methods

Unlike time domain simulation methods the direct methods assess the stability without explicitly solving the differential equation of the system. In power literature, the Lyapunov method has become the transient energy function method because the energy-based methods are a special case of the more general Lyapunov second method or the direct method. The inkling behind this method is the replacement of post-fault system equations by a stability measure. P. Kundur [20] has depicted the concept of *TEF* in quite an excellent manner by an example of rolling ball in the inner surface of the bowl. As shown in Figure 2.2 [20] the bottom of the bowl is referred as *Stable Equilibrium point (SEP)* whereas the bowl's rim is regarded as *Potential Energy Boundary Surface (PEBS).* The area inside the bowl is the region of stability whereas the region outside is called as

region of instability. *PEBS* has a number of *Unstable Equilibrium Point (UEP)*. If the bowl is perturbed, the ball which is initially at *SEP* will move from its location due to the injection of kinetic energy and will roll up the bowl's surface. If the ball is able to convert all the kinetic energy into potential energy before getting to the rim (*PEBS*), then it will eventually roll back and settles at *SEP*. On contrary to this, if the kinetic energy injected is high enough to make the ball roll over the rim then it will enter the region of instability and will never return to *SEP*. Conceptually similar to this are power system's dynamics. At the fault occurrence, the generator speeds up, gains the kinetic energy and potential energy and moves towards the *PEBS* away from the *SEP*. After the fault clearance, same as in the case of ball rolling the kinetic energy is converted into potential energy. For the system to be stable it must be able to absorb the kinetic energy to make the generators operate at a new equilibrium point.

The TEF method is well supported by the concept of equal area criterion and can be considered as analogy of each other as depicted in Figure 2.3.[20]. As in equal area criterion the equality of area A_1 and A_2 establishes the critical clearing angle (δ_{cc}), the critical clearing angle in TEF is specified in terms of kinetic and potential energy.
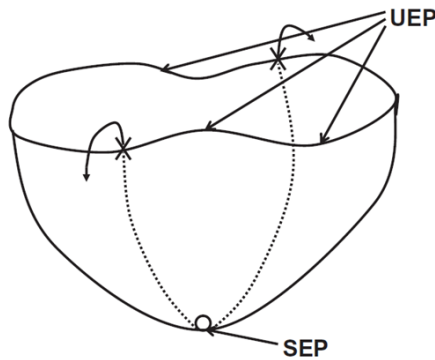
Figure 2.2:   Ball rolling example [20].

To assess the transient stability of the system, a comparison is made between two energies, the energies being, the total energy (E_{cl}) injected in the faulted period i.e. the sum of kinetic energy gained during the fault and the potential energy at the corresponding rotor angle; and critical potential energy (E_{cr}) at δ_u, where δ_u being the rotor angle at the unstable equilibrium point. If $E_{cr} > E_{cl}$ then the system is stable otherwise unstable.
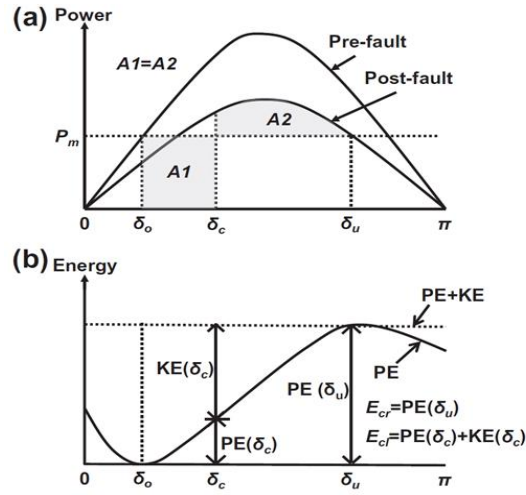
Figure 2.3:   Equal Area criterion and TEF equivalence [20].

A number of TEF formulation has been used in the literature however (5) (details in [21]–[24]) is the most simplest and has been employed in most of the literature derived for the power system in the reference of Center of Inertia (COI) given by (6) and (7) [23]

$$V = \frac{1}{2}\sum_{i=1}^{N_G}M_i\tilde{\omega}_i^2 - \sum_{i=1}^{N_G}P_i\left(\theta_i - \theta_i^S\right) - \sum_{i=1}^{N_G-1}\sum_{j=i+1}^{N_G}\left[C_{ij}\left(Cos\theta_{ij} - Cos\,\theta_{ij}^S\right) - I_{ij}\right] \qquad (2.5)$$

where,

$$I_{ij} = D_{ij}\frac{\theta_i^b - \theta_i^a + \theta_j^b - \theta_j^a}{\theta_{ij}^b - \theta_{ij}^a}\left(Sin\theta_{ij}^b - Sin\theta_{ij}^a\right) \qquad (2.6)$$

16

I_{ij} is the path dependent integral. Approximated using straight line approximation, where a and b are the starting and ending points respectively of the path.

$$M_i \, \dot{\tilde{\omega}}_i = P_i - P_{ei} - \frac{M_i}{M_T} P_{COI} - D_i \tilde{\omega}_i \tag{2.7}$$

$$\dot{\theta}_i = \tilde{\omega}_i \tag{2.8}$$

where, $i = 1, ..., N_G$

The angular displacement θ_i and angular velocity $\tilde{\omega}_i$ are defined as

$$\theta_i = \delta_i - \delta_{COI} \tag{2.9}$$

$$\tilde{\omega}_i = \omega_i - \omega_{COI} \tag{2.10}$$

where,

$$M_T = \sum_{i=1}^{N_G} M_i \tag{2.11}$$

$$\delta_{COI} = \frac{1}{M_T} \sum_{i=1}^{N_G} M_i \delta_i \tag{2.12}$$

$$\omega_{COI} = \frac{1}{M_T} \sum_{i=1}^{N_G} M_i \omega_i \tag{2.13}$$

$$P_{COI} = \sum_{i=1}^{N_G} (P_i - P_{ei}) \tag{2.14}$$

$$P_i = P_{mi} - E_i^2 G_{ii} \tag{2.15}$$

17

$$P_{ei} = \sum_{\substack{i=1 \\ j \neq i}}^{N_G} \left[C_{ij} Sin\left(\delta_i - \delta_j\right) + D_{ij} Cos\left(\delta_i - \delta_j\right) \right] \tag{2.16}$$

where,

$$\begin{aligned} C_{ij} &= E_i E_j B_{ij} \\ D_{ij} &= E_i E_j G_{ij} \end{aligned} \tag{2.17}$$

M_T = Inertia constant of system.

A large number of papers are published on utilization of Transient Energy Function method for transient stability analysis. Chen *et al* [25] used the transient energy to effectively point out the source of oscillation in power system in case of electromechanical transient and has proposed wide area measurement based energy calculation method within the network. This not only shines out the use of TEF method in transient stability assessment but also provides ground to be used as real-time stability assessment tool. Another real time application of TEF method can be found in [26] which utilizes the rate of change of kinetic energy to assess the transient stability in real time. The authors in [26] has also used resistive dynamic braking to improve the transient stability margin for the simulated power system. To take into account the ever growing renewable energy sources for transient stability, a structure preserved stochastic transient energy function method is proposed in [27] proving the generality of TEF method with the developing diversified energy resources. Yorino *et al* [28] proposed a new method for direct CCT computation. This method utilizes TEF to compute the critical trajectory where the transient stability problem has been formulated as a minimization problem with critical synchronism conditions to assess the stability of the system in different

contingencies. Ref. [29] presents an example of integration of HVDC dynamics in the transient energy function to assess the stability of hybrid (AC/DC) transmission system. Author has derived a new TEF for HVDC dynamics inclusion and a new algorithm to compute Transient Energy Margin so as to reduce the computational time. [30] presents the integration of FACTS devices. The author has developed energy function for Unified Power Flow Controller (UPFC) and has tested to prove the authenticity in different conditions and scenarios. Jing Shi *et al* [31] has diversified the use of energy function method by proposing an energy based controller for Superconducting Magnetic Energy Storage (SMES) system in order to improve the transient stability of the power system. The author has first analyzed the energy interaction between SMES and power system and then designed an energy based controller for optimal utilization of SMES in transient stability enhancement. Similarly, Ref. [32] presents the use of energy function to develop the control strategy for Interline power flow controller (IPFC). Despite of the frequent usage and advantages the TEF method has certain drawbacks as follows:

- The equations of the system during the fault period must be integrated for obtaining post-fault SEP and CCT.

- If the system is initialized outside the stability region, nothing can be said about stability of the system.

2.3 Hybrid Methods

To overcome the deficiencies in both the numerical integration method and transient energy function method a hybrid method was introduced by [33] combining the accuracy of numerical integration method and generalization power and speed of TEF methods.

One of the major advantage of the hybrid method is incorporation of details of models like higher order generator model, auxiliary controls and other aids within the power system and there is no need to compute the UEP[34]. After the hybrid method proposal for transient stability assessment many forms of hybrid methods are reported in the literature, however there are three major forms that have been used extensively a) *the hybrid method* [33], b) *the two phase method* [35] and c) *the second kick method* [36]. The details of the methods can be found in references cited.

Al Marhoon *et al* [37] presented a hybrid method by simulating the system step-by-step up to the fault clearance point and then divides the machines into two groups, based on accelerating power the generators are classified as severely disturbed. The decision on stability is made on the basis of comparison of the potential energies of one group to the kinetic energies of the other group. A unique hybrid of Single machine equal area criterion and TEF method has been presented in [38]. The proposed method selects the critical couple of generator based on energies of the machine and applies time step simulation to assess the stability of the system. This saves the computation time and reduces the complexity as there is no need for network reduction and generator aggregation as in EEAC. The concept of transient stability for distributed generators is given in [39] which uses a hybrid of TEF and equal area criterion. The author has also proposed a control strategy for countering the transient phenomena for distributed generators. Ref. [40] have proposed to study the energy balance of critical machines only to determine the stability of the system and has proposed a new method to determine the stability margin in order to give a quantitative insight for the stability of the system. Ref. [41] have used clustering analysis techniques and hybrid TEF to assess the stability of a

large power system. The authors have described a real time transient stability assessor which requires information only from the step by step simulation. The author has also derived a transient stability index based on hybrid TEF and has depicted its performance with the application on a practical power system of UK. Kwok *et al* [42] has used a new approach named Marginally Unstable Injection (MUI) to formulate an accurate transient stability index based on the hybrid TEF method and has illustrated it with an application on a huge network of 700-buses, highlighting its accuracy and reliability. The author has also presented the conceptual differences between applied approach and few of the earlier hybrid approaches.

2.4   Artificial Neural Network based Methods

With the advancement in the computational capabilities and metering technology the application of the artificial intelligence for the power system problems has gained a significant boost. The power of these systems lies in the fact of mimicking the natural phenomenon giving them ability to generalize and predict. One example of this can be neural networks which tries to replicate the structure of human brain to solve the problem for which it is designed for.

For transient stability assessment problem different intelligent techniques have been formulated and applied. Among the different techniques applied the Artificial Neural Networks (ANN) has shown promising prospect in this regards.

Artificial Neural Networks (*ANN*) composed of highly interconnected network of nodes called as *neurons* which are the main elements responsible for processing the data. *ANN* presents a complete replica of human brain. Just as in the human brain the neurons

are connected via links called *synapse*, similarly the *ANN* neurons are also interconnected by weighted *synapse*. These networks are to be trained rather than to be programmed.
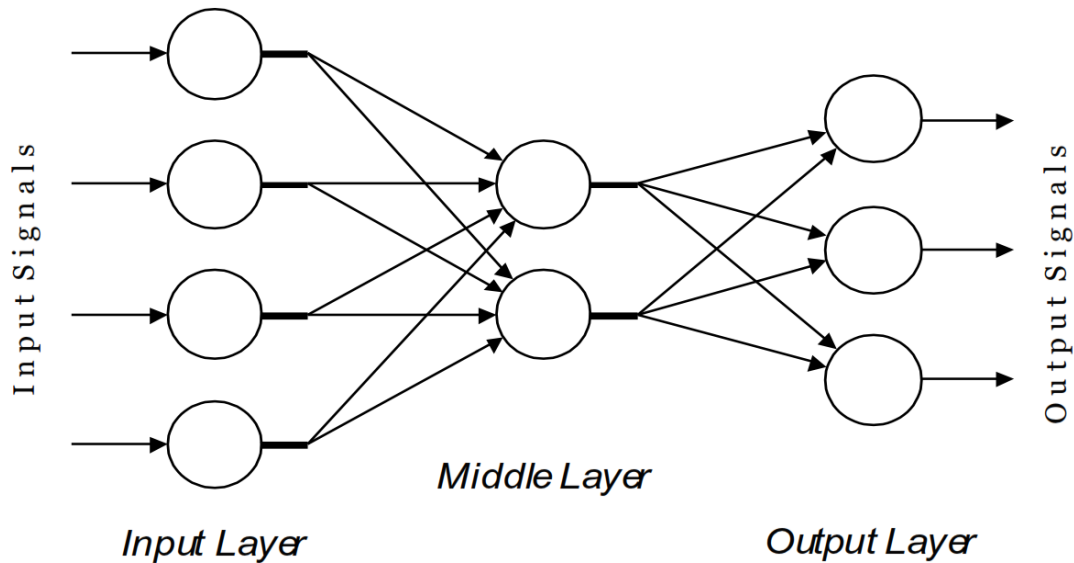
Figure 2.4:   Basic structure of ANN.

There exist many architectures for *ANN*, although the core elements (*neurons* and *synapse*) remains the same, the variants differ in training algorithm or structure. Multi-Layer Perceptron (MLP) with Back-propagation (BP) training algorithm is the most commonly used architecture and training algorithm respectively as shown in Figure 2.4.

The precise objective of *ANN* is to develop a functional association between the data presented during the training phase. *ANN* once trained with selected data for a particular problem has the ability to classify or can recognize the data pattern to produce a specific output. The fore mentioned objective of developing a functional association is achieved in two phases.

- Selection / Extraction of feature.

- Classification of the system.

In the first phase the training set is generated for stable and unstable system conditions based on the offline simulations for each of the contingency and operating condition. Data is generated for each of the state (feature) of the system. For a given contingency a classifier function (rules) is applied online to declare the system stable or unstable.

As no calculations are to be done, the *ANNs* are fast and do not depend on the system initial conditions. Due to this ability *ANN* has proven to be a viable candidate for Dynamic Stability Assessment (DSA) of power system, as it can be used in classification as well as prediction of power system stability. Different training vectors has been used in literature to assess the stability of power system. Usually a stability index or a manipulated state proves to be good choice for the training vector.

Hashiesh and Mostafa [43] has designed a real time intelligent wide area phasor measurement unit based stability predictor. The authors have used a two layer feed-forward neural network with the input vector $X = \left\{ \frac{dV_i}{dt}, \frac{d\delta_i}{dt} \right\}$, the rate of change of generator *i* bus voltage and rate of change of generator *i* bus voltage angle. The predictor takes 6 reading after the fault clearance at an interval of each cycle to predict the stability status of the system. Xu *et al* [44] have applied Extreme Learning Machine (ELM) theory to assess the power system stability in real time. ELM is essentially an *ANN* differing from the conventional one in training algorithm which reduces the computational efforts required during training. The authors have shown the effect of feature selection of ELM through reduction in training time and accuracy of the network. The training vector used

is the maximum relative rotor angle during the fault-on period. If the angle is within pre-specified limits then the system is classified stable otherwise unstable. Gomez *et al* [45] have presented yet another variant of the *ANN* called *Support Vector Machine* (*SVM*) to overcome the disadvantages of orthodox *ANN*. The *SVM* unlike the *ANN* can learn from a very small training set also it is easily applicable to large system without any increase in complexity that depends on the support vector rather than on dimensionality of the training vector. Other benefits of *SVM* includes more prone to over fitting and has a better performance if the data presented is outside the training data. The authors [45] have used transient stability index η to classify the power system as stable or unstable. If η is positive then system is stable and unstable otherwise. η is defined as

$$\eta = \frac{360° - |\Delta\delta|_{max}}{360° + |\Delta\delta|_{max}} \tag{2.18}$$

where, $|\Delta\delta|_{max}$ is the maximum separation angle between two generators during the post fault period. Another application of Neural Networks in power system stability assessment can be found in [46]. The author has used voltage magnitude at all buses and power flow through the lines as an input pattern to predict the Critical clearing time and hence the transient stability of the system.[47] has used TEF method based neural network to assess the transient stability of the system. The input vector used is the normalized transient stability margin ΔV_n calculated from the TEF method of transient stability assessment. If the value of $\Delta V_n > 0$ then the system is stable and if $\Delta V_n < 0$ the system is classified unstable. The reason behind using such classifier is that it not only gives a qualitative measure but also gives a quantitative (degree of stability) measure of the system stability. Another approach to intelligent transient stability prediction is

presented in [48], which predicts the rotor angle stability by using voltage trajectories in the post fault period. The author has used SVM as a classifier and generator bus voltages as the input vector. Ref. [49] presented a novel *Synchronism Status Index* (*SSI*) based on hyperbolic functions.

$$SSI\left(\delta_{i,COI}\right) = \begin{cases} 1 + tgh\left(\dfrac{\delta_{i,COI}}{\delta_{max} - \delta_{i,COI}}\right) & ; if \ \delta_{i,COI} < \delta_{max} \\ 2 & ; if \ \delta_{i,COI} > \delta_{max} \end{cases} \qquad (2.19)$$

where, tgh(.) is the hyperbolic tangent function.

$$SSI\left(\delta_{i,COI}\right) = \begin{cases} 1; & if \ i^{th} \ unit \ is \ stable \\ 2; & if \ i^{th} \ unit \ is \ unstable \end{cases} \qquad (2.20)$$

First the measured rotor angles are transformed into COI reference and then *SSI* is calculated by applying hyperbolic transformation. This *SSI* is then presented to a hybrid classifier to predict the synchronism status of the system. The author has also shown the use of the algorithm to detect the tripped generators.

Sawhney and Jeyasurya [50] has presented a neural network classifier based on aggregated equal area criterion application on multi-machine to device a transient stability classifier. The classifier η lies between -100 to 100 and is defined as

$$\eta = \begin{cases} \dfrac{A_{dec} - A_{inc}}{A_{dec}} \times 100 & , system \ stable \ if \ (A_{dec} > A_{inc}) \\ \dfrac{A_{dec} - A_{inc}}{A_{dec}} \times 100 & , system \ stable \ if \ (A_{dec} < A_{inc}) \end{cases} \qquad (2.21)$$

Another training vector i.e. the active and reactive power of critical generator buses has been used in [51] to assess the transient stability. The authors has made use of the Support Vector machine and a binary classifier is used to classify the system stable or unstable.

Sanyal [52] has applied a unique strategy in feature selection. The author has used 6 features that represents the whole of the system effectively. The features being a) *Accelerating parameter* (*AC*) [53], b) *Asynchronous Kinetic Energy* [54] (*AE*), c) *Transmission Power Margin* [54] (*TMAR*), d) Fault clearing time, e) Location of fault and f) Critical clearing time.

$$AC_i = \frac{\left(P_{mi} - P_{ei}\right)}{M_i} \tag{2.22}$$

$$AE = \sum_{i=1}^{N_G} E_i = \frac{1}{2} \sum_{i=1}^{N_G} M_i \cdot [\frac{d\delta_i}{dt} - \frac{d\delta_{COI}}{dt}]^2 \tag{2.23}$$

$$TMAR = \sum_{i=1}^{N_G-1} \sum_{j=i+1}^{N_G} \left[E_i.B_{ij}.E_j.\left(1 - Sin\delta_{ij}\right) \right] \tag{2.24}$$

Each of the above parameter is calculated in the fault on period. The author has shown the application of proposed method on a test system to validate its authenticity. Despite the advantages of less computational time and modelling requirement, the AI based methods still have some room for improvement in the area of extensive training requirement and validation. The main vulnerability lies in the fact that if a data out of the training data is presented to the network, what would be the output or response of the network. Due to this these techniques are rarely applied in a practical system and

conventional techniques are preferred over these in spite of the heavy computational requirements. Based on this it is possible to apply these algorithms in practical system as secondary line of defense with the conventional protection system to mitigate with the instability of the system. In future with the advancement in the technologies an increase in the capabilities of AI system is expected making it a real contender for the online and practical stability assessment.

2.5   Transient Stability Constrained Optimal Power Flow

Unlike the transient stability problem, optimal power flow (OPF) [55] is a steady state nonlinear programming (NLP) problem that involves the determination of optimal control parameters in order to achieve the desired objectives subjected to a number of system constraints [8], [56] . The results from the conventional OPF may lead to infeasibility in terms of transient stability, as usually the objective of OPF is to minimize operating cost of the power system. In today's deregulated market environment, the reconciliation of transient stability and economics is achieved by embedding the transient stability constraints with in the optimal power flow which gives rise to Transient Stability Constraint Optimal Power Flow (TSC-OPF) [57], [58], achieving a set of control parameters that not only makes the system to withstand severe contingencies also to achieve the desired objectives. As with the addition of constraint the resulting cost is naturally higher than the conventional OPF case. Therefore, the power market participants and operators has a great interest in depressing this additional cost to maximum extent, which in turn demands improvement in the quality of solution of TSC-OPF.

The TSC-OPF is a highly non-linear optimization problem that involves algebraic and differential constraints that are difficult to handle even for a small power system, due to which the conventional mathematical optimization techniques are ill-fit for solving such kind of a problem.

Various *ad hoc* algorithms and its variants have been proposed for solving TSC-OPF. Xin *et al.* [59] presents a critical review of different variants of TSC-OPF. Ref. [60]–[62] have employed a constraint transcription based on the functional transformation technique to convert the original TSC-OPF into an optimization problem.

Ref. [63] and [58], have transformed the differential equations governing the transient stability constraint into algebraic equations, which are introduced in OPF as a constraint, at each time step. This technique on one hand helps in simplifying the problem but at the same time results in a larger size of problem. This problem was only formulated for a single contingencies case. Ref. [64] extends this problem to include multiple contingencies. Also [64] and [65], reduced the size of the problem considerably from the usage of reduced bus admittance matrix.

Another technique to handle the transient stability constraint is presented in [66]–[68]. The proposed technique introduced bounds, with in the standard OPF problem, on power generation capacity of selected generator or a group of selected generators by using the results of transient stability assessment that is done separately. Due to separate handling of transient stability problem higher order models of the system can easily be incorporated. The only drawback being the non-guarantee of obtaining an optimal

solution as the stability limits were only imposed on the power generating capacity of the gensets.

One of the highlighting facts in all the above mentioned techniques (except for [68])is the stability criteria used to determine the stability status of the system. Ref. [58], [60], [62], [64]–[67], [69] uses the relative machine rotor angle deviations to assess the stability of the system. The limits imposed are arbitrary and differ from reference to reference. Table 2.1 depicts the stability criteria used in different references. A change in the criterion may lead to sub optimal results.

Ref. [61] and [63] uses the energy function criterion to assess the stability of the system. This type of assessment criteria cannot ensure the instability status of the system, also heavy computation is required if higher order models are considered. Ref. [68] proposed an objective based stability criteria by transforming multi-machine system to SIngle Machine Equivalent (SIME) to avoid arbitrary stability criteria. This technique can introduce numerical inaccuracies, whereas transforming the multi- machine system into a SIME is not an easy task.

TABLE 2.1:   ROTOR ANGLE DEVIATION LIMITS USED IN LITERATURE

Reference	Rotor angle deviation limit [degrees]
[58], [64], [65], [70]	100
[62]	120
[60]	144
[67]	180
[66]	270

CHAPTER 3

OPTIMAL PMU PLACEMENT (OPP) PROBLEM

It is neither economical nor necessary to install a PMU at each bus of a wide-area power network. To achieve the fault-location observability over the entire network, it is important to examine minimal PMU placement considering the installation cost of PMUs in the PMU-based applications. The optimal PMU placement (OPP) problem concerns with where and how many PMUs should be installed in a power system to achieve full observability at minimum number of PMUs. [71][72]

When a PMU is placed at a bus in a power system, the voltage phasor at that bus and current phasors in all branches that are incident on that bus can be obtained. A bus is said to be observable if the voltage phasor at that bus is known and the power system is said to be completely observable when all the buses are observable. Clearly, installation of a PMU at a bus makes that bus observable. Since all branch currents at such a bus are also known, the voltage phasors at buses adjacent to this PMU bus can be calculated from

knowledge of the line parameters. Therefore, a PMU placed at a bus makes that bus and all buses adjacent to it observable.[73]–[76]

Being an area of a great research interest, different techniques have been used to solve OPP problem as summarized in [77], [78]. References [73], [79]–[81] propose an integer linear programming formulation to solve OPP problem. In [79] OPP problem is solved under different cases of redundant PMU placement, full observability and incomplete observability.

In [80], OPP problem is solved considering not only the base case operating conditions but also the contingency cases. The proposed method makes use of a voltage stability based contingency ranking method and a graph theoretic approach to modify the constraints under contingency. Reference [81] proposes a procedure for multistage scheduling of PMU placement in a given time horizon taking into account the zero injection constraints. In [73], the problem of joint OPP and conventional measurements to ensure full network observability is addressed. The problem is first formulated as a nonlinear integer programming problem and then recast into an equivalent integer linear programming problem by introducing auxiliary variables and constraints. The branch and bound optimization method is adopted in [82] to solve OPP problem considering secondary voltage control. Constraint functions considering adjacent zero-injection buses are constructed using a novel hybrid topology transformation nonlinear constraint method. References [83], [84] propose solution methods to OPP problem based on particle swarm (PSO) optimization. The objective in [89] is to solve OPP problem using the minimum number of PMUs while maximizing the measurement redundancy at the power system buses. In [90], the performance of the proposed PSO algorithm is

31

compared with that of adaptive GA, CLONALG and adaptive CLONALG. An integer quadratic programming approach is used in [85] to solve OPP problem by minimizing the total number of PMUs required and, at the same time, maximizing the measurement redundancy at the power system buses. The proposed formulation considers the existing conventional measurements, outage of a single transmission line or a single PMU. The binary search method, proposed in [86], accounts also for single branch outages and seeks to maximize the measurement redundancy with minimum number of PMUs. An evolutionary-based approach is proposed in [87] to solve OPP problem for a power system such that a minimum mean square error (MSE) for state estimation is gained in normal operating conditions. The proposed approach employs differential evolution (DE) algorithm to do a state estimation for a power system, calculate the corresponding MSE and then determine the minimum number of PMU needed to make a minimum MSE for the system. Convex relaxation method is proposed in [88] to solve the OPP problem. Different OPP problem formulations considering probabilistic cost/benefit analysis [89], a defined number of PMUs [90] and existing smart meters [91] have also been proposed.

This chapter presents a multi objective formulation for OPP problem to achieve full network observability with minimum number of PMUs which reflects the cost of investment. At first the OPP problem is described a constrained minimization problem with single objective to achieve full network observability using minimum number of PMUs. Then the formulation is extended to include another objective to increase the redundancy of measurement in the system. Strength Pareto Evolutionary Algorithm (SPEA) is applied to the extended formulation and results are compared with published

32

literature in the field of PMU placement. This chapter also details several topological observability rules which are applied to assess the electric network observability.

3.1   OPP Problem Formulation

While formulating the OPP problem, one might require to PMUs to be installed at particular buses due to their specific importance or to better suit a certain PMU application. The two end of a tie line connecting two areas of a power system represent an example falling under the set of *"must place"* buses. Moreover we may sometimes need to prohibit PMU installation at some buses to meet the problem constraint. Power system buses lacking communication facilities and virtual buses that are nonexistent in reality represent some of the example falling under the set *"don't place"* buses. Based on the above the OPP problem is treated as a constrained minimization problem and it is mathematically formulated as shown in equation (3.1).

$$Min\, F\left(x\right)$$

$$F\left(x\right)=\sum_{k=1}^{N_b}C_i n_{ki} + \sum_{k=1}^{N_b}C_r n_{kr} + \sum_{k=1}^{N_b}W_k U_k \qquad (3.1)$$

$$such\,that\,S \in S_{MP}\ ,S \notin S_{DP}$$

where

N_b :   Number of buses

C_i :   Investment Cost of a new PMU

C_r :   Removal and relocation cost of an existing PMU

n_{ki} :   Binary bit to indicate PMU installation at bus 'k'. $n_{ki} = 1$ if a new PMU is

installed at bus 'k' otherwise $n_{ki} = 0$

n_{kr} :   Binary bit to indicate PMU removal at bus 'k'. $n_{kr} = 1$ if a PMU is

removed from bus 'k' otherwise $n_{kr} = 0$

W_k : Penalty factor for bus unobservability. Since the aim is to place the PMUs to have a completely observable system, W_k is set be very high in case of incomplete observability.

U_k : A binary number to indicate unobservability of bus 'k'. it is set to 0 if bus 'k' is observable and 1 other wise

S_{MP} : A set of "must place" buses, if any.

S_{DP} : A set of "don't place" buses, if any.

S : A candidate solution represented by a set of binary numbers indicating PMU installation at system buses. Mathematically it can be represented as follows

$$S = \{x_1 \quad x_2 \quad x_3 \dots \dots \quad \dots \dots \dots \dots x_{N_b}\}$$

Such that $x_i = 1 \ if \ i \in \ S_{MP}$ and $x_i = 0 \ if \ i \in \ S_{DP}$

3.2   Extended OPP Problem Formulation

Traditionally, OPP problem is formulated with a single objective to find the minimum numbers of PMUs and their respective locations, required to have power system fully observable. A natural extension of such formulation is to combine two or more objectives. In this section OPP is formulated to achieve dual objectives, to minimize the number of PMUs and to maximize the PMU measurement redundancy at the power system buses. The following topological observability rules are applied for network observability analysis.[92]–[95]

1.   If a PMU is installed on a bus, voltage phasor of that bus and currents phasors of all incident branches to that bus are known. These are called as direct measurements.

2.   If voltage phasors of both ends of a branch are known then the current phasor of this branch can be obtained directly. These are called pseudo measurements.

3.   If there is a bus whose all incident branches current phasors are known but one, then the current phasor of the unknown one can be obtained using KCL equations.

Based on the above rules an index called as *Observability Redundancy Index ORI* is defined which serves as measure of the redundancy. Higher the value of *ORI* more is the redundancy of measurement. Therefore, extended OPP problem is mathematically formulated as shown below.

$$Min \, F_1(x)$$

$$F_1(x) = \sum_{k=1}^{N_b} C_i n_{ki} + \sum_{k=1}^{N_b} C_r n_{kr} + \sum_{k=1}^{N_b} W_k U_k \qquad (3.2)$$

$$such \, that \, S \in S_{MP} \, , S \notin S_{DP}$$

$$Max \, F_2(x)$$

$$F_2(x) = ORI \qquad (3.3)$$

$$such \, that \, ORI = \sum_{k=1}^{N_b} R_k$$

where,

R_k :   An integer number to indicate bus 'k' observability redundancy index. If N_k indicates number of times bus 'k' is observed, then:

35

$$R_k = \begin{cases} N_k - 1, & N_k \geq 2 \\ 0 & , \quad otherwise \end{cases}$$

(3.4)

3.3   Strength Pareto Evolutionary Algorithm (SPEA)

3.3.1   Multi-Objective Optimization Overview

Multi-objective optimization is a very important research topic for engineers, not only because of the multi-objective nature of most real-world problems, but also because there are still many open questions in this area. In fact, there is not even a universally accepted definition of "*optimum*" as in single-objective optimization.[96], [97]

The principles of multi-objective optimization are different from that in a single objective optimization. The main goal in a single objective optimization is to find the global optimal solution, resulting in the optimal value for the single objective function. However, in a multi-objective optimization problem, there is more than one objective function, each of which may have a different individual optimal solution. If there is sufficient difference in the optimal solutions corresponding to different objectives, the objective functions are often known as conflicting to each other.[98]

Multi-objective optimization with such conflicting objective functions gives rise to a set of optimal solutions, instead of one optimal solution. The reason for the optimality of many solutions is that no one can be considered to be better than any other with respect to all objective functions. These optimal solutions have a special name of *Pareto optimal solutions*.

A general multi-objective optimization problem consists of a number of objectives to be optimized simultaneously with a number of inequality and equality constraints. It can be formulated as follows:

$$\underset{x}{Minimize} \; f_i(x) \quad i=1,...,N_{obj} \tag{3.5}$$

$$Subject \; to: \quad \begin{cases} g_j(x)=0 & j=1,...,M \\ h_k(x) \le 0 & k=1,...,K \end{cases} \tag{3.6}$$

Where, f_i is the ith objective function, x is the set of parameter to be optimized, N_{obj} is the number of objectives, M and K are the number of equality and inequality constraints respectively.

3.3.2 Dominance and Pareto Optimal Solutions

For a multi-objective optimization problem, any two solutions x^1 and x^2 can have one of two possibilities: one dominates the other or none dominates the other. In a minimization problem, without loss of generality, a solution x^1 dominates x^2 *if and only if* the following two conditions are satisfied:

$$\begin{aligned} &1. \; \forall \, i \in \{1,2,...,N_{obj}\}: f_i(x^1) \le f_i(x^2) \\ &2. \; \exists \, j \in \{1,2,...,N_{obj}\}: f_j(x^1) < f_j(x^2) \end{aligned} \tag{3.7}$$

If any of the above condition is violated, the solution x^1 does not dominate the solution x^2. If x^1 dominates the solution x^2, x^1 is called the nondominated solution. The solutions that are nondominated within the entire search space are denoted as *Pareto optimal solutions* and constitute the *Pareto-optimal set* or *Pareto-optimal front*

From the theory of multi-objective optimization [99] the main objectives of multi-objective optimization algorithm are:

- Lead the exploration towards *Pareto-optimal frontier.*

- Maintain the population's diversity in *Pareto-optimal frontier.*

The first task is a natural goal of any optimization algorithm. The second task is unique to multi-objective optimization. Since no one solution in the Pareto-optimal set can be said to be better than the other, what an algorithm can do best is to find as many different Pareto-optimal solutions as possible.

3.3.3 Pareto Set Reduction by Clustering

Generally, the Pareto optimal set can be extremely large. Therefore, reducing the set of nondominated solutions without destroying the characteristics of the trade-off front is desirable from the decision maker's point of view. An average linkage based hierarchical clustering algorithm [100] is employed to reduce the Pareto set to manageable size. It works iteratively by joining the adjacent clusters until the required number of groups is obtained. It can be described as:

"Given a set P for which its size exceeds the maximum allowable size N, it is required to form a subset P* with the size N"

The algorithm is illustrated in the following steps.[99]

Step 1:   Initialize cluster set C; each individual $i \in P$ constitutes a distinct cluster.

Step 2: If number of clusters ≤ *N*, then go to Step 5, else go to Step 3.

Step 3: Calculate the distance of all possible pairs of clusters. The distance d_c of two clusters c_1 and $c_2 \in C$ is given as the average distance between pairs of individuals across the two clusters

$$d_c = \frac{1}{n_1 \times n_2} \sum_{i_1 \in c_1, i_2 \in c_2} d(i_1, i_2)$$

Step 4: Determine two clusters with minimal distance d_c. Combine these clusters into a larger one. Go to Step 2.

Step 5: Find the centroid of each cluster. Select the nearest individual in this cluster to the centroid as a representative individual and remove all other individuals from the cluster.

Step 6: Compute the reduced nondominated set *P** by uniting the representatives of the clusters.

3.3.4 Best Compromise Solution Extraction

On completion of evolution process the multi objective algorithm must offer a best compromise solution to the decision maker. Fuzzy concepts are applied to model the impreciseness in ruling of the decision maker. The membership function μ_i for i^{th} objective function F_i is given as

$$
\mu_i = \begin{cases} 1 & F_i \leq F_i^{\text{min}} \\ \dfrac{F_i^{\text{max}} - F_i}{F_i^{\text{max}} - F_i^{\text{min}}} & F_i^{\text{min}} < F_i < F_i^{\text{max}} \\ 0 & F_i \geq F_i^{\text{max}} \end{cases}
\tag{3.8}
$$

where, F_i^{min} and F_i^{max} are the minimum and maximum of the ith objective function among all nondominated solutions, respectively. The membership function value ranges from 0 to 1 as shown in Figure 3.1. The maximum of normalized membership function μ^k gives the best compromise solution [99], whereas normalized membership function for k^{th} nondominated solution is given as

$$
\mu^k = \frac{\displaystyle\sum_{i=1}^{N_{Obj}} \mu_i^k}{\displaystyle\sum_{k=1}^{M}\sum_{i=1}^{N_{Obj}} \mu_i^k}
\tag{3.9}
$$

where, M is the number of nondominated solutions in Pareto set.
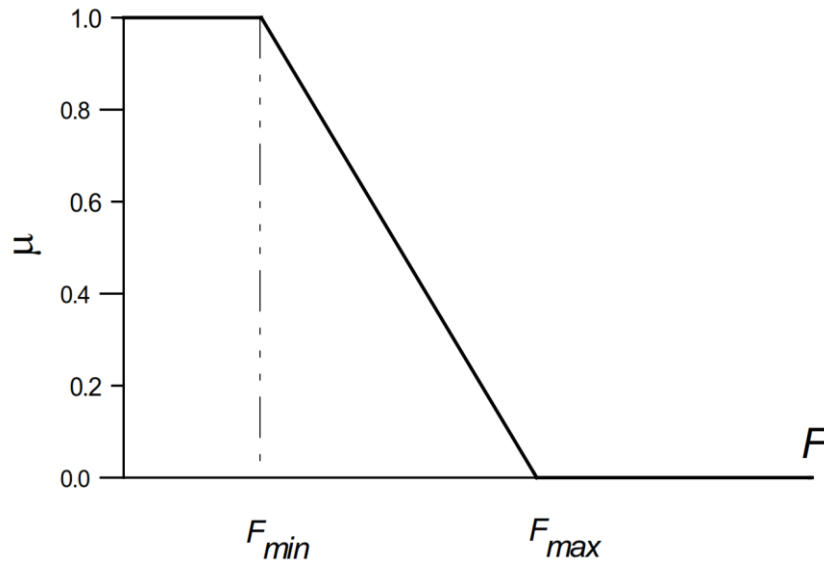
Figure 3.1:   Membership function of the objective functions

3.3.5 SPEA Overview

Zitzler and Thiele [97] presented SPEA as a potential algorithm for multi objective optimization. This technique stores externally the individuals that represent a nondominated front among all solutions considered so far. All individuals in the external set participate in selection. SPEA uses the concept of Pareto dominance in order to assign scalar fitness values to individuals in the current population.

3.3.6 Basic Definitions

The basic elements of the SPEA technique are briefly stated and defined as follows:

***External set*: -** It is a set of Pareto optimal solutions. These solutions are stored externally and updated continuously. Ultimately, the solutions stored in this set represent the Pareto optimal front.

***Strength of a Pareto optimal solution*: -** It is an assigned real value $s \in [0,1)$ for each individual in the external set. The strength of an individual is proportional to the number of individuals covered by it.

***Fitness of population individuals*: -** The fitness of each individual in the population is the sum of the strengths of all external Pareto optimal solutions by which it is covered. It is worth mentioning that, unlike NSGA [96] and NPGA [96], the fitness of a population member is determined only from the individuals stored in the external set. This reduces significantly the computational burden of the fitness assignment process. It is worth mentioning that the strength of a Pareto optimal solution is at the same time its fitness.

3.3.7 The Algorithm

Generally, the algorithm can be described in the following steps.

Step 1)   **(Initialization)**: Generate an initial population and create the empty external Pareto-optimal set.

Step 2)   **(External set updating):** The external Pareto-optimal set is updated as follows.

    i. Search the population for the nondominated individuals and copy them to the external Pareto set.

    ii. Search the external Pareto set for the nondominated individuals and remove all dominated solutions from the set.

    iii. If the number of the individuals externally stored in the Pareto set exceeds a pre-specified maximum size, reduce the set by means of clustering.

Step 3)   **(Fitness assignment)**: Calculate the fitness values of individuals in both external Pareto set and the population as follows.

    i. Assign the strength s for each individual in the external set. The strength is proportional to the number of individuals covered by that individual.

ii. The fitness of each individual in the population is the sum of the strengths of all external Pareto solutions which dominate that individual. A small positive number is added to the resulting sum to guarantee that Pareto solutions are most likely to be produced.

Step 4)   **(Selection)**: Combine the population and the external set individuals. Select two individuals at random and compare their fitness. Select the better one and copy it to the mating pool.

Step 5)   **(Crossover and Mutation)**: Perform the crossover and mutation operations according to their probabilities to generate the new population.

Step 6)   **(Termination)**: Check for stopping criteria. If anyone is satisfied *then* stop *else* copy new population to old population and go to Step 2. In this study, the search will be stopped if the generation counter exceeds its maximum number.

3.3.8 Implementation

The fore mentioned algorithm is implemented and coded in MATLAB. Due to difficulties of binary representation when dealing with continuous search space with large dimensions, the proposed approach has been implemented using real-coded genetic

algorithm (RCGA) [101]. A decision variable x_i is represented by a real number within its lower limit a_i and upper limit b_i, i.e. $x_i \in [a_i, b_i]$. The RCGA crossover and mutation operators are described as follows:
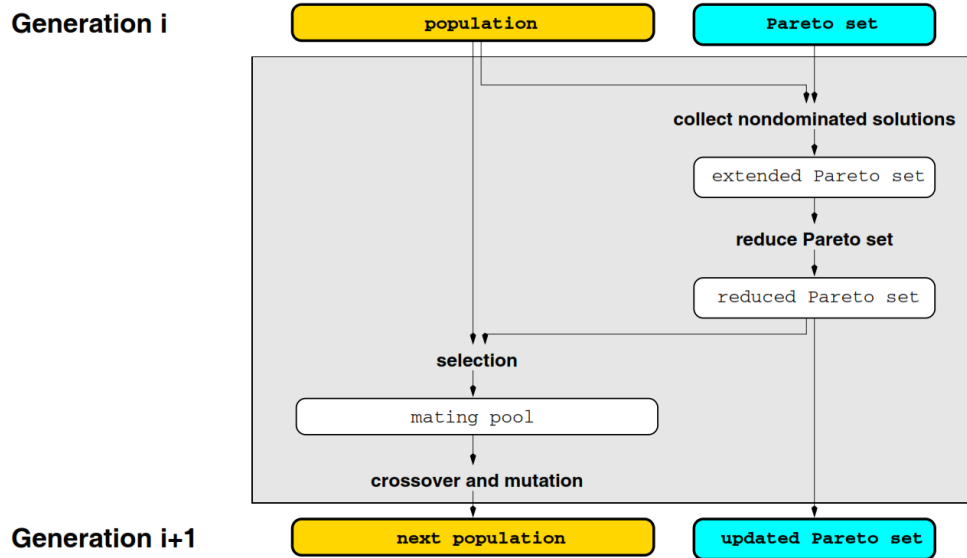
Figure 3.2:   General outline of SPEA. [97]

Crossover:- To proceed onto the next generation as in any evolutionary algorithm first step is to perform crossover operation on the current generation. Different crossover techniques exist for crossover, however a blend crossover *(BLX-α)* is employed in this study. In this type of crossover, a random number is selected from the interval given as

$$[x_i - \alpha(y_i - x_i), y_i - \alpha(y_i - x_i)] \tag{3.10}$$

where x_i and y_i are the ith parameter values of the parent solutions and $x_i < y_i$. α is chosen to be 0.5 to ensure exploration and exploitation.
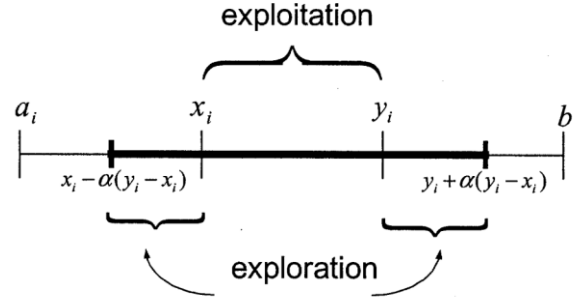
Figure 3.3:   Blend Crossover Operator (BLX-α)

Mutation:- Mutation is applied in the evolutionary algorithm in order to diversify the solutions and to avoid premature convergence. A non-uniform mutation technique is applied in this study. The mutated child x_i' for parameter x_i at for a specific generation '*t*' is given as

$$x_i' = \begin{cases} x_i + \Delta(t, b_i - x_i), & \text{if } \tau = 0 \\ x_i - \Delta(t, x_i - \alpha_i), & \text{if } \tau = 1 \end{cases} \tag{3.11}$$

and

$$\Delta(t, y) = y(1 - r^{(1-t/g_{max})^{\beta}}) \tag{3.12}$$

where *r* is a random number $r \in [0,1]$, τ is a binary random number, g_{max} is the maximum number of generations and β is a random number selected arbitrarily, in this study $\beta = 5$ is selected. During the start of evolutionary process when *t* is small the search is uniform as the algorithm advances the probability of having a mutated child x_i' close to the parent x_i, increases.

Finally, Figure 3.4 shows the detailed computation flow of SPEA.

45
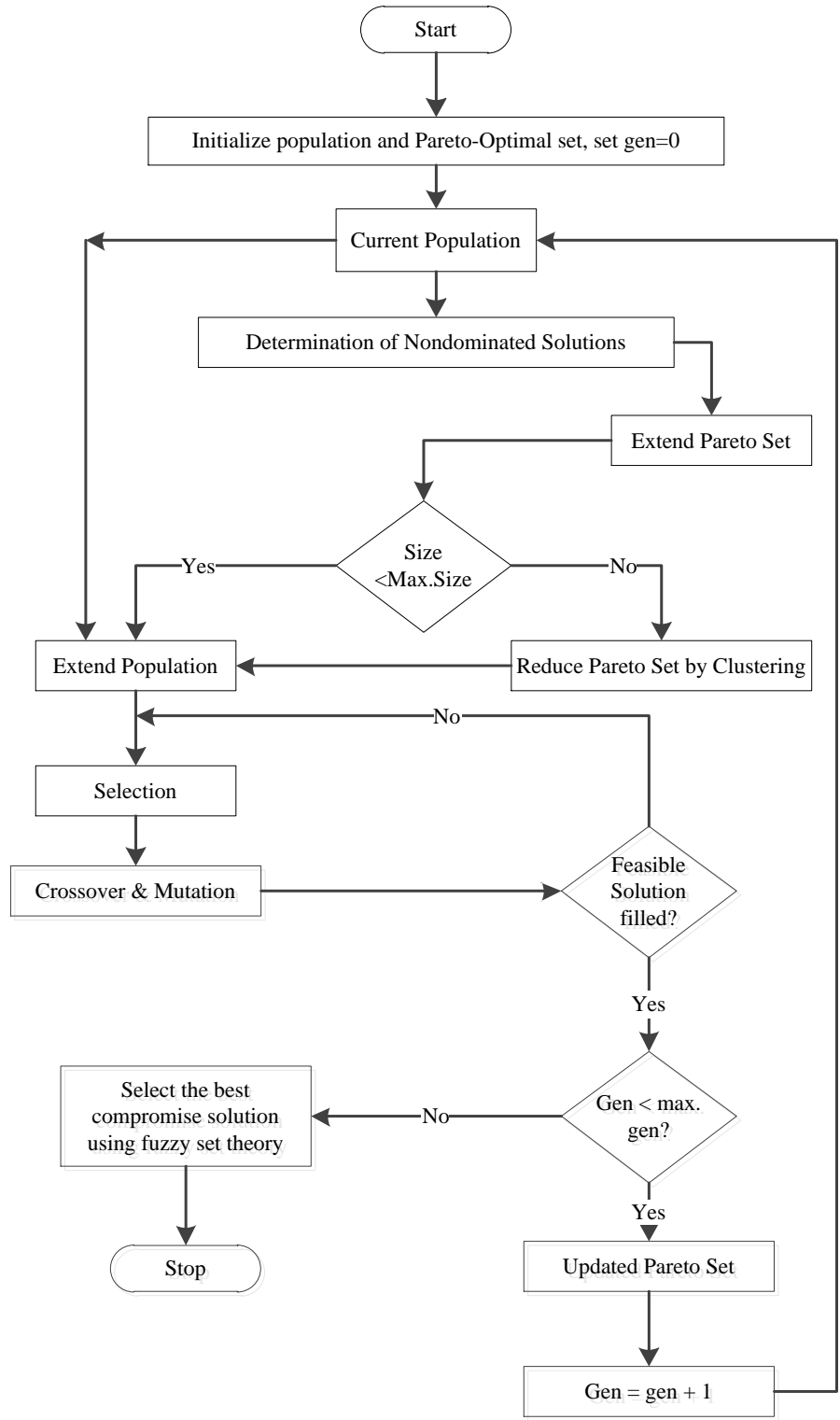
Figure 3.4:   SPEA Computational Flow

3.4   SPEA Implementation for OPP Problem:

The extension of the OPP problem makes it a multi objective optimization problem with conflicting objectives. One trivial way of handling a multi-objective or vector objective problems is to combine the desired goals of the optimization problem and construct a scalar function and then use a common scalar optimization approach to solve the problem. The major problem of this methodology is the unavailability of any straightforward methods for combining the objectives or goals of the problem while they vary constantly. The other approach is to use a multi objective based heuristic or intelligent technique as it is a non-convex optimization problem to determine the optimal solution(s). As from the extended formulation, (3.2) and (3.3), it is clear that two objectives under consideration are conflicting to each other, i.e. one is to be minimized and other need to be maximized. A SPEA minimization code is implemented in MATLAB as described in section (3.3.7). Without the loss of generality, one of the objective i.e. F_2 is taking as inverted as shown below.

$$Max\, F_2\left(x\right)=-\,Min\, F_2\left(x\right) \tag{3.13}$$

Making use of formulation, observability rules and algorithm as described in equations (3.2), (3.3) and (3.13), section (3.2) and section (3.3.7) respectively the OPP problem is solved by finding the minimum number of PMUs, required to have full network observability, their location with maximizing the measurement redundancy for IEEE 14- and IEEE 30- bus systems. The next subsections presents the simulation results obtained and compare them with those obtained and published in literature using some other optimization techniques.

3.4.1 Application to IEEE 14-bus test system

Figure 3.5 shows the one line diagram for the IEEE 14-bus test system. The SPEA parameters that are population size N_{pop}, desired size of Pareto set N_{Des}, crossover probability P_{CROSS} and mutation probability P_{MUT} are set as 30 (almost twice the size of buses in the system), 10, 0.8 and 0.01 respectively.
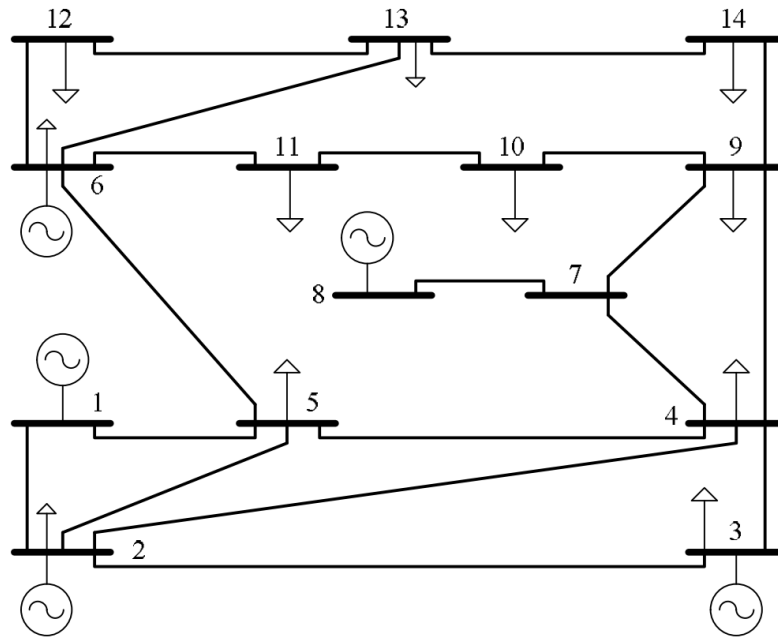
Figure 3.5:   IEEE 14-bus test system

The result of optimization for IEEE 14-bus case is tabulated in Table 3.1. The location of the PMUs and required number of PMUs i.e. N_{PMU} and the respective *ORI* are also incorporated in Table 3.1. As described in 3.3.1 for multi objective optimization rather than existence of one optimum there exist a set of optimal solutions. The Pareto front obtained as a result of optimization is shown in Figure 3.6. One of the advantage that can be seen for formulating OPP problem as multi objective optimization problem, is the solutions presented by the algorithm are unique and the decision maker has

opportunity to choose from variety of solutions rather than only one solution. Another advantage being unlike in single objective optimization (where there are two or more objective) e.g. weighted sum or goal programming, there is no need to make number of runs to find the optimum solution.
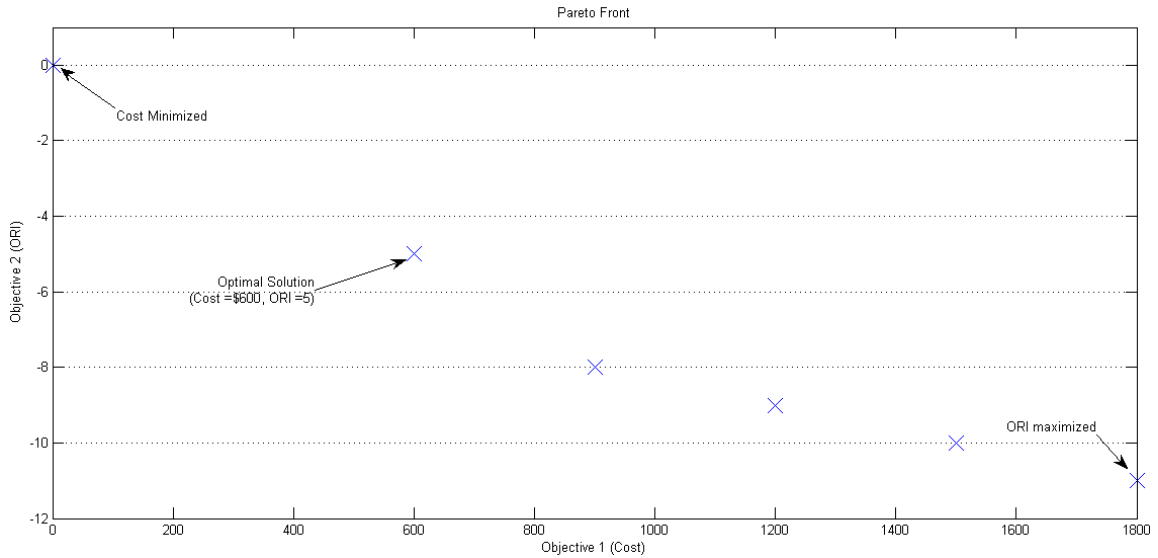
Figure 3.6:   Pareto front for IEEE 14-Bus Test System

TABLE 3.1:   OPP FOR IEEE 14-BUS TEST SYSTEM

P_{CROSS}	P_{MUT}	N_{PMU}	Location	ORI
0.8	0.01	4	2, 6, 7, 9	5

It is considered that each of the PMU installed or replaced incurs a cost of $150. Simulation results reveal three solutions that are minimum cost solution, best compromise solution and maximum *ORI* solution. The minimum cost i.e. $0, results naturally when there are no PMUs placed in the system, the solution presented in the best compromise case is the one we are interested in, as it gives balanced importance to each objective. The cost associated with this solution is $600 which in turn means 4 PMUs are

required to completely observe the system with a redundancy index of 5, which means some of the buses in the system are observed more than once as per equation (3.3). For maximum *ORI* solution the cost incurred is the highest, this kind of solution can be used as reference for future installations of PMUs in the system which results in maximum measurement redundancy.

Another run is made for 14-bus test system OPP problem, without maximizing the *ORI*. Table 3.2 compares the effect of maximizing the *ORI* case with the case where *ORI* was not considered as an objective. It can be seen that for the case where the *ORI* is maximized bus 4 is observed 3 times whereas bus 5, 7 and 9 are observed twice. Physically it can be seen as, for the case where *ORI* is maximized, a failure of PMU on bus 2 will make bus number 1, 2 and 3 unobservable, on the other hand for the case where *ORI* is not maximized, a failure of PMU on bus number 2 will make bus number 1, 2, 3, 4 and 5 unobservable. More number of buses are affected due to the failure of PMU(s) when *ORI* is not maximized as compared to the case where *ORI* is maximized.

TABLE 3.2: EFFECT OF MAXIMIZING *ORI* FOR IEEE 14-BUS TEST SYSTEM

Case	N_{PMU}	Location	ORI	N_k
With maximizing ORI	4	2, 6, 7, 9	5	1,1,1,3,2,1,2,1,2,1,1,1,1,1
Without maximizing ORI	4	2,8,10,13	0	1,1,1,1,1,1,1,1,1,1,1,1,1,1

3.4.2 Application to IEEE 30-bus test system

Figure 3.7 shows the one line diagram for the IEEE 30-bus test system. The SPEA parameters that are population size N_{pop}, desired size of Pareto set N_{Des}, crossover

probability P_{CROSS} and mutation probability P_{MUT} are set as 60 (twice the size of buses in the system), 20, 0.8 and 0.01 respectively.
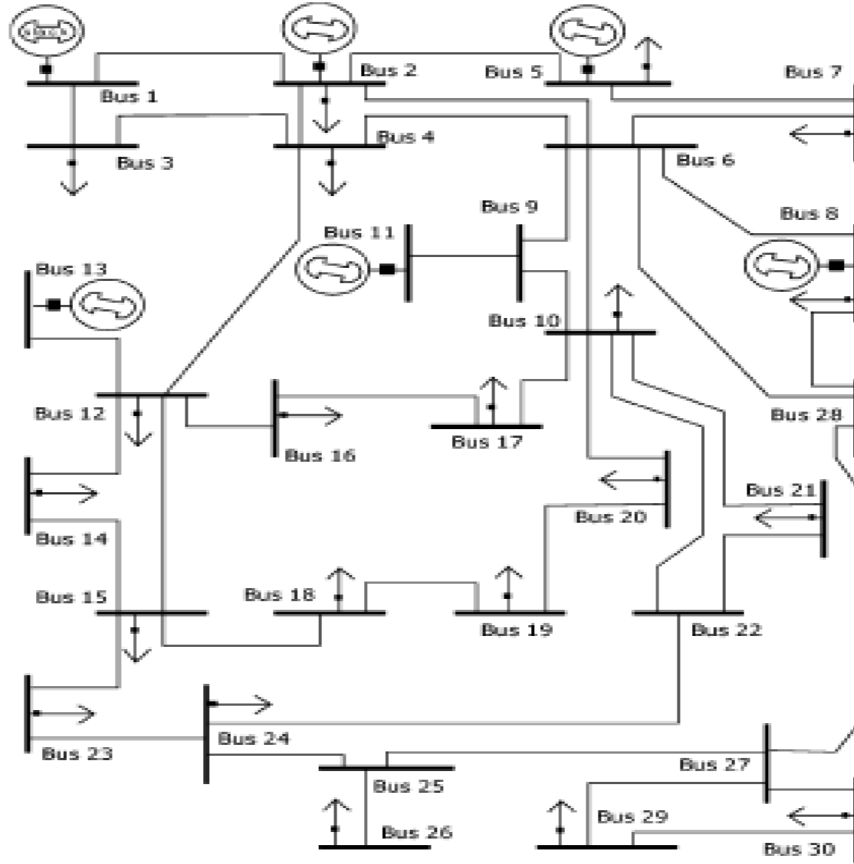
Figure 3.7:   IEEE 30-bus test system.

The result of optimization for IEEE 30-bus case is tabulated in Table 3.3. The location of the PMUs and required number of PMUs i.e. N_{PMU} and the respective *ORI* are also incorporated in Table 3.3. The Pareto front obtained as a result of optimization is shown in Figure 3.8.

It is considered that each of the PMU installed or replaced incurs a cost of $150. Simulation results reveal three solutions that are minimum cost solution, best compromise solution and maximum *ORI* solution. The minimum cost i.e. $0, results

51

naturally when there are no PMUs placed in the system, the solution presented in the best

compromise case is the one we are interested in, as it gives balanced importance to each

objective.
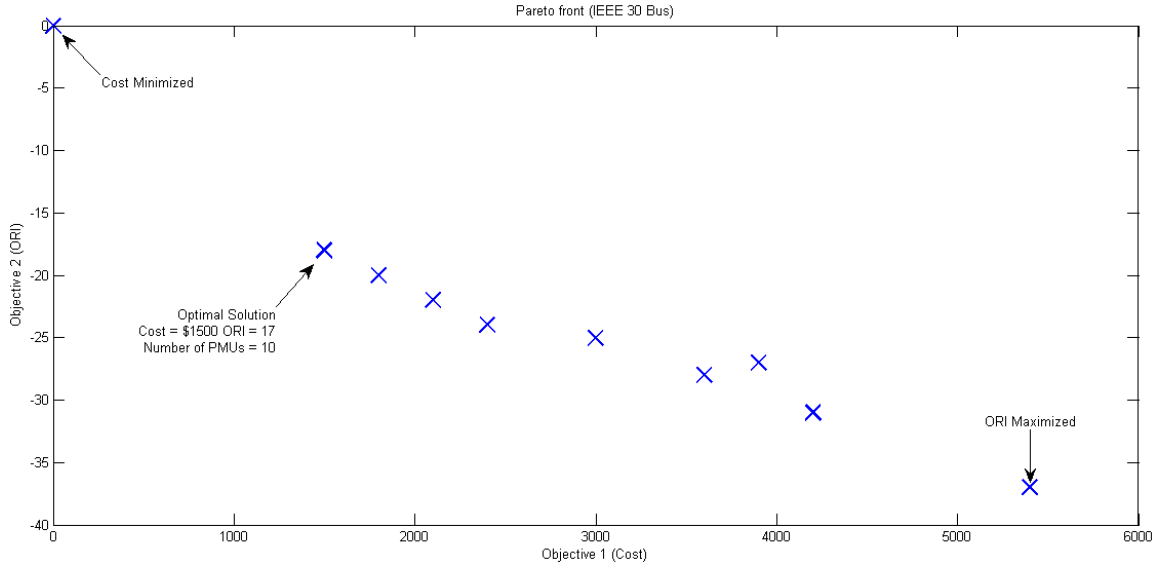
Figure 3.8:   Pareto Front for IEEE 30-bus Test System.

TABLE 3.3:   OPP FOR IEEE 30-BUS TEST SYSTEM

P_{CROSS}	P_{MUT}	N_{PMU}	Location	ORI
0.8	0.01	10	2, 4, 6, 10, 11, 12, 19, 24, 26, 27	17

The cost associated with best compromise solution is $1500 which in turn means

10 PMUs are required to completely observe the system with a redundancy index of 17,

which means some of the buses in the system are observed more than once as per

equation (3.3). For maximum *ORI* solution the cost incurred is the highest, this kind of

solution can be used as reference for future installations of PMUs in the system, which

results in maximum measurement redundancy.

52

3.5 Comparison with other optimization techniques

To validate the results obtained using SPEA algorithm a comparison is made with the published results obtained using other optimization techniques, namely Differential Evolution (DE) namely Branch and Bound (B&B), Binary Particle Swarm Optimization (BPSO), Integer Quadratic Programming (IQP), Binary Search Algorithm (BSA), Integer Linear Programming (ILP) and Genetic Algorithm (GA). Table 3.4 shows an acceptable performance of DE algorithm when compared to these optimization techniques.

TABLE 3.4:   NUMBER AND LOCATION OF PMUS FROM SPEA AND OTHER OPTIMIZATION
ALGORITHMS

Algorithm		14-Bus	30-Bus
SPEA	No.	4	10
	Loc.	As per Table 3.1	As per Table 3.3
DE [102]	No.	4	10
	Loc.	2,6,7,9	1,5,6,9,10,12,18,24,25,27
ILP [79]	No.	4	10
	Loc.	Not reported	Not reported
ILP [73], [103]	No.	4	--
	Loc.	2,6,7,9	--
B&B [82]	No.	--	10
	Loc.	--	1,5,6,9,10,12,15,19,25,29
BPSO [104]	No.	4	10
	Loc.	2,7,10,13	1,5,6,9,10,12,15,19,25,27
IQP [85]	No.	4	10
	Loc.	2,7,10,13	2,4,6,9,10,12,15,19,25,27
BSA [86]	No.	4	10
	Loc.	2,6,7,9	1,2,6,9,10,12,15,19,25,27
GA [105]	No.	4	10
	Loc.	2,6,7,9	2,4,6,9,10,12,15,19,25,27

CHAPTER 4

OPTIMAL STATCOM PLACEMENT AND SIZING

PROBLEM

Series capacitor, shunt capacitor, and phase shifter are different approaches to increase the power system load ability. In past decades, all these devices were controlled mechanically and were, therefore, relatively slow. They were very useful in a steady state operation of power systems but from a dynamical point of view, their time response was too slow to effectively damp transient oscillations. If mechanically controlled systems were made to respond faster, power system security would had significantly improved, allowing the full utilization of system capability while maintaining adequate levels of stability. This motivation led to the changes in the structure and control of these devices. With emergence of power electronics and continual advancement in this field led to a new approach introduced by the Electric Power Research Institute (EPRI) in the late 1980 called Flexible AC Transmission Systems or simply FACTS. Generally, the main

objectives of FACTS are to increase the useable transmission capacity of lines and control power flow over designated transmission routes.[106]

Hingorani and Gyugyi [106] and Hingorani [107], [108] proposed the concept of FACTS. Edris in [109] proposed terms and definitions for different FACTS controllers. Flexible AC Transmission System (FACTS) is an alternating current transmission system incorporating power electronic-based and other static controllers to enhance controllability and increase power transfer capability [106]. FACTS devices have become very important applications of power electronics in controlling power flow by controlling any of the AC transmission system parameters, that are voltage magnitude, phase and load impedance [110].

FACTS devices were the solution to the difficulties arising with the geographically irregular growing power demand. FACTS met the transmission system requirement to use the existing power facilities without decreasing system availability and security. In addition, the use of FACTS provides voltage support to prevent voltage collapses when the electricity network is under heavy loading. The main objectives of FACTS are to increase transmission capacity of lines and to control the power flow over chosen transmission routes [111]. As supplementary functions, damping the inter-area modes and enhancing power system stability using FACTS controllers have been extensively studied and investigated. Generally, it is not cost-effective to install FACTS devices for the sole purpose of power system stability enhancement.

A FACT offers the possibility of meeting many recent power demands. FACTS devices are routinely employed in order to enhance the power transfer capability of the

otherwise under-utilized parts of the interconnected network [112]. To install FACTS devices in realistic system, it is necessary to study the power network to choose the best locations for them for power stability improvement and voltage regulation during dynamic disturbances [113].

4.1   First Generation FACTS Devices

Developments in the field of high voltage power electronics have made possible the practical realization of FACTS controllers. By the 1970s, the voltage and current rating of Thyristor had been increased significantly making them suitable for applications in high voltage power systems [116]. This made construction of modern Static Var Compensators (SVC), Thyristor Controlled/Switched Series Capacitors (TCSC/TSSC), and Thyristor Controlled Phase Shifter Regulators (TCPS). A fundamental feature of the thyristor based switching controllers is that the speed of response of passive power system components such as a capacitor or a reactor is enhanced, but their compensation capacity is still solely determined by the size of the reactive component.

4.2   Second Generation FACTS Devices

The field of FACTS devices was completely revolutionized with emergence of Gate Turn-Off (GTO) Thyristor in start of 1990s. The basic difference between the first and second generation of FACTS devices was the use of switching devices, the first generation FACTS devices used conventional thyristor which requires gate pulse to turn on but no control was there to turn it off, whereas second generation of FACTS devices employed Gate Turn-Off Thyristor which uses Pulse Width Modulation (PWM) to be switched on or off allowing more flexibility in control. This allowed to give birth to more

dynamic family of FACTS devices. STATCOM, UPFC and IPFC are to be named as a few in this class. Only STATCOM is given consideration in this survey as the scope of this study is to optimally place them to improve power system transient stability.

4.2.1 STATic synchronous COMpensator (STATCOM)

STATCOM is a shunt-connected FACTS controller, which can be utilized to control the voltage at the point of connection [117], [118]. It senses the AC system terminal voltage and compensate for the voltage difference across the coupling transformer connecting it to the AC system by exchanging active and reactive power. If the output voltage is greater than the AC voltage, it supplies power to the AC system and if the output voltage is less than the AC voltage, it absorbs power from the AC system.

The building block for STATCOM is a six-pulse voltage-sourced DC to AC inverter (VSI). The output voltage waveforms of this block have high harmonic contents. To reduce these harmonics, a number of six-pulse VSI's are combined to generate a balanced three-phase voltage whose amplitude and phase are controllable by power electronic devices such as Gate Turn-Off (GTO) thyristor and Integrated Gate-Commutated Thyristor (IGCT).

STATCOM can be used to obtain desired reactive power compensation and regulate the bus voltage. It can dramatically increase the stability of electric power grid and decrease disturbance to the rest of the electric power grid [115]. Regulating the reactive and active power transferred by STATCOM to the network controls the power flow in the line and the DC link voltage inside STATCOM. Compared to the old style

reactive power support methods using capacitor banks and thyristors, STATCOM can offer much higher dynamic performance. These benefits are well-recognized [119].

$$V_m$$

$$x_t \quad i_s$$

$$V_s$$

VSC

$$C$$

$$\phi$$

$$I_{DC} \quad V_{DC}$$

$$C_{DC}$$
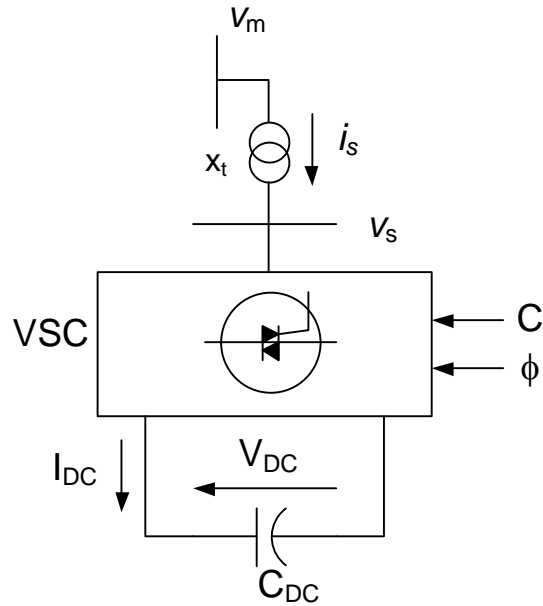
Figure 4.1:   Basic structure of STATCOM

Compared to SVC and other conventional reactive power compensators, STATCOM has several advantages. STATCOM has a dynamic performance far exceeding the other VAR compensators. The overall system response time of STATCOM can reach 10 ms and sometimes less than that. STATCOM can maintain full capacitive output current even at low system voltage. Thus, it is more effective than SVC in improving transient stability. Also, STATCOM has a smaller installation space, about half of that for SVC. STATCOM controllers are generally Pulse Width Modulated (PWM) controllers that are used to control the output voltage of STATCOM to supply or absorb reactive power [120].

The optimal location of the STATCOM in a four-machine power system and its coordinated design with power system stabilizers for power system stability improvement has been studied by Panda and Narayana in 2008 [121]. The location of the STATCOM has been formulated as an optimization problem to improve transient stability and particle swarm optimization has been used to search for its optimal location. In addition, the optimal parameters of the STATCOM have been determined. Genetic algorithm technique was used to design STATCOM controllers. Other intelligent techniques were also used, such as particle swarm optimization [120] in and fuzzy logic in [119].

Although it has been 15 years since the advent of the STATCOM, it has mostly been used to enhance the voltage stability or to increase the low frequency oscillation damping in the power system as the main objective behind the installation of these devices is to support the bus voltage where it is installed, by injecting or absorbing reactive power. As FACTS has capability to change the network conditions very abruptly these devices can be exploited to enhance the transient stability of the power system. To the best of knowledge of author there is none work being done in the field of optimal placement of STATCOM to enhance transient stability of the power system. In the subsequent section a novel formulation for placing the STATCOM optimally is presented, which is an optimization problem solved using Differential Evolution Algorithm (DEA).

4.3 Optimal STATCOM Placement and Sizing Problem Formulation

Whenever a solid three phase fault occurs in a power system on a bus, the voltage of that bus decreases and eventually goes to zero, this results in machine acceleration as a result of imbalance between electrical and mechanical power of the machines. From the theory

of energy functions of the power system it is known that, if a system is stable after contingency the Kinetic Energy (KE) and Potential Energy (PE) are positive and small; otherwise, if the system goes unstable the KE increases drastically and PE drops rapidly to keep the Total Energy (TEF) constant [22].

$$TEF = KE + PE \tag{4.1}$$

$$KE = \frac{1}{2}\sum_{i=1}^{N_G} M_i \tilde{\omega}_i^2 \tag{4.2}$$

$$PE = -\sum_{i=1}^{N_G} \int_{\theta_i^{SEP}}^{\theta_i} PAC_i^P d\theta_i \tag{4.3}$$

where

$$PAC_i = P_{mi} - P_{ei} - \frac{M_i}{M_T} P_{COI} \tag{4.4}$$

and

$$P_{COI} = \sum_{i=1}^{N_G} (P_{mi} - P_{ei}) \tag{4.5}$$

θ_i^{SEP} :   Rotor angle of the ith machine for post fault system's SEP.

PAC_i^P :   Accelerating power of ith machine for post fault period.

From equation (4.2) it can be observed that KE is in proportion to square of the speed ω of the machines, therefore the increment rate of KE is very large. Using this characteristic of the energy functions the transient stability of the system is quantified and regarded as

an objective to place the STATCOM in the system in order to improve the transient stability of the system. Now the objective for the problem can be given as follows

$$F = Minimize\,(max(KE_{cl}))$$ (4.6)

$$Subject\,to : V_{Bus_{STATCOM}} \leq 1.05\ p.u.$$ (4.7)

where

$$KE_{cl} = \frac{1}{2}\sum_{i=1}^{N_G} M_i \tilde{\omega}_{i_{cl}}^2$$ (4.8)

KE_{cl} :   Kinetic Energy of the system at instance of fault clearance.

$\tilde{\omega}_{icl}$:   Speed of ith machine at instance of fault clearance.

A voltage limit constraint is imposed on the objective function to keep the system under physical constraint. As too high value of STATCOM or overcompensation may result in overvoltage at the bus at which the STATCOM is installed.

Until now we have quantified the transient stability of the system, so another constraint of system stability is added to check the feasibility i.e. if the system is stable or not. Although the stability status of the system can be determined by energy functions, but the computational requirement for calculating PE serves as a drawback for this scenario. Instead a hybrid system synchronism classifier "η" is introduced for each machine in the system given as

$$\eta_i = \frac{180 - |\theta_i|}{180 + |\theta_i|}$$ (4.9)

θ_i :   Rotor angle of ith machine in COI reference frame.

The value of η_i varies from -1 to 1. For a stable system $\eta_i \geq 0$.

Now the complete formulation for the problem can be written as

$$F = Minimize\,(max(KE_{cl}))$$
$$Subject\ to: \qquad V_{Bus_{STATCOM}} \leq 1.05\ p.u. \qquad\qquad (4.10)$$
$$\eta_{i_m} \geq 0$$

where, η_{i_m} denotes the synchronism status of ith generator for m^{th} contingency.

From equation (4.10) it is evident that it is a single objective constrained minimization problem, in this study Differential Evolution Algorithm (DEA) for optimization is applied which is briefly described in the section to follow.

4.4   DE Optimization Algorithm

DE is a relatively new population-based optimization technique as it was first proposed by Storn and Price at Berkeley over 1994–1996. Since then, DE has been attracting increasing attention for a wide variety of engineering applications including power engineering. Unlike the conventional evolutionary algorithms (EAs) that depend on pre-defined probability distribution function for mutation process, DE uses the differences of randomly sampled pairs of objective vectors for its mutation process. As a result, the object vectors' differences will pass the objective functions topographical information toward the optimization process and therefore provide more efficient global optimization capability. DE is a stochastic direct search optimization method. In general, it is considered to be simple, accurate, reasonably fast and robust. It is easy to use in solving optimization problems that require a minimization process with real-valued and multimodal objective functions. DE uses a non-uniform crossover that makes use of child vector parameters to guide through the minimization process. In comparison with GAs,

the mutation operation with DE is performed by arithmetical combinations of individuals rather than perturbing the genes in individuals with small probability. Another main advantage of DE over many basic EAs is its ability to search with floating point representation instead of binary representation [87], [122]–[124]

4.4.1 DE Fundamentals

Being a member of the EA family, DE also depends on the initial population generation, mutation, recombination and selection through repeated generations until the stopping criteria is met. DE uses a population of *NP* parameter vectors for each generation. At each generation *G*, the population P^G is composed of $x_i^G, i = 1,2,...,NP$. If there is nothing known about the problem to be optimized, the initial population P^{G0} can be chosen randomly under uniform probability distribution [122], [125].

The key characteristic of a DE is the way it generates trial parameter vectors throughout the generations. A weighted difference vector between two individuals is added to a third individual to form a new parameter vector. The newly generated vector will be evaluated by the objective function. The value of the corresponding objective function will be compared with a pre-determined individual. If the newly generated parameter vector has lower objective function value, it will replace the pre-determined parameter vector. The best parameter vector is evaluated for every generation in order to track the progress made throughout the minimization process. The random deviations of DE are generated by the search distance and direction information from the population. This adaptive approach is associated with the normally fast convergence properties of a DE. [122], [125]

DE generates, for each parent parameter vector, a candidate child vector based on the distance of two other parameter vectors. For each dimension $\in [1,d]$ this process is shown in equation (4.11).

$$x^{'} = x^{'}_{r3} + F * (x^G_{r1} - x^G_{r2})$$
(4.11)

where the random integers $r1 \neq r2 \neq r3 \neq i$ are used as indices to index the current parent object vector. F is a real constant positive scaling factor, normally $F \in (0,1)$, that controls the scale of differential variation $(x^G_{r1} - x^G_{r2})$. Selecting this newly generated vector is based on comparison with another control variable, the crossover constant $CR \in [0,1]$, to ensure the search diversity. Some of the newly generated vectors will be used as child vector for the next generation and others will remain unchanged. The selection process of DE follows the typical EA process. Each new vector $x^{'}$ is compared with x_i. The new vector $x^{'}$ replaces x_i as a member of next generation if it produces a better solution than x_i [122], [125].

4.4.2 DE Key Operators

In this section, some specific operators of DE are analyzed in more details to achieve better understanding and application of the technique. These include mutation, crossover and other operators. The objective of *mutation* is to enable search diversity in the parameter space and to direct the existing object vectors with suitable amount of parameter variation in a way that will lead to better results at a suitable time. It keeps the search robust and explores new areas in the search domain. In DE, the mutation vectors are generated by adaptively scaling and correlating the output of pre-defined, multivariate probability distribution. The mutation operation is considered as the first step towards the

generation of new solutions. After initial population generation, for every solution (individual) in the population in G^{th} generation $X_i^{(G)}, i = 1, ..., NP$ a mutant vector $V_i^{(G+1)}$ is generated [122], [125], [126] given as

$$V_i^{(G+1)} = X_i^{(G)} + F*(X_{best}^{(G)} - X_i^{(G)}) + F*(X_{r1}^{(G)} - X_{r2}^{(G)}) \qquad (4.12)$$

where, $X_{r1}^{(G)}, X_{r2}^{(G)}$ are randomly selected solution vectors from the current generation (different from each other and the corresponding X_i) and $X_{best}^{(G)}$ is the solution achieving best value. $F \in (0, 1)$ is a mutation constant and plays an important role in controlling the convergence speed.

To further perturb the generated solutions and enhance the diversity, a *crossover* operation is applied by the DE shown in Figure 4.2. In this step the parameters of the generated mutant vector and its corresponding vector I in the original population are copied to a trial solution according to a certain crossover factor $CR \in [0, 1]$. For each parameter, a random number in the range [0, 1] is generated and compared with *CR*, and if its value is less than or equal to *CR*, the parameter value is taken from the mutant vector, otherwise, it will be taken from the parent. Crossover process is shown in Figure 4.2. However, in case *CR* was defined to be zero, then all the parameters of the trial vector are copied from the parent vector X_i, except one value (randomly chosen) of the trial vector is set equal to the corresponding parameter in the mutant vector. On the other hand, if *CR* is set equal to one. Then, all parameters will be copied from the mutant vector, except one value (randomly chosen) of the trial vector is set equal to the corresponding parameter in the parent vector. The factor *CR* plays a role in controlling the smoothness of the convergence. As *CR* becomes very small, it becomes very probable

that the trial solutions would have characteristic of their parent vectors and therefore, slow the convergence.
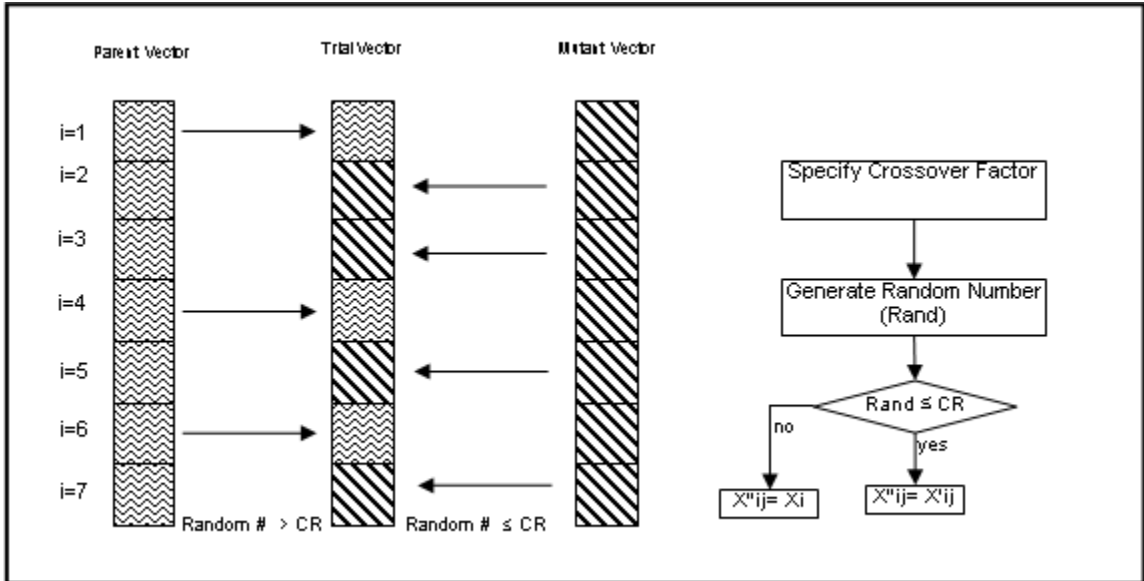
Figure 4.2:   Crossover process.

Among other operators, *population size* and *selection operation* are considered to be the most important. DE usually employs fixed population size *NP* throughout the search process. Selection of the population size *NP* involves conflicting objectives. The population size should be as small as possible to achieve fast computational speed. However, too small may lead to premature convergence or stagnation. Figure 4.3 shows the typical computational flow of the Differential Evolution.
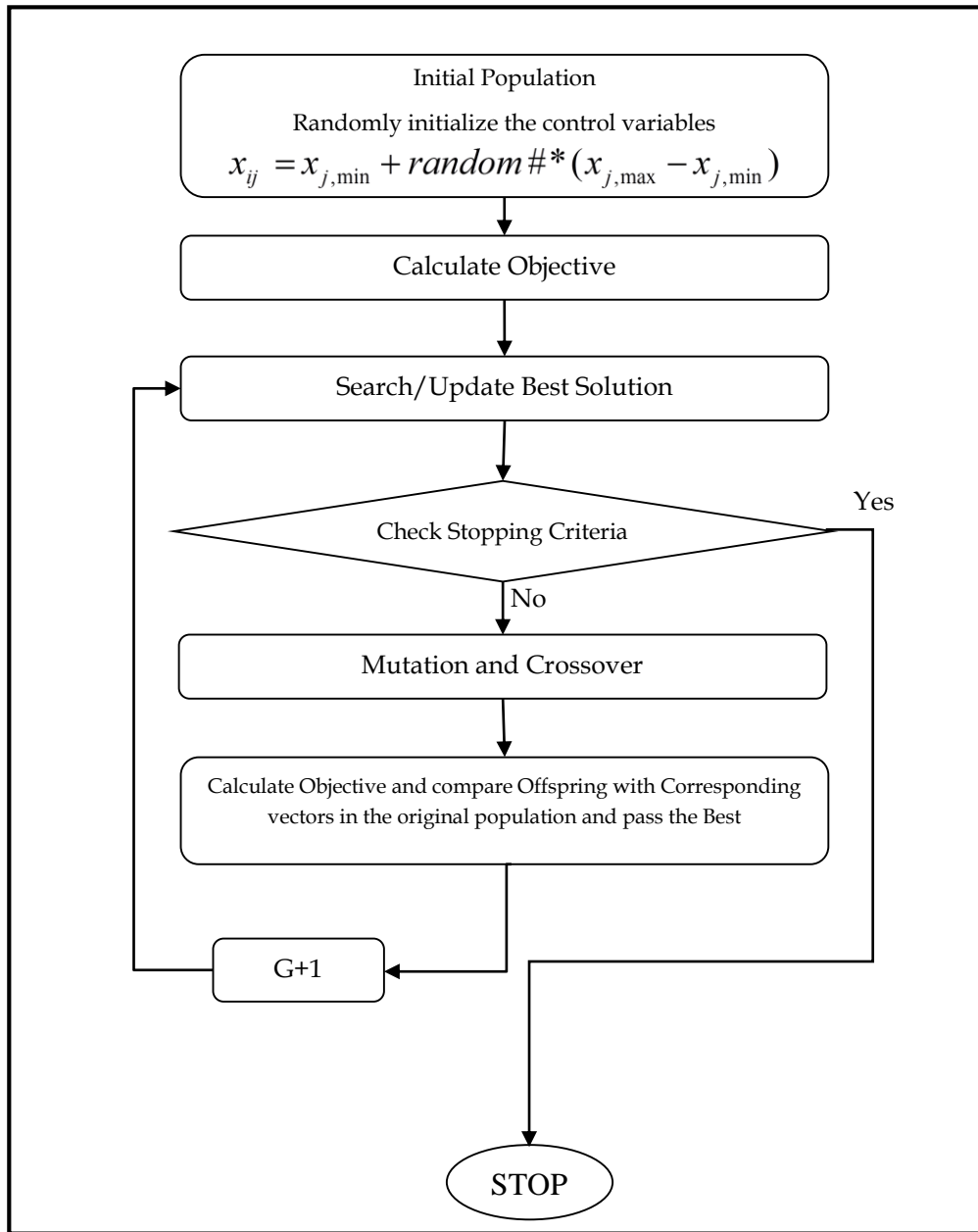
Figure 4.3: Typical DE Optimization Process

4.5   DE Application to Optimal STATCOM Placement Problem

A MATLAB program is developed to simulate a DE-based algorithm to solve the optimal STATCOM placement problem formulated as described in section (4.3). The system under consideration is Western System Coordinating Council. (WSCC) Three Machine Nine Bus System given in Figure 4.4.
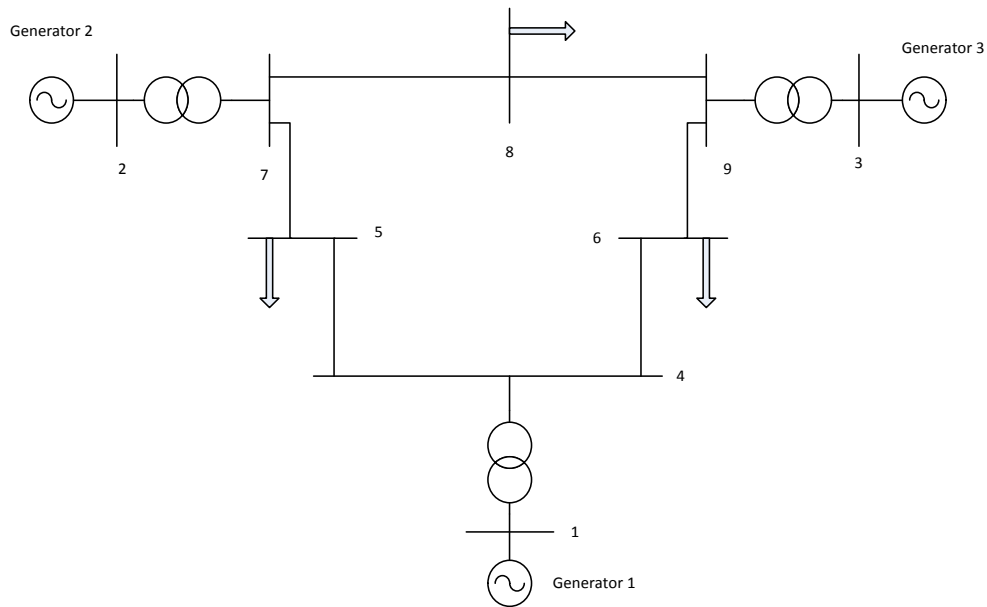
Figure 4.4:   WSCC 3 Machine 9 Bus Test System.

As per section (4.4), for each STATCOM in the system, there are two control parameters, one is the location or bus number at which STATCOM need to be placed and other is the STATCOM size or rating. Before the optimization, a priority list of all the possible faults in the system is created, to determine the faults that have the lowest critical clearing time and make the system instable. A group of top faults is created and is named as *critical fault group*. The priority list of the faults cleared by subsequent isolation of the lines, for WSCC 3 Machine 9 Bus Test System is given in Table 4.1

TABLE 4.1:   PRIORITY LIST OF FAULTS FOR WSCC 3 MACHINE 9 BUS TEST SYSTEM.

Faulted Bus	Line tripped	Critical Clearing Time (CCT) (sec)
7	5-7	0.1620
7	7-8	0.1813
9	6-9	0.2142
9	8-9	0.2350
8	7-8	0.2579
4	4-5	0.3004
8	8-9	0.3017
4	4-6	0.3098
5	5-7	0.3171
5	4-5	0.3573
6	6-9	0.3895
6	4-6	0.4494

As it can be seen in Table 4.1, fault on bus number 7 is the worst with reference to the critical clearing time. For the purpose of demonstrating the said formulation top four faults are selected as *critical fault group* for optimization. To treat each of the fault fairly an average clearing time for faults is used in optimization. Also as a worst case scenario it is assumed that the STATCOM is working at full capacity prior to the fault application. Moreover to this the STATCOM only works in reactive power injection mode.

As the primary purpose of FACTS is not the improvement of stability, therefore the number of STATCOMs in the system for this purpose are limited. For a small system such as the WSCC 3 Machine 9 Bus System one or two STATCOMs are sufficient depending on the primary requirements (minimization of losses or voltage support). In this study it is assumed that the maximum allowable number of STATCOM in the system

is two. First only one STATCOM is allowed and is optimally placed and test are carried out to see the effect of placement, if the placement is able to achieve global improvement in transient stability then it is declared optimal, otherwise the number of STATCOMs are increased by 1 and optimization is carried out again. Figure 4.5 shows the complete computational flow of DE for Optimal STATCOM Placement.

At first, only one STATCOM is allowed to be placed in the system. Table 4.2 shows the location and size of the STATCOM obtained after optimization. Table 4.3 shows the effect of STATCOM on CCT of all the possible faults in the system.

TABLE 4.2: OPTIMAL STATCOM LOCATION AND SIZE

No of STATCOM	Mutation Factor (F)	Crossover Ratio (CR)	Location	Size (MVA)
1	0.8	0.4	9	76.15

As it is evident from Table 4.3, the placement is able to improve the CCT for most of the faults except fault at bus 9 and bus 6 cleared by line 6-9 and 4-6 isolation respectively. As the aim of our placement is to improve the global transient performance of the system, therefore this placement is regarded as infeasible.
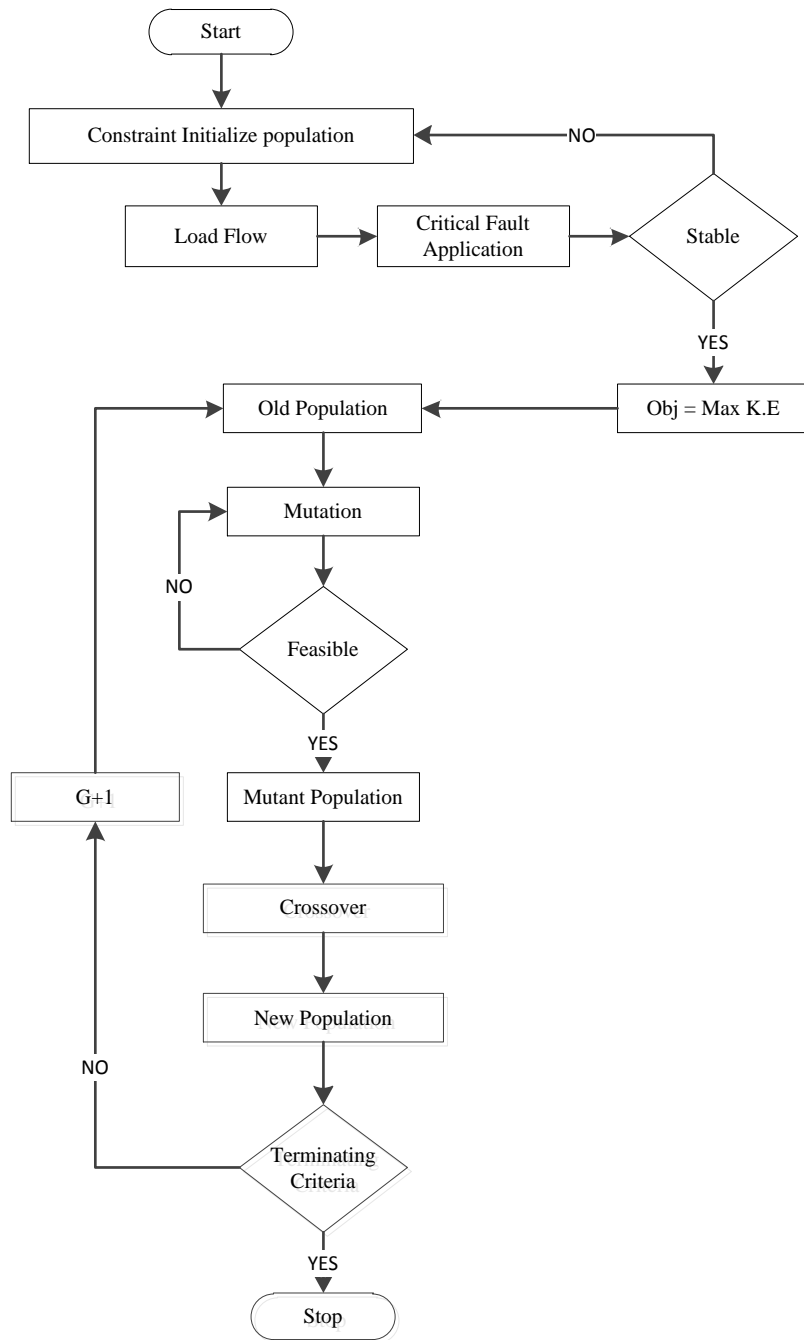
Figure 4.5:　　DE for Optimal STATCOM Placement.

72

TABLE 4.3:   EFFECT OF STATCOM PLACEMENT ON WSCC 3 MACHINE 9 BUS SYSTEM

Faulted Bus	Line tripped	Critical Clearing Time (CCT) (sec) without STATCOM	Critical Clearing Time (CCT) (sec) with STATCOM	Percentage Improvement (%)
7	5-7	0.1620	0.1742	7.53
7	7-8	0.1813	0.1743	-3.86
9	6-9	0.2142	0.2193	2.38
9	8-9	0.2350	0.2452	4.34
8	7-8	0.2579	0.2602	0.89
8	8-9	0.3017	0.2980	-1.22
4	4-5	0.3004	0.3030	0.86
4	4-6	0.3098	0.3160	2.00
5	5-7	0.3171	0.3400	7.22
5	4-5	0.3573	0.3810	6.63
6	6-9	0.3895	0.3925	0.77
6	4-6	0.4494	0.4499	0.11

The optimization is carried out again but with increased number of STATCOMs in the system Table 4.4 summarizes the simulation results obtained for WSCC 3 machine 9 bus test system. Three different values of mutation factor or probability F, namely 0.9, 0.8 and 0.7 are considered. For each value of F, the crossover constant CR is varied from 0.4 to 0.9 with an increment of 0.1. The population size is fixed throughout the search process and it is selected as 100. Table 4.4 also incorporates the location and size of STATCOMs for each combination of *F* and *CR* values. It can be seen that for WSCC 3 machine 9 bus test system, the location of the two STATCOMs is similar for different combination of *F* and *CR*. Figure 4.6-Figure 4.8 depicts the convergence curves for different values of *F* and *CR*. At first instance the curves seems to converge at different

points but the difference is in the order of 10^{-4}. It can also be seen that the combination $F = 0.7$ and $CR = 0.7$ produces the best result i.e. 0.9829 p.u., within 100 generations. Finally Table 4.5 shows the effect of STATCOM placement on the CCTs of all the possible faults for WSCC 3 machine 9 bus test system. This placement is able to improve the global transient performance of the system hence it is declared as optimum number of STATCOMs required to improve the global transient stability of the system.

TABLE 4.4:   OPTIMAL STATCOM LOCATION AND SIZE

F	CR	Optimum			
		Location (Bus no.)	Size/Rating(MVA)	Location (Bus no.)	Size/Rating(MVA)
0.7	0.4	6	75.6	7	69.05
0.7	0.5	6	75.33	7	69.11
0.7	0.6	6	76.43	7	68.09
0.7	0.7	6	75.85	7	68.25
0.7	0.8	6	76.11	7	69.6
0.7	0.9	6	75.76	7	68.27
0.8	0.4	6	75.36	7	68.87
0.8	0.5	6	75.03	7	69.45
0.8	0.6	6	76.27	7	69.56
0.8	0.7	6	76.41	7	68.62
0.8	0.8	6	75.87	7	68.94
0.8	0.9	6	76.38	7	68.23
0.9	0.4	6	76.24	7	69.28
0.9	0.5	6	75.31	7	69.32
0.9	0.6	6	76.02	7	68.36
0.9	0.7	6	76.12	7	68.96
0.9	0.8	6	76.4	7	68.44
0.9	0.9	6	76.23	7	68.19
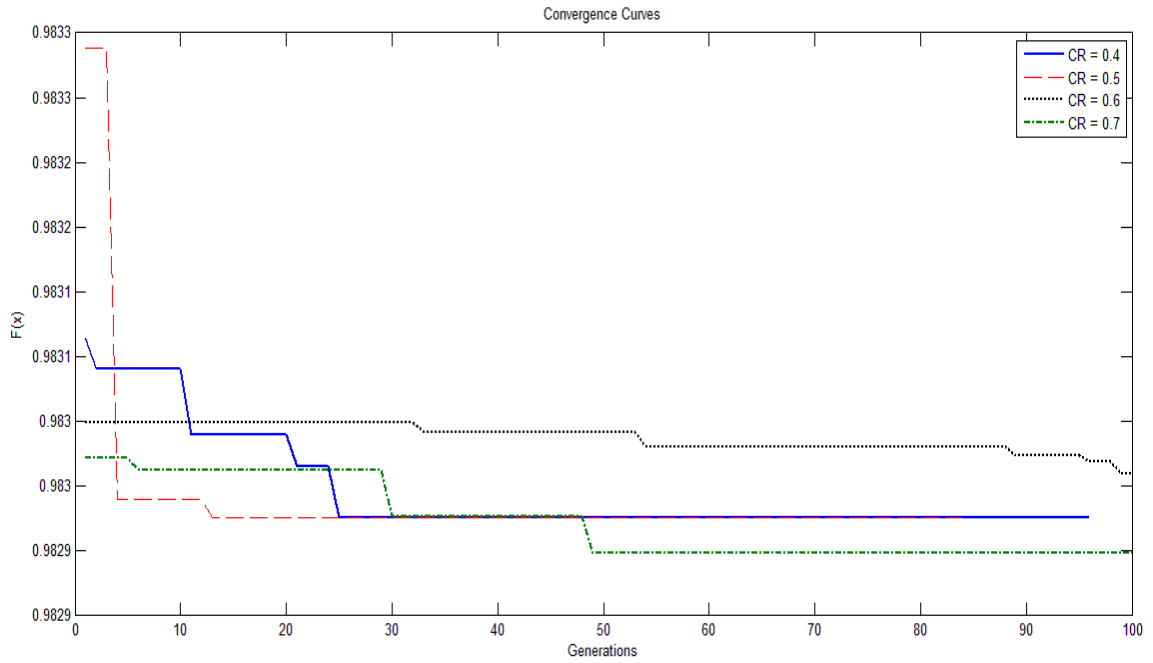
Figure 4.6:   Convergence curves for *F* = 0.7 with different values of *CR*.
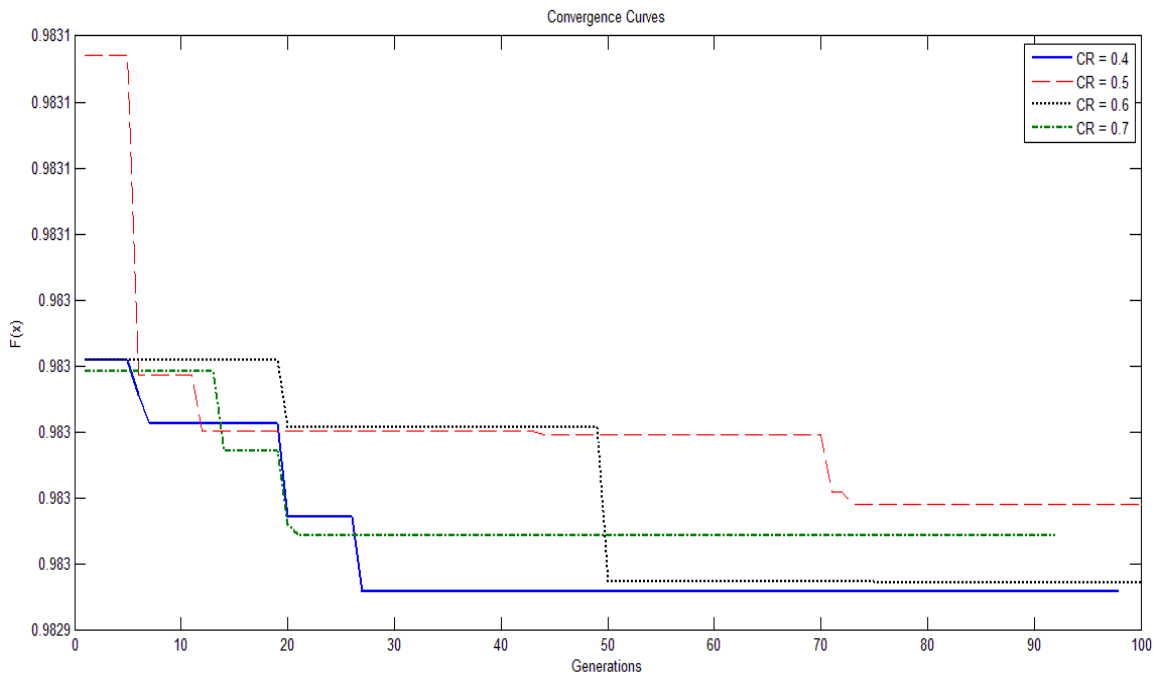
Figure 4.7:   Convergence curves for *F* = 0.8 with different values of *CR*.

76
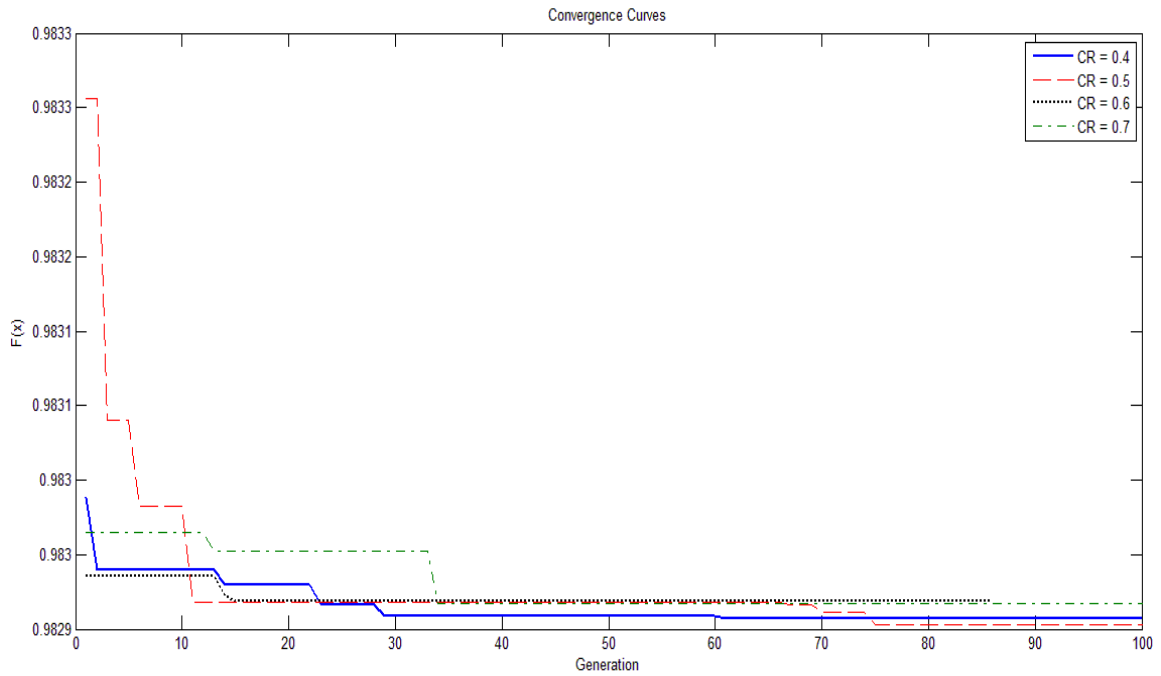
Figure 4.8:   Convergence curves for *F* = 0.8 with different values of *CR*.

TABLE 4.5:   EFFECT OF STATCOM PLACEMENT ON WSCC 3 MACHINE 9 BUS SYSTEM

Faulted Bus	*Line tripped*	*Critical Clearing Time (CCT) (sec) without STATCOM*	*Critical Clearing Time (CCT) (sec) with 2 STATCOM*	*Percentage Improvement (%)*
7	5-7	0.1620	0.1818	12.22
7	7-8	0.1813	0.1953	7.72
9	6-9	0.2142	0.2233	4.24
9	8-9	0.2350	0.2390	1.70
8	7-8	0.2579	0.2730	5.85
8	8-9	0.3017	0.3109	3.04
4	4-5	0.3004	0.3090	2.86
4	4-6	0.3098	0.3226	4.13
5	5-7	0.3171	0.3420	7.85
5	4-5	0.3573	0.3630	1.59
6	6-9	0.3895	0.3905	0.25
6	4-6	0.4494	0.4553	1.31

77

4.6 Dynamic Performance Evaluation

During the placement of the STATCOMs it was considered as a worst case scenario that the STATCOM placed in the system is loaded up to its full capacity prior to the occurrence of the fault. To worsen the scenario no dynamics (controllers) were considered during or after the fault. In order to simulate the dynamics involved and to see the reasonable effect of STATCOM placement in the system, STATCOM dynamics are also considered in this section. The simulations considering the dynamics of the system and STATCOMs are carried out on SIMULINK® module of MATLAB. Few details of the modelling of STATCOM is provided in the following subsections.

4.6.1 STATCOM Modelling

The Static Synchronous Compensator (STATCOM) is a shunt device of the Flexible AC Transmission Systems (FACTS) family using power electronics to control power flow and improve transient stability on power grids [106]. The STATCOM regulates voltage at its terminal by controlling the amount of reactive power injected into or absorbed from the power system. When system voltage is low, the STATCOM generates reactive power (STATCOM capacitive). When system voltage is high, it absorbs reactive power (STATCOM inductive).

The variation of reactive power is performed by means of a Voltage-Sourced Converter (VSC) connected on the secondary side of a coupling transformer. The VSC uses forced-commutated power electronic devices (GTOs, IGBTs or IGCTs) to synthesize a voltage V_S from a DC voltage source. The principle of operation of the STATCOM is explained on the Figure 4.9 showing the active and reactive power transfer

between a source V_m and a source V_S. In this Figure 4.9, V_m represents the system

voltage to be controlled and V_S is the voltage generated by the VSC.
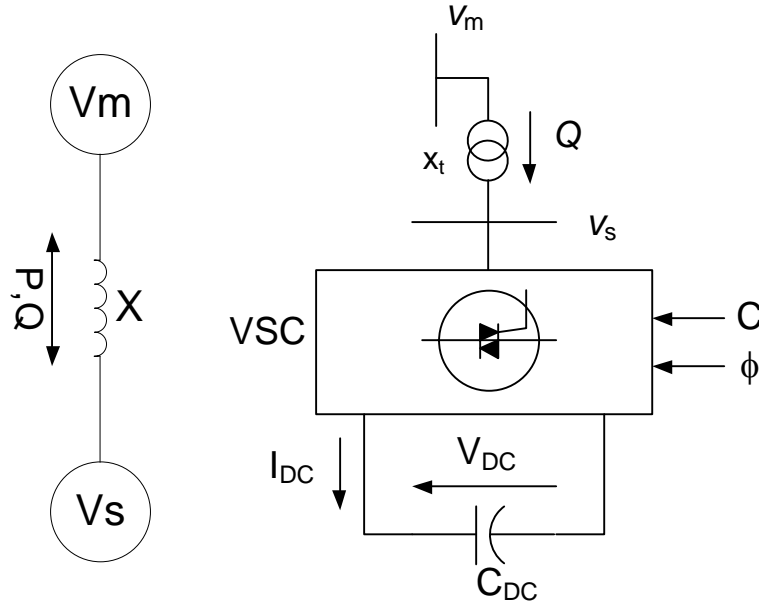
Figure 4.9:   Operating Principle of STATCOM.

$$P = \frac{V_m * V_s}{X} * Sin\delta \qquad (4.13)$$

$$Q = \frac{V_m(V_m - V_s Cos\delta)}{X} \qquad (4.14)$$

where,

V_m :   Line to line voltage of source *m*

V_S :   Line to line voltage of VSC

δ :   Phase Angle of voltages

X :   Reactance of interconnecting transformers and filters.

Although the STATCOM has the capability of interchanging real power as well with

reactive power but this capability is limited. Therefore, in steady state operation, the

voltage V_S generated by the VSC is in phase with V_m ($\delta=0$), so that only reactive power is flowing (P=0). If V_S is lower than V_m, reactive power is flowing from V_m to V_S (STATCOM is absorbing reactive power). On the reverse, if V_S is higher than V_m, reactive power is flowing from V_S to V_m (STATCOM is generating reactive power). The amount of reactive power is given by

$$Q = \frac{V_m(V_m - V_s)}{X} \qquad (4.15)$$

A capacitor connected on the DC side of the VSC acts as a DC voltage source. In steady state the voltage V_S has to be phase shifted slightly behind V_m in order to compensate for transformer and VSC losses and to keep the capacitor charged.

In this study, an IGBT - based STATCOM (fixed DC voltage) is modelled, no power electronics details e.g. switching inertia and delays, are incorporated as the aim of this study is to perform transient analysis of STATCOM and power system.
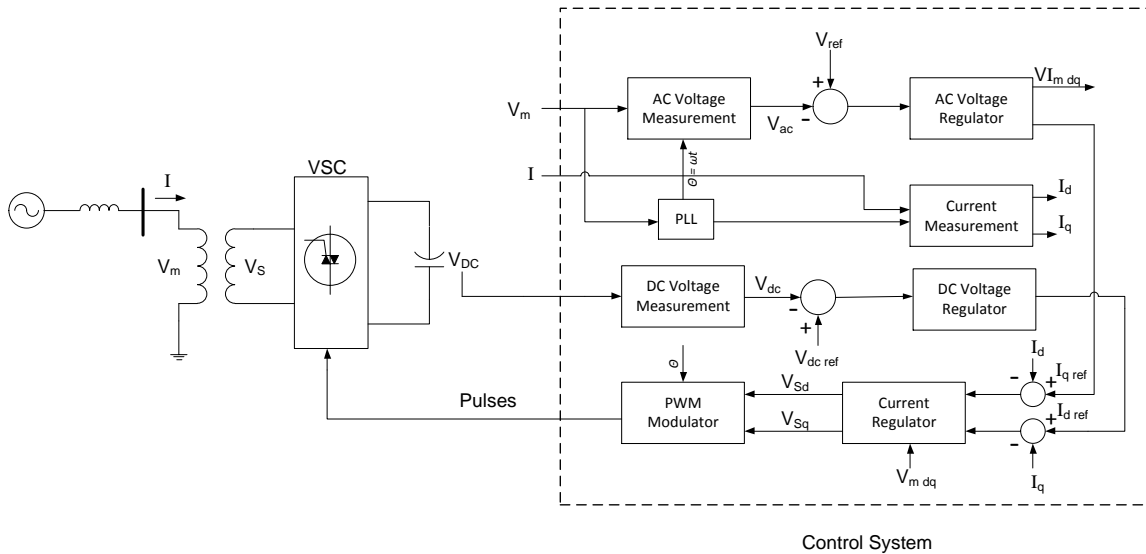

Figure 4.10:   Single line diagram of a STATCOM and its Control System Block Diagram

Figure 4.10 shows a single-line diagram of the STATCOM and a simplified block diagram of its control system. The control system consist of:

- A phase-locked loop (PLL) which synchronizes on the positive-sequence component of the three-phase primary voltage V_m. The output of the PLL (angle $\Theta=\omega t$) is used to compute the direct-axis and quadrature-axis components of the AC three-phase voltage and currents (labeled as V_{md}, V_{mq} or I_{md}, I_{mq} on the Figure 4.10).

- Measurement systems measuring the d and q components of AC positive sequence voltage and currents to be controlled as well as the DC voltage V_{dc}.

- An outer regulation loop consisting of an AC voltage regulator and a DC voltage regulator. The output of the AC voltage regulator is the reference current I_{qref} for the current regulator (I_q = current in quadrature with voltage which controls reactive power flow). The output of the DC voltage regulator is the reference current I_{dref} for the current regulator (I_d = current in phase with voltage which controls active power flow).

- An inner current regulation loop consisting of a current regulator. The current regulator controls the magnitude and phase of the voltage generated by the PWM converter (V_{sd} V_{sq}) from the I_{dref} and I_{qref} reference currents produced respectively by the DC voltage regulator and the AC voltage regulator (in voltage control mode). The current regulator is assisted by a feed forward type regulator which predicts the V_S voltage output (V_{Sd} V_{Sq}) from the V_m measurement (V_{md} and V_{mq}) and the transformer leakage reactance.

4.6.2 STATCOM V-I Characteristics

The STATCOM can be operated in two different modes:

- In voltage control mode (the voltage is regulated within limits).

- In VAR control mode (the STATCOM reactive power output is kept constant).

When the STATCOM is operated in voltage regulation mode, it implements the following V-I characteristics [106].

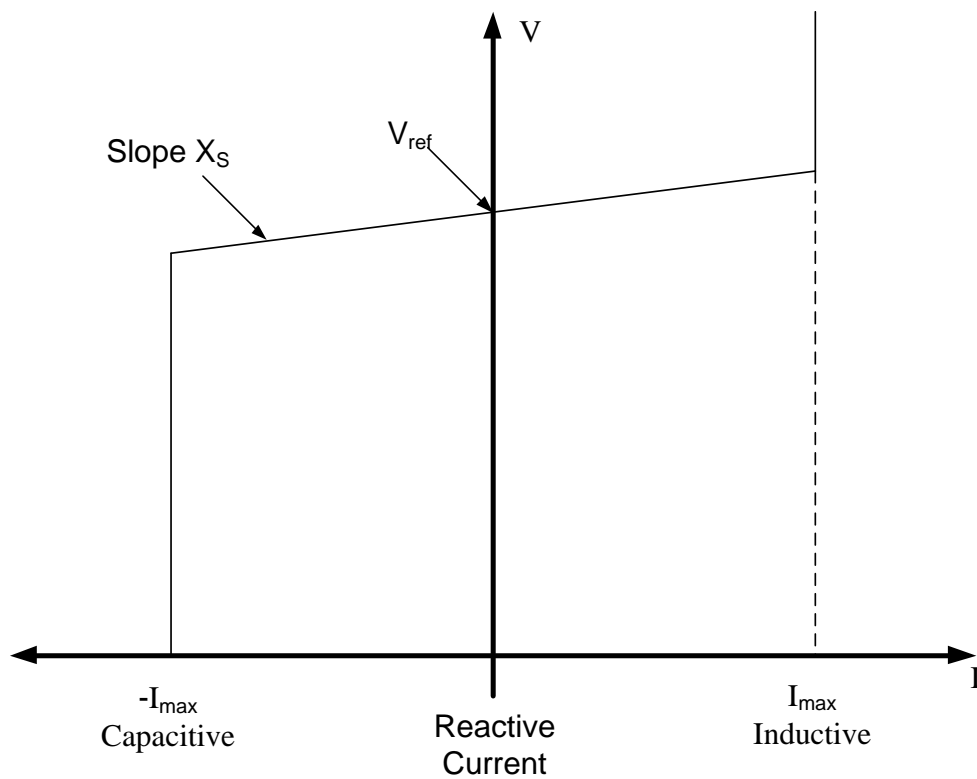Figure 4.11: STATCOM V-I Characteristics

As long as the reactive current stays within the minimum and minimum current values (-Imax, Imax) imposed by the converter rating, the voltage is regulated at the reference voltage V_{ref}. However, a voltage droop is normally used (usually between 1% and 4% at maximum reactive power output), and the V-I characteristic has the slope X_S indicated in

the Figure 4.11. In the voltage regulation mode, the V-I characteristic is described by the following equation:

$$V = V_{ref} + X_S I \qquad (4.16)$$

where,

V	:	Positive sequence voltage (p.u.)
I	:	Reactive current (p.u./Pnom). ($I > 0$ indicates an inductive current).
X_S	:	Slope or droop reactance (p.u./Pnom)
$Pnom$	:	Three-phase nominal power of the converter.

4.6.3 Simulation and Results

A WSCC 3 Machine 9 Bus Test System is implemented in SIMULINK®. Simplified synchronous machine models i.e. a constant voltage source behind a transient reactance, is used without models of governor or Automatic Voltage Regulator (AVR). Pi-models of the transmission lines and breaker are modelled as ideal switching devices. Two STATCOM are placed in the system with the modelling described in 4.6.1). The ratings and locations of the STATCOM are decided based on the best solution from the optimization i.e. $F = 0.7$ and $CR = 0.7$, which gives ratings as ±76.43 MVA and ±68.09 MVA for bus number 6 and 7 respectively, whereas the control parameters are arbitrarily selected, as the aim of this study is demonstrate the effect of the STATCOM in the system. Naturally, if the control parameters are optimized a better performance can be expected. Two faults that are fault on bus 7 with line 5-7 isolation and fault on bus 9 with line 6-9 isolation, are simulated in the system.

Arrangement is made such that prior to the fault the two STATCOMs are in floating state i.e. no power is exchanged between the system and two STATCOMs. Two different control strategies for controlling the STATCOMs are also evaluated based on the CCTs of the faults. Two fault cases are simulated in the system namely case A which is fault on bus 7 with line 5-7 cleared and case B which is fault on bus 9 with line 6-9 clearance. Table 4.6 summarizes the improvement of CCT in the presence of STATCOM in the system. It can easily be seen that the STATCOMs in voltage control mode has outperformed the STATCOMs in VAR control mode in both the cases.

TABLE 4.6:   CCT WITH DYNAMIC RESPONSE OF STATCOM

Case	CCT without STATCOM (sec)	CCT with STATCOM (sec)			
		Voltage Control mode	Improvement (%)	VAR Control mode	Improvement (%)
A	0.1834	0.2221	21.10	0.2157	17.6
B	0.2480	0.2718	9.59	0.2716	9.51

Figure 4.12 - Figure 4.25 shows the comparison of system without STATCOM and with STATCOM in terms of generator relative rotor angles, generator rotor angle in COI reference frame and voltages on bus 7 and 9 in each case. The fault applied in each case has a clearing time equal to that to CCT of fault without STATCOM. For each of the scenario under consideration it can be seen that for the system without STATCOM the first swing peak is much higher than the system with STATCOM optimally placed. It can also be seen that the first swing peak in each case when the STATCOM works in voltage control mode is lower than the first swing peak when the STATCOM operates in reactive

power control mode. Another advantage of operating the STATCOM in voltage control mode is increase in the damping as well as prevention of over voltages on the system.

Figure 4.12:   Generator 2 Relative Rotor Angle Response Comparison for Case A

Figure 4.13:   Generator 3 Relative Rotor Angle Response Comparison for Case A

Figure 4.14:   Generator 1 COI Reference Rotor Angle Response Comparison for Case A.

Figure 4.15:   Generator 2 COI Reference Rotor Angle Response Comparison for Case A.

Figure 4.16:   Generator 3 COI Reference Rotor Angle Response Comparison for Case A.

Figure 4.17:   Voltage Comparison at bus number 7 for Case A.

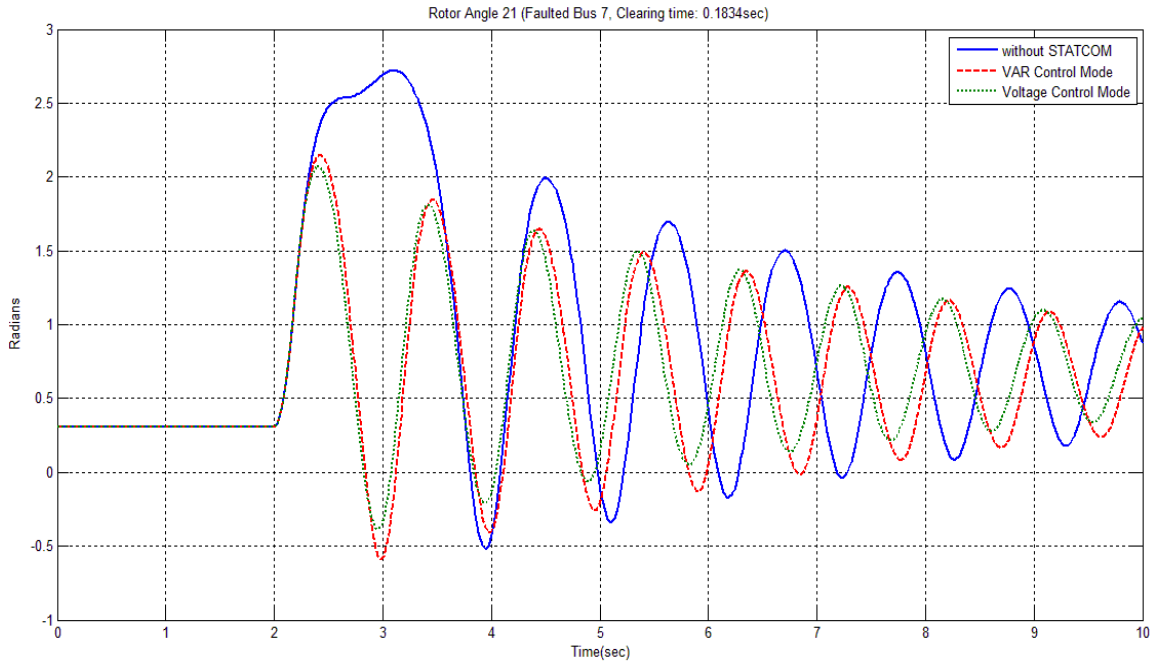Figure 4.18:   Voltage Comparison at bus number 9 for Case A.

Figure 4.19:   Generator 2 Relative Rotor Angle Response Comparison for Case B.
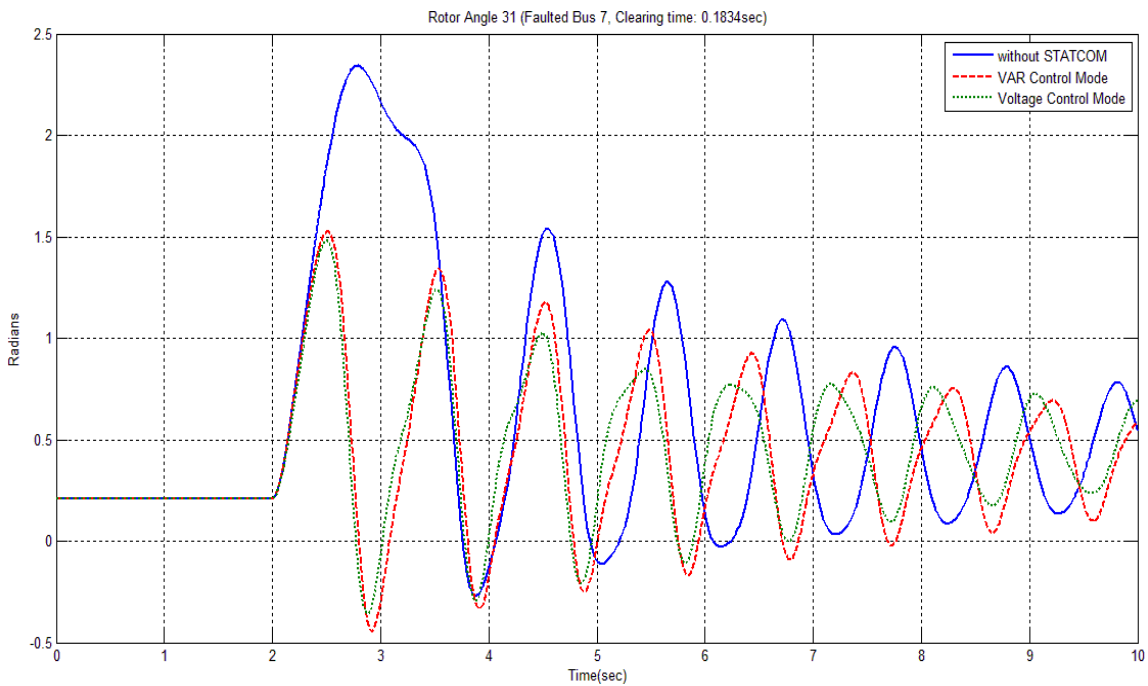
Figure 4.20:   Generator 3 Relative Rotor Angle Response Comparison for Case B.
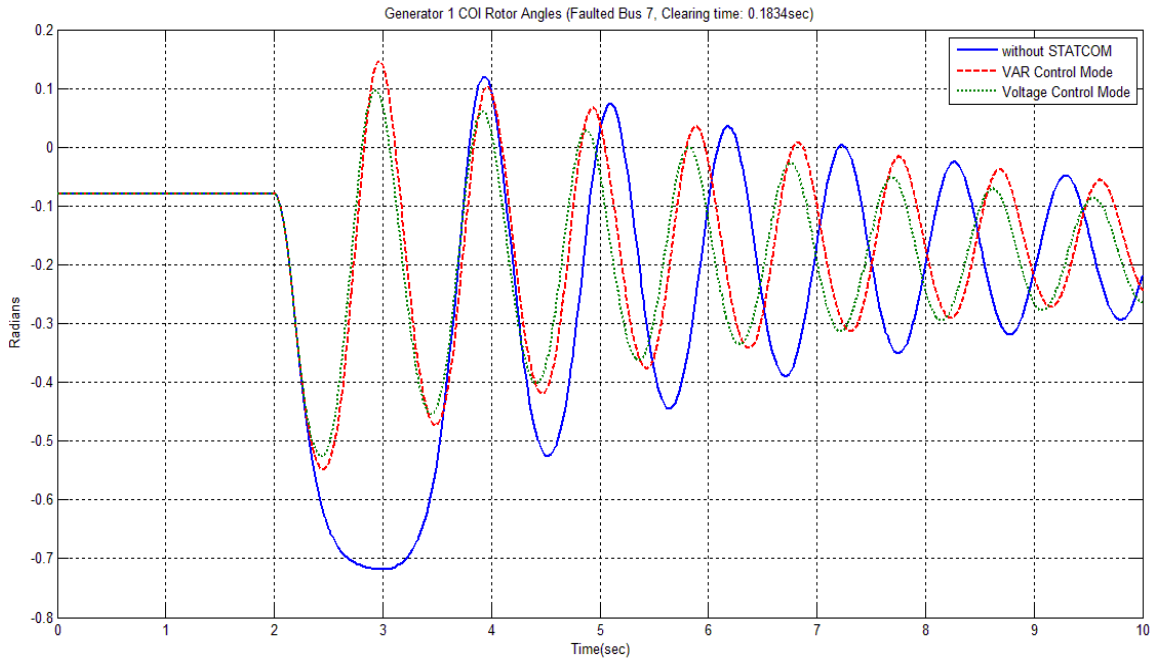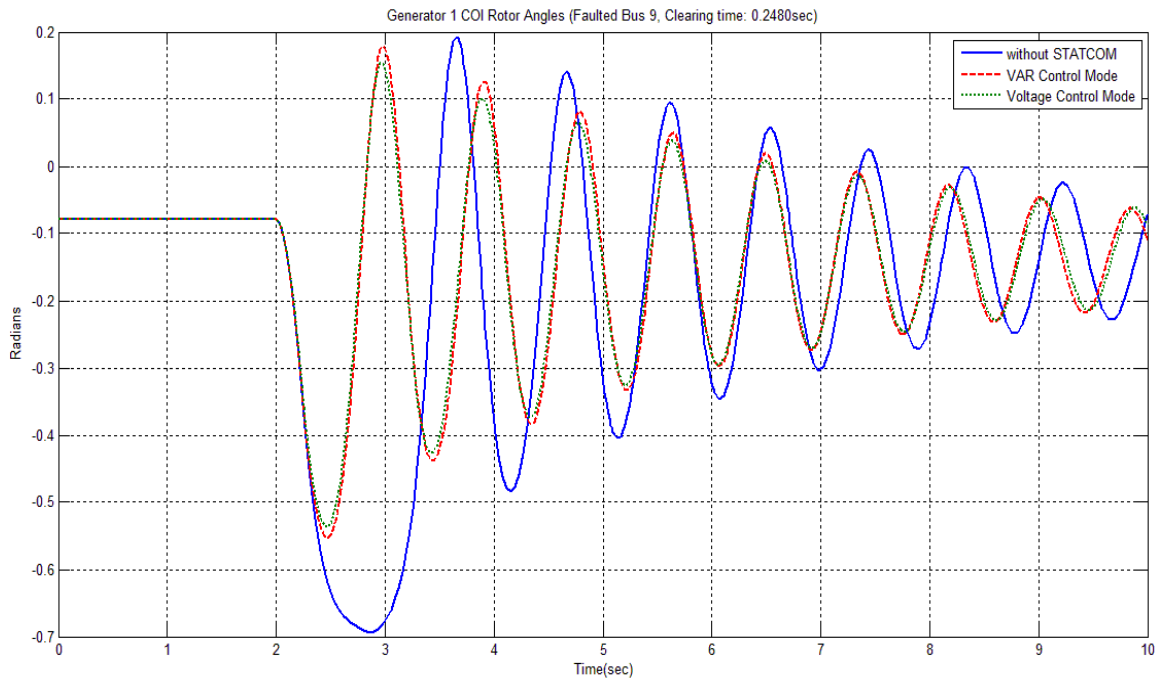

Figure 4.21:   Generator 1 COI Reference Rotor Angle Response Comparison for Case B.
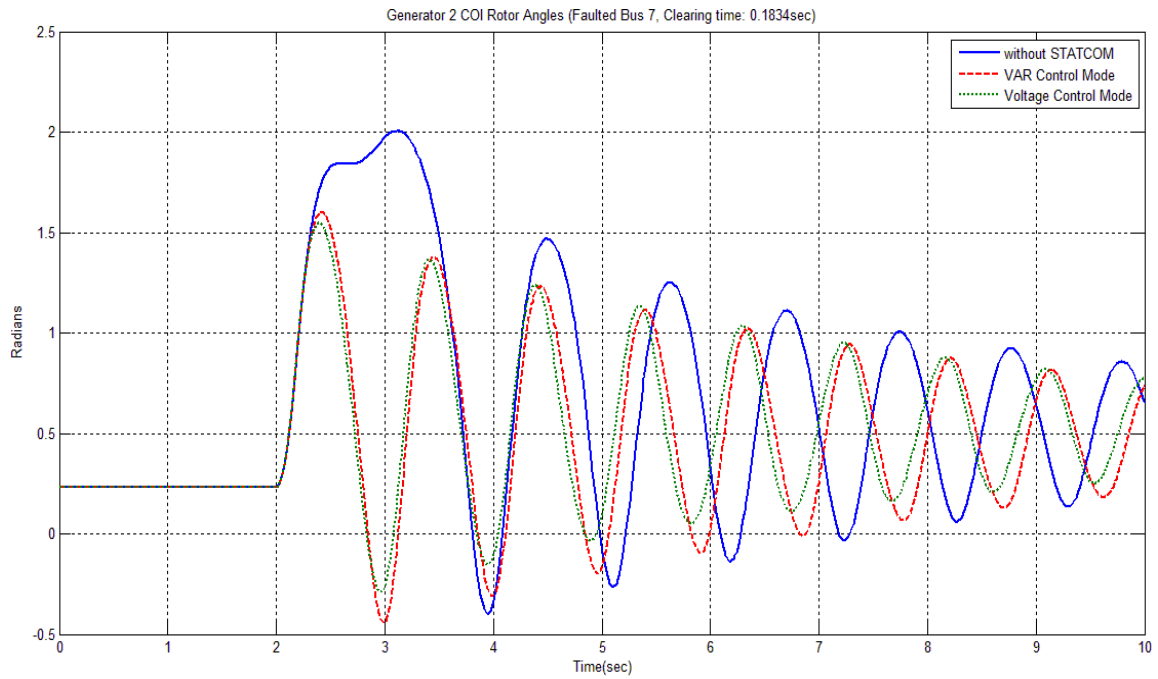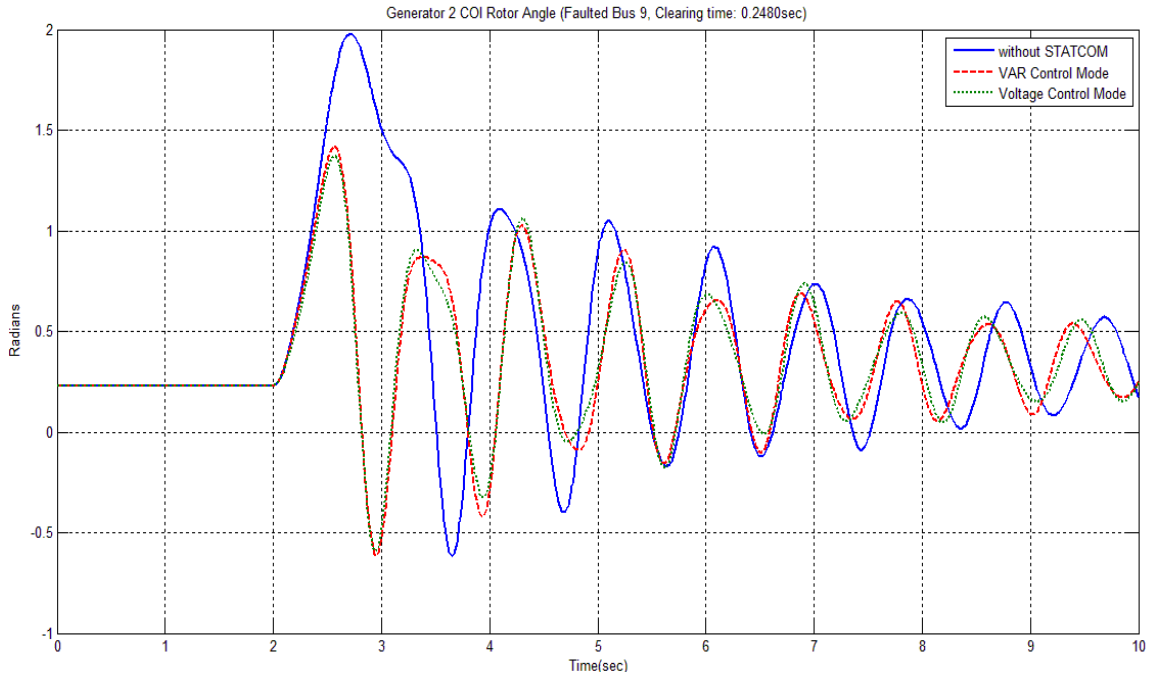
Figure 4.22:   Generator 2 COI Reference Rotor Angle Response Comparison for Case B.
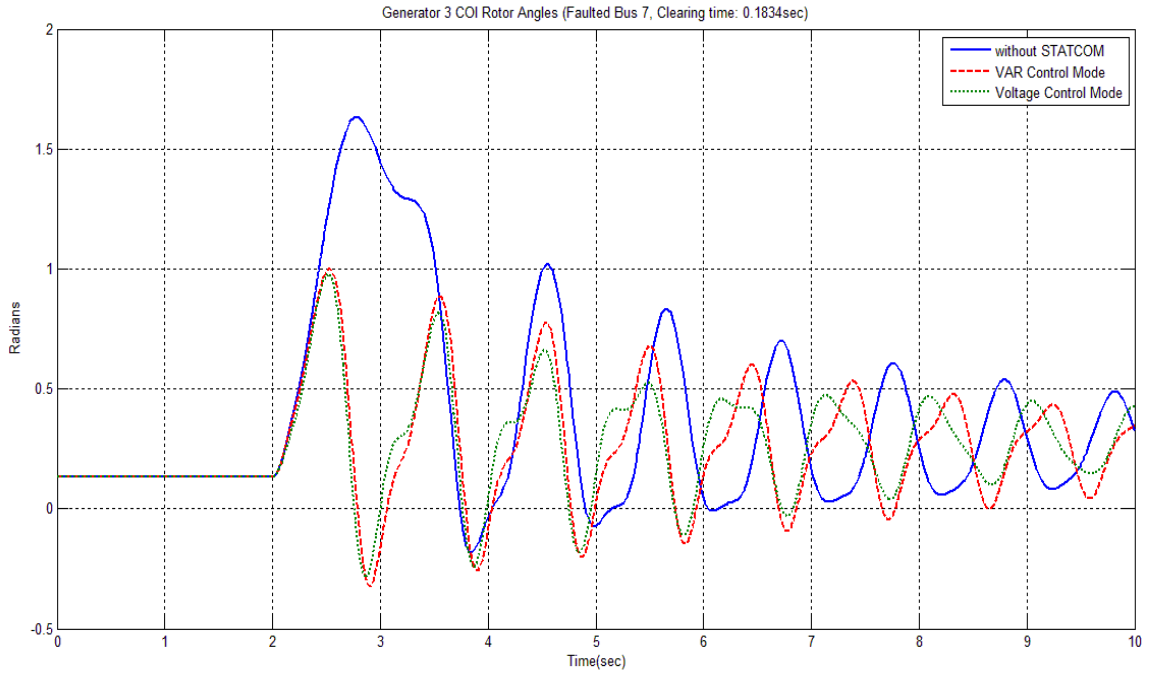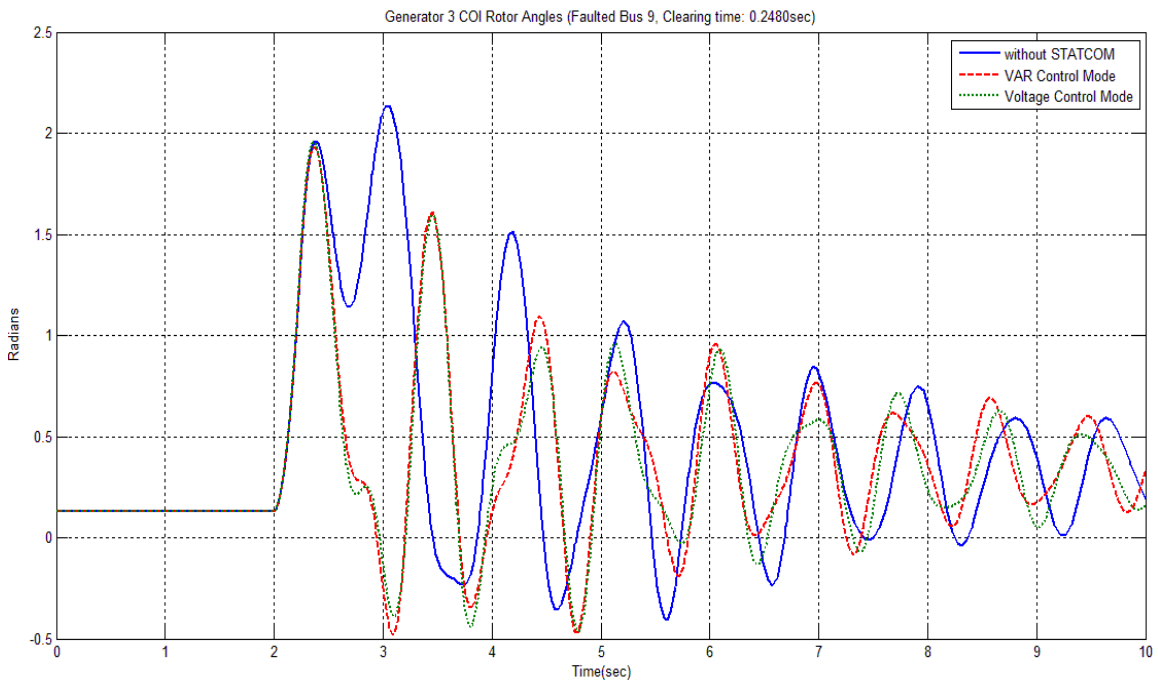

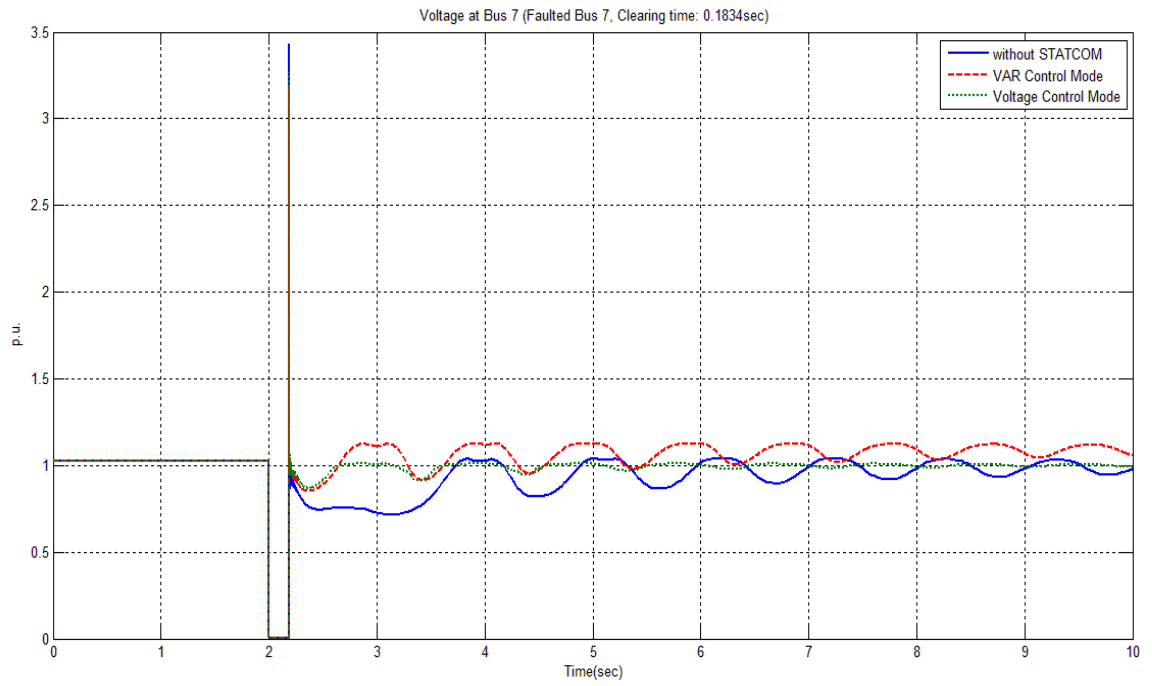Figure 4.23:   Generator 3 COI Reference Rotor Angle Response Comparison for Case B.

90
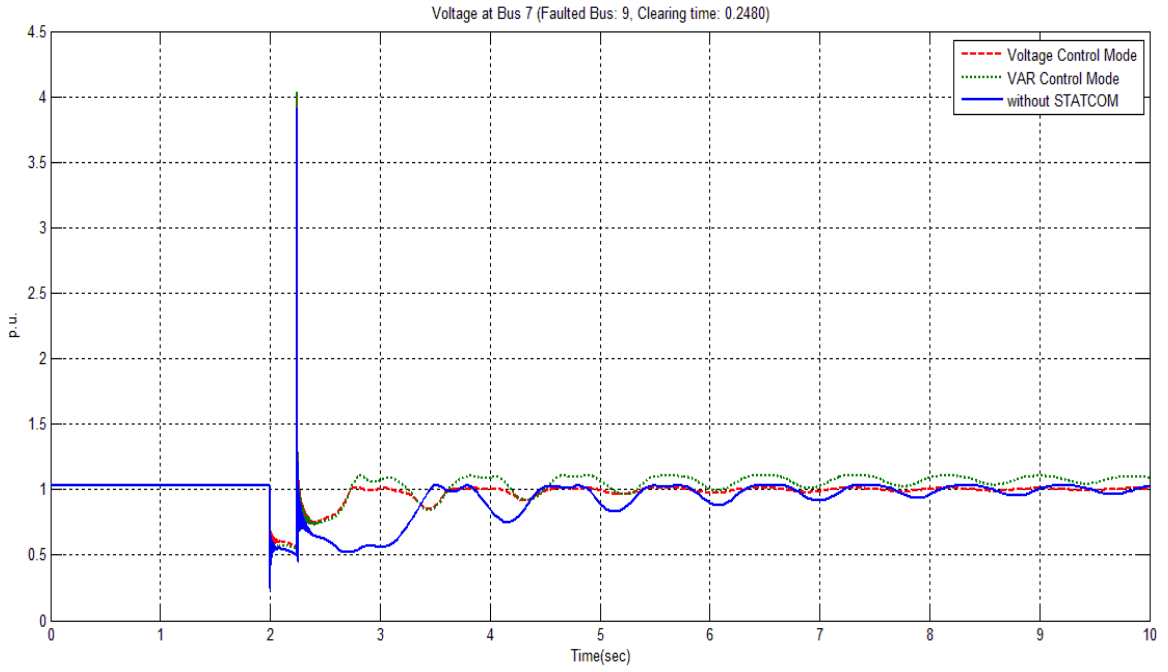
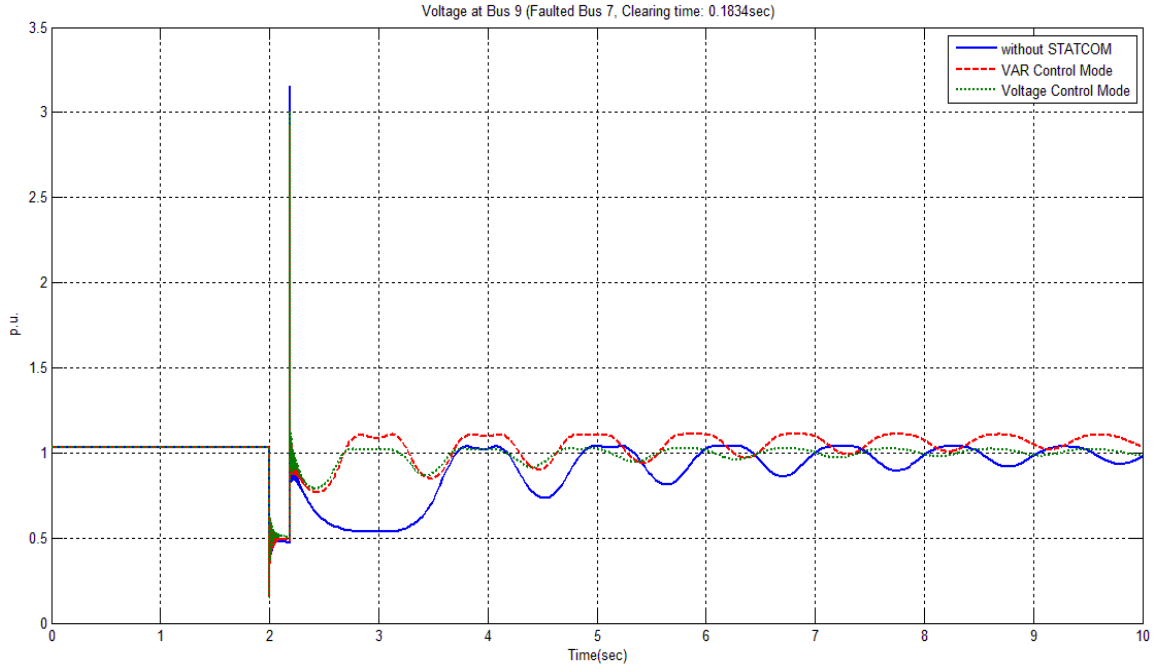Figure 4.24:   Voltage Comparison at bus number 7 for Case B.

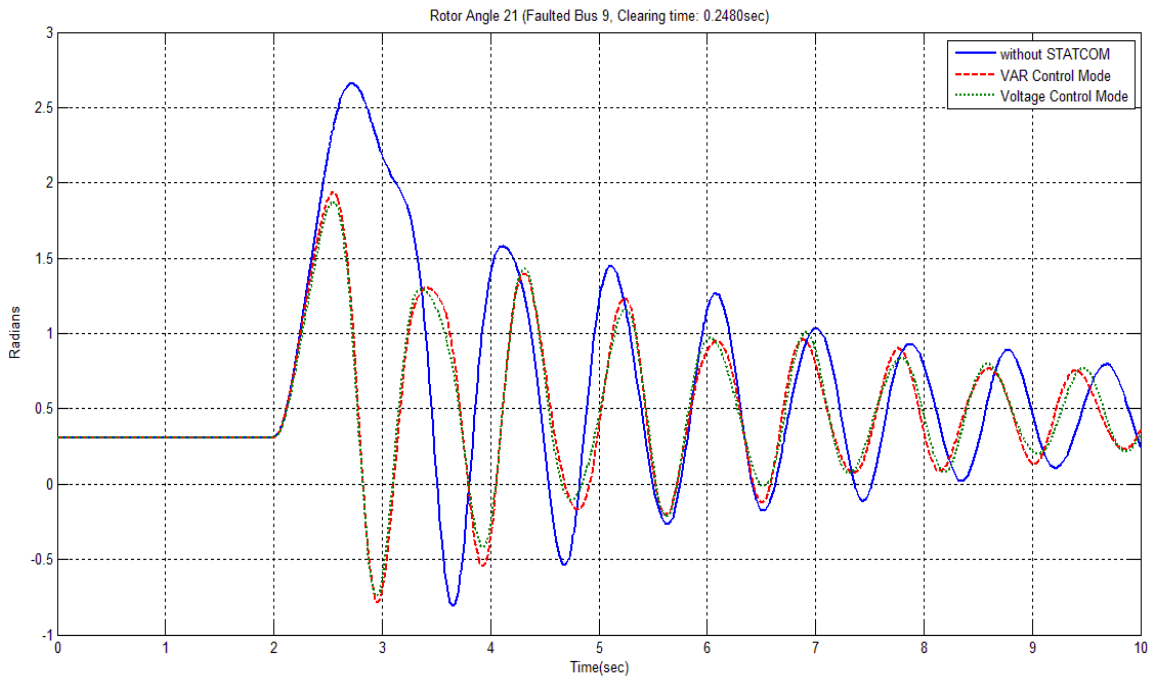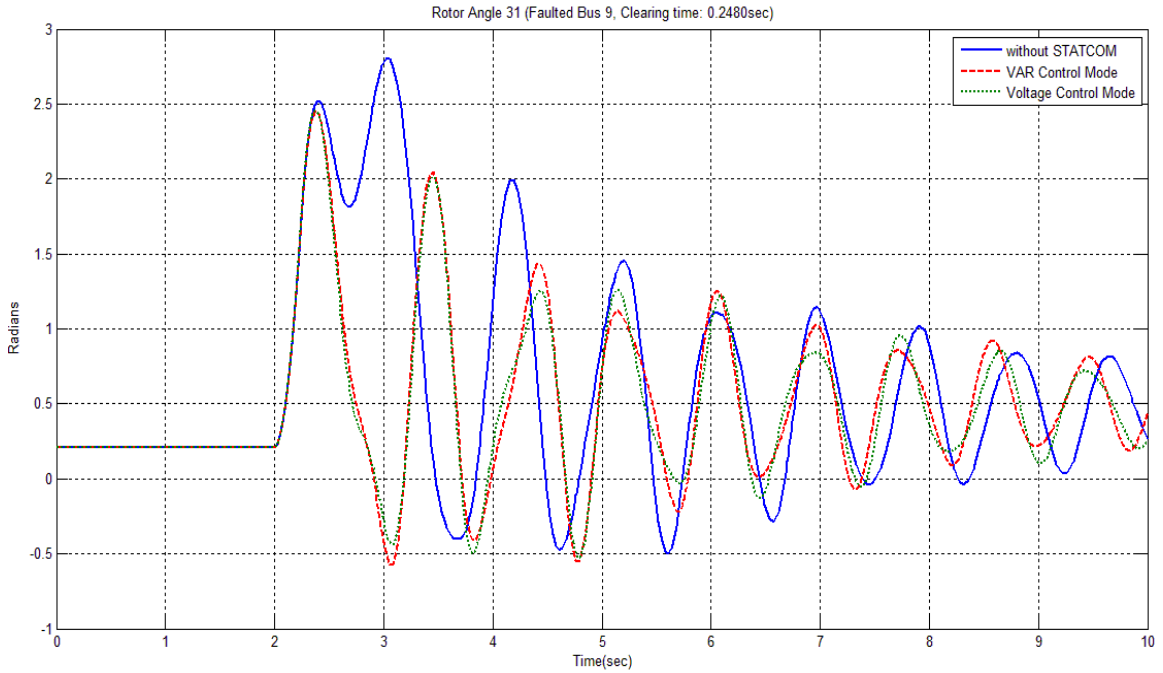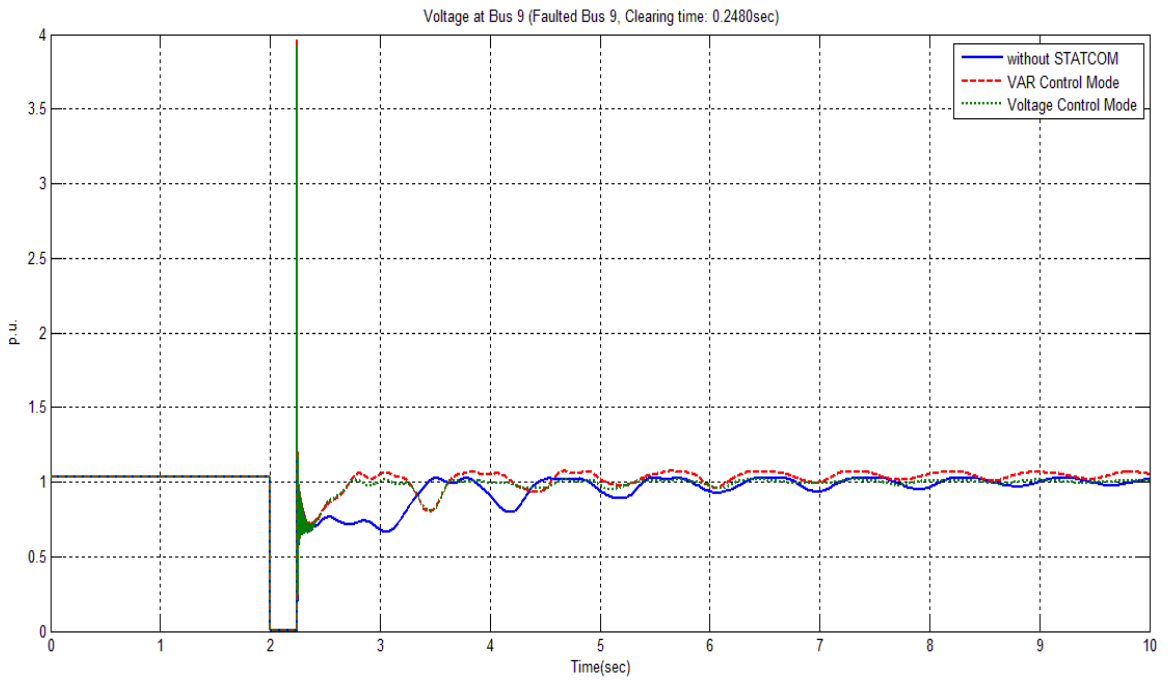Figure 4.25:   Voltage Comparison at bus number 9 for Case B.

CHAPTER 5

TRANSIENTLY STABLE OPTIMAL POWER FLOW

In order to improve the transient stability of the power system without extra investment on the infrastructure of the power system, researchers are continuously striving to achieve better transient performance of the system by altering the available control parameters of the system. This led to the formulation of Transient Stability Constrained Optimal Power Flow (TSC-OPF) [57],[58]. TSC-OPF merges the transient stability, which is a dynamic problem, with steady state economic and feasible operations of power system.

With inclusion of transient stability constraint the optimal power flow problem becomes more complex due to inherent high non linearity of the power system and results in higher cost naturally due to constraint addition. Unlike conventional OPF problem the constraint in TSC-OPF are differential as well as algebraic. After emergence of TSC-OPF on the scene as an effective countermeasure [63], a number of different variants, in order to effectively solve TSC-OPF, have been proposed in literature. In general they can be classified as *"traditional methods"* [2], [4]–[8], *"direct methods"* [67], [68], [127]–[130] and *"Evolutionary Algorithm (EA) based methods"* [131]–[134]. The philosophy behind

traditional method is conversion of differential constraints into algebraic one by fundamental functional transformation of swing equation, which allows the application of classical mathematical programming techniques for solving transformed optimal power flow problem. In *direct method* transient stability constraint is handled via direct stability assessment method e.g. SIngle Machine Equivalent (SIME) or Transient Energy function (TEF) method. This method employs rescheduling of generation to stabilize the system for contingency under consideration. Although traditional and direct methods helps in simplifying the TSC-OPF but suffer from poor numerical convergence, sub optimality, outsized inaccuracy due to number of approximation employed for simplification and heavy computation requirements. Whereas, EA based methods suffer from problem of inconsistency, due to which it mislays its chances of practical application.

This chapter aims to present a novel formulation for Optimal Power Flow (OPF) which improves the overall transient stability of the power system. To overcome the fore mentioned short comings of the techniques in the literature, this study formulates OPF as a true multi-objective optimization problem. One objective is to operate the system economically within the system's physical bounds, other being, to with stand severe contingencies. Strength Pareto Evolutionary Algorithm (SPEA) is employed for solving multi-objective optimization which overcomes the inconsistency and sub optimality problems, hybrid time domain simulation employed for handling transient stability problem which knocks out the numerical inaccuracies and convergence problem and to speed up the computation a hybrid stability classifier is employed.

5.1 Multi Objective Transiently Stable Optimal Power Flow Formulation

The transient stable optimal power flow problem requires to obtain optimal parameter settings for two conflicting objective functions, minimizing operating fuel cost and maximizing the system stability, without violating the system physical constraints. The problem is formulated as follows [135].

5.1.1 Minimization of Operating Cost

Quadratic cost curve modelling is used to represent the generators' operating cost, given as follows:

$$f_1 = \sum_{i=1}^{N_G} a_i + b_i P_{G_i} + c_i P_{G_i}^2 \tag{5.1}$$

where, N_G is the number of generators'; a_i , b_i and c_i are the cost coefficients of the ith generator; and P_{Gi} is the real power output of the ith generator. P_G is the real power outputs of the generators and defined as

$$P_G = [P_{G_1}, P_{G_2}, ..., P_{G_{N_G}}]^T \tag{5.2}$$

5.1.2 Maximization of Transient Stability Index

The estimation of power system capability to survive the stated contingencies by withstanding the succeeding transient events and attain a stable steady state operating condition is called Transient Stability Assessment [136]. Different techniques have been used to assess the transient stability of power system. In general these techniques can be classified into *numerical time domain simulation* (*TDS*), *direct assessment methods* or

transient energy function (*TEF*) *method* and *hybrid method*. The time domain simulation method lacks to quantify the stability of the system, an arbitrary value for relative rotor angle deviation is selected as a threshold based on the experience and trials. Different threshold values have been used in literature; e.g. 100 degrees [58], [60], [64], [65] and 180 degrees [67]. The threshold of 180 degrees has proven to be a logical and effective choice as any system is sure to loose synchronism if the rotor angle deviation reaches 180 degrees. The TEF methods, unlike time domain simulation can quantify the stability but suffers from convergence problem, limited modelling capability and high computation requirement. In order to overcome these problems a hybrid of TDS and TEF is used in this paper. The TEF method allows to quantify the stability of system effectively, whereas the TDS is utilized for fast classification of system's synchronism. Following describes the formulation for transient stability maximization and its handling procedure.

From the theory of energy functions [136],[22], in post contingency case if the system is unstable the *KE* of the system increases drastically as it is proportional to the square of machines' speed. Therefore, *KE* of the system at the point of fault clearance is an effective measure of system's stability. Now defining the objective function for transient stability improvement as minimizing the maximum of *KE* at fault clearance for the selected weakest faults in the system, given as

$$f_2 = \min(\max(KE_{cl})) \tag{5.3}$$

where

$$KE_{cl} = \frac{1}{2} \sum_{i=1}^{N_G} M_i \tilde{\omega}_{i_{cl}}^2 \tag{5.4}$$

where, $\tilde{\omega}_{icl}$ is the angular speed of ith machine at point of fault clearance.

In order to avoid extensive computation involved in PE calculation a synchronism status classifier "η" is associated with each of the generator for post fault period, given as

$$\eta_i = \frac{180 - |\theta_i|}{180 + |\theta_i|} \tag{5.5}$$

The value of η_i varies from -1 to 1. For a stable system $\eta_i \geq 0$ for $i = 1, \ldots, N_G$.

5.1.3 Constraints

1) *Generating Units Constraint:*

Each generating unit is limited by it generating capacity upper and lower bounds, given as

$$P_{G_i}^{\min} \leq P_{G_i} \leq P_{G_i}^{\max}, \quad i = 1, \ldots, N_G \tag{5.6}$$

$$Q_{G_i}^{\min} \leq Q_{G_i} \leq Q_{G_i}^{\max}, \quad i = 1, \ldots, N_G \tag{5.7}$$

2) *Power Balance Constraint:*

For a power system to operate satisfactorily the total generation must be enough to meet up the load demand and also cover the losses in the transmission line. Therefore,

$$\sum_{i=1}^{N_G} P_{G_i} - P_D - P_{loss} = 0 \tag{5.8}$$

Calculating P_{loss} requires solving the load flow problem which imposes following constraints.

$$P_{G_i} - P_{D_i} - V_i \sum_{j=1}^{NB} V_j [G_{ij} \cos(\delta_i - \delta_j) + B_{ij} \sin(\delta_i - \delta_j)] = 0 \tag{5.9}$$

$$Q_{G_i} - Q_{D_i} - V_i \sum_{j=1}^{NB} V_j [G_{ij} \sin(\delta_i - \delta_j) - B_{ij} \cos(\delta_i - \delta_j)] = 0 \qquad (5.10)$$

where, $i = 1,2, ..., NB$; NB is the number of buses; Q_G and P_G are the reactive and real power generation at bus i respectively. V_i and V_j are the voltages at bus i and j respectively; G_{ij} and B_{ij} are the transfer conductance and suseptance between bus i and j respectively; δ_i and δ_j are the voltage bus angles at bus i and j respectively. Solving (5.9) and (5.10), voltage magnitudes and angles can be found at each bus. Then the power loss in transmission network can be calculated as

$$P_{loss} = \sum_{k=1}^{N_L} g_k [V_i^2 + V_j^2 - 2V_i V_j \cos(\delta_i - \delta_j)] \qquad (5.11)$$

where N_L is the number of transmission lines in the network and g_k is the conductance of the kth line connecting bus i and j.

3)   *Security Constraint:*

To ensure secure operation each branch flow is limited by its upper limit as follows

$$S_{l_k} \le S_{l_k}^{\max}, \quad k = 1,..., N_L \qquad (5.12)$$

4)   *Voltage Constraint:*

Each of the bus voltage is constrained by its upper and lower limit for reliable operation of power system, given as

$$V_i^{\min} \le V_i \le V_i^{\max} \qquad (5.13)$$

97

Accumulating the constraints and objectives, the complete formulation for transient stable optimal power flow can be stated as

$$\text{Minimize} \quad [f_1(\boldsymbol{u}, \boldsymbol{x}), f_2(\boldsymbol{u}, \boldsymbol{x})] \tag{5.14}$$

$$\begin{aligned} \textit{subject to} \quad & g(\boldsymbol{u}, \boldsymbol{x}) = 0 \\ & h(\boldsymbol{u}, \boldsymbol{x}) \leq 0 \\ & \eta_{i_m} \geq 0 \end{aligned} \tag{5.15}$$

where $\boldsymbol{x}$ and $\boldsymbol{u}$ denotes the vector of dependent parameters on $\boldsymbol{u}$ and control parameters respectively, whereas η_{i_m} denotes the synchronism status of ith generator for mth contingency; g and h are the equality and inequality constraints respectively.

5.2 SPEA Implementation on Transient Stable Optimal Power Flow

5.2.1 Control Parameters

The control parameters selected in this study are the generators' active power except for the slack bus and the voltages at the voltage controlled buses and the slack bus in the system. Therefore, the set of control parameter can be given as follows

$$\boldsymbol{u}^T = [P_{G_2}, ..., P_{G_{N_G}}, V_{G_1}, ..., V_{G_{N_G}}] \tag{5.16}$$

where P_{G1} is the real power output of the slack generator which is a dependent parameter calculated from the load flow of the system.

5.2.2 Constrained Feasible Initialization

To avoid unnecessary computation, the control parameters are initialized randomly according to (5.17) with a uniform distribution within its given bounds to form the parent population for the first generation.

$$u_{i,j}^0 = Rand(u_j^{\min}, u_j^{\max}) \tag{5.17}$$

where $i \in \{1,2,\ldots,N_{pop}\}$, $j \in \{1,2,\ldots,N_{var}\}$; $u_{i,j}^0$ is the control parameter j in individual i at the first generation; N_{pop} is the population size and N_{var} is the number of control parameters in the system. Each individual in the initial population is checked for feasibility against each objective. First the load flow is conducted and parameters' bounds are checked, if feasible it is checked for transient stability objective, if solution is still feasible then it is included in the population otherwise it is discarded and a new solution is generated and checked for feasibility. This not only lightens the computational efforts as only load flow feasible solution goes under transient stability assessment and only feasible population is presented for crossover and mutation operators to produce new generation which speeds up the algorithm.

5.2.3 Transient Stability Objective Handling

The strategy employed in this study to improve the transient stability of the system, involves determination of priority list of faults according to their severeness. The severeness criteria being the critical clearing time (CCT) of the fault, which is the largest allowable fault clearing time after which the system loses stability. The lower the CCT of a fault higher is the priority. A group of most severe faults called critical fault group is selected, the number of faults in the group can vary according to the system and operator

requirements. Naturally, as the size of this group grows, the operating price will increase. During the optimization process, each of the load flow feasible individual goes under transient stability assessment, the selected faults in the group are applied one after another with an average fault clearing time of the faults under consideration and respective KEs are recorded at the point of fault clearance. For worst case each fault is cleared by tripping the subsequent line. The feasibility of the individual under consideration is checked according to (5.5) if feasible then the maximum of recorded KE is substituted as the objective function value otherwise the solution is discarded and a new solution is generated.

5.3   Performance Evaluation

The proposed SPEA based transient stable optimal power flow performance is evaluated in this section. The approach is applied on WSCC 3 machine 9 Bus system and New England 10 machine 39 bus system. As a worst case scenario the synchronous machine in each system is modelled using classical two state model whereas the loads are modelled as constant impedance type load. To solve the differential equation in transient stability assessment third order Runge-Kutta method with adaptive time step is applied. Transient stability time window is selected as 5 sec which is large enough to observe multiple swings of the system. For SPEA, the population size, the maximum size of Pareto set and the maximum number generations are selected as 100. The probabilities for crossover and mutation we selected as 0.8 and 0.01 respectively. All the simulations are performed on codes developed in MATLAB® environment running on an Intel® Core i7 2.00GHz CPU and 6GB RAM.

5.3.1 Simulation Results for WSCC 3 Machine 9 Bus Test System

Figure 4.4 shows the single line diagram of WSCC 3 machine 9 bus test system. The system data is taken from [137]. The fuel cost coefficients are available in [67]. The voltage upper and lower bounds are set as 0.95 and 1.05 p.u. respectively. Generator 1 is the chosen as the slack generator. Therefore, according to (5.16) there are 5 control parameters, being real power outputs of generator 2 and generator 3 and voltages at each of the generator buses.

As per the procedure stated in (5.2.3) the priority list for the 3 Machine 9 Bus system is given in Table 4.1. As a method to depict the effectiveness of the proposed algorithm the critical fault group consist of the top four faults in the priority list. The optimization is done for an average clearing time of faults under consideration i.e. 0.2 sec.

As stated earlier, the algorithm successfully achieves the desired objectives of finding the pareto front with preservance of diversity. The minimum cost solution comes out to be 1133$/h which is well in accordance with the literature [67], [133]. The pareto front is shown in Figure 5.1. Results extracted from Figure 5.1 are tabulated in Table 5.1. As discussed, the algorithm suggests three solutions; best compromise solution, solution for minimum cost and solution for minimum K.E. Unlike the algorithm presented in [133], the proposed approach covers the whole search space and the decision maker has freedom to choose from wide variety of solutions depending on the system conditions and requirements, rather than having only one solution to choose from.
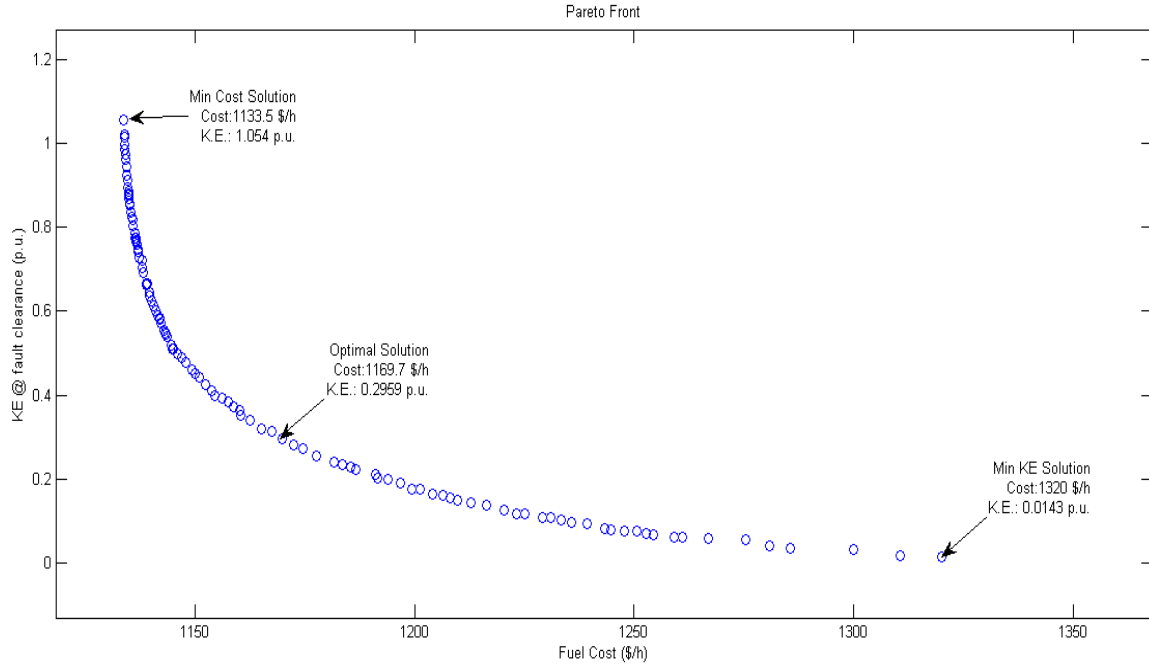
Figure 5.1:   Pareto-Front for WSCC 3 Machine 9 Bus Test System

TABLE 5.1:   PARETO SOLUTIONS FOR WSCC 3 MACHINE 9 BUS TEST SYSTEM

Parameters	Solution		
	Best Compromise	*Min. Cost*	*Min. K.E*
$P_{G_1}(MW)$	162.476	106.478	242.448
$P_{G_2}(MW)$	98.074	115.898	53.3127
$P_{G_3}(MW)$	57.617	96.228	24.351
$V_1(p.u.)$	0.9811	0.9951	0.9888
$V_2(p.u.)$	1.0101	0.9958	1.0021
$V_3(p.u.)$	1.026	1.0078	1.0189
$Cost\,(\$/\,h)$	1169.54	1133.59	1326.85
$K.E.(p.u.)$	0.2959	1.054	0.0143

TABLE 5.2: CCT COMPARISON FOR WSCC 3 MACHINE 9 BUS TEST SYSTEM

Faulted Bus	Line tripped	CCT(sec) for base case	CCT(sec) for Best compromise solution	CCT(sec) for Min. cost solution	CCT(sec) for Min. KE solution	CCT(sec) Reported in	
						[133]	[67]
7	5-7	0.1620	0.4080	0.2317	0.8246	0.3897	0.5556
7	7-8	0.1813	0.3932	0.2389	1.1265	0.4075	0.5244
9	6-9	0.2142	0.4044	0.2239	0.9755	0.2454	0.2184
9	8-9	0.2350	0.3579	0.2212	0.9810	0.2308	0.2111
Cost ($/h)		1132.30	1169.54	1133.59	1326.85	1140.06	1191.56

Improvement in transient stability of the system is shown in Table 5.2. For the case of best compromise solution, a balance between economics and stability is maintained by the proposed algorithm, the solution obtained improves the transient stability of the system with the best possible cost. Naturally, the cost in this case is higher than the base cost as the economy is sacrificed for transient stability enhancement. In case of minimum cost solution, more emphasis is given to economy of the system. This solution is unable to improve the overall transient stability of the system as shown in Table 5.2, for minimum cost case the CCT for the fault at bus 9 cleared by tripping line 8-9 the CCT comes out to be 0.2212 sec whereas it was 0.2350 sec for base case. The third solution that maximizes the transient stability of the system has the highest cost compared to all the solutions as more emphasis is laid on improving the transient

103

performance of the system. These kind of solutions can be extremely helpful in case of emergency scenarios. Table 5.2 also compares the proposed approach with the state of the art transient stability constrained OPF published in literature. The proposed approach is robust enough to improve the overall transient stability of the system unlike the algorithms presented in [67] and [133], which relies on improving the transient stability of one fault. Comparing the best compromise solution of proposed approach with reported results. Ref. [133] has employed DE for solving transient stability constrained optimal power flow for fault at bus 7 cleared by tripping line 5-7. The CCT for this particular fault is greatly enhanced as compared to the base case but the rescheduling has deteriorated the CCT of fault at bus 9 cleared by line 8-9 tripping. It is worth mentioning that the base case referred here is original system settings without any optimization applied. The cost of the proposed approach is higher as compared to [133] as the aim of approach presented in this study is to improve the overall transient performance of the system rather than for a single fault. Similarly, in [67] a trajectory sensitivity approach is applied to reschedule the generators for fault at bus 7 cleared by line 5-7, this approach also improves the CCT for the fault under consideration but has depreciated the CCT from the base case of fault at bus 9 cleared by tripping line 8-9 proving the solution presented is suboptimal.

To illustrate the effectiveness of the proposed approach a comparison has been made with state of the art methods in the field of TSCOPF. To make a fair and logical comparison, the SPEA optimization routine is executed again with fault at bus 7 with line 5-7 clearance as a critical fault and fault at bus 9 with 6-9 clearance as a critical faults for case A and B respectively. The pareto fronts resulted from optimization are shown in
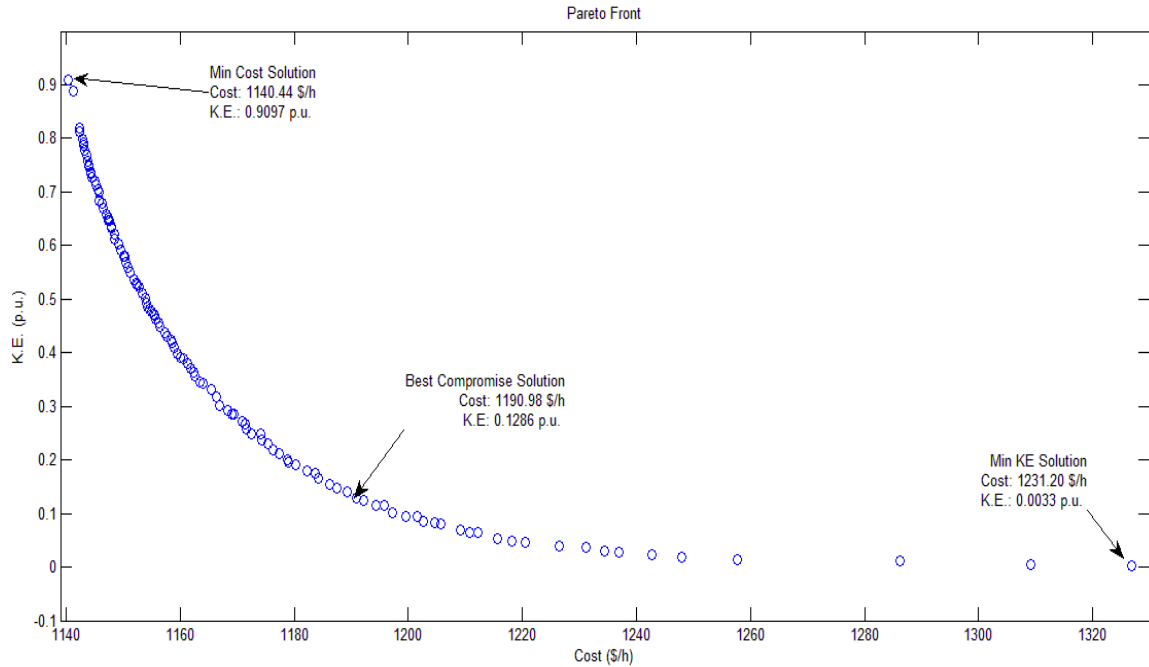
Figure 5.2:   Pareto Front for 3 Machine 9 Bus Test System for Case A.
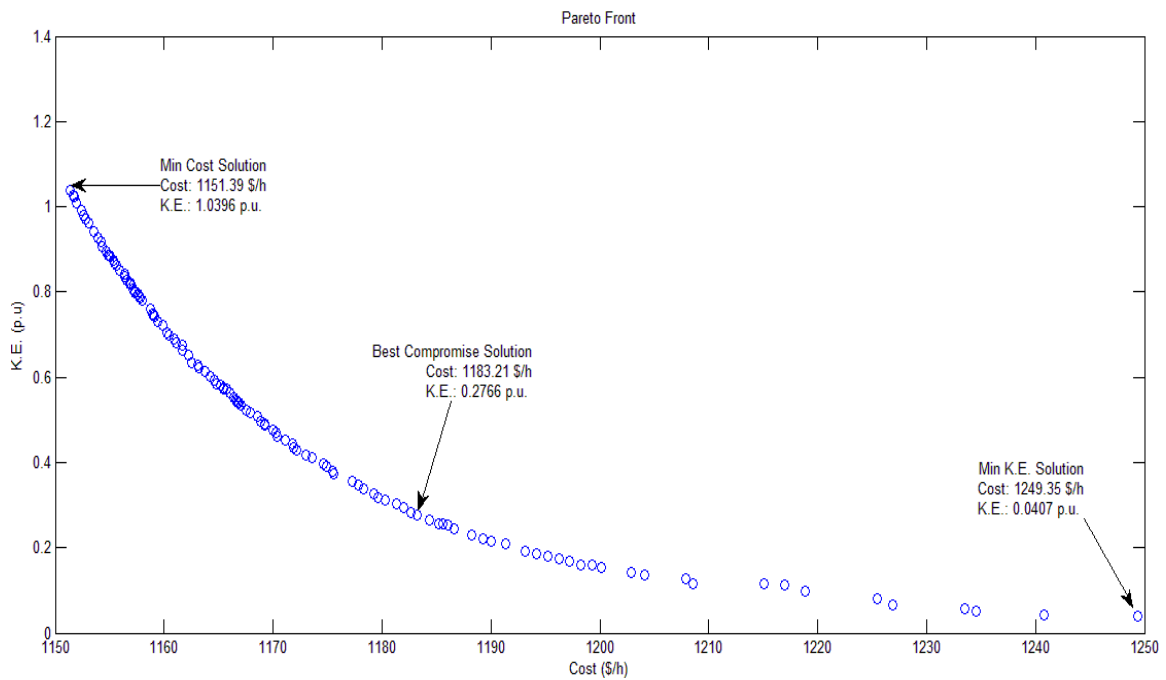

Figure 5.3:   Pareto Front for 3 Machine 9 Bus Test System for Case B.

Figure 5.2 and Figure 5.3 for Case A and Case B respectively. The pareto solutions for
the two cases are shown in Table 5.3.

TABLE 5.3:   PARETO SOLUTIONS FOR INDIVIDUAL CRITICAL FAULTS CASES

Solution	Case A			Case B		
Parameters	Best Compromise	Min. Cost	Min. K.E	Best Compromise	Min. Cost	Min. K.E
$P_{G_1}(MW)$	175.0859	128.7672	242.6353	156.6279	132.4447	207.1070
$P_{G_2}(MW)$	57.2989	92.7405	44.4828	127.3337	126.4623	89.3018
$P_{G_3}(MW)$	85.9137	96.7918	32.9123	34.3801	59.3990	22.488
$V_1(p.u.)$	0.9887	0.9792	0.9965	0.9836	0.9809	0.9925
$V_2(p.u.)$	1.0123	1.0118	1.0225	1.0331	1.0162	1.0233
$V_3(p.u.)$	1.0482	1.0308	1.0366	1.0210	1.0215	1.0245
$Cost(\$/h)$	1190.98	1140.44	1326.89	1183.21	1151.39	1249.35
$K.E_{Cl}(p.u)$	0.1286	0.9096	0.0032	0.2766	1.0369	0.0407

TABLE 5.4:   PERFORMANCE COMPARISON OF PROPOSED SPEA BASED APPROACH WITH
DIFFERENTIAL EVOLUTION BASED TSCOPF

Case	Cost for SPEA (Min. Cost) ($/h)	Cost reported in [133]	Increment in cost (%)	CCT for SPEA (Min. Cost) (sec)	CCT reported in [133]	Increment in CCT (%)
A	1140.44	1140.06	0.0335	0.401	0.3897	2.899
B	1151.39	1148.58	0.2443	0.3856	0.3707	4.019

TABLE 5.5:   PERFORMANCE COMPARISON OF PROPOSED SPEA BASED APPROACH WITH
TRAJECTORY SENSITIVITY APPROACH

Case	CCT for SPEA (Min. K.E) (sec)	CCT reported in [67]	Increase in CCT (%)
A	1.7300	0.5556	211.375
B	1.1220	0.5725	95.98

TABLE 5.4 compares the proposed approach with differential evolution based transient stability constrained optimal power flow (TSCOPF) [133]. Only the minimum cost solutions of SPEA is compared in these cases as the algorithm in [133] emphasize on minimizing the cost with increasing the transient stability. For both cases portrayed in TABLE 5.4 it can easily been seen that for a negligible increase in cost, the increment in CCT is quite higher proving the superiority of the proposed algorithm. In TABLE 5.5, another comparison has been rendered between the proposed approach and generator rescheduling through trajectory sensitivity approach [67]. The comparison is however

made on grounds of CCT only as the technique in [67] focuses on making the system stable for the contingency under consideration without concerning the cost of solution. Comparing only the minimum K.E solutions, as cost is considered rather inconsequential, for both cases, it can easily been seen that the proposed approach far surpasses the technique presented in [67]. A significant improvement in CCT can be seen in case A where the CCT by proposed approach is nearly three times the CCT by technique in [67]. This speaks for the quality of solutions provided by the proposed approach.

Finally, Figure 5.4 - Figure 5.7 shows the stable system trajectories in Center of Inertia (COI) reference frame with the parameter settings as shown in Table 5.1 and the fault timings as depicted in Table 5.2 for best compromise solutions.
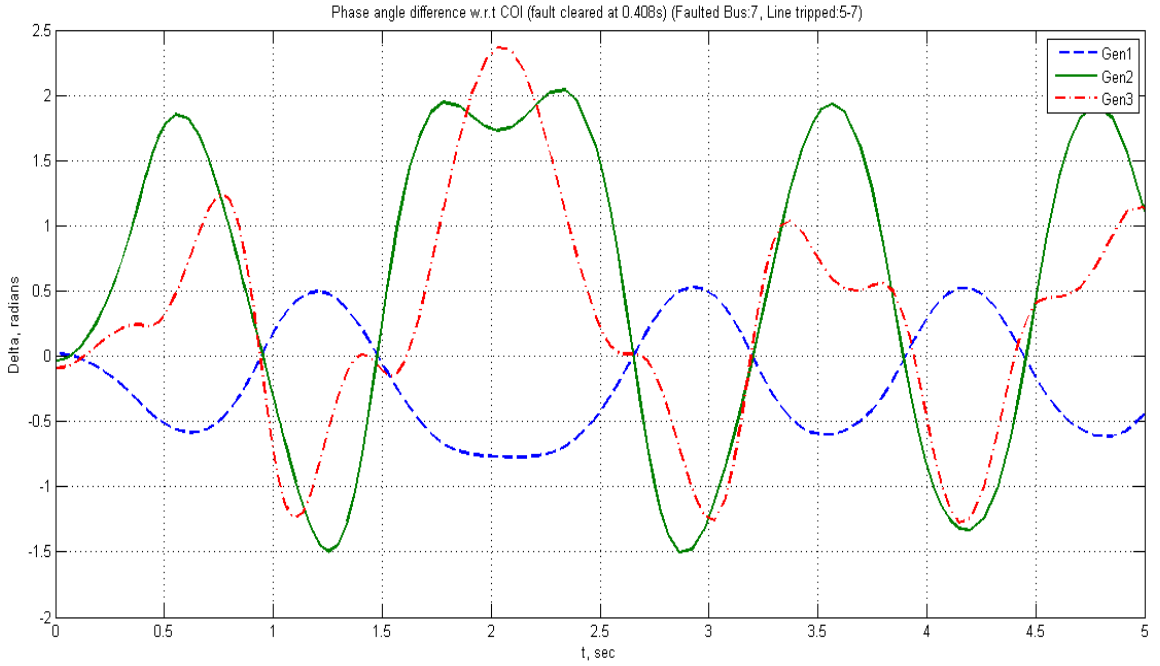
Figure 5.4:   Stable trajectory for fault at bus 7 cleared by line 5-7 tripping, fault clearing time 0.408 sec
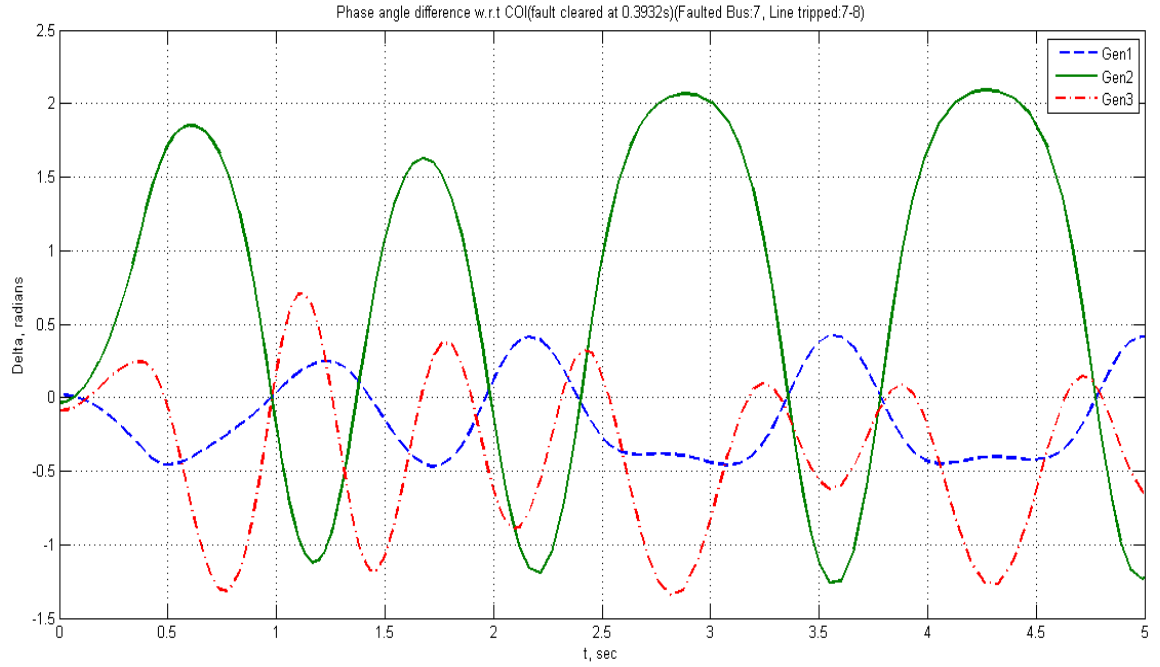

Figure 5.5:   Stable trajectory for fault at bus 7 cleared by line 7-8 tripping, fault clearing time 0.3932 sec.
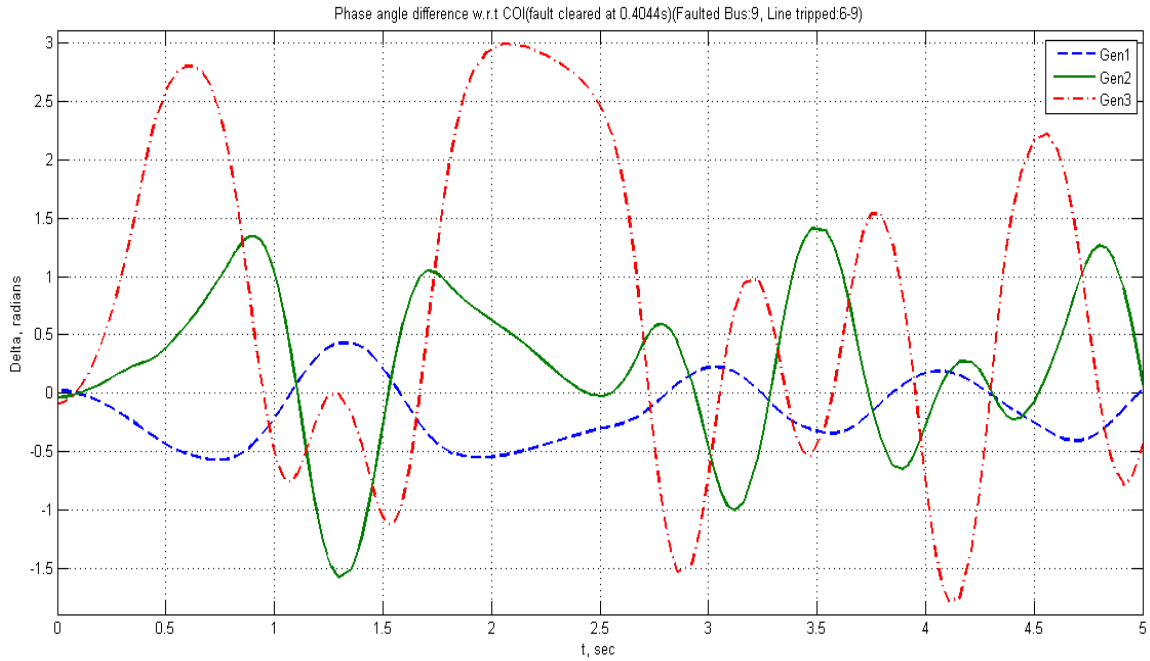
Figure 5.6:   Stable trajectory for fault at bus 9 cleared by line 6-9 tripping, fault clearing time 0.4044 sec.
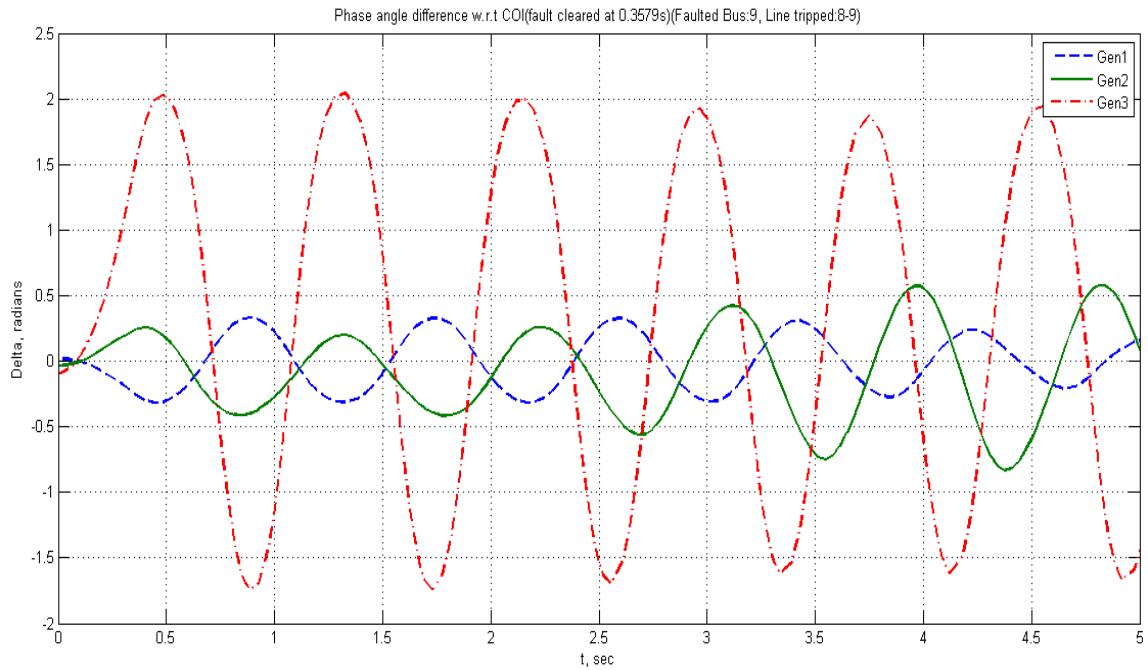

Figure 5.7:   Stable trajectory for fault at bus 9 cleared by line 8-9 tripping, fault clearing time 0.3579 sec.

5.3.2 Simulation Results for New England 10 Machine 39 Bus Test System

Figure 5.8 [67] shows the one line diagram for New England 39 Bus system. The system data is in accordance with [22], the fuel cost parameters are taken from [67], the generators' rating and the system physical bounds are taken from [138]. As per equation (5.16) there are 19 control parameter that includes 9 generator active powers and voltage at each of the generator bus.

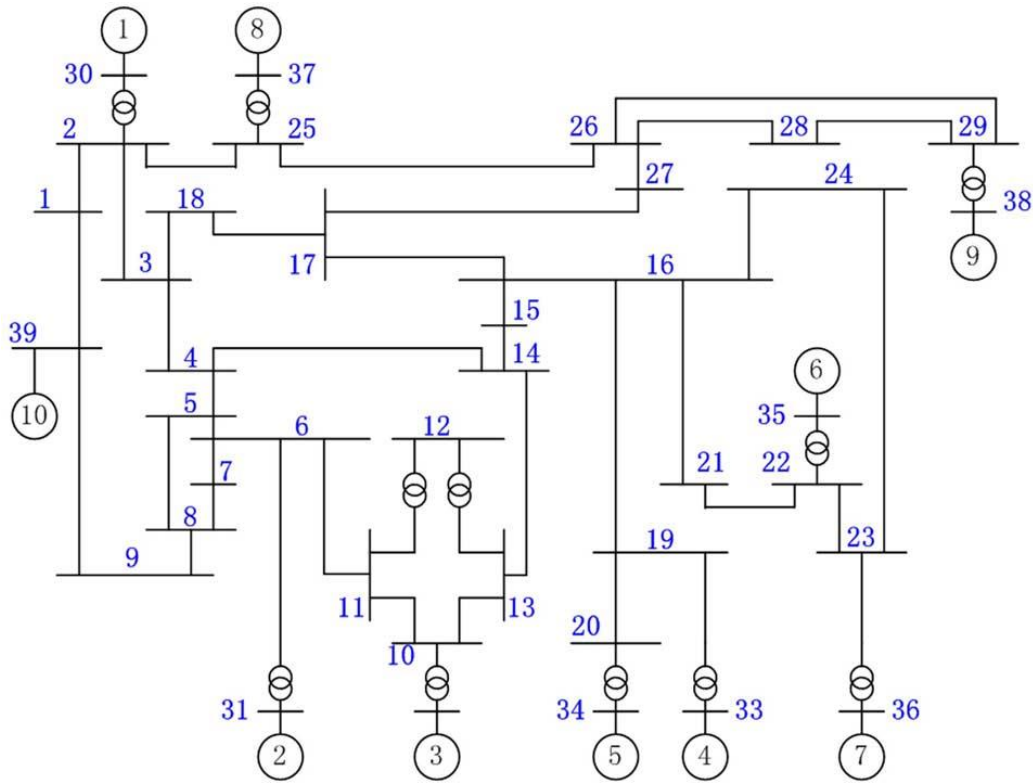Figure 5.8:   Single Line Diagram for New England 10 Machine 39 Bus Test System

According to the strategy described in section (5.2.3) a priority list of all possible faults in the system is formed first. Out of the 33 possible faults the top four faults as shown in TABLE 5.6 are selected as critical fault group. The optimization is done for an average clearing time of faults under consideration i.e. 0.0625 sec.

TABLE 5.6:   CRITICAL FAULT GROUP FOR NEW ENGLAND 10 MACHINE 39 BUS TEST SYSTEM

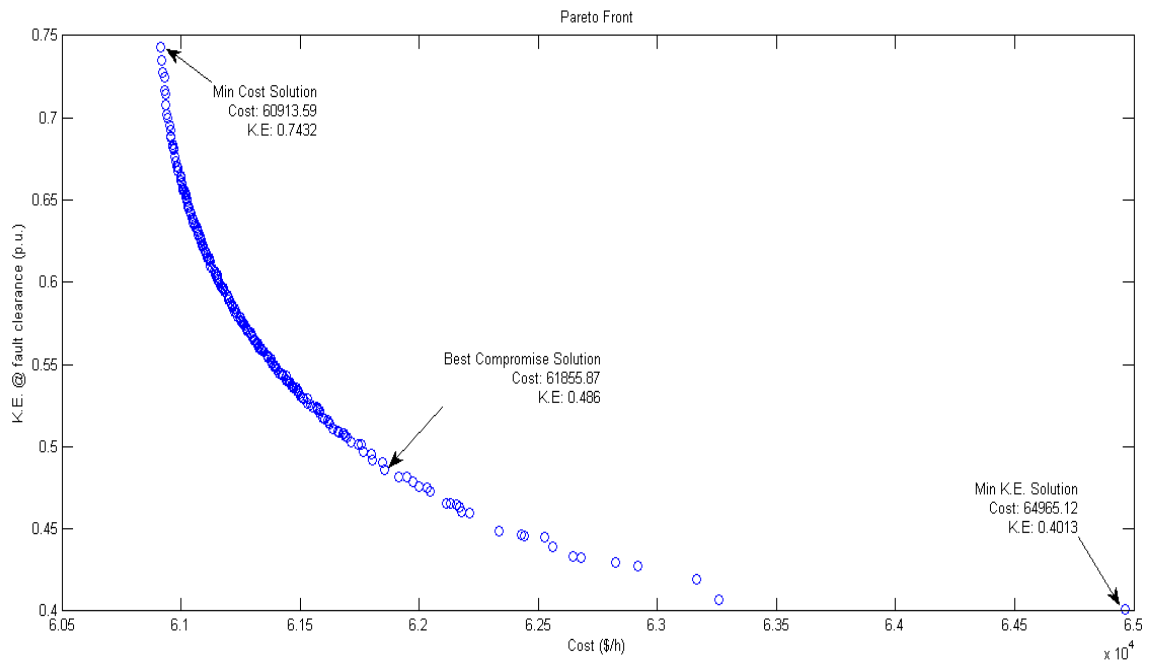| *Faulted Bus*	*Line tripped*	*Critical Clearing Time (CCT) (sec)*
29	28-29	0.04849
28	28-29	0.05656
29	26-29	0.06906
26	26-29	0.07620

Figure 5.9:   Pareto Front for New England 10 Machine 39 Bus Test System.

TABLE 5.7: PARETO SOLUTIONS FOR NEW ENGLAND 10 MACHINE 39 BUS TEST SYSTEM

Solution Parameters	Best Compromise	Min. Cost	Min. K.E
$P_{G_1}(MW)$	262.21	251.32	321.28
$P_{G_2}(MW)$	602.64	576.37	659.03
$P_{G_3}(MW)$	681.85	649.39	676.98
$P_{G_4}(MW)$	641.23	640.89	407.23
$P_{G_5}(MW)$	518.60	494.04	602.80
$P_{G_6}(MW)$	668.29	659.23	551.87
$P_{G_7}(MW)$	571.32	548.57	836.36
$P_{G_8}(MW)$	499.52	526.65	311.15
$P_{G_9}(MW)$	538.01	806.63	471.64
$P_{G_{10}}(MW)$	1146.21	983.77	1292.82
$V_1(p.u.)$	1.0264	1.0199	1.0350
$V_2(p.u.)$	1.0302	1.0204	1.0207
$V_3(p.u.)$	1.0324	1.0200	1.0142
$V_4(p.u.)$	1.0206	1.0221	1.0119
$V_5(p.u.)$	1.0365	1.0396	1.0260
$V_6(p.u.)$	1.0329	1.0319	1.0224
$V_7(p.u.)$	1.0366	1.0294	1.0450
$V_8(p.u.)$	1.0049	1.0273	1.0351
$V_9(p.u.)$	1.0314	1.0397	1.0078
$V_{10}(p.u.)$	1.0373	1.0149	1.0210
$Cost(\$/h)$	61855.87	60913.59	64965.12
$K.E_{Cl}(p.u)$	0.486	0.7432	0.4013

Figure 5.9 shows the pareto front obtained as a result of optimization and the results extracted are tabulated in TABLE 5.7. Again there are three possible solutions, minimum cost solution, minimum K.E. solution and best compromised solution, presented by the algorithm for decision maker. As depicted by pareto front in Figure 5.9 the proposed algorithm not only achieves the optimal solution but also covers the whole search space hence maintaining diversity. The influence of optimization towards the improvement in transient stability of the system can be seen in TABLE 5.8. To prove the claim of improving the overall stability of the system, a fault on bus 17 with line 17-18 clearance has been applied. It should be noted that this particular fault is not included in the critical fault group. The proposed algorithm is able to improve the CCT of this fault as well, as shown in TABLE 5.8.

TABLE 5.8:   CCT COMPARISON FOR NEW ENGLAND 10 MACHINE 39 BUS TEST SYSTEM

Faulted Bus	Line tripped	CCT(sec) for base case	CCT(sec) for Best compromise solution	CCT(sec) for Min. cost solution	CCT(sec) for Min. KE solution	CCT(sec) Reported in [67]
26	26-29	0.0762	0.2584	0.1007	0.2739	0.0743
29	26-29	0.06906	0.2500	0.0893	0.2954	0.0672
28	28-29	0.05656	0.2884	0.0857	0.3454	0.0539
29	28-29	0.04849	0.2433	0.0730	0.2896	0.0462
17	17-18	0.1293	0.1551	0.1226	0.1559	0.1873

A comparison is made between the proposed algorithm and trajectory sensitivity approach for improving stability of the system [67]. As in [67] fault at bus 17 with line 17-18 clearance is selected as a critical fault. Figure 5.10 shows the pareto front obtained as result of optimization. TABLE 5.9 shows the comparison of CCTs of the fault for each approach
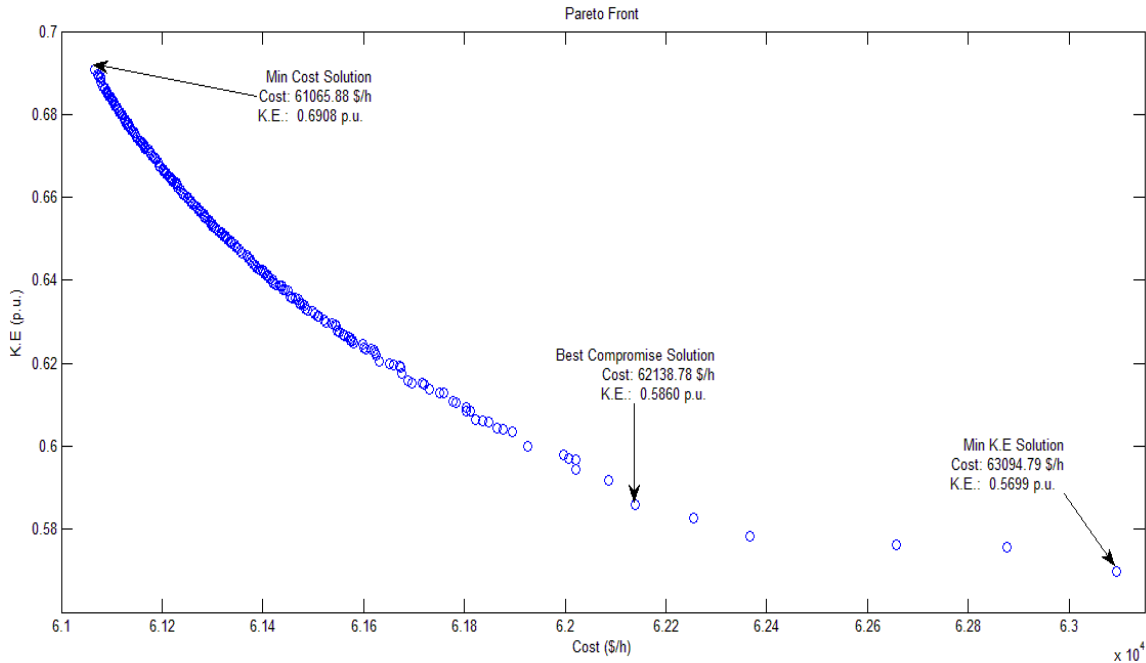

Figure 5.10:   Pareto Front for New England 10 Machine 39 Bus Test System for fault at bus 17

TABLE 5.9:   PERFORMANCE COMPARISON OF PROPOSED SPEA BASED APPROACH WITH TRAJECTORY SENSITIVITY APPROACH.

Case	CCT for SPEA (Min. K.E) (sec)	CCT reported in [67]	Increase in CCT (%)
Fault: 17, Line cleared: 17-18	0.2315	0.1873	23.59

As in the case of three machine nine bus case only the minimum K.E. solution is compared as cost of the solution is considered secondary as compared to stability of the

system. Again the proposed approach presents a solution that far surpasses the trajectory sensitivity approach [67]. Finally, Figure 5.11 - Figure 5.15 shows the stable system trajectories with respect to COI for best compromise case with system operating conditions, faults applied and fault clearance time as depicted in TABLE 5.7 and TABLE 5.8 respectively.
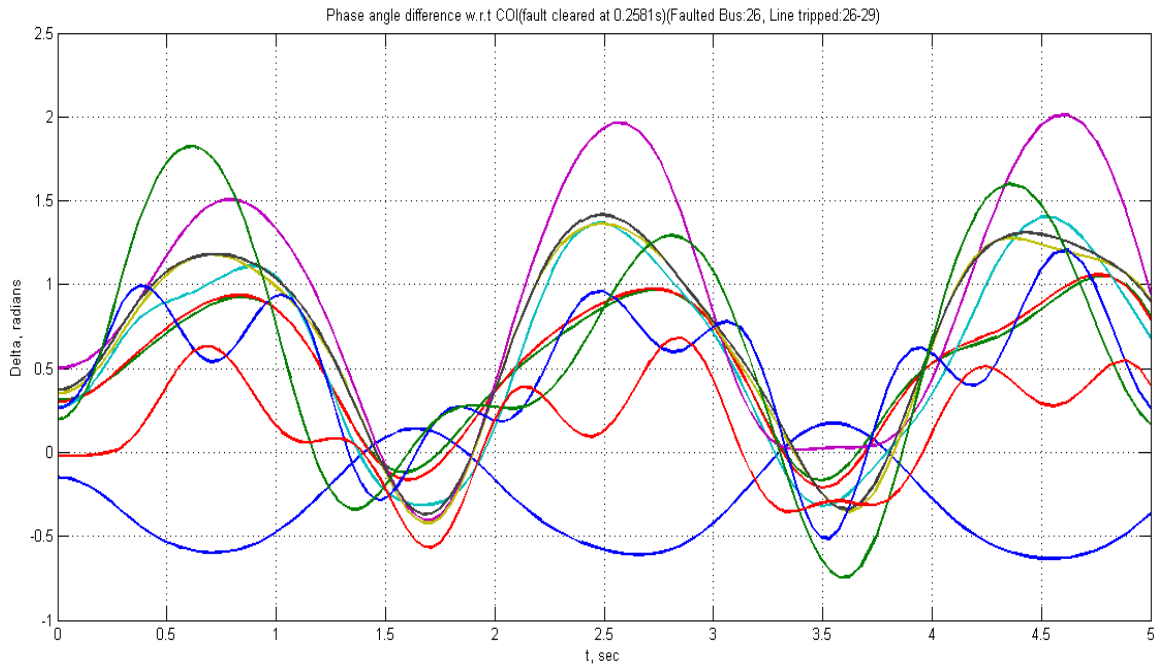

Figure 5.11:   Stable trajectory for fault at bus 26 cleared by line 26-29 tripping, fault clearing time 0.2584 sec.
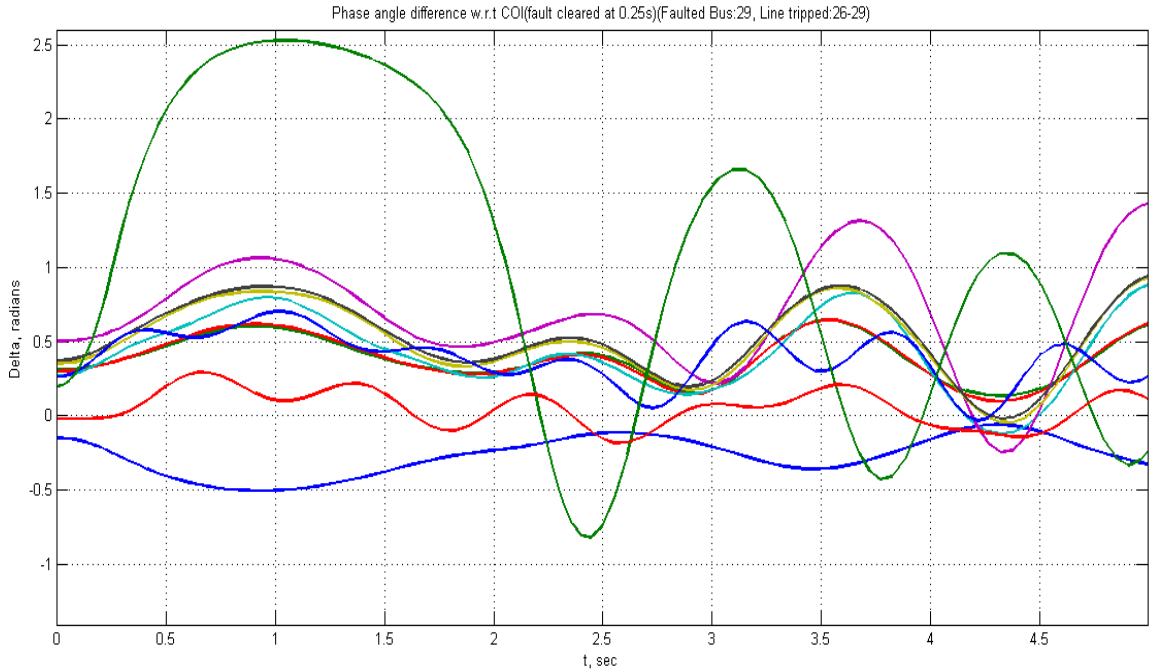
Figure 5.12:   Stable trajectory for fault at bus 29 cleared by line 26-29 tripping, fault clearing
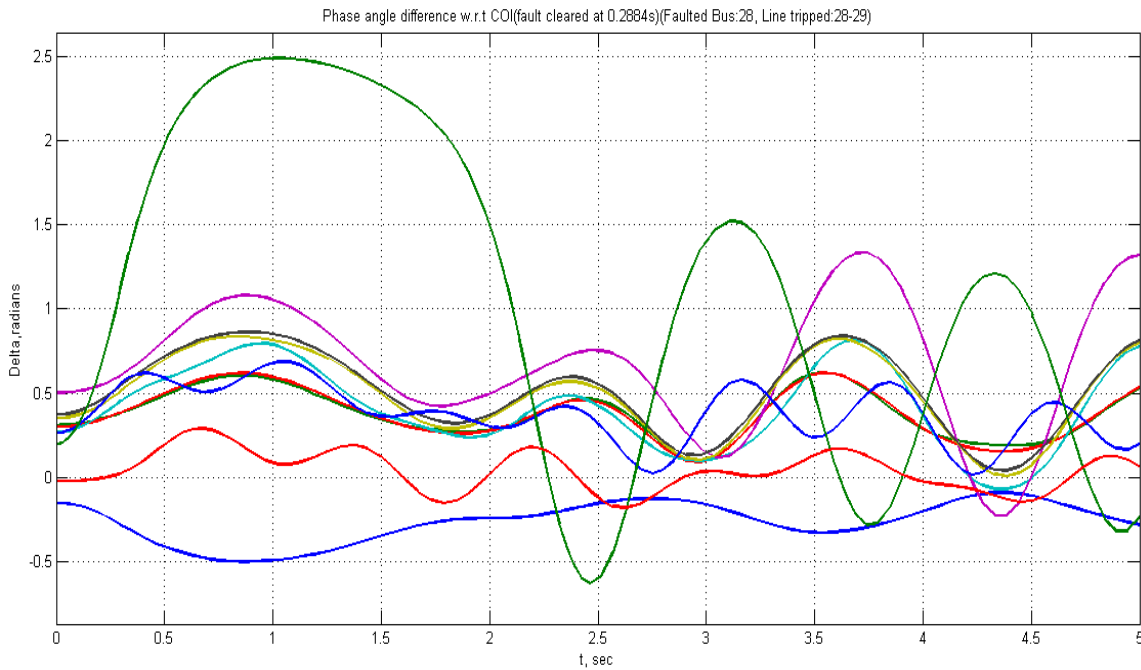
time 0.25 sec

Figure 5.13:   Stable trajectory for fault at bus 28 cleared by line 28-29 tripping, fault clearing
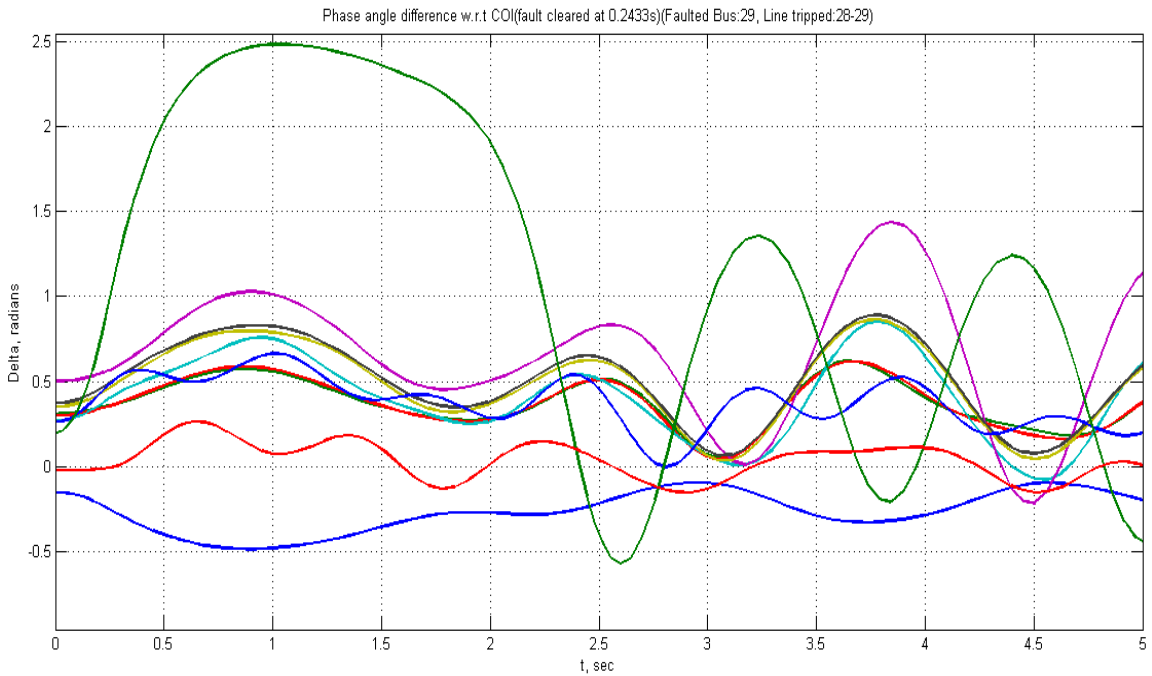
time 0.2884 sec..

117

Figure 5.14:   Stable trajectory for fault at bus 29 cleared by line 28-29 tripping, fault clearing
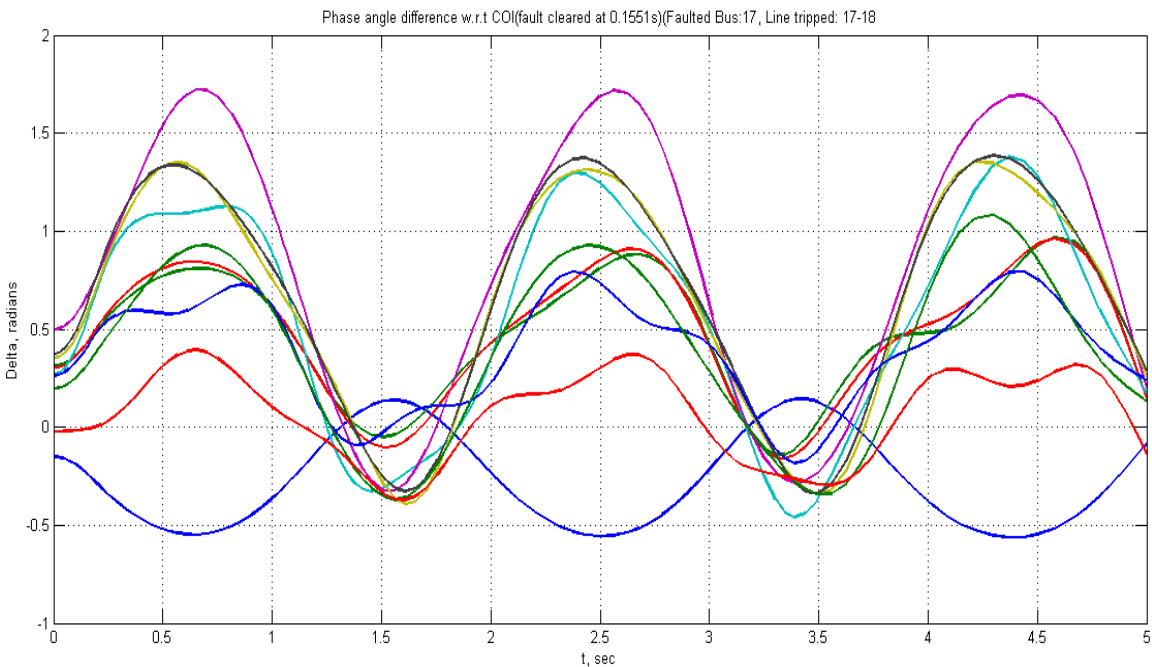
time 0.2433 sec.

Figure 5.15:   Stable trajectory for fault at bus 17 cleared by line 17-18 tripping, fault clearing

time 0.1551 sec.

118

5.4   RTDS Implementation

The said SPEA based Transient Stable Optimal Power Flow is also implemented on Real Time Digital Simulator (RTDS) to prove the claim of robustness. An overview of RTDS hardware and software is given in Appendix A:. The WSCC 3 Machine 9 Bus System is implemented on RTDS and faults are simulated at bus number 7 and bus number 9 with line 5-7 and line 6-9 clearance respectively. Real time breaker models are implemented to simulate the actual real time scenario. The machines in the system are modelled as two axis machine without damper windings. All the machines are modelled with IEEE Type 1 Speed Governor and Turbine model and IEEE Type 1 Static Excitation models. As the system is modelled in real time with different power system components and platform different than MATLAB® therefore the CCT of the faults obtained from RTDS are expected to be different than MATLAB®, but it is expected the same trend will be there as in MATLAB®. FIGURE shows the draft file implementation of WSCC 3 machine 9 Bus test system on RTDS, also the fault and breaker logics are shown FIGURE II. The powers and voltages obtained from the optimization are plugged in one at a time and effects of optimization is seen on the basis of improvement in CCT of the faults. Faults are simulated and CCT for each fault is obtained by repeating the simulation over and over again. The stability of the system in RTDS is determined by the speed of the machines and per ANSI standards an over frequency instability is declared whenever one of the machine reaches 390 rad/sec.
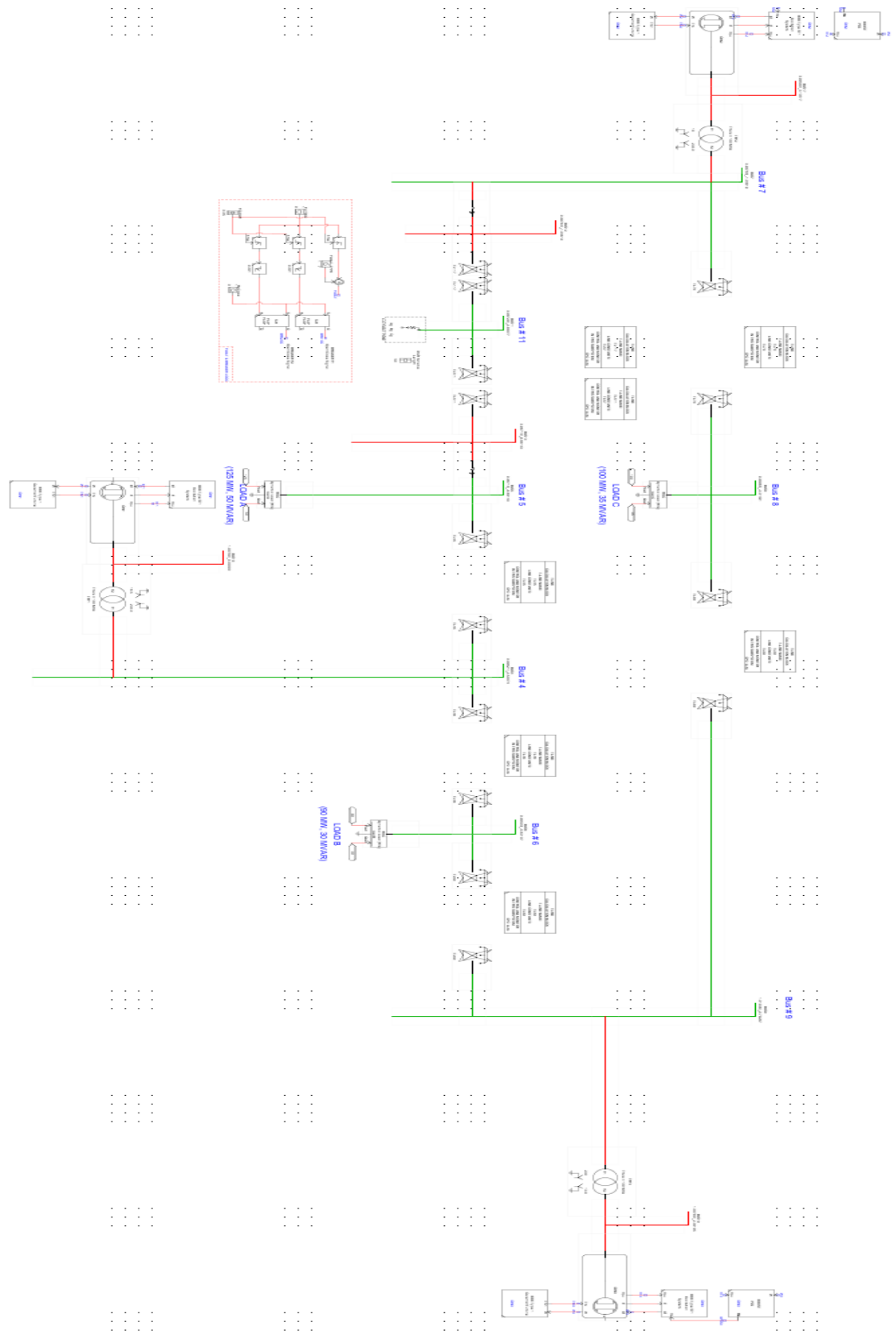
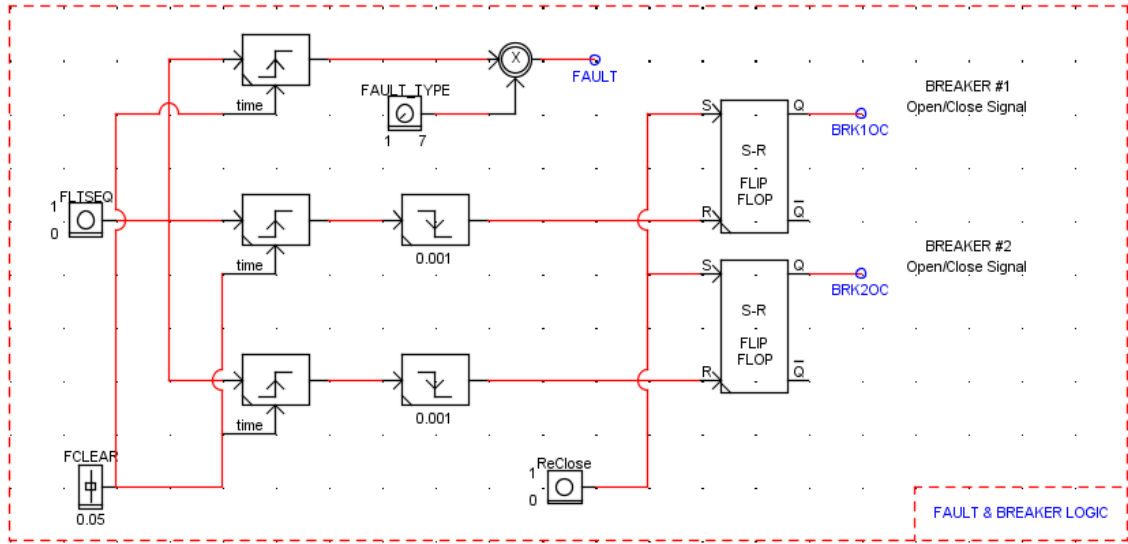Figure 5.16:   RTDS Implementation of WSCC 3 Machine 9 Bus Test System

Figure 5.17:   Fault and Breaker logic

TABLE 5.10 shows the CCT for base case i.e. for original system settings, for minimum cost case, best compromise case and minimum K.E. case of the optimization. It can be seen in TABLE 5.10 that the similar trend as in MATLAB® platform is shown by the CCT of the system on RTDS platform. As for each of the case the min cost solution gives the worst CCT for all solutions in both the cases. As in both platform a similar trend that is worst CCT for min cost solution can be seen in TABLE 5.10 and Figure 5.18 and Figure 5.19. Similarly, a moderate improvement in CCT for both platform in case of best compromise solution can be seen in TABLE 5.10. The maximum improvement in CCT is for the minimum K.E. case as the stability of the system is given more importance over cost in the optimization algorithm. Finally Figure 5.20-Figure 5.27 show the machine speed trajectories, fault clearing time and breaker statuses for each breaker on the end of the line, for each fault with the clearing time as depicted in TABLE 5.10 for RTDS platform.

TABLE 5.10:   CCT COMPARISON FOR MATLAB AND RTDS

Solution	CCT for Base Case		CCT for Min. Cost Solution		CCT for Best Compromise Solution		CCT for Min. KE Solution	
Case	MATLAB	RTDS	MATLAB	RTDS	MATLAB	RTDS	MATLAB	RTDS
A	0.1620	0.2589	0.2317	0.4605	0.4080	0.6286	0.8246	0.8500
B	0.2142	0.3870	0.2239	0.4010	0.4044	0.6508	0.9755	1.1050

MATLAB vs. RTDS (Case A)
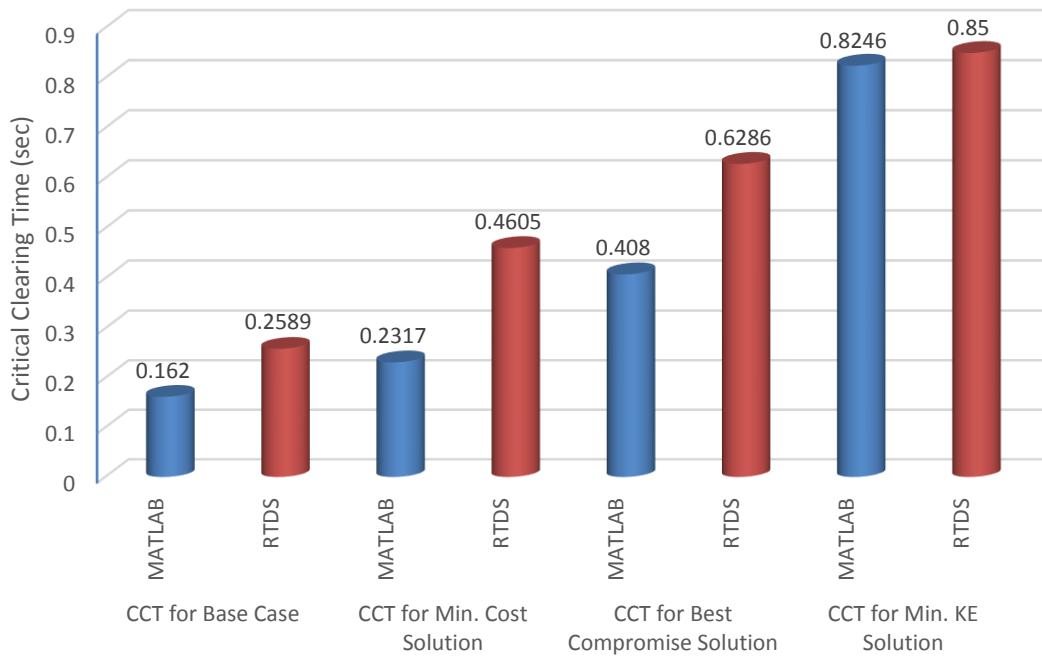
Figure 5.18:   MATLAB vs. RTDS for Case A.
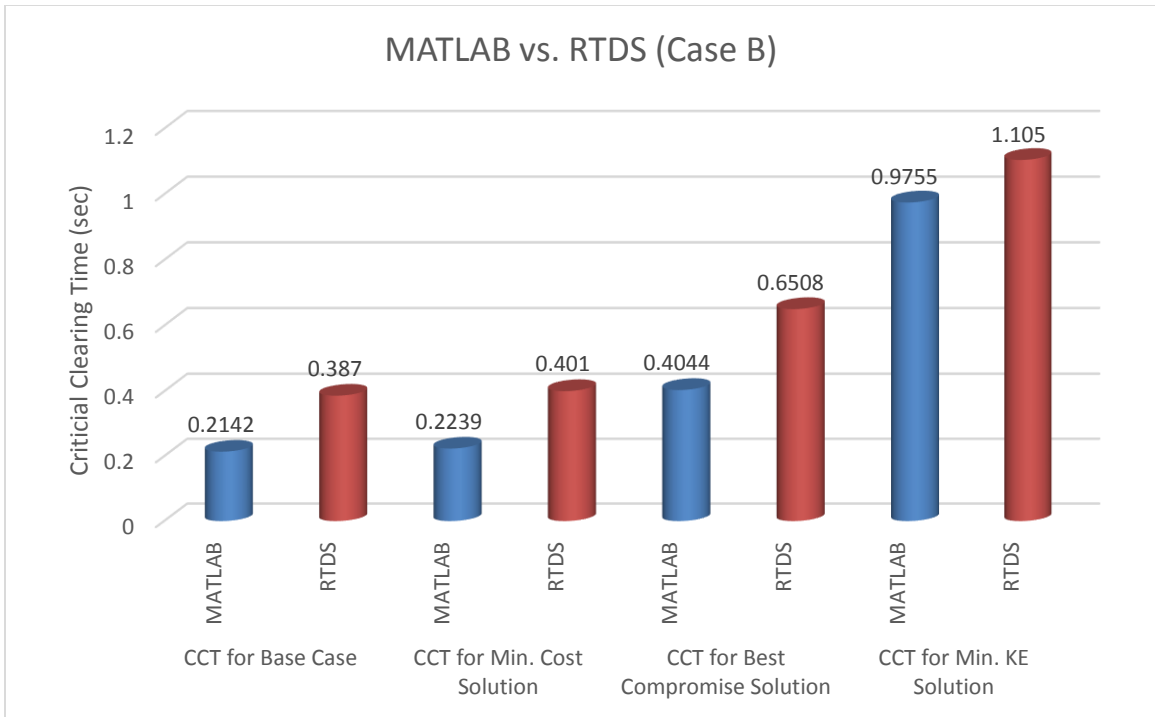
Figure 5.19:   MATLAB vs. RTDS for Case B.

Figure 5.20:   System response for base setting, fault at bus 7 line cleared 5-7.

Figure 5.21: System response for min cost solution, fault at bus 7 line cleared 5-7.

Figure 5.22: System response for best compromise solution, fault at bus 7 line cleared 5-7.
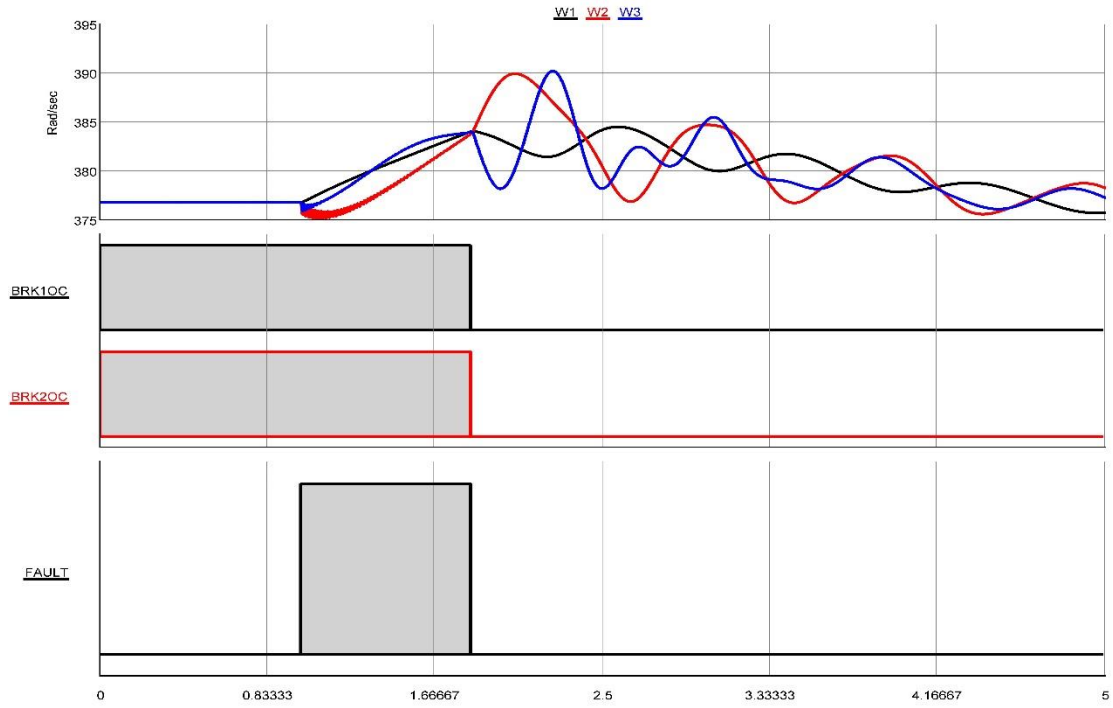
Figure 5.23:   System response for min. K.E solution, fault at bus 7 line cleared 5-7.
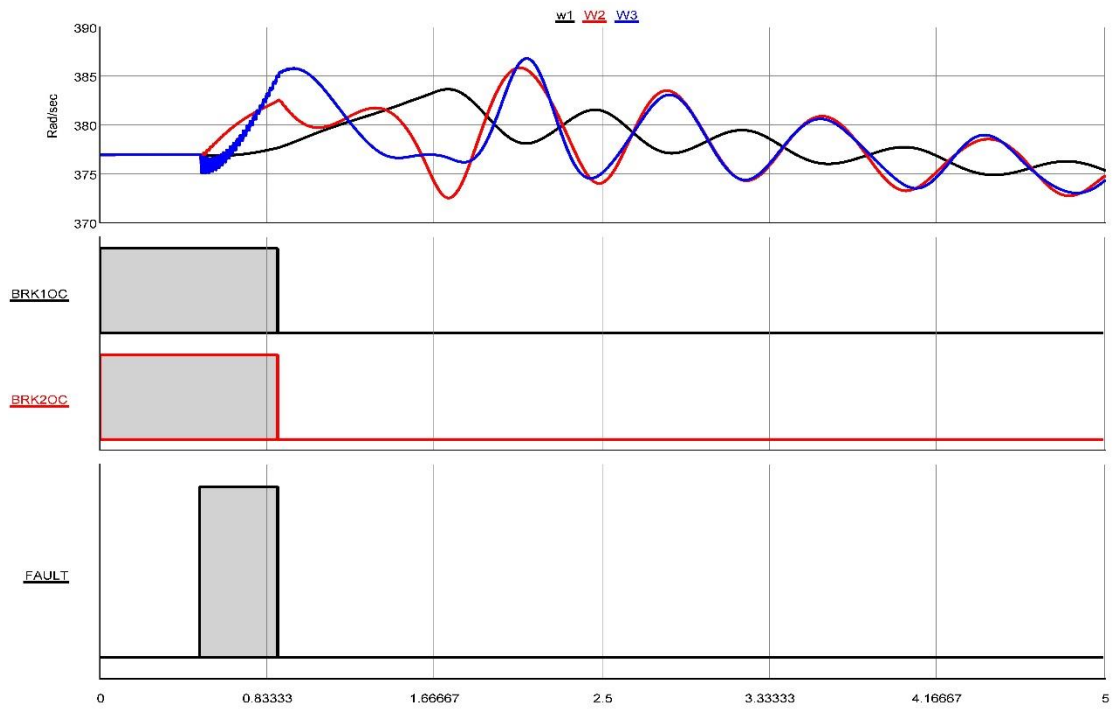
Figure 5.24:   System response for base setting, fault at bus 9 line cleared 6-9

125
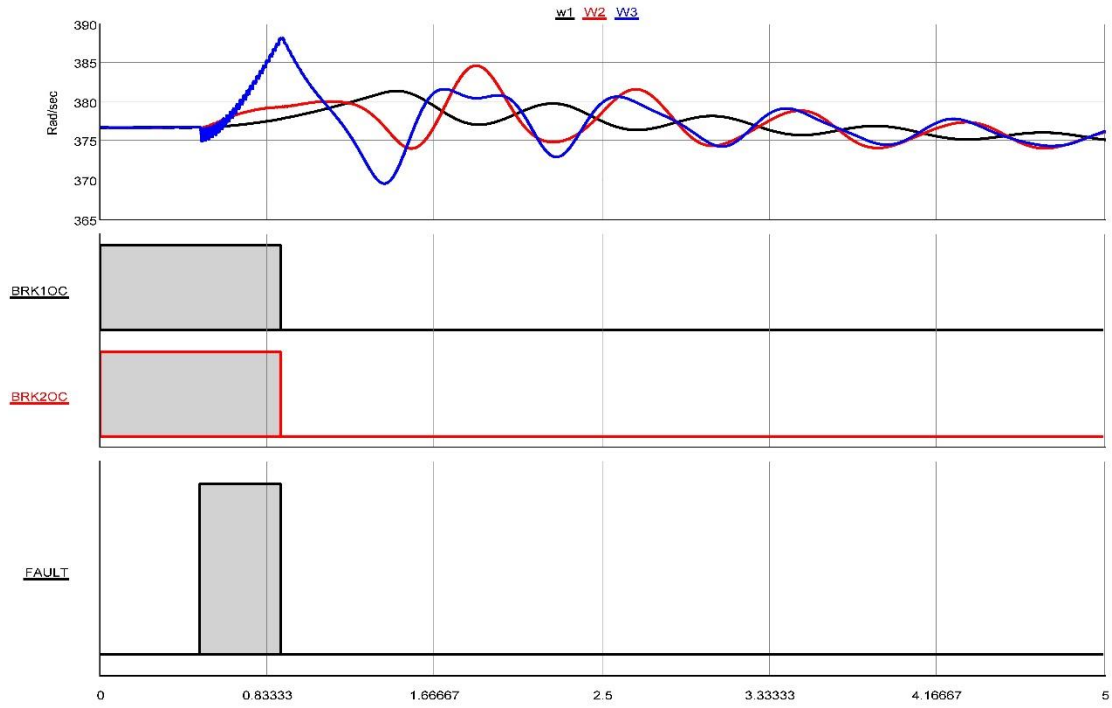
Figure 5.25:   System response for min cost solution, fault at bus 9 line cleared 6-9.
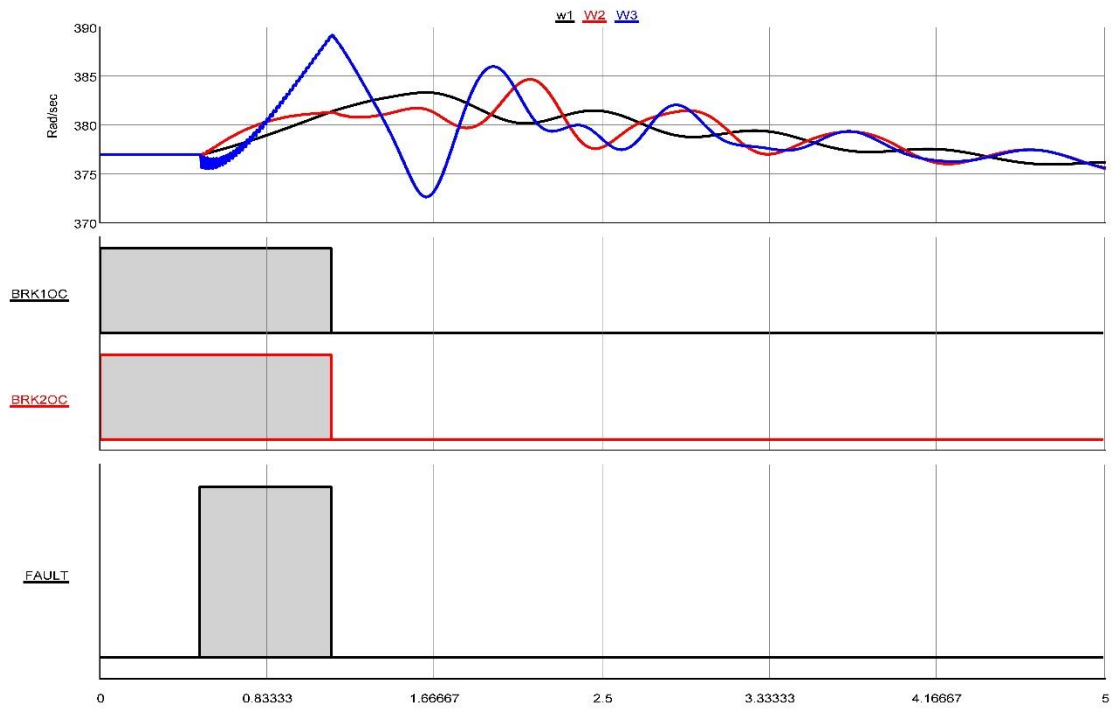
Figure 5.26:   System response for best compromise solution, fault at bus 9 line cleared 6-9.

126

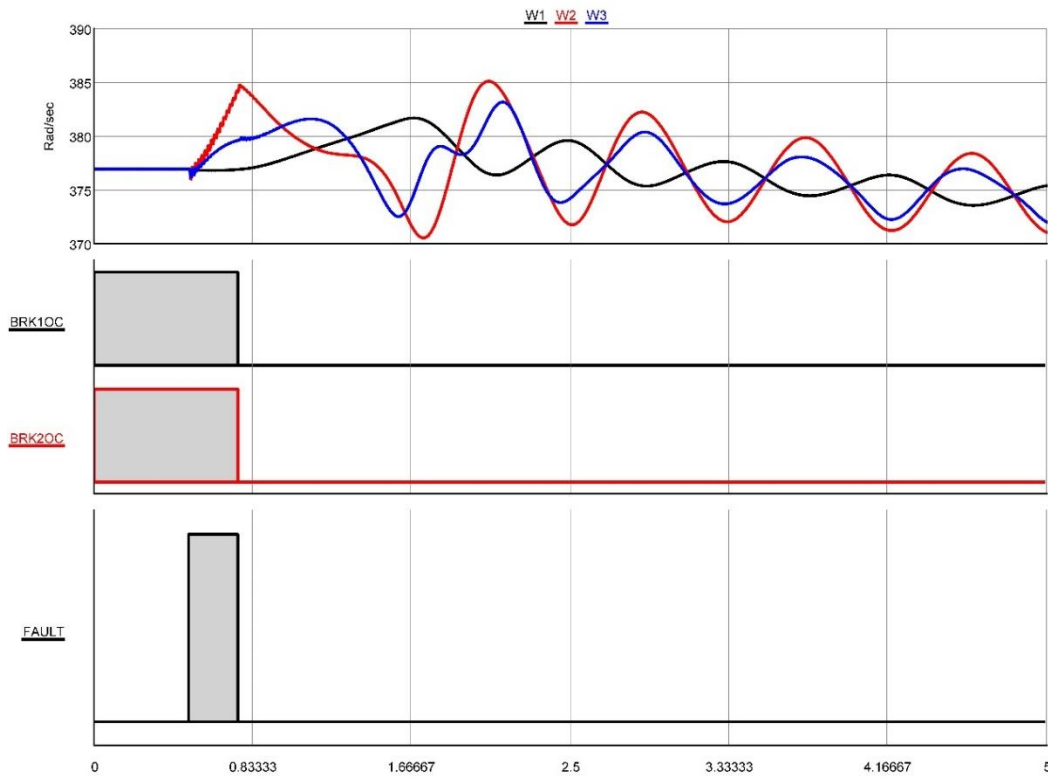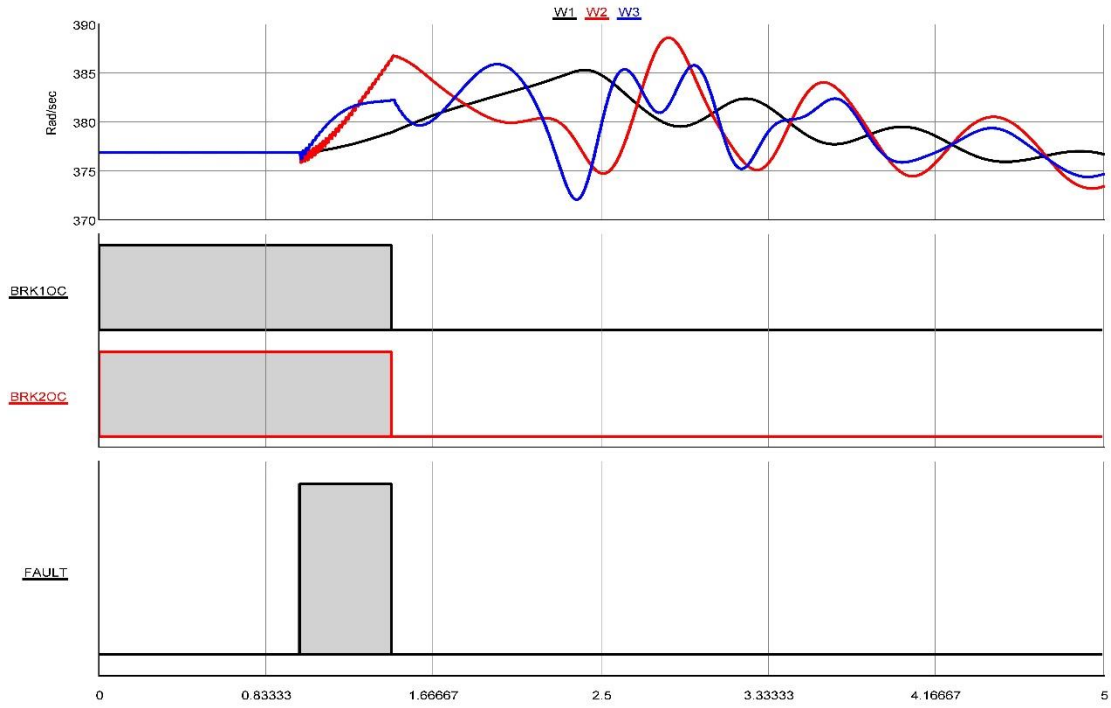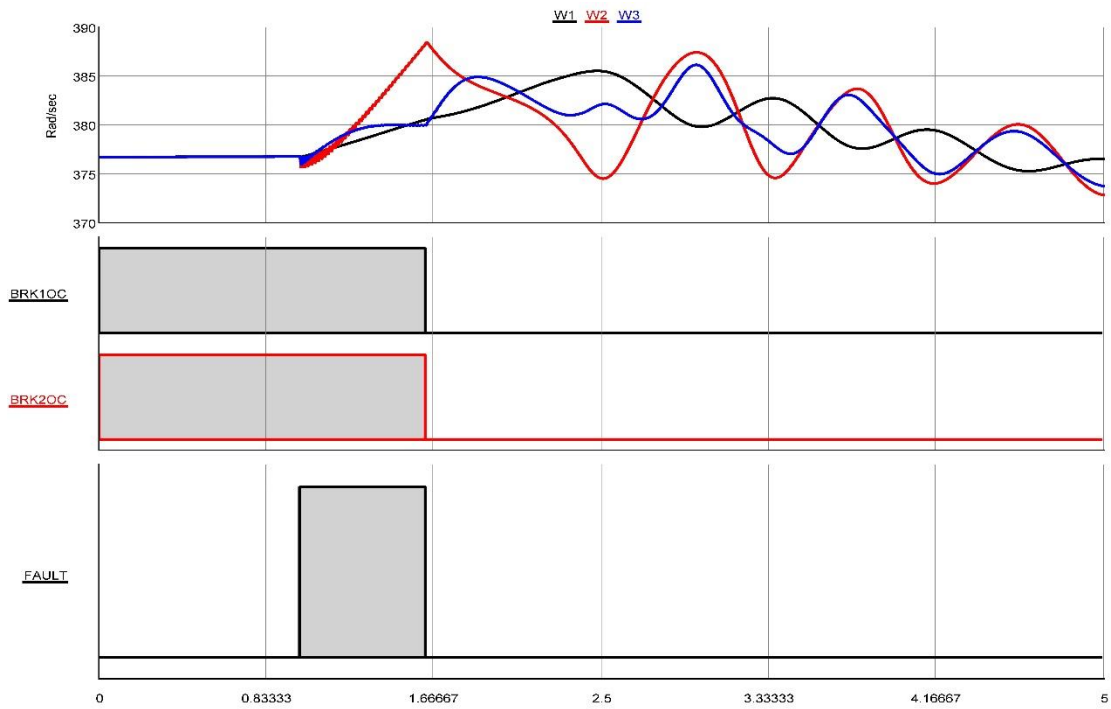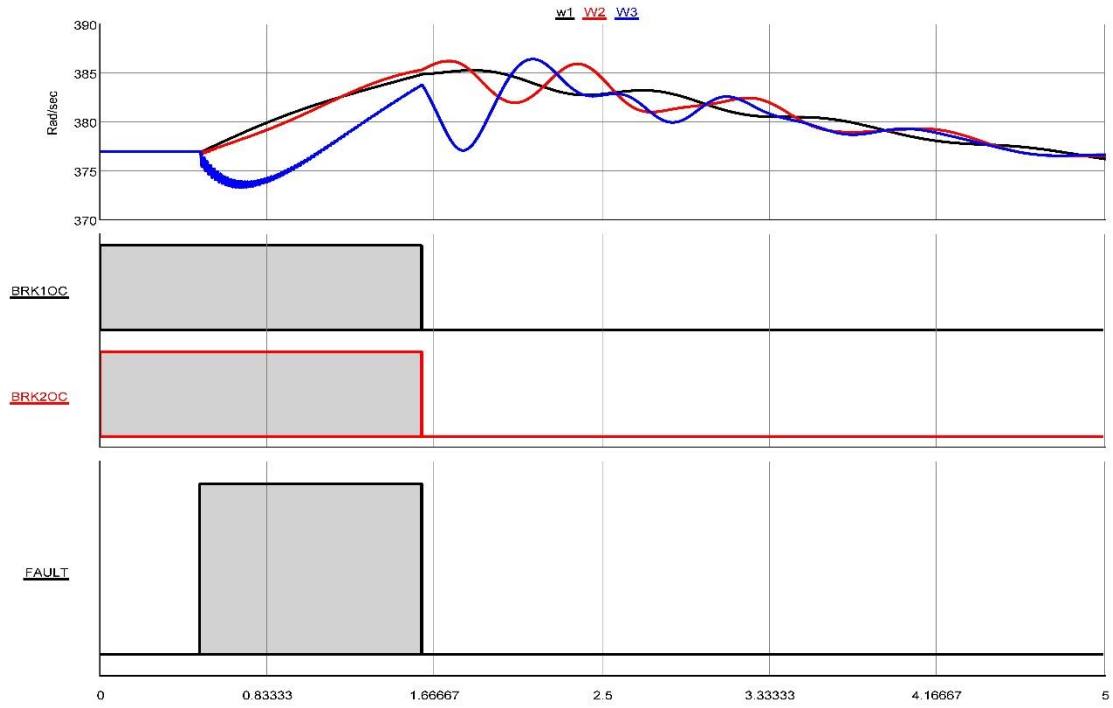Figure 5.27:   System response for best compromise solution, fault at bus 9 line cleared 6-9.

CHAPTER 6

PMU BASED TRANSIENT INSTABILITY PREDICTION

AND MITIGATION

The introduction of PMUs in power systems greatly improves the possibilities of power system monitoring and analyzing of its dynamics. PMUs can directly measure phase angles between corresponding phasors in different locations within the power system. With PMU improved monitoring and remedial action capabilities, network operators can utilize the existing power system in a more efficient way. Synchronized measurements not only allow fast and reliable emergency actions but also make it possible to reduce the need for relatively high transmission margins required by potential power system disturbances.

Synchronized phasor measurements are no longer an academic curiosity as they presently provide solutions that otherwise would have been too expensive or too complicated to implement with traditional approaches. This chapter provides a brief

introduction to PMU technology, its uses and application, later in the chapter a PMU based transient instability prediction algorithm is presented based on which Remedial Schemes are designed to mitigate with the detected instability.

6.1   PMU Based Transient Instability Prediction Scheme

One of the main feature of the PMU which gives it an upper hand over conventional measurement units is the ability of measuring phasors and time stamping, which allows faster and accurate control of the power system. Keeping this idea in mind, in this section a real time intelligent transient instability predictor based on the PMU measurements is developed and demonstrated. The proposed scheme is called intelligent as it makes use of intelligent computational technique i.e. Artificial Neural Networks and ability of PMUs to present the current and voltage measurements in form of phasors makes it real time. The output of the scheme will serve as an arming signal for the Remedial Action Schemes (RAS) which will take necessary action to mitigate with the predicted instability. An advantage of this kind of implementation is the risk reduction posed by the conventional detection and mitigation scheme i.e. to miss classify the event as stable or unstable. Figure 6.1 and Figure 6.2 shows the difference between the conventional and PMU based intelligent scheme. The arming signal in Figure 6.1 is decided based on offline simulations and pre-decided events, one example being the RAS will be armed when the power flowing through a line is more than the critical power, which may not always be case, where as in intelligent scheme RAS will be armed when actual instability is detected. Moreover to this stability information can be seen in case of fault event or disturbance as shown in Figure 6.3 and Figure 6.4. In the sections to follow first Artificial Neural Networks (ANN) are introduced and the predictor scheme design is

presented. The system under consideration is WSCC 3 Machine 9 Bus Test System. To test the performance of the proposed scheme the time domain simulation results are shown in conjunction with the ANN output to verify it. An Artificial Neural Network (ANN) is an information processing paradigm that is inspired by the way biological nervous systems, such as the brain, process information. The human brain consist of highly complex, nonlinear, parallel information processing system. Information is stored and processed in the biological neural network simultaneously, much faster than the fastest computers in existence today. Topologically a brain consist of interconnected set of nerve cells or basic information processing units called *neurons* and their connections called as synapses. There exist nearly 10 billion neurons and 60 trillion synapses in an average human brain. Each neuron has a very simple structure, but collection of such elements constitutes a tremendous processing power. The key element of this paradigm is the novel structure of the information processing system. It is composed of a large number of highly interconnected processing elements (neurons) working in harmony to solve specific problems. ANNs, like people, learn by example. An ANN is configured for a specific application, such as pattern recognition or data classification, through a learning process. Learning in biological systems involves adjustments to the synaptic connections that exist between the neurons. This is true of ANNs as well.

TABLE 6.1:   ANALOGY BETWEEN BIOLOGICAL AND ARTIFICIAL NEURAL NETWORKS

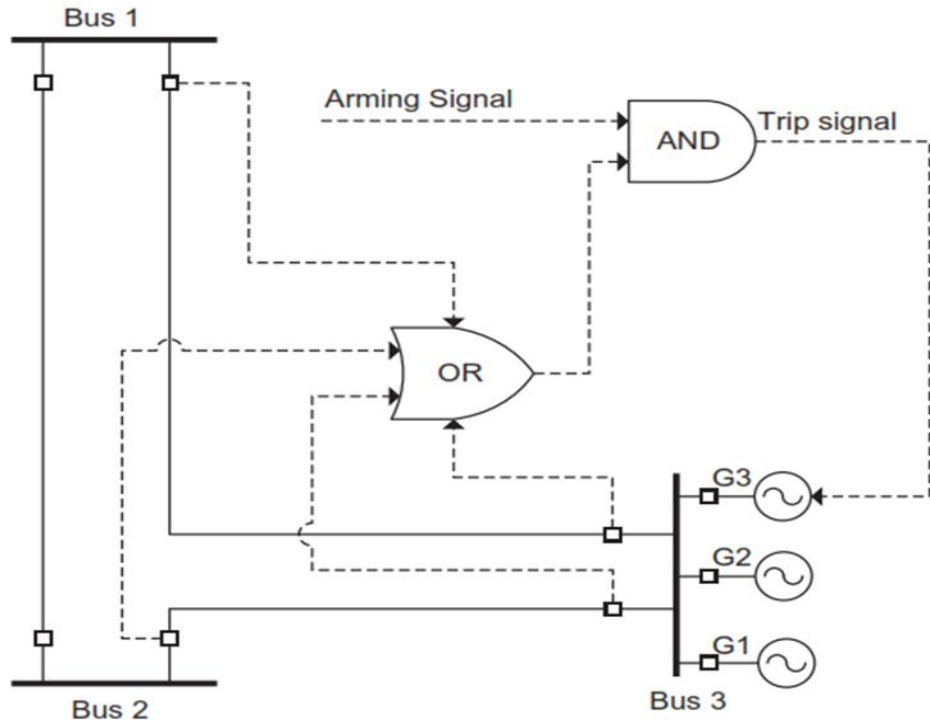| *Biological NN*	*Artificial NN*
Soma	Neuron
Dendrite	Input
Axon	Output
Synapse	Weight

Figure 6.1:　　　Conventional Remedial Action Scheme
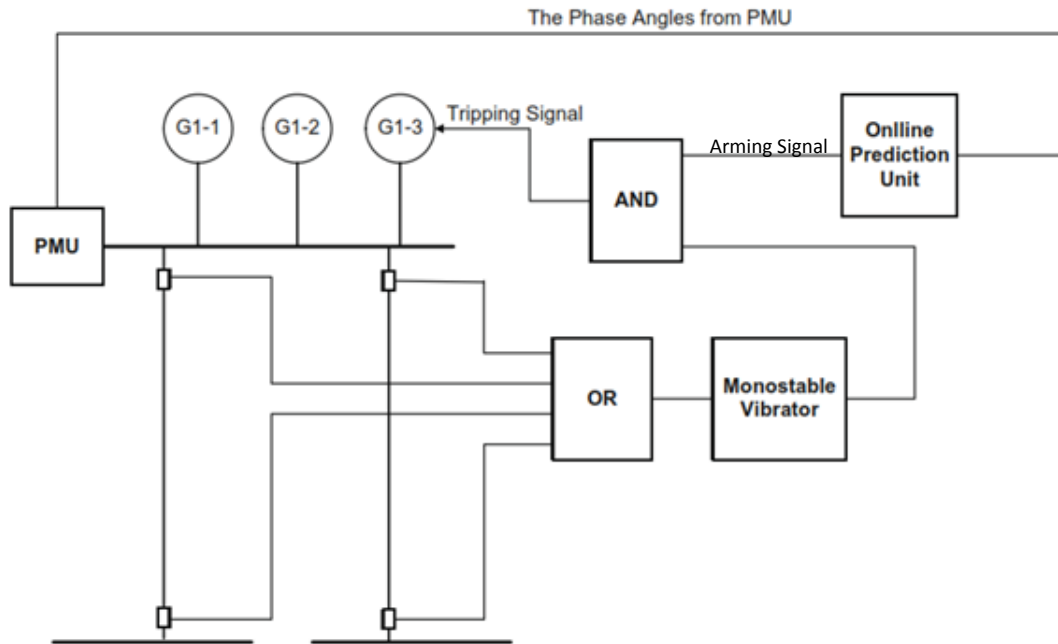
Figure 6.2:　　　PMU Based Remedial Action Scheme

131
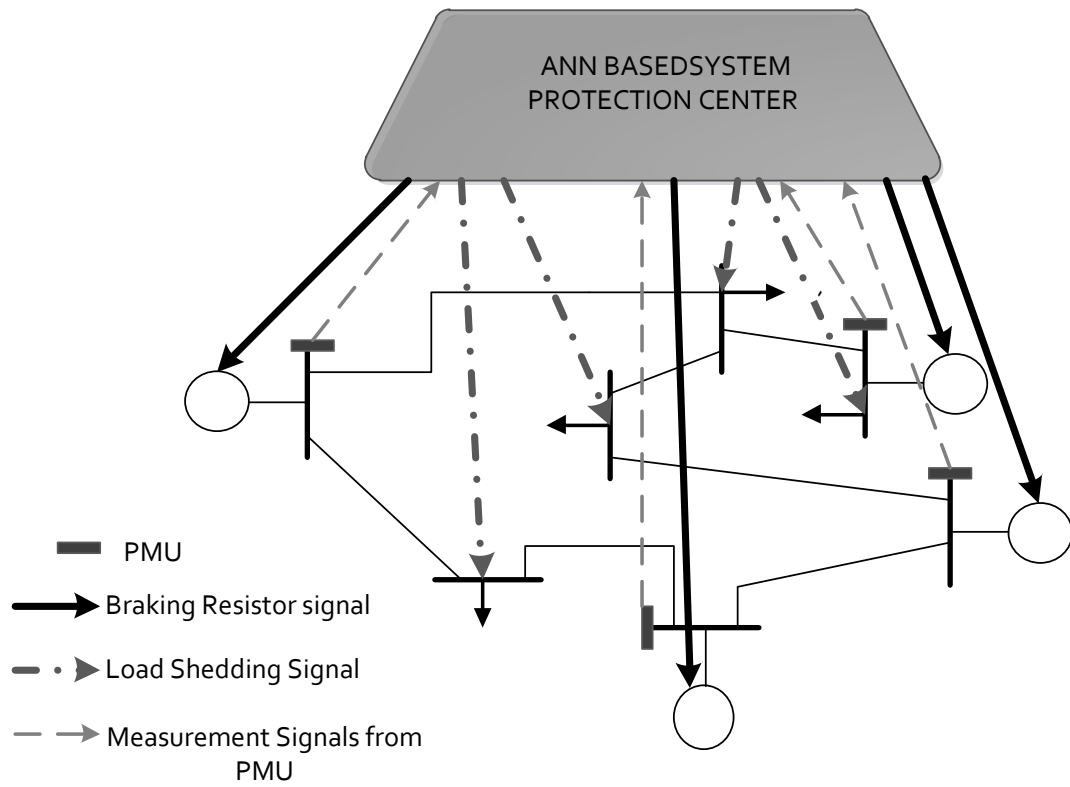
Figure 6.3:   Proposed Remedial Action Scheme
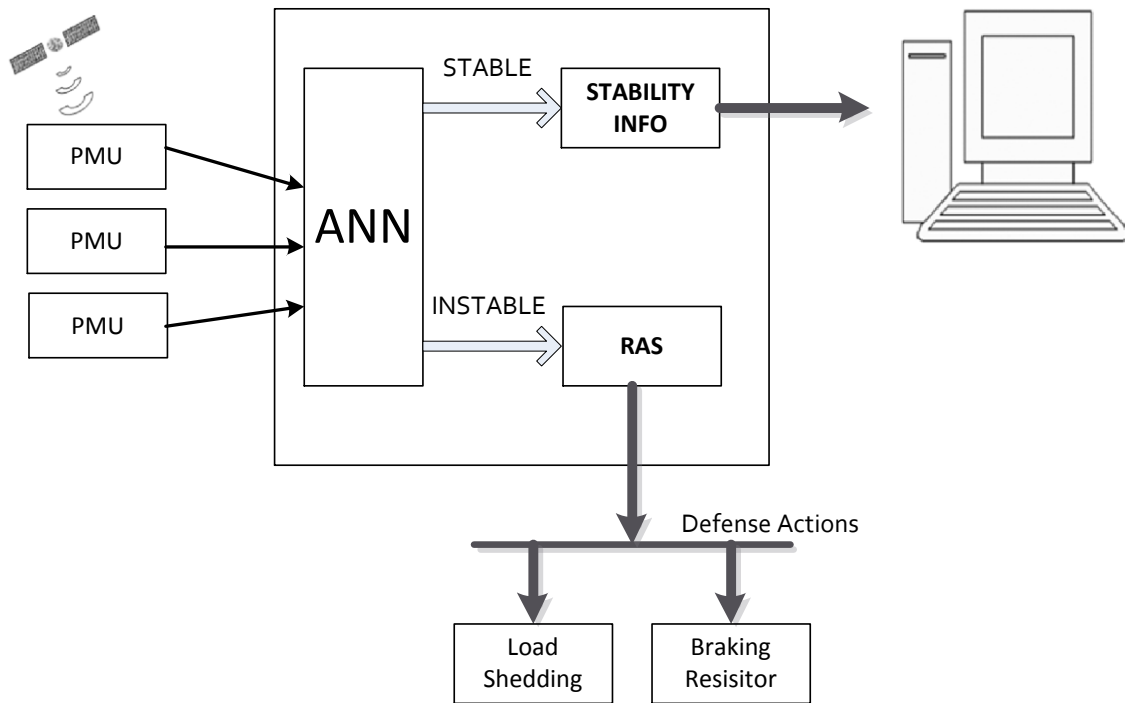
Figure 6.4:   Proposed Structure of ANN based RAS

The most common type of artificial neural network consists of three groups, or layers, of units: a layer of "input" units is connected to a layer of "hidden" units, which is connected to a layer of "output" units.

- The activity of the input units represents the raw information that is fed into the network.

- The activity of each hidden unit is determined by the activities of the input units and the weights on the connections between the input and the hidden units.

- The behavior of the output units depends on the activity of the hidden units and the weights between the hidden and output units.

This simple type of network is interesting because the hidden units are free to construct their own representations of the input. The weights between the input and hidden units determine when each hidden unit is active, and so by modifying these weights, a hidden unit can choose what it represents.

To make a neural network that performs some specific task, we must choose how the units are connected to one another, and we must set the weights on the connections appropriately. The connections determine whether it is possible for one unit to influence another. The weights specify the strength of the influence. We can teach a three-layer network to perform a particular task by using the following procedure also shown in Figure 6.5:

1. We present the network with training examples, which consist of a pattern of activities for the input units together with the desired pattern of activities for the output units.

133

2. We determine how closely the actual output of the network matches the desired output.

3. We change the weight of each connection so that the network produces a better approximation of the desired output.
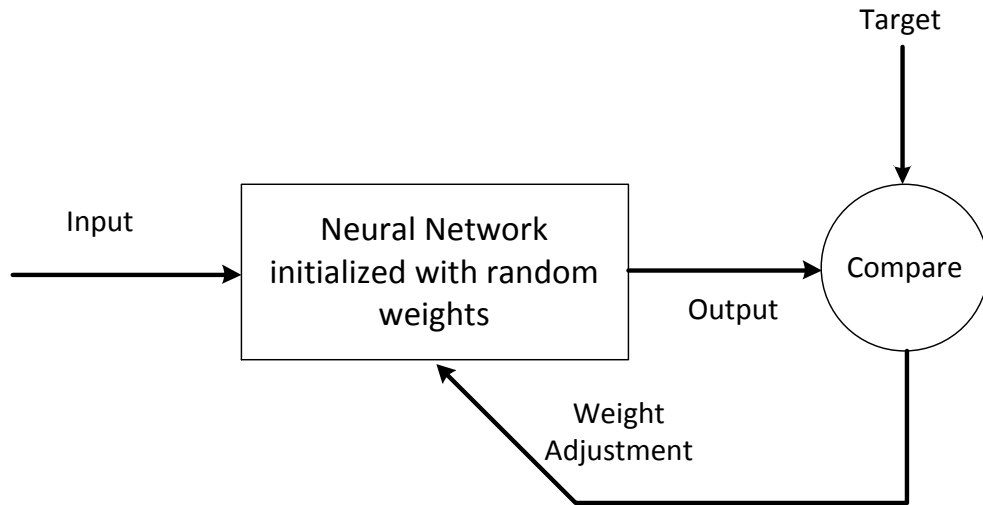
Figure 6.5:   Back error propagation algorithm

One way to change the weight is to use the Back-propagation algorithm which is described below, and has become nowadays one of the most important tools for training neural networks.

6.1.1 Back-propagation Algorithm

There is a real number associated with each connection, which is called the weight of the connection. We denote by W_{ij} the weight of the connection from unit u_i to unit u_j. It is then convenient to represent the pattern of connectivity in the network by a weight matrix W whose elements are the weights W_{ij}. Two types of connection are usually distinguished: excitatory and inhibitory. A positive weight represents an excitatory

connection whereas a negative weight represents an inhibitory connection. The pattern of connectivity characterizes the architecture of the network.

A unit in the output layer determines its activity by following a two-step procedure.

First, it computes the total weighted input x_j, using the formula:

$$X_j = \sum_i y_i W_{ij} \tag{6.1}$$

where y_i is the activity level of the jth unit in the previous layer and W_{ij} is the weight of the connection between the ith and the jth unit.

Next, the unit calculates the activity y_j using some transfer function of the total weighted input. The most commonly used transfer function is sigmoid function given as

$$y_j = \frac{1}{1 + e^{-x_j}} \tag{6.2}$$

Once the activities of all output units have been determined, the network computes the error E, which is defined by the expression:

$$E = \frac{1}{2} \sum_i (y_i - d_i)^2 \tag{6.3}$$

where y_i is the activity level of the ith unit in the top layer and d_i is the desired output of the ith unit.

Now the back-propagation algorithm is given as

1. Compute how fast the error changes as the activity of an output unit is changed. This error derivative (*EA*) is the difference between the actual and the desired activity.

$$EA_j = \frac{\partial E}{\partial y_j} = y_j - d_j \qquad (6.4)$$

2. Compute how fast the error changes as the total input received by an output unit is changed. This quantity (*EI*) is the answer from step 1 multiplied by the rate at which the output of a unit changes as its total input is changed.

$$EI_j = \frac{\partial E}{\partial x_j} = \frac{\partial E}{\partial y_j} \times \frac{\partial y_j}{\partial x_j} = EA_j y_j (1 - y_j) \qquad (6.5)$$

3. Compute how fast the error changes as a weight on the connection into an output unit is changed. This quantity (EW) is the answer from step 2 multiplied by the activity level of the unit from which the connection emanates.

$$EW_{ij} = \frac{\partial E}{\partial W_{ij}} = \frac{\partial E}{\partial x_j} \times \frac{\partial x_j}{\partial W_{ij}} = EI_j y_j \qquad (6.6)$$

4. Compute how fast the error changes as the activity of a unit in the previous layer is changed. This crucial step allows back propagation to be applied to multilayer networks. When the activity of a unit in the previous layer changes, it affects the activation of all the output units to which it is connected. So to compute the overall effect on the error, we add together all these separate effects on output units. But each effect is simple to calculate. It is the answer in step 2 multiplied by the weight on the connection to that output unit.

136

$$EA_i = \frac{\partial E}{\partial y_i} = \sum_j \frac{\partial E}{\partial x_j} \times \frac{\partial x_j}{\partial y_i} = \sum_j EI_j W_{ij} \qquad (6.7)$$

By using steps 2 and 4, we can convert the EAs of one layer of units into EAs for the previous layer. This procedure can be repeated to get the EAs for as many previous layers as desired. Once we know the EA of a unit, we can use steps 2 and 3 to compute the EWs on its incoming connections.

6.1.2 Stages needed to build an ANN predictor

Following are the stages required generally to build any ANN. Each of the stage has its own importance and are briefly described for transient instability prediction algorithm for WSCC 3 machine 9 bus test system.

Stage 1 (Input Selection)

Before designing and deciding for the inputs of the prediction algorithm it is essential to know the location of PMUs in the system. For this purpose initially the PMU placement algorithm is applied as described in chapter 3) but with generator buses or buses directly connected to the generator as must place buses. For SPEA algorithm application on WSCC 3 machine 9 bus test system, the parameters chosen are N_{pop} = 20, N_{DES} = 10, P_{CROSS} = 0.8 and P_{MUT} = 0.01. The application of SPEA algorithm on WSCC 3 machine 9 bus test system results in a Pareto front as shown in Figure 6.6. Table 6.2 tabulates the results extracted from the Pareto front. It can be seen in Table 6.2 that the system can be fully observed with 3 number of PMUs in the system with the location specified in Table 6.2.
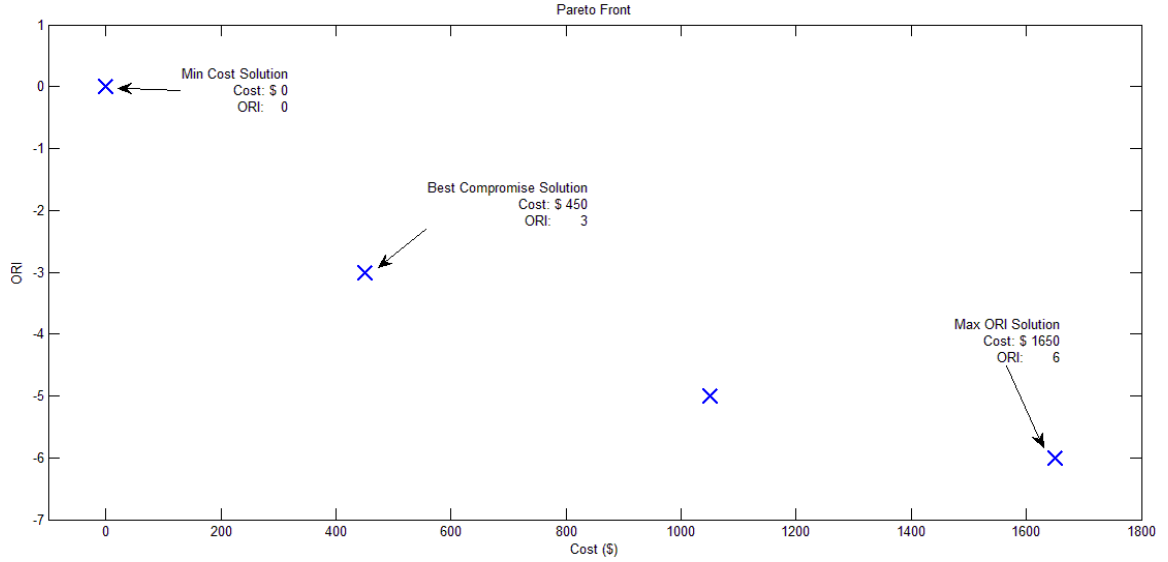
Figure 6.6:   Pareto front for WSCC 3 machine 9 bus test system

TABLE 6.2:   OPP FOR WSCC 3 MACHINE 9 BUS TEST SYSTEM

PCROSS	PMUT	NPMU	Location	ORI
0.8	0.01	3	4,7,9	3

Using the features of the ANN and location of PMUs from the OPP as described above a transient instability predictor is proposed. In this study the algorithm for online determination of instability employs the separation of angle between the generator buses and center of angle of the system. The center of angle of a system is defined as

$$\delta_{COA} = \frac{\sum_{i=1}^{N_G} \delta_i H_i}{\sum_{i=1}^{N_G} H_i} \qquad (6.8)$$

where

N_G :   Number of generators in the system

138

δ_i :   Rotor angle of the machine i (degrees/radians)

H_i :   Per unit Inertia constant of machine i ($MJ/_{MVA}$)

To decide whether a generator is stable or unstable, the hybrid classifier given in equation (5.5), repeated here for the reader convenience, is used to classify the generator as stable or unstable.

$$\eta_i = \frac{180 - |\theta_i|}{180 + |\theta_i|} \tag{6.9}$$

The value of η_i varies from -1 to 1. For a stable system $\eta_i \geq 0$ for $i = 1, \dots, N_G$.

The input data is based on number of phasor measurements cycles window, which begins after the fault clearing. In this study as a method of demonstration a window of 6 cycle i.e. 0.1 sec for 60 Hz, is selected. As the location of PMUs are directly connected to the generator therefore, generator rotor angle can be directly measured. The difference of the generator rotor angle and the center of angle after the fault clearance for 6 cycles serves as the input for the ANN.

Stage 2 (Selection of Training Data)

After the input selection stage, it is necessary to collect the data for training. This data should be accurate and vast enough to cover all the possible operating points of the systems. In this study, fault on each bus is simulated from 0.01 sec to 5 sec one at a time. A training pair, i.e. each generator rotor angle difference from center of angle for 6 cycles after the fault clearance and stability status of the system, is formed. A total of 1200 pairs were formed and presented to ANN as training and validation data.

Stage 3 (Selection of ANN Size)

The next stage in the ANN development is the selection of layers and neurons in the hidden layer. There is no hard and fast rule for the size of ANN. Generally we start from a small number of hidden neurons and one hidden layer, if these number of neurons are sufficient to produce desired performance, it is accepted; otherwise the number of neurons or number of layers are increased until the desired performance is achieved by the network.

In this study, a 3 layered ANN is used after extensive trails as shown in Figure 6.7. The first hidden layer consist of 6 neurons with sigmoid transfer function, the second hidden layer consist of 3 hidden neurons with sigmoid transfer function whereas the output layer consist of 2 hidden neuron with pure linear transfer function. Again, for the selection of type of neuron there is no criteria defined, rather it is dependent on the user and application.

The output of the ANN selected, is the stability status, given by neuron 1 in the output layer. Its value varies as follows

0 → System is stable after fault clearing

1 → System is unstable after fault clearing

The detailed connections for each layer is given in Figure 6.8 - Figure 6.13
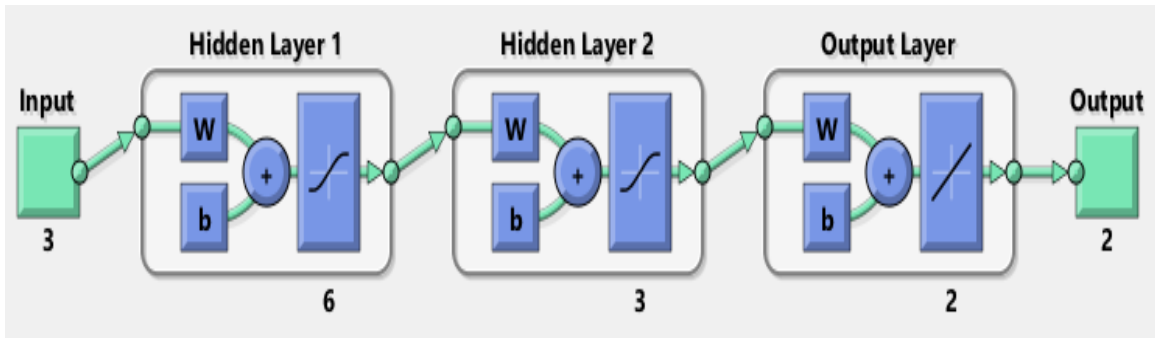
Figure 6.7:   Neural Network Architecture for proposed transient instability predictor.
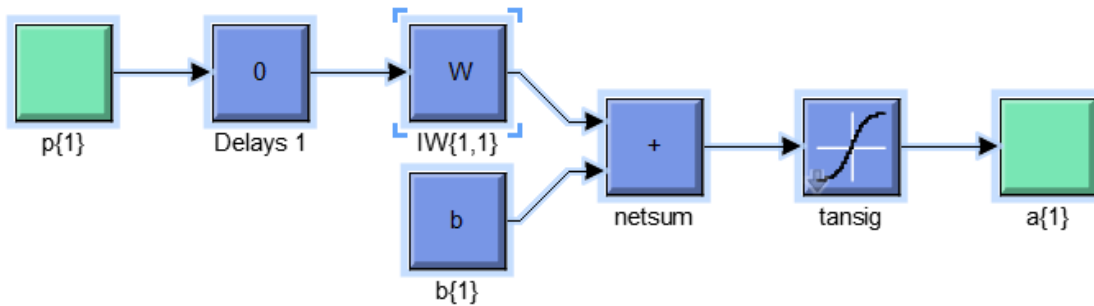
Figure 6.8:   Layer 1 details
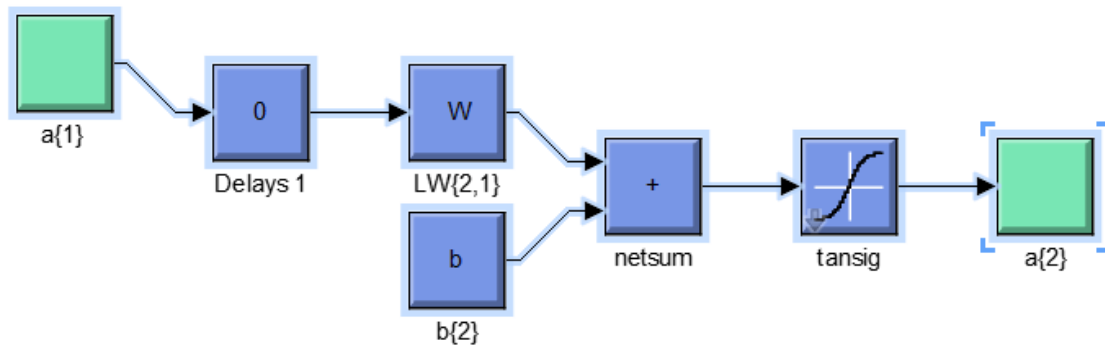
Figure 6.9:   Layer 2 details
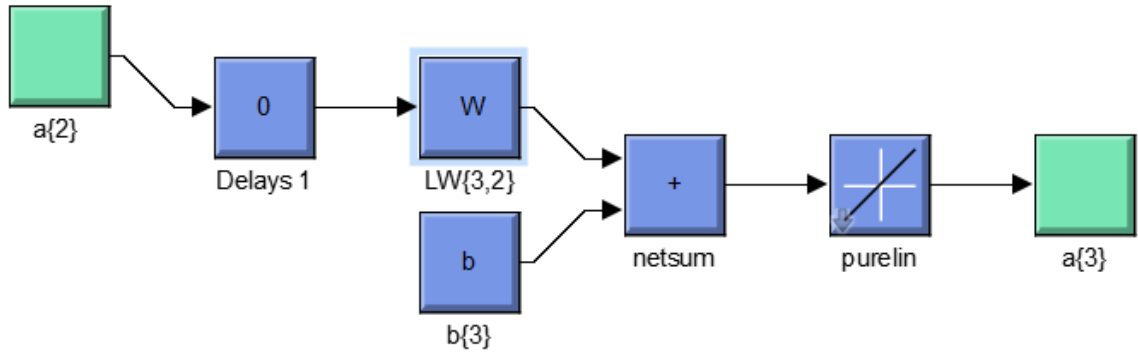
Figure 6.10:   Layer 3 details
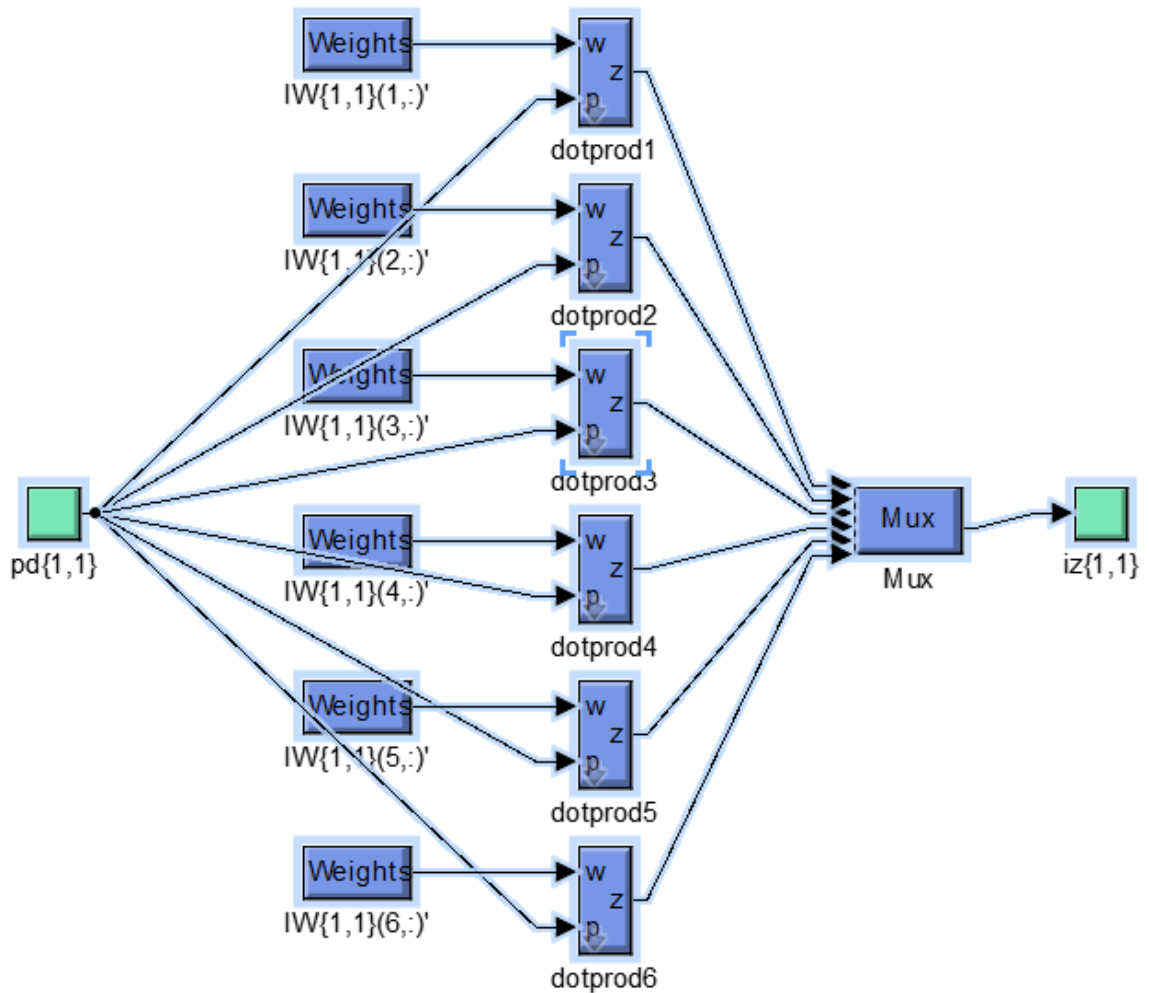
Figure 6.11:   Layer 1 weight connections details
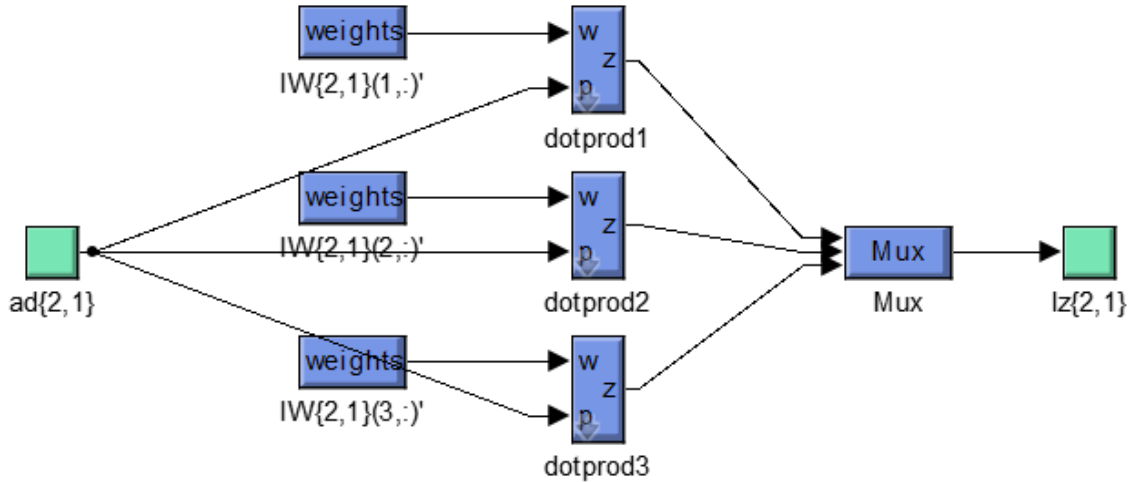
Figure 6.12:   Layer 2 weight connections details
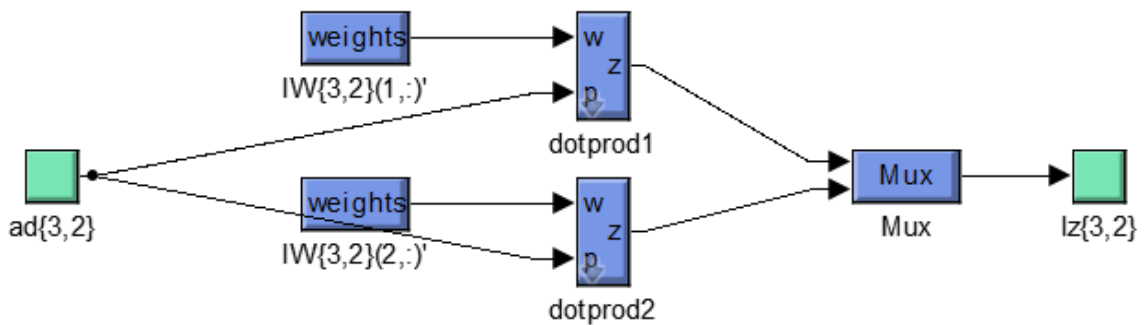
Figure 6.13:   Layer 3 weight connections details

Stage 4 (Train ANN)

The next stage in the development of ANN is the training of ANN from the data collected in the previous stage. The MATLAB Neural Network Toolbox is used for designing and training the ANN. For training, the back propagation algorithm as described in the previous section is used in this study, in order to minimize the mean square error (MSE) between the output produced by the . Out of total 1200 cases, 70% are selected randomly for training whereas 30% leftover cases are used in validation and testing in order to

143

terminate the training when the termination criteria is met. The minimum MSE achieved for this case is 0.012 at 82nd iteration as shown in Figure 6.14. It is worth mentioning that in back propagation algorithm each iteration is called as Epoch.
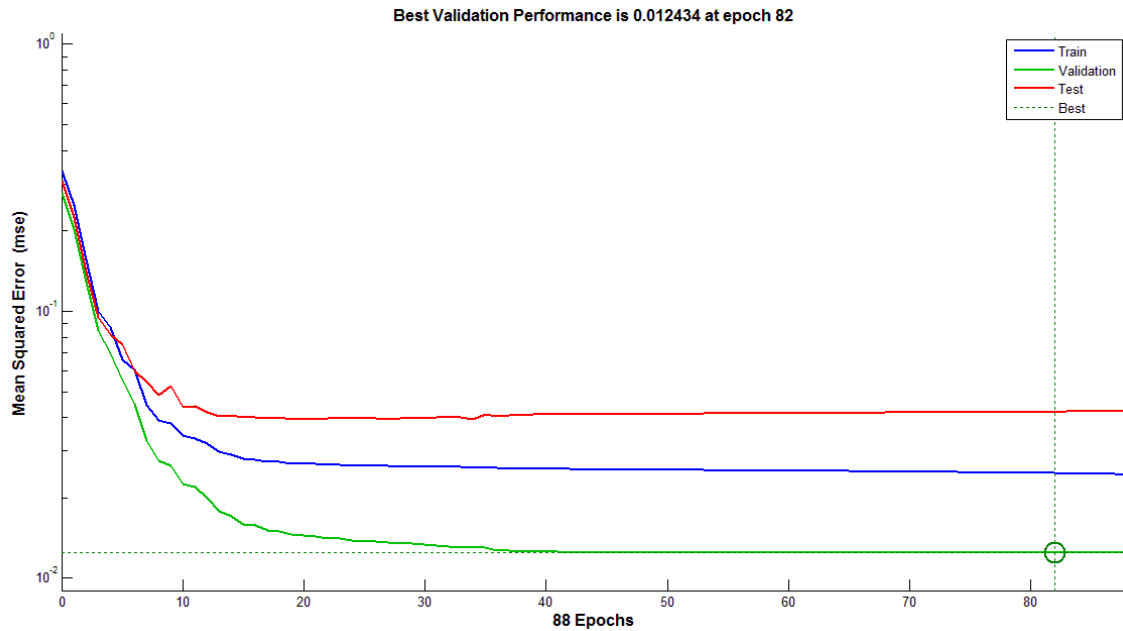
Figure 6.14:   Performance of proposed ANN based predictor

Stage 5 (Tests and result comparison)

To test the proposed ANN for performance authenticity, faults on bus 7 and bus 9 are applied with line 5-7 and line 6-9 clearance respectively. For each of the fault a stable and unstable case is presented to the system which was not there in the training. Figure 6.15 shows the time domain simulation result for a stable case with fault on bus 7 with line 5-7 cleared, whereas Figure 6.16 shows the ANN output for the same case. It can be seen in Figure 6.16 that the output produced by ANN is very near to zero declaring the system to be stable which complements with the time domain simulation result shown in Figure 6.15. The reason that the ANN doesn't produce exactly zero

144

being, the ANN utilized in here is a function approximator rather than a classifier, therefore as the system moves towards instability the value of the output grows and become nearly equal to 1 when the system is unstable. This is shown in Figure 6.17 and Figure 6.18, which presents an unstable case for fault at bus 7. As discussed the ANN output again complements the time domain simulation declaring the system as unstable by producing an output very near to 1. Similarly, for bus 9 a stable case with ANN output is shown in Figure 6.19 and Figure 6.20 respectively, whereas for unstable case for bus 9 are presented in Figure 6.21 and Figure 6.22.
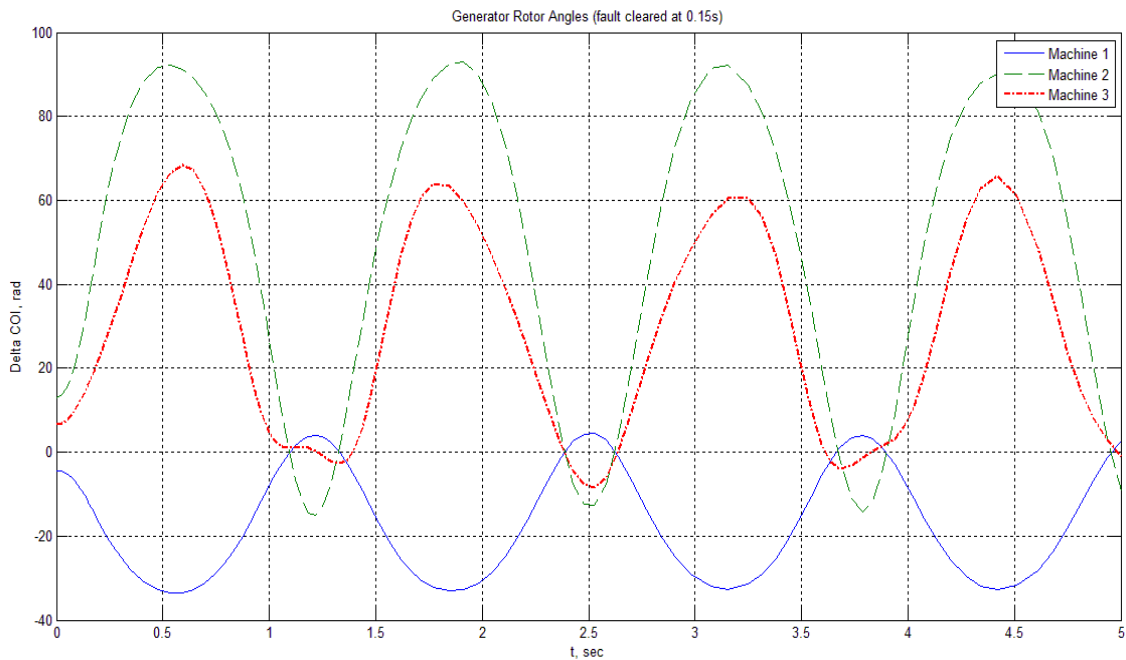
Figure 6.15:   Time domain simulation for stable case for fault at bus 7
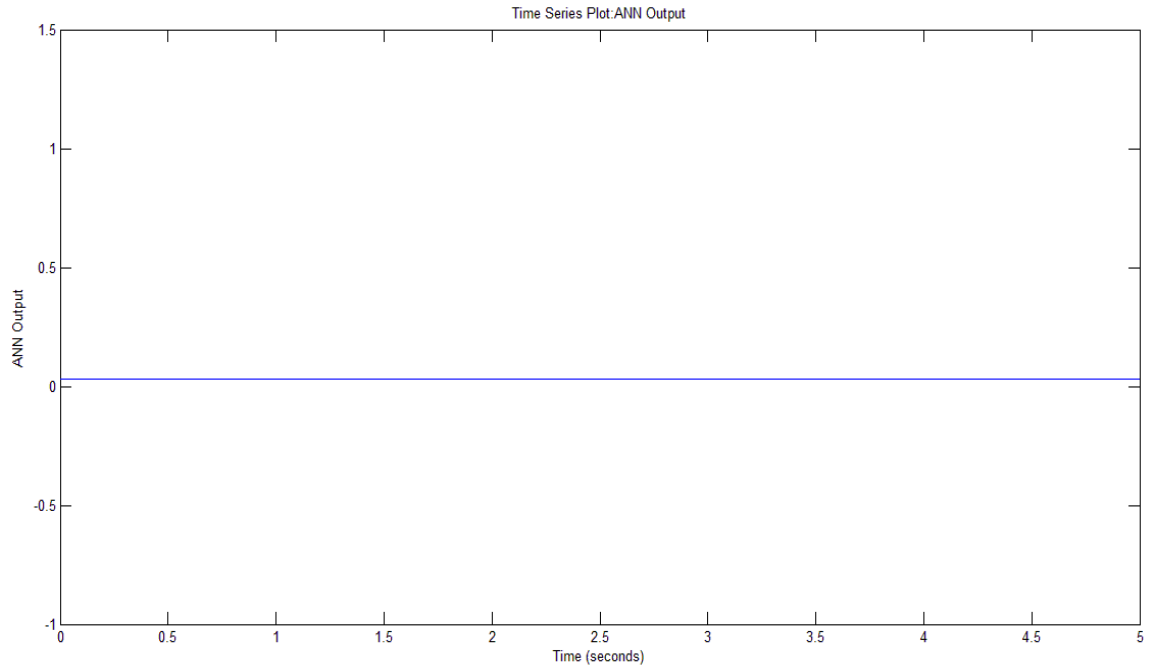
Figure 6.16:   ANN output for stable case for fault at bus 7
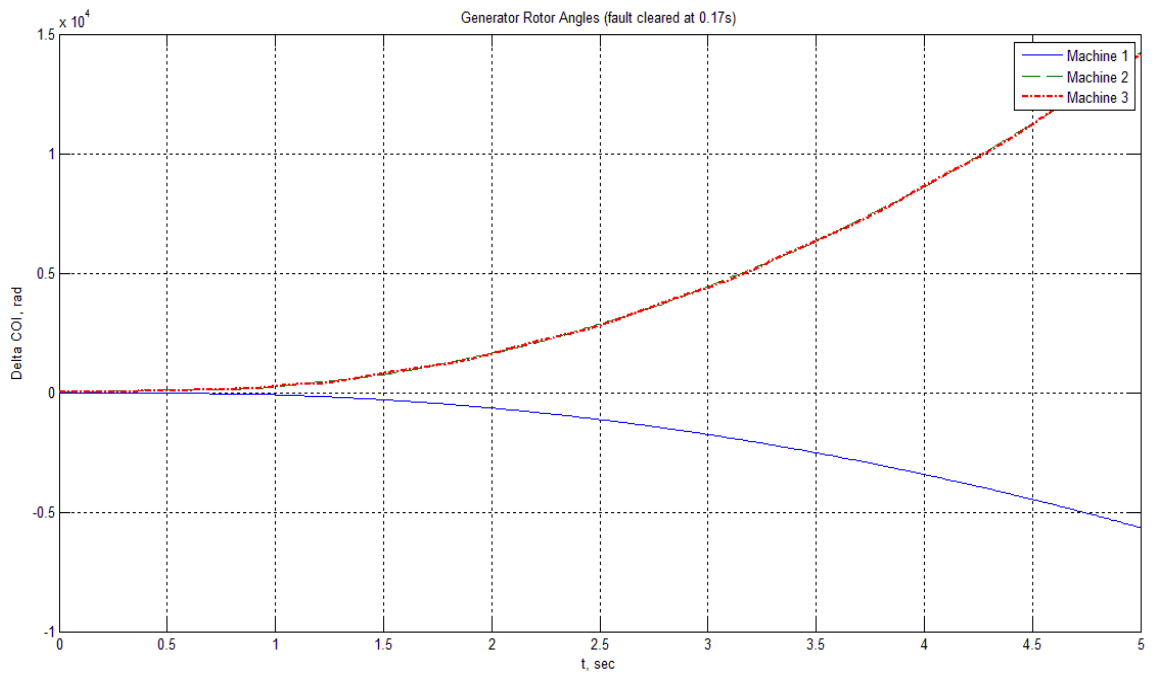
Figure 6.17:   Time domain simulation for unstable case for fault at bus 7

146
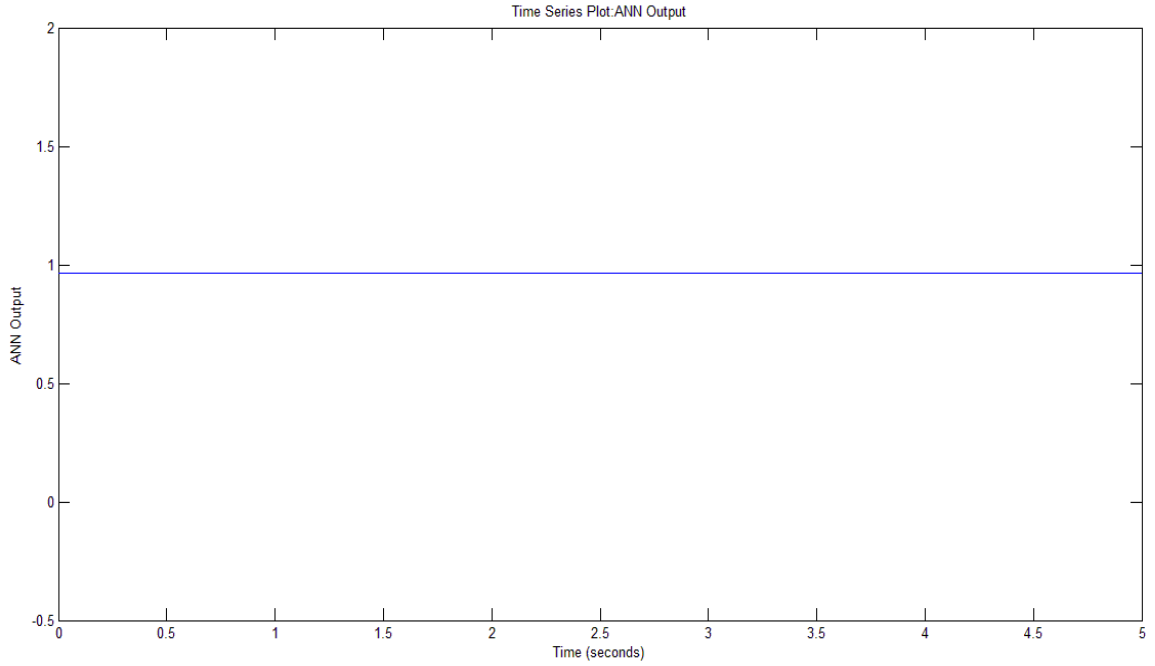
Figure 6.18:   ANN output for stable case for fault at bus 7
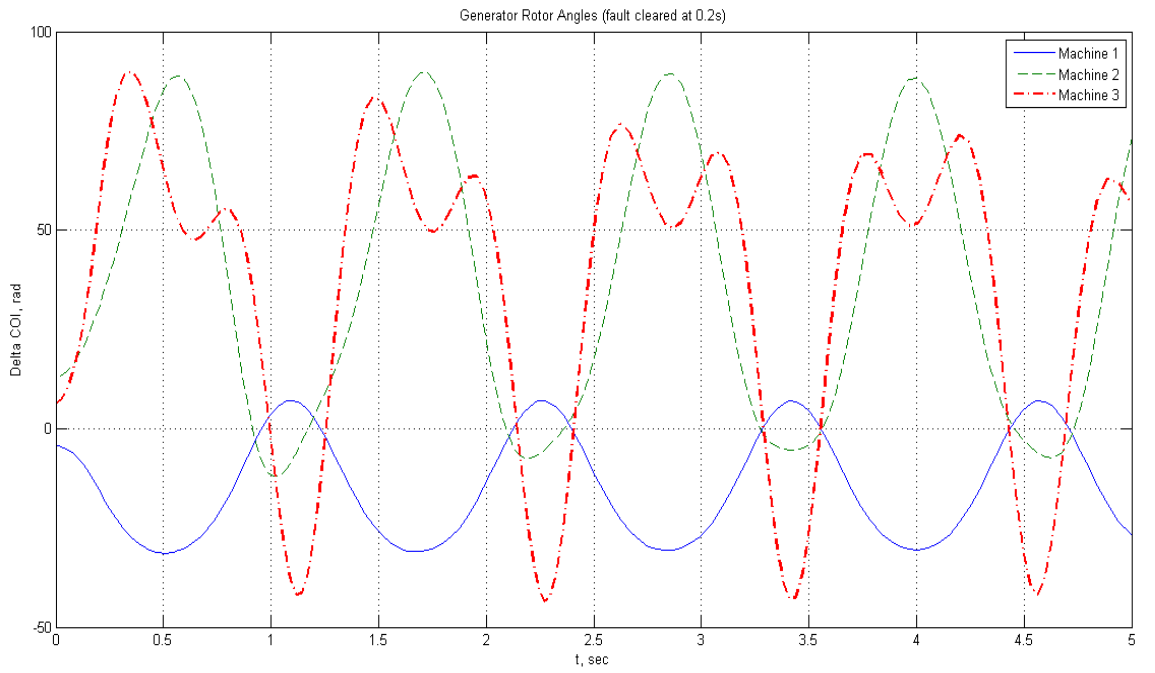
Figure 6.19:   Time domain simulation for stable case for fault at bus 9

147
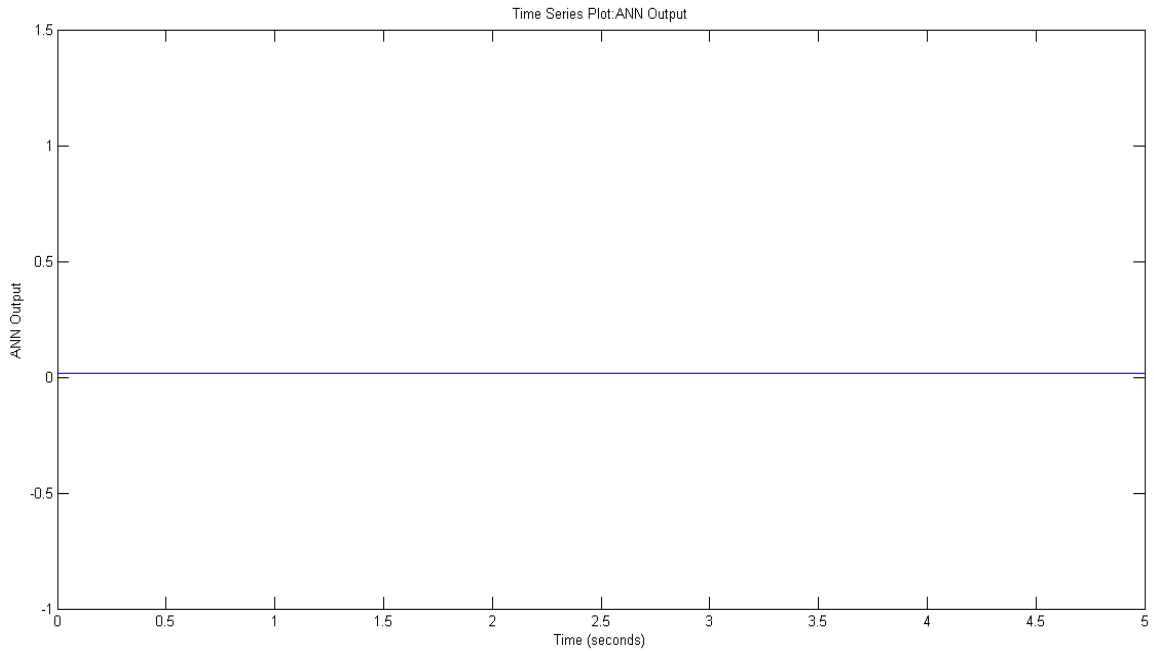
Figure 6.20:   ANN output for stable case for fault at bus 9
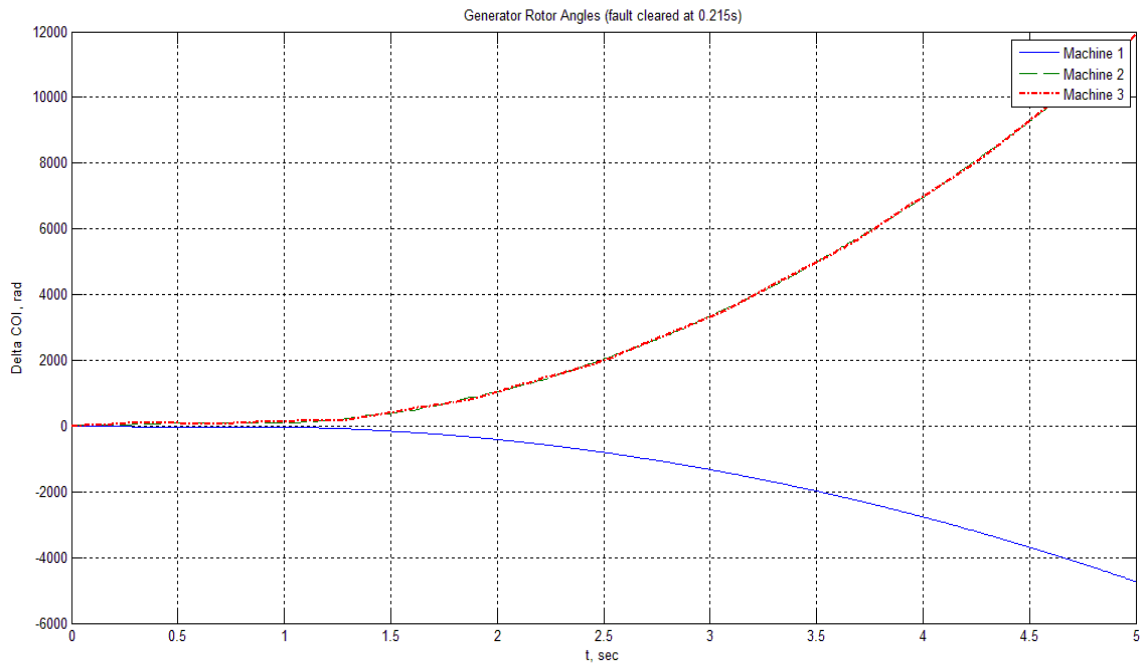
Figure 6.21:   Time domain simulation for unstable case for fault at bus 9
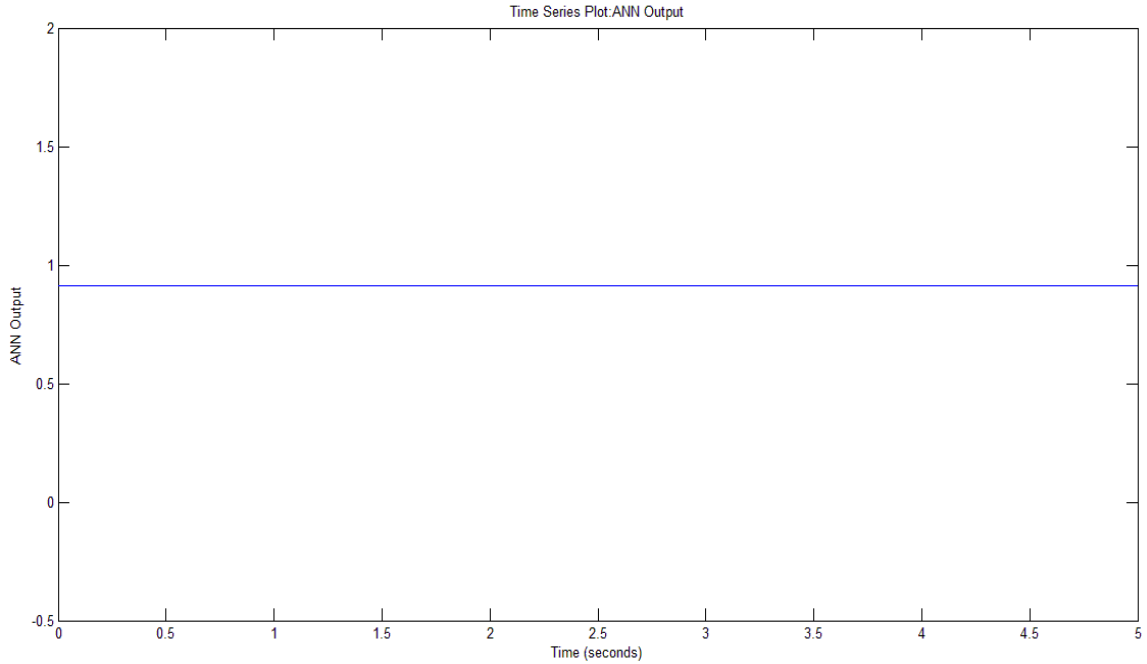
Figure 6.22:   ANN output for stable case for fault at bus 9

6.2   Remedial Action Schemes

Based on the output produced by the ANN based transient instability predictor the Remedial Action Schemes can be armed and if needed can take action against the detected instability. These schemes include generator tripping, islanding, braking resistor insertion and under frequency or under voltage load shedding. As a method to demonstrate the power of PMUs in the application of these schemes only braking resistor and under frequency load shedding schemes are designed and applied in this study. Each of the RAS counter one type of instability; braking resistor counters the over frequency which occurs in case of faults or load loss, whereas under frequency load shedding (UFLS) counters the under frequency occurred due to generation loss or load addition. Each of the scheme is applied on WSCC 3 machine 9 bus test system and developed on

SIMULINK for simulation purposes and is experimentally implemented on RTDS and SEL SYS-310 with power hardware in loop PMUs.

6.2.1   Braking Resistor Scheme

This scheme as name depicts is insertion of a dummy load or often called as *Braking resistor* in case the machines' speeds in system goes beyond a certain set point. It is regarded as helpful tool in damping the transient energies injected as a result of large disturbances in the system. Usually modelled as a shunt load and is connected directly to the generator terminal, this is the point where the effectiveness of this resistor is maximum. The duty of these resistors are generally small ranging from 2 cycles to 10 cycles limited by the thermal properties of the material from which the resistor is made up of. Some of the practical implementation includes the Peace river system, the four corner plant of the Arizona Public Service Company and the BPA. The insertion criteria of these resistor is done on the basis of open loop and pre specified control strategies. Different models, simulation and theories have been in reported in also on different test systems.

In this study the dynamic braking scheme is applied on WSCC 3 machine 9 bus test system. It is assumed that only generator number 2 and generator number 3 are equipped with braking resistors as from the analysis of WSCC 3 machine 9 bus test system, it is found that these two are most prone to instability. The effect of different values of braking resistors and their duty cycles are evaluated and optimal size and switching duty is found after analysis.

Figure 6.23 shows the WSCC 3 machine 9 bus test system with two braking resistor installed as mentioned earlier. The location of the PMUs come from the OPP problem solution as depicted in the previous section. As per the introduction of PMUs in section previous sections the frequency information is directly embedded into the data packet. Using this feature of the PMUs a braking resistor switching scheme is designed on the basis of machines' speed.
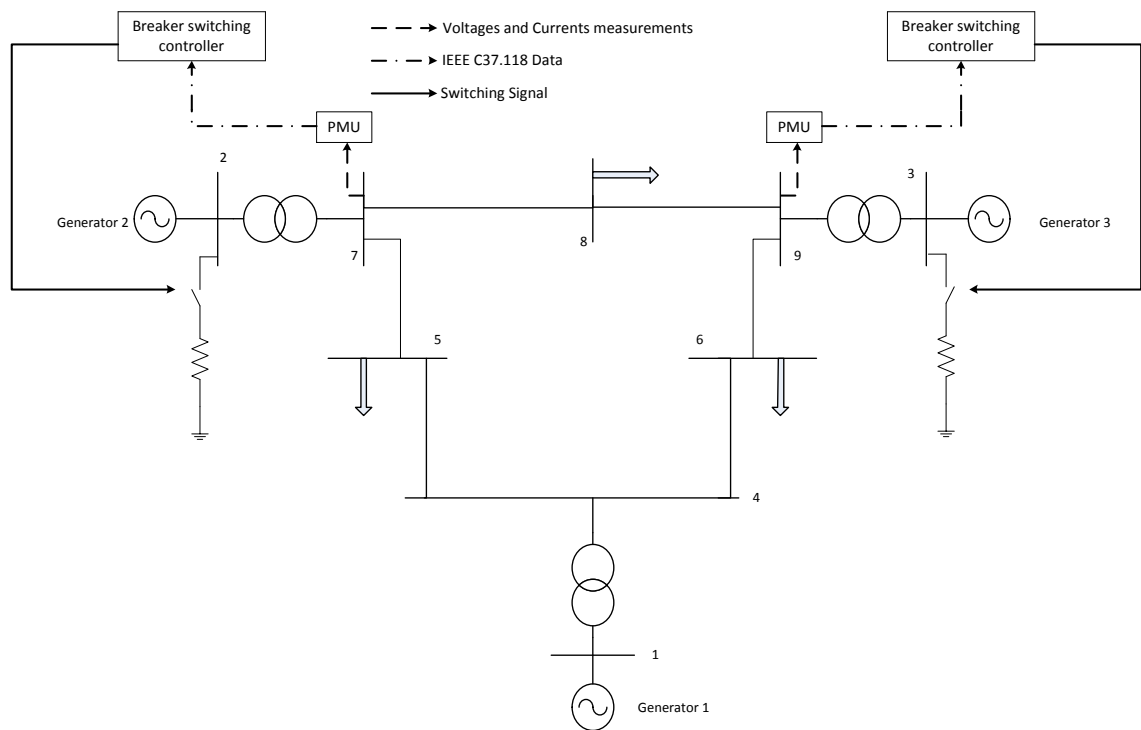
Figure 6.23:   Proposed PMU based braking resistor scheme

Figure 6.24 shows the PMU based algorithm for the breaking resistor insertion in case of over frequency. If a fault is applied and the ANN based predictor, predicts the instability in the system, the RAS will be armed or enabled. Once armed, the PMU measurements from the system are made available to the controller. The scheme to switch the resistor used in this study makes use of the frequency of the bus which is apparently the machine

frequency to which the bus is directly connected. If during the fault the frequency of the machine surpasses a certain set point i.e. 60.5 Hz in this study, the resistor is switched in. The switching frequency of the resistor is decided by a pulse generator connected directly to the breaker of the resistor. After fault is cleared which can easily be detected by the fault currents or the line switching, a delay of 6 cycles is introduced before the frequency is rechecked. If the maximum frequency during this window is less than the set point i.e. 60.5 Hz, the arming signal is disabled otherwise the resistor keep on switching until the frequency is under 60.5 Hz. This kind of scheme allows the resistor only to be switched when there are large transient energies injected in the system as a result of large faults or disturbances.
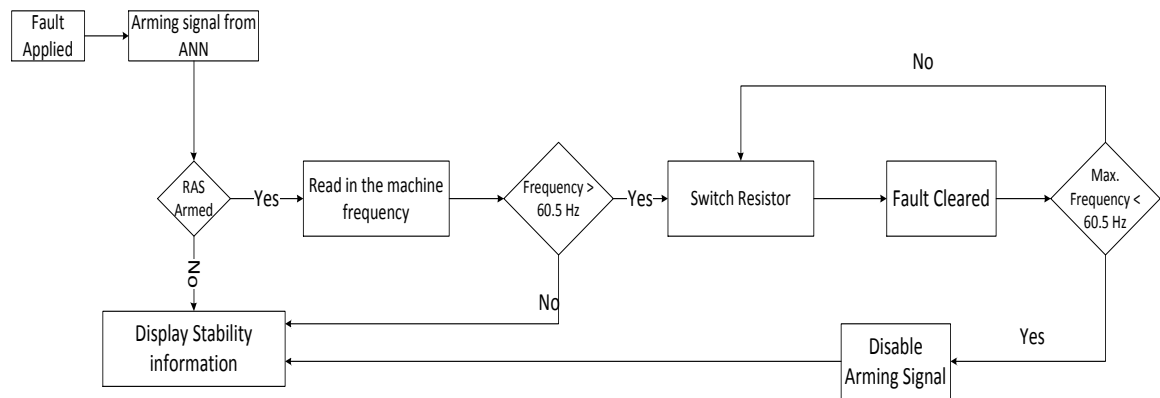
Figure 6.24:   Proposed braking resistor switching scheme

6.2.2 Results

Three different sizes of resistors that are 50, 100 and 150 MW with three different switching duties namely. 2, 4 and 6 cycle switching are applied on generator 2 and 3. For each of the generator the severest of the fault i.e. fault on generator bus is simulated and effect of braking resistor is seen. Table 6.3 and Table 6.4 tabulates the improvement in the CCT for two different faults when the each resistor is switched individually the faults being, fault on bus 7 with line 5-7 clearance and fault on bus 9 with line 6-9 clearance. It can be seen that when the braking resistor at generator number is only allowed to switch as per the proposed scheme, the CCT for the fault increases as the resistor size and switching cycle increase. The maximum improvement in the CCT is there when 150 MW resistor is switched at a duty (on-off) of 6 cycle. This is reasonable, as the inertia of machine 2 is large more energy i.e. longer switching is required, to prevent the machine from speeding up in case of fault

TABLE 6.3:   CCT COMPARISON FOR FAULT AT BUS 7 AND RESISTOR AT GENERATOR 2 ONLY

Switching Duty *Size (MW)*	*CCT without braking resistor (sec)*	*CCT for 2 cycles (sec)*	*CCT for 4 cycles (sec)*	*CCT for 6 cycles (sec)*
50		0.1941	0.1965	0.2014
100	*0.1834*	0.2037	0.2049	0.2064
150		0.2104	0.2111	0.2140

TABLE 6.4:   CCT COMPARISON FOR FAULT AT BUS 9 AND RESISTOR AT GENERATOR 3 ONLY

Switching Duty Size (MW)	CCT without braking resistor (sec)	CCT for 2 cycles (sec)	CCT for 4 cycles (sec)	CCT for 6 cycles (sec)
50		0.2513	0.2501	0.2497
100	0.2480	0.2595	0.2525	0.2517
150		0.2636	0.2618	0.2613

From Table 6.4, it can be seen that when the resistor at generator 3 is allowed to switch only, the CCT of the fault improves with increase in size of the resistor but decreases with the increase in the switching duty. This physically can be interpreted as the machine 3 is the lightest in the system so relatively small switching duties are sufficient to prevent it from over speed. A longer switching duty in this case with decrease the speed too much and in turn will depreciate the stability of the system.

From the CCT analysis it is found that the optimal size of the resistor at bus number 2 is 150 MW with an optimal switching duty of 6 cycles whereas for the resistor at generator 3 has an optimal size of 150 MW with 2 cycle switching frequency. To these optimal sizes and switching duties, the resistors are allowed to switch simultaneously on the application of fault with proposed switching scheme. Table 6.5 shows the improvement in CCT of fault at bus 7 with line 5-7 clearance and fault at bus 9 with line 6-9 clearance when the resistors are allowed to switch simultaneously.

CCT for fault at bus 7 with line 5-7 cleared		CCT for fault at bus 9 with line 6-9 cleared	
Without resistor	Optimal size and switching	Without resistor	Optimal size and switching
0.1834	0.2149	0.2480	0.2649

Finally, Figure 6.25 - Figure 6.34 shows the comparison of system rotor angle trajectories for the system without resistor and with resistor as tabulated in Table 6.3, Table 6.4 and Table 6.5. It can clearly be seen that braking resistor serves as an effective tool in mitigating the instabilities of the system.
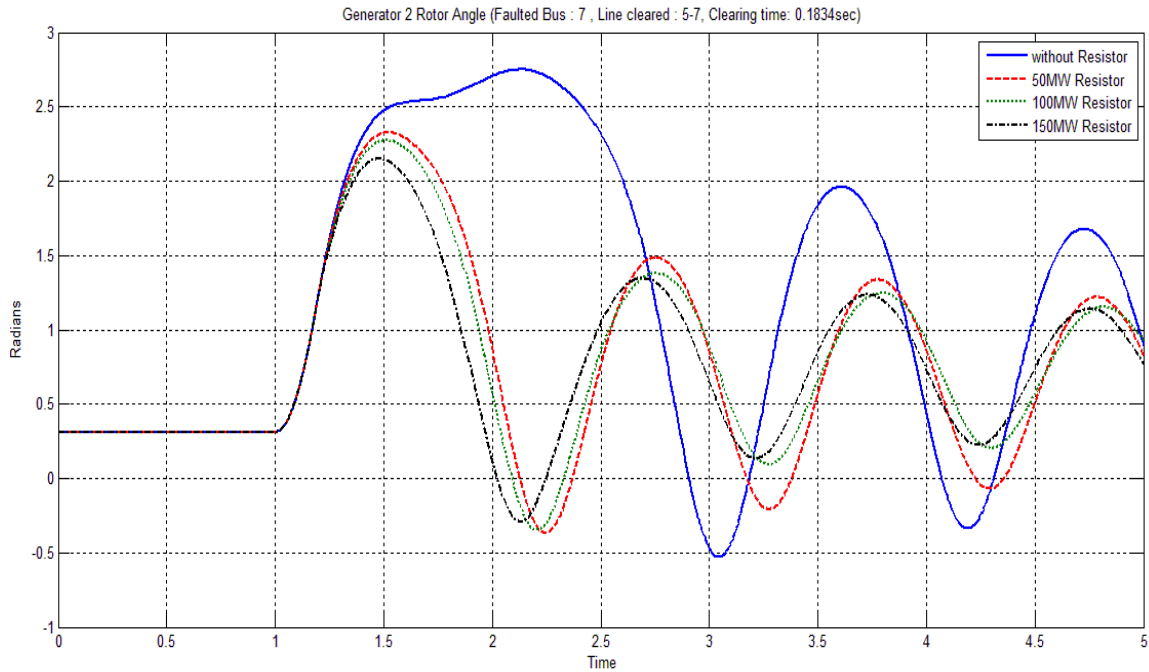
Figure 6.25: Rotor angle response for generator 2 for individual resistor switching at 2 cycle switching frequency.

155
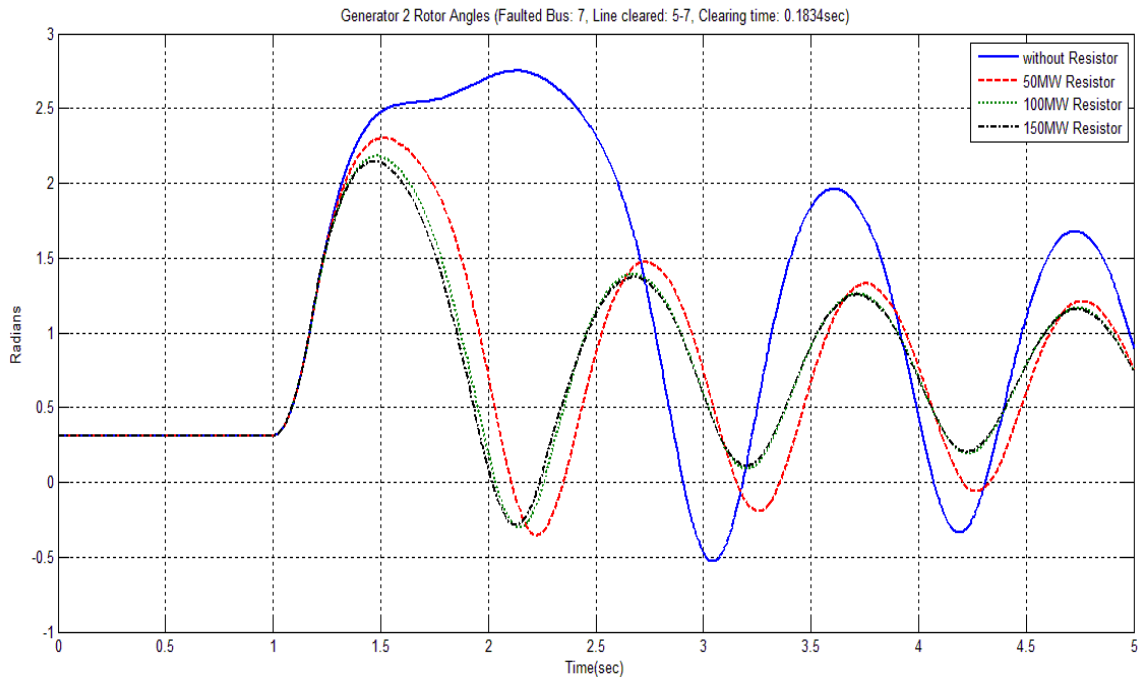
Figure 6.26:   Rotor angle response for generator 2 for individual resistor switching at 4 cycle

switching frequency.
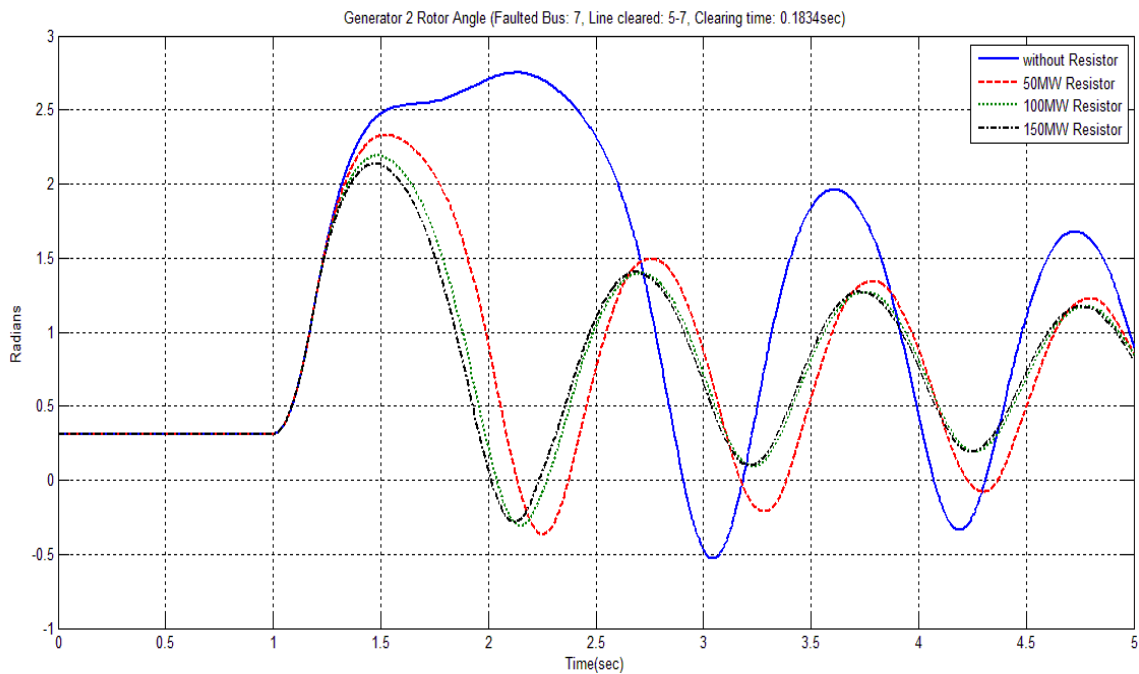
Figure 6.27:   Rotor angle response for generator 2 for individual resistor switching at 6 cycle

switching frequency.
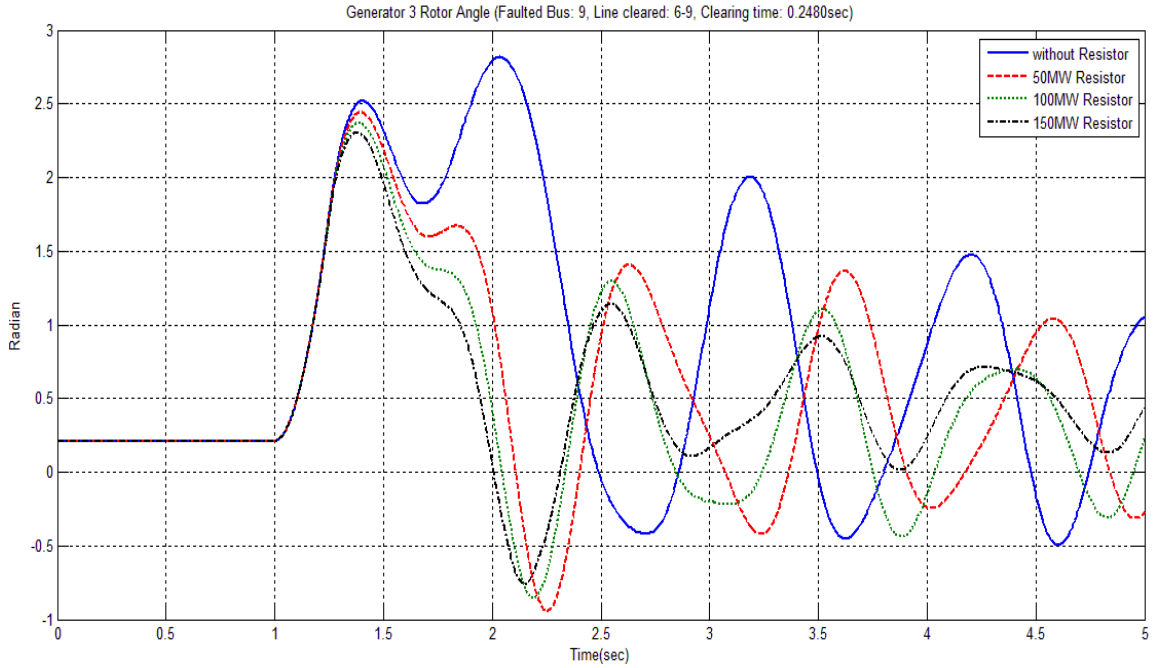
Figure 6.28:   Rotor angle response for generator 3 for individual resistor switching at 2 cycle

switching frequency.
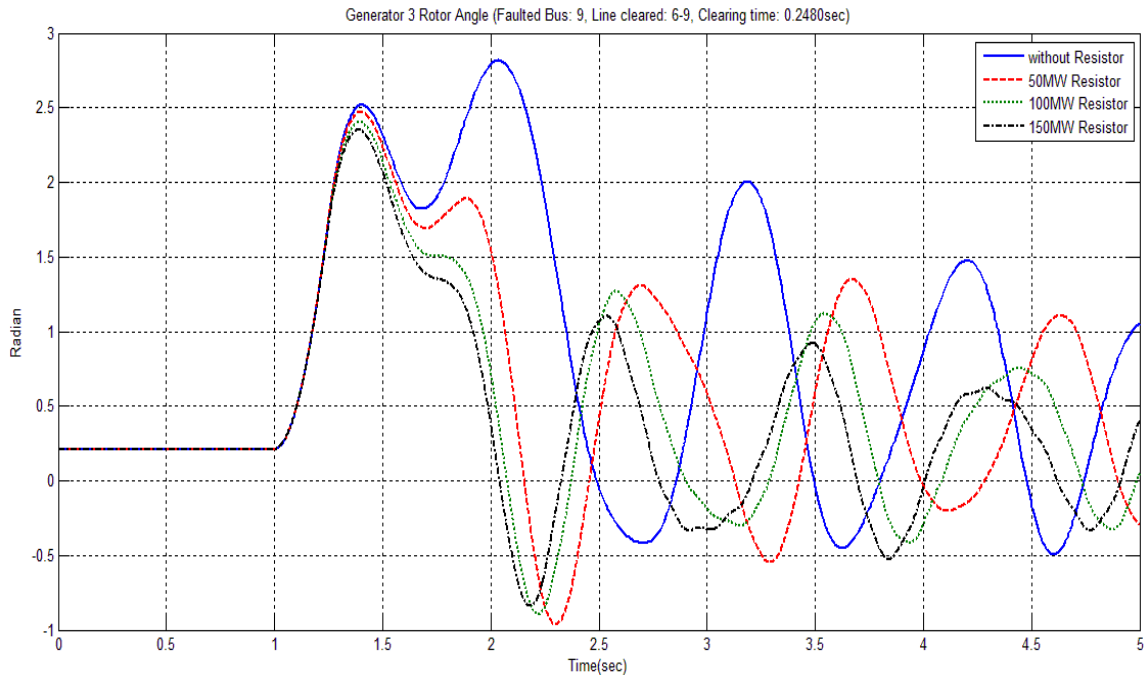
Figure 6.29:   Rotor angle response for generator 3 for individual resistor switching at 4 cycle

switching frequency.

157
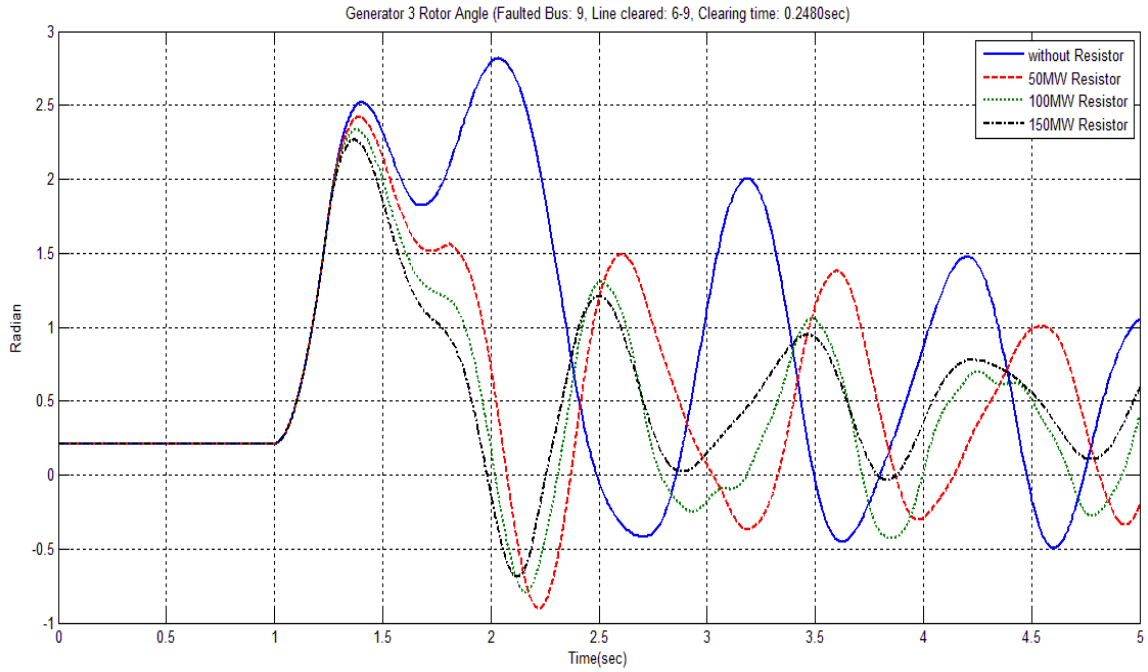
Figure 6.30:   Rotor angle response for generator 3 for individual resistor switching at 6 cycle

switching frequency.
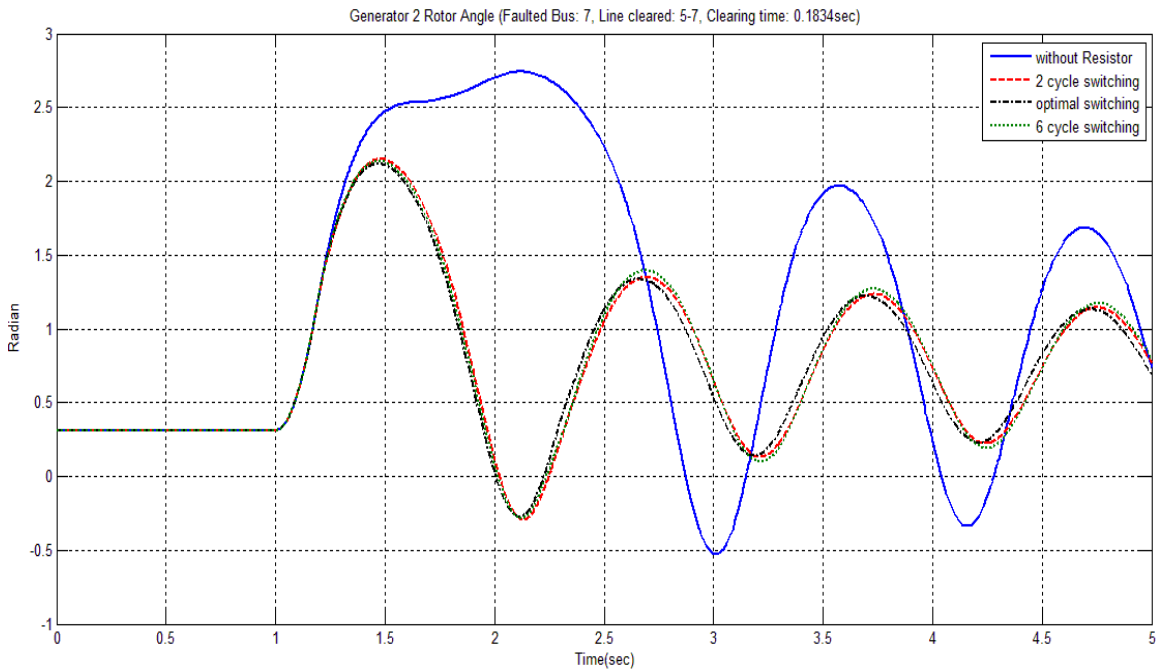
Figure 6.31:   Rotor angle response for generator 2 for optimal and simultaneous switching for
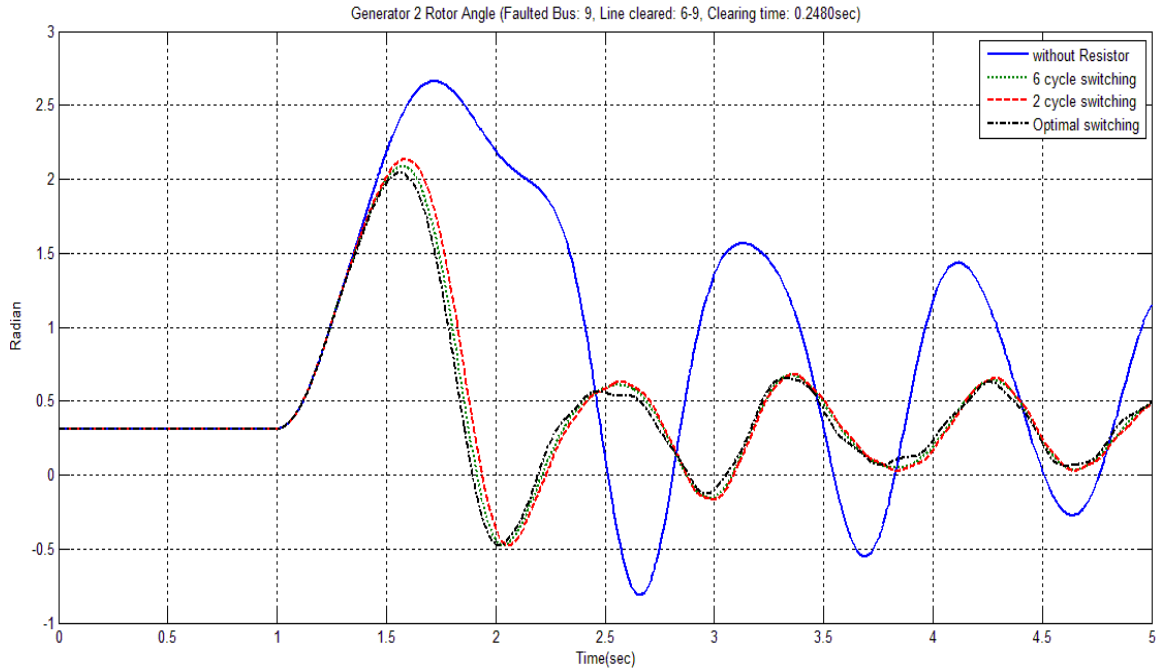
fault at bus 7

Figure 6.32:   Rotor angle response for generator 2 for optimal and simultaneous switching for
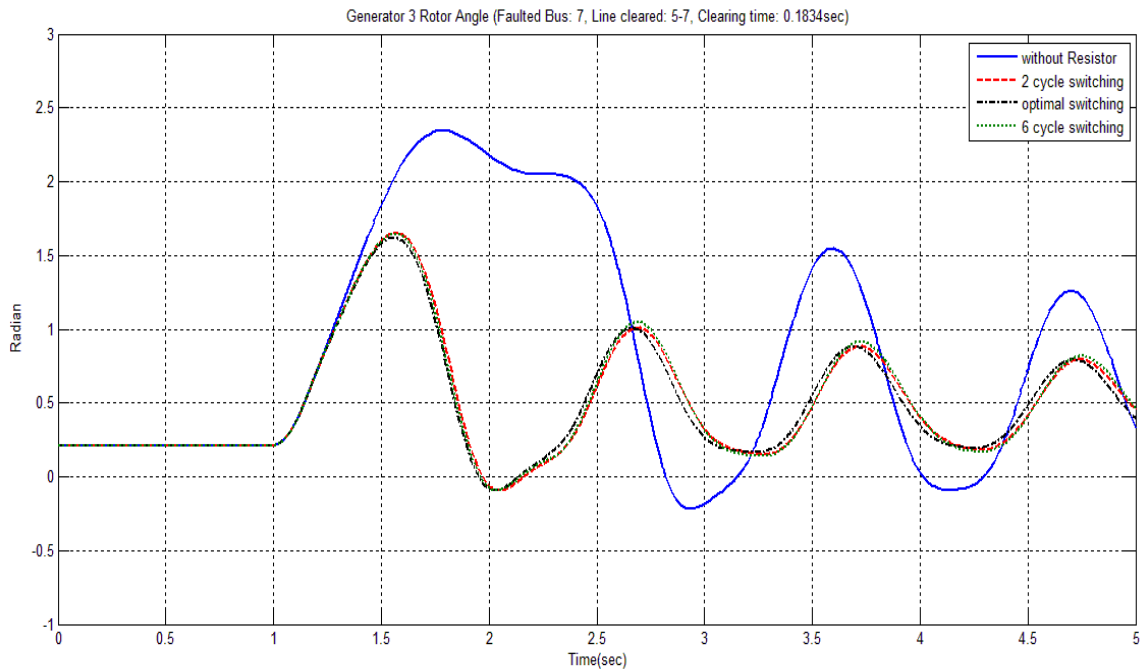
fault at bus 9

Figure 6.33:   Rotor angle response for generator 3 for optimal and simultaneous switching for
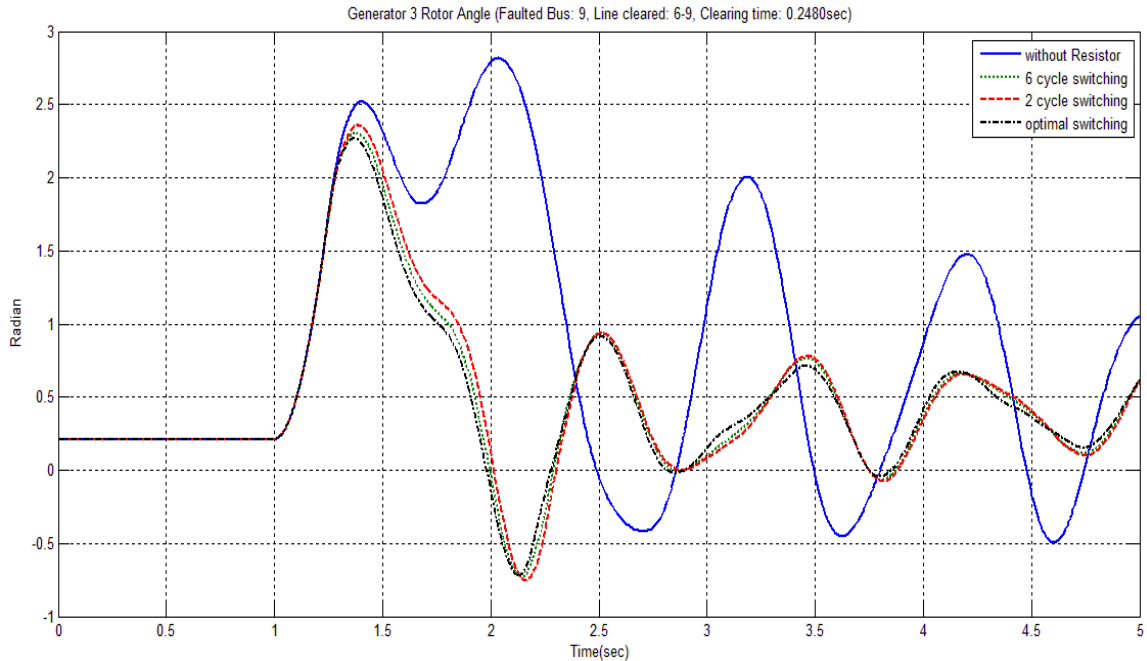
fault at bus 7

Figure 6.34: Rotor angle response for generator 3 for optimal and simultaneous switching for

fault at bus 9

6.2.3 Experimental validation of Braking Resistor Scheme

To verify the proposed braking resistor scheme experimentally, the WSCC 3 machine 9 bus test system is implemented on RTDS with governor and AVR models, whereas the proposed braking resistor controller is implemented on Synchrophasor Vector Processor (SVP). Figure 6.35 shows the connection details between RTDS and SVP.

Simulated Current Transformers (CTs) and Potential Transformers (PTs) are placed on bus 7 and bus 9 with in the RTDS as shown in Figure 6.36. These simulated CTs and PTs signals are sent out as analog outputs of ±10VDC range from GTAO card in the RTDS rack. These signals are then amplified by Doble Amplifier to an appropriate level for the PMUs i.e. currents are converted to a range of ±1-5Amperes AC and voltages are converted to ±110 -150Volts AC. As shown in Figure 6.35 there are two PMUs in the system which are connected to a GPS clock.

160
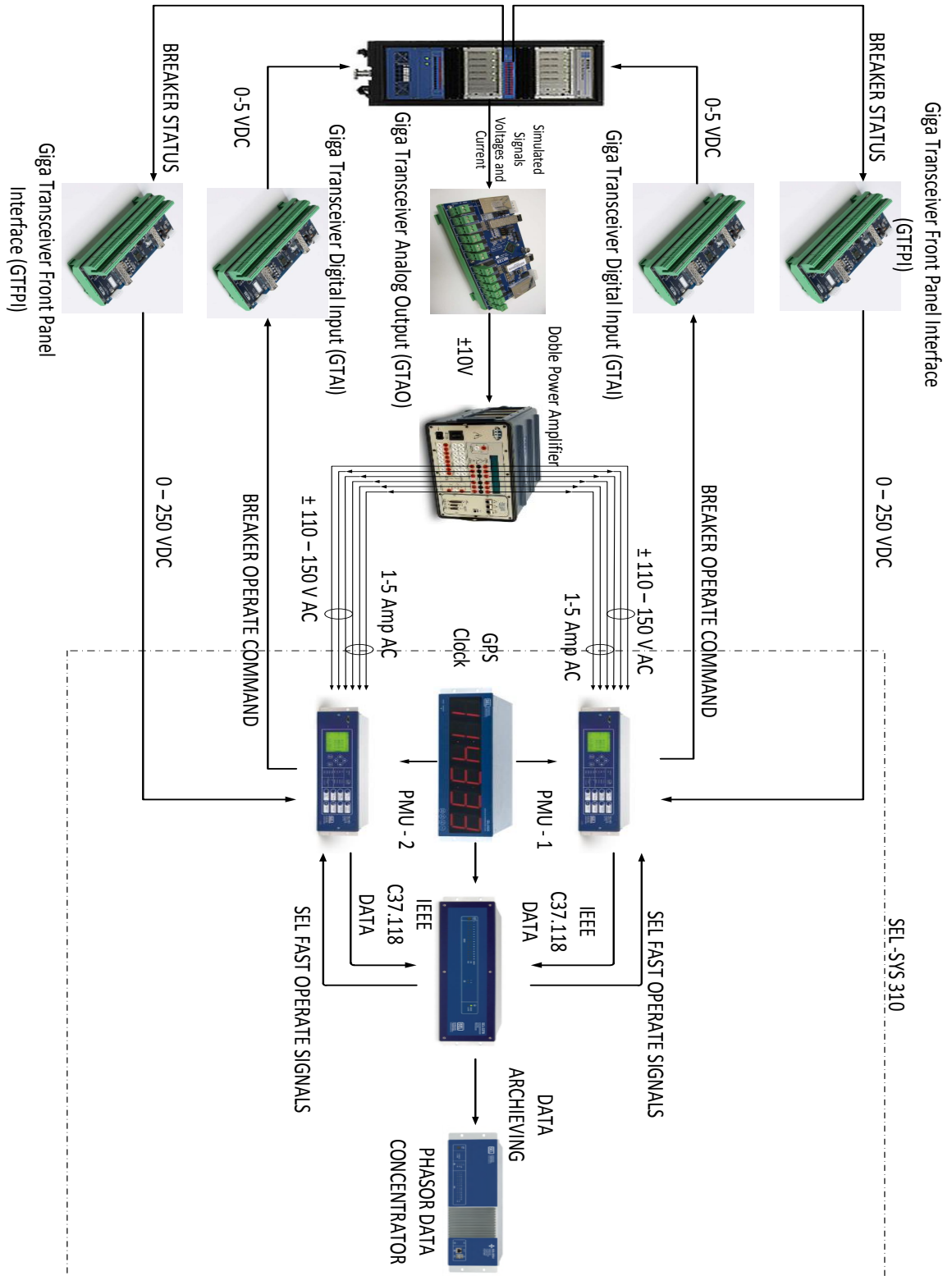
Figure 6.35:   RTDS and SYS-310 interconnection details
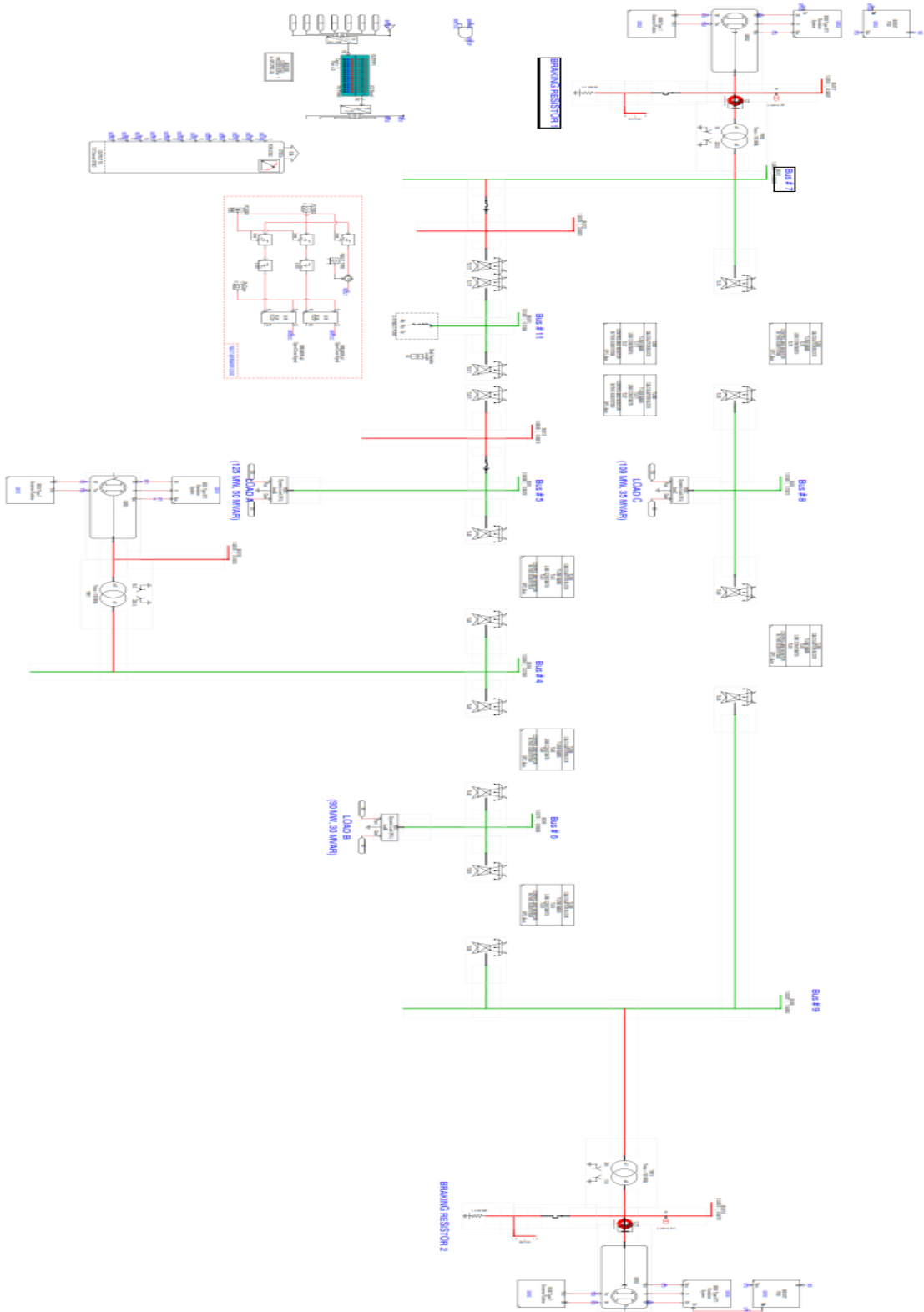
Figure 6.36:   RTDS Implementation of WSCC 3 Machine 9 Bus Test System with braking

resistors.

These PMUs reads in the voltages and currents from the amplifier and convert these measurements into standard IEEE 37.118C data. This data is then transferred to SVP which is the heart of processing in this scenario. SVP is a specialized hardware from SEL Inc. that allows the use of synchronized phasor measurements (synchrophasor) for real-time power system monitoring, control, and protection. The SEL-3378 acquires and time correlates synchrophasor data from various Phasor Measurement and Control Units (PMCUs). The SEL SVP combines the power of synchrophasor data processing with customizable programmable logic controller (PLC). SVP can be programmed by standard IEC 61131-3 programming languages. The controller proposed earlier is implemented on SVP in Continuous Flow Configuration language (CFC) shown in Figure 6.37.
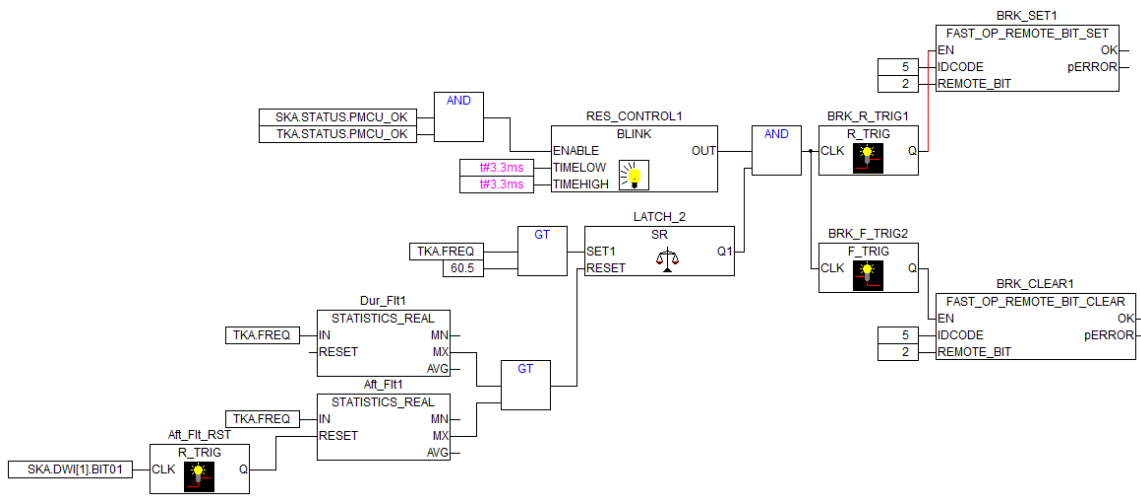
Figure 6.37:   SVP Implementation of proposed braking resistor controller

Again, the two faults namely, fault at bus 7 with line 5-7 clearance and fault at bus 9 with line 6-9 clearance are simulated on RTDS and the effects of proposed scheme is compared with the system without braking resistor. Only the optimal size and switching frequency is implemented to show the effectiveness of the proposed scheme in the presence of governor and AVR. The fault clearing time for each fault is the CCT of the

fault without the braking resistor. Figure 6.38 compares the speed of machine 2 for the system with and without resistor, for fault at bus 7. It can clearly be seen that not only the first swing peak is decreased with the application of braking resistor, but also the system is damped faster. In the case of machine 3 and fault at bus 7 as shown in Figure 6.39, the peak magnitude is the almost the same but first peak in case of system with braking resistor has appeared much earlier than the system without braking resistor, also in this case the system damping has also improved. Figure 6.40 and Figure 6.41 shows the comparison of speed of machine 2 and 3 respectively with fault at bus 9 with line 6-9 clearance. For this fault as well the system with braking resistor shows a better performance and highlights the effectiveness of proposed control scheme.
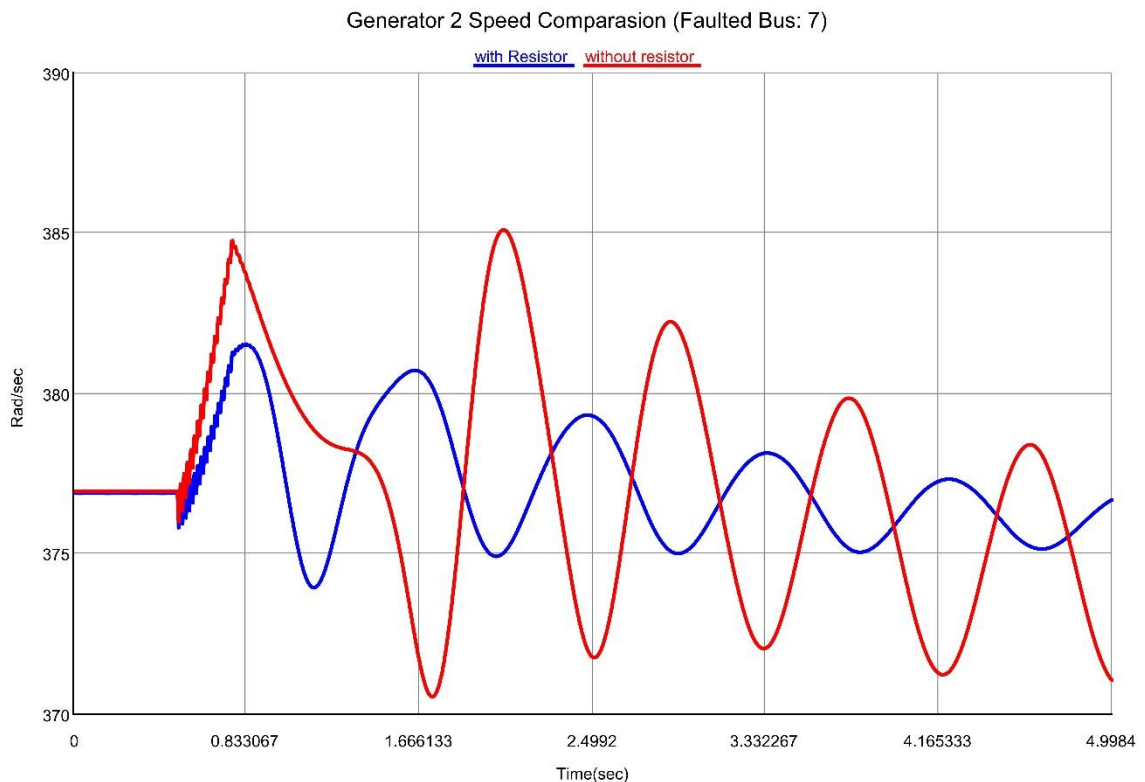
Figure 6.38:   Machine 2 Speed Comparison for fault at bus 7.
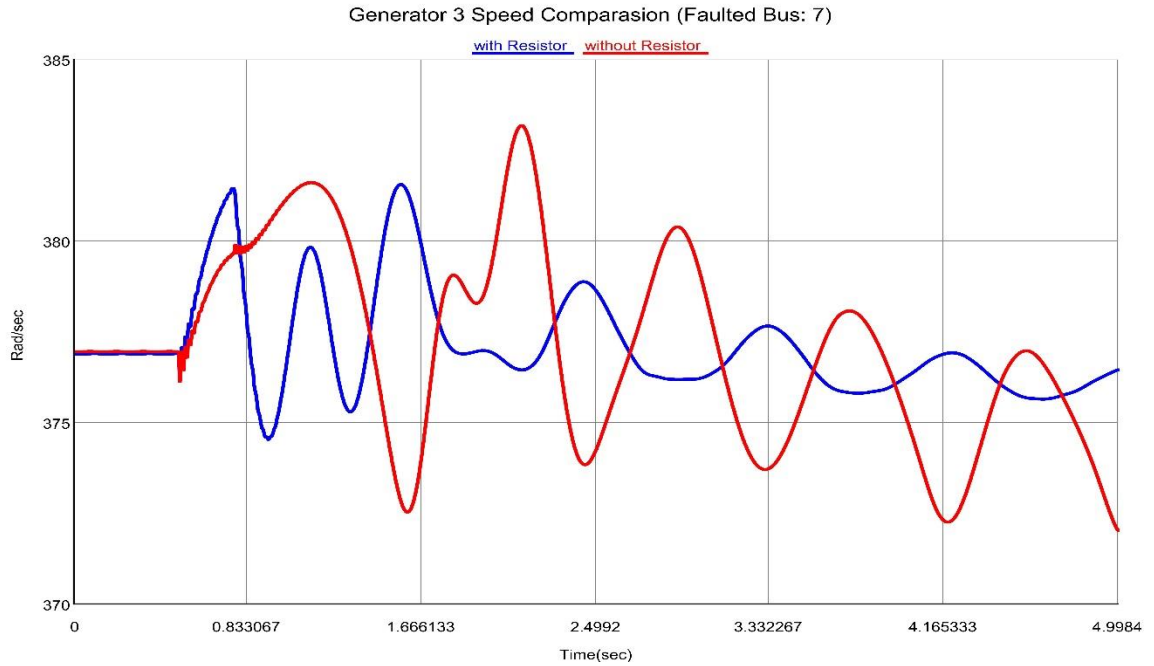
Figure 6.39:   Machine 3 Speed Comparison for fault at bus 7.
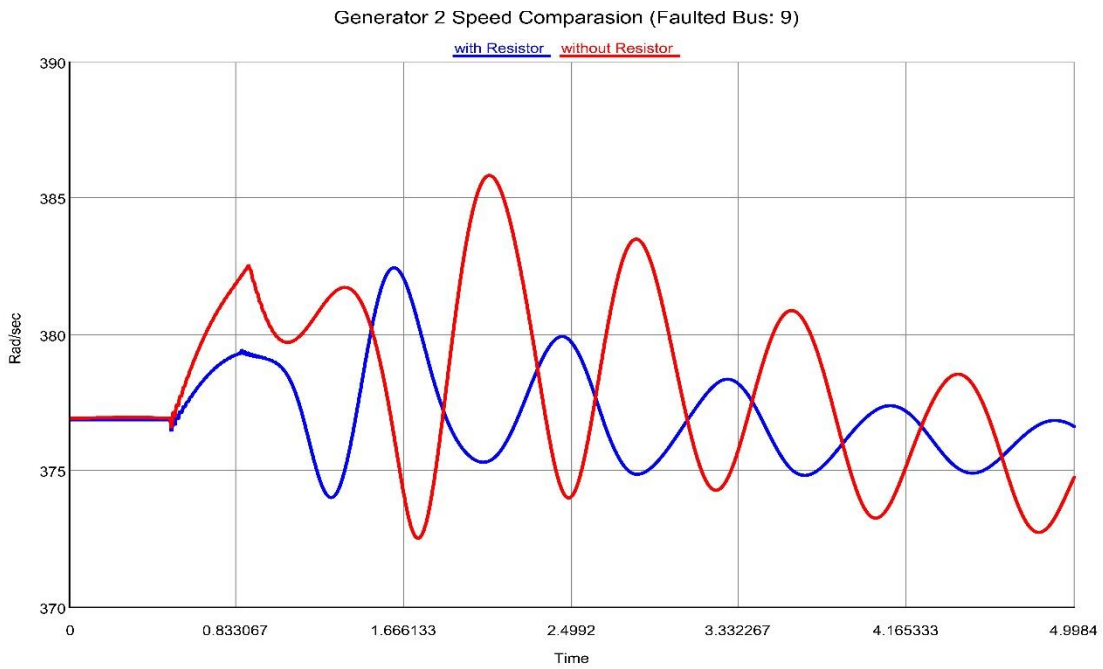
Figure 6.40:   Machine 2 Speed Comparison for fault at bus 9
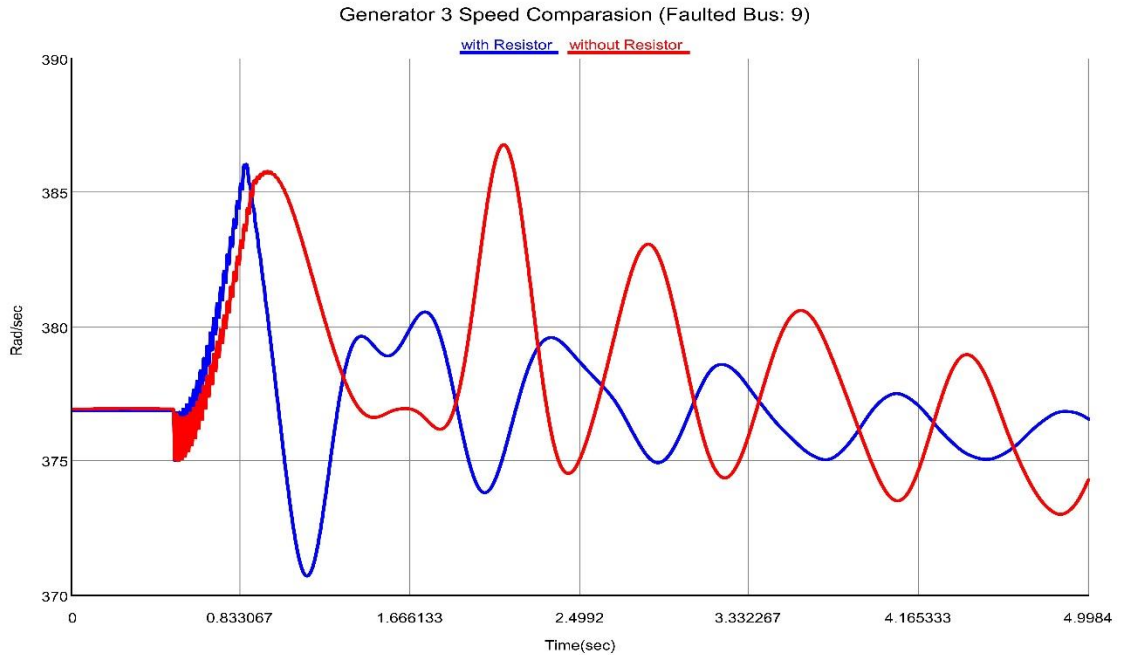
Figure 6.41:   Machine 3 Speed Comparison for fault at bus 9

6.2.4 Under frequency Load Shedding Scheme

On the occurrence of a transient disturbance such as generation loss or large load addition would cause the system frequency to decline due to the imbalance between generation and load. Whenever the state of the power system changes from normal operation to emergency under frequency conditions, *under frequency load shedding* (UFLS) becomes of extreme significance for restoring secure operation of power system. *UFLS* is simply a harmonized set of control measures which results in decrement of the electrical load and thus balancing the electrical and mechanical power of the machines. Therefore, whenever the system frequency falls below a pre-specified threshold, some part of the load should be disconnected or shed in a number of steps to restore the power balance. The reason behind the protection of system against under frequencies being if the generators in the system operate below its nominal speed at a decreased frequency, a

166

aggregated damage is produced on turbine generator shaft due to excessive vibrations [148], [149]. Table 6.6 shows the maximum allowable operating time for a machine at different levels of reduced frequencies [148], [149].

TABLE 6.6:   TYPICAL TIME LIMITS FOR THE OPERATION OF GENERATOR AT DECREASED FREQUENCY

Percentage of rated frequency at full load (%)	*Maximum permissible time (min)*
99.0	Continuous
97.3	90
97.0	10
96.0	1

For a generator, if the limits depicted in Table 6.6 are not observed and the frequency is not restored to its optimum operating point, the related generator is disconnected which leads to further imbalance of load and generation and in turn reduces the frequency further which may cause tripping of other generators in the system and at last through this cascaded tripping of generators the system encounter a blackout.

Deeming to the importance of encountering the under frequency in the system, a PMU based under frequency load shedding scheme is designed and implemented on the WSCC 3 machine 9 bus test system. The system is simulated and tested on SIMULINK and experimentally verified by implementation on RTDS and SYS-310.

Figure 6.42 shows the flow chart of the ULFS to be used in conjunction with ANN based transient instability detector.
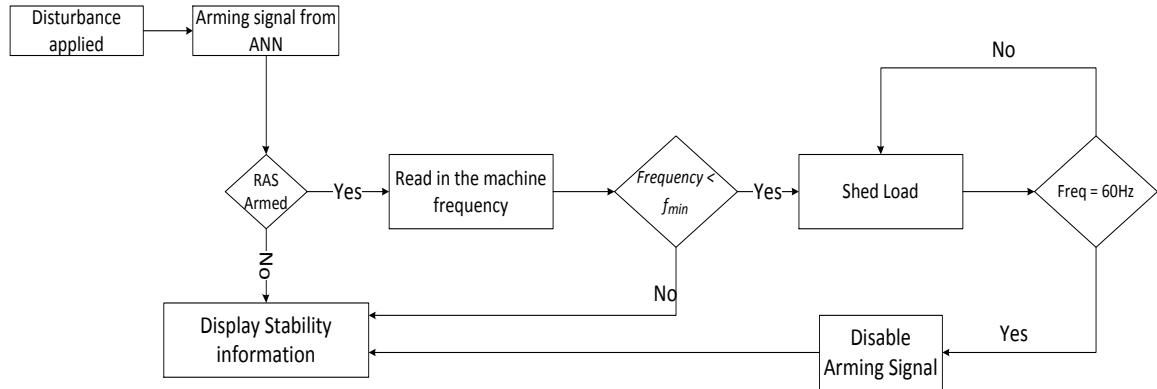
Figure 6.42:   Flow chart for under frequency load shedding

Design Steps for Under Frequency Load Shedding Scheme

1. First step towards the design of UFLS is the determination of anticipated overload. This is an important parameter for the representation of protection provided and the extent of service interrupted during the overloading event. The value of anticipated overload (p.u.) is calculated as

$$L = \frac{Total\ Load - Total\ Generation}{Total\ Generation} \qquad (6.10)$$

This parameter L is decided during the design phase. The physical interpretation of (6.10) can be, if the system is balanced then there will be no overload. However, due to a fault or any other disturbance a loss of 33% of total generation will lead to 50% overload, similarly a loss of 50% generation will result in a 100% overload. The value of anticipated overload is kept between 10-40% and a value over 50% is not recommended due to possible over shedding in case of

small magnitude of disturbance. In this study the anticipated overload is taken to 30% [150].

2. Second step involves the determination of number of steps required for the load shedding. Typically the number of these steps vary from three to six [148]. The UFLS instigated in this work involves 4 steps, with steps of 20%, 20%. 30% and 30% of the total load to be shed.

3. The amount of load to be shed is the next step in the designing of UFLS in order to maintain operate able system frequency. The amount of load to be shed (LD) is given as

$$LD = \frac{\dfrac{L}{(1+L)} - d\left(1 - \dfrac{f_{min}}{f_n}\right)}{1 - d\left(1 - \dfrac{f_{min}}{f_n}\right)} \qquad (6.11)$$

where

L	:	Anticipated overload (p.u.)
f_{min}	:	Minimum allowed operating frequency (Hz)
f_n	:	Nominal system frequency (Hz)
d	:	Load reduction factor

In this study f_{min} is taken as 59.5 Hz, the point at which the load shedding will start, d is assumed to be 1.7 [151] [150] which is a design parameter and ranges from 1.5 − 1.8. Applying these values, result in LD as 0.440 p.u. of total

connected load in the system (138 MW). These makes the steps of 28MW, 28MW, 41MW and 41 MW. The first three steps are applied on bus 5 and the other step is applied on bus 6. In this study, it is assumed that the overloading is produced by a connection of load of 100 MW at bus number 5.

6.2.5 Results

Figure 6.43 shows the layout of the scheme and it implementation. Whereas Figure 6.44 shows the implementation of WSCC 3 machine 9 bus system with UFLS on SIMULINK. The PMU measurements of bus 1 are used as a criteria to determine the initialization of load shedding. In Figure 6.45 - Figure 6.47 the machine speeds are compared, whereas in Figure 6.48 the average system frequency is shown, when the system is equipped with UFLS and without UFLS. It can be seen that without UFLS the system is never able to recover from the frequency dip whereas the system frequency with UFLS is restored as soon as system hits the minimum allowable frequency limit of 59.5Hz.
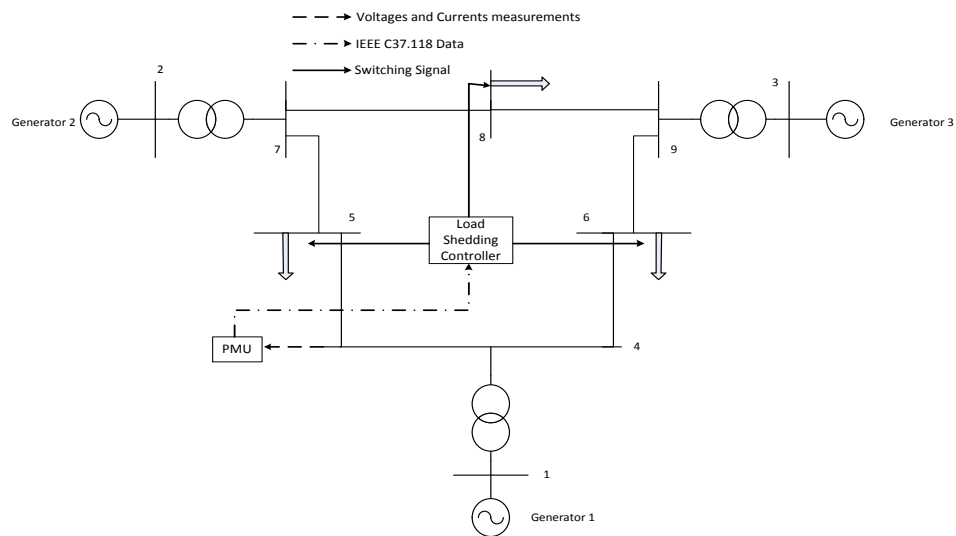
Figure 6.43:   UFLS Layout for WSCC 3 Machine 9 Bus Test System
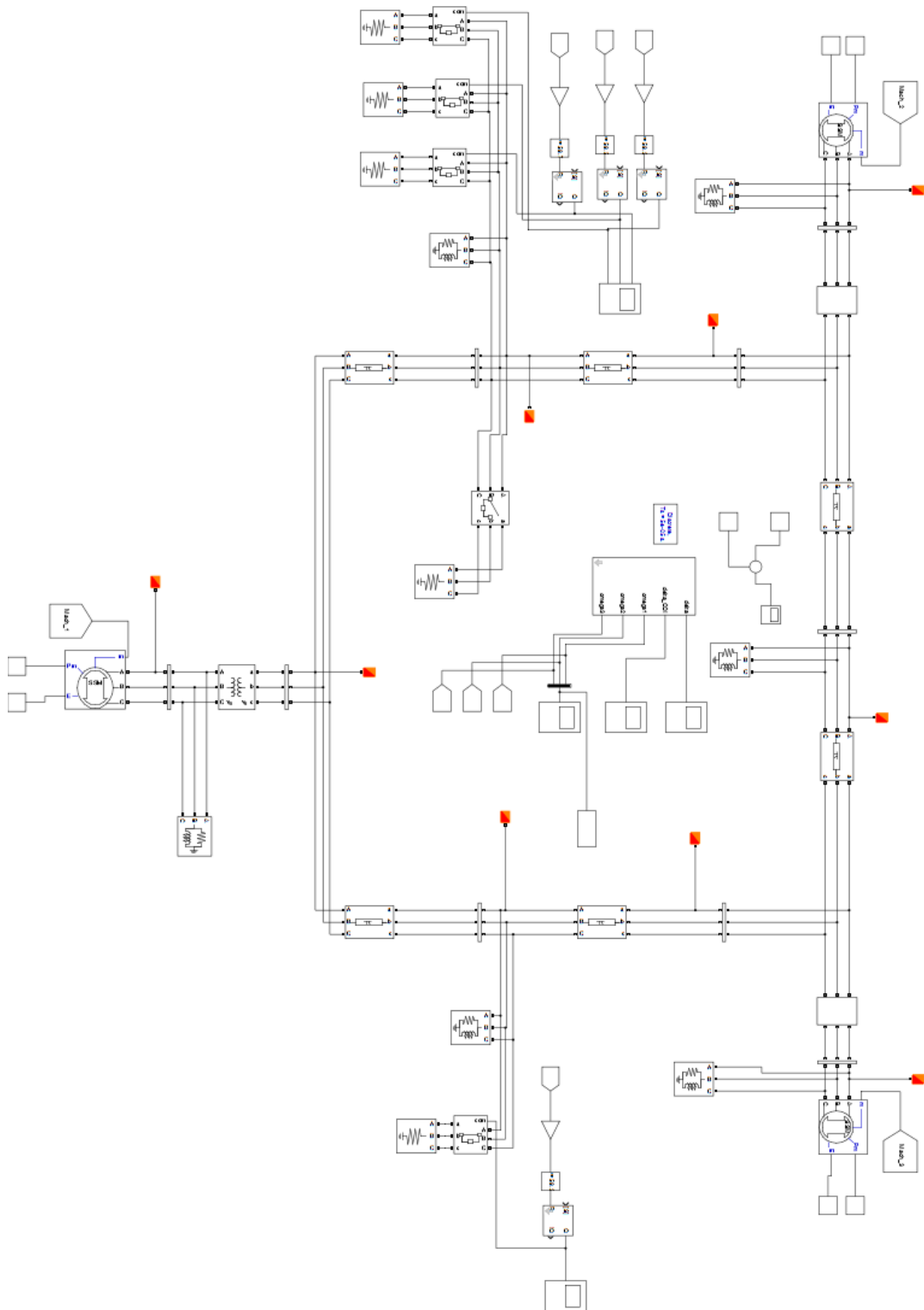
Figure 6.44:   UFLS Implementation on SIMULINK
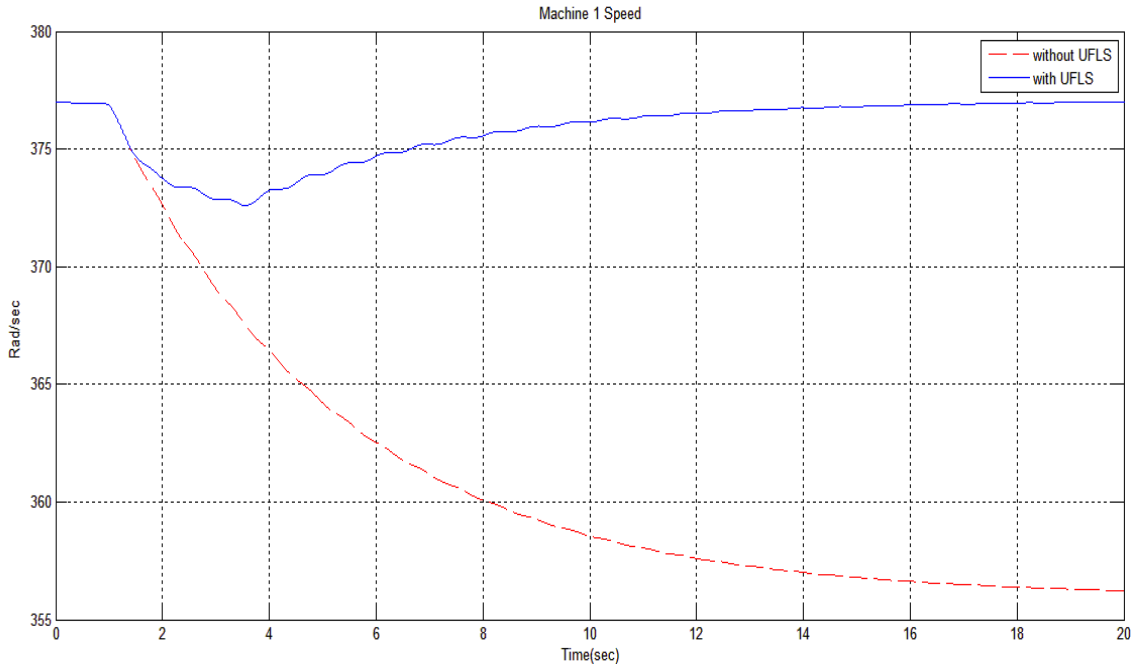
Figure 6.45:   Machine 1 Speed comparison for UFLS
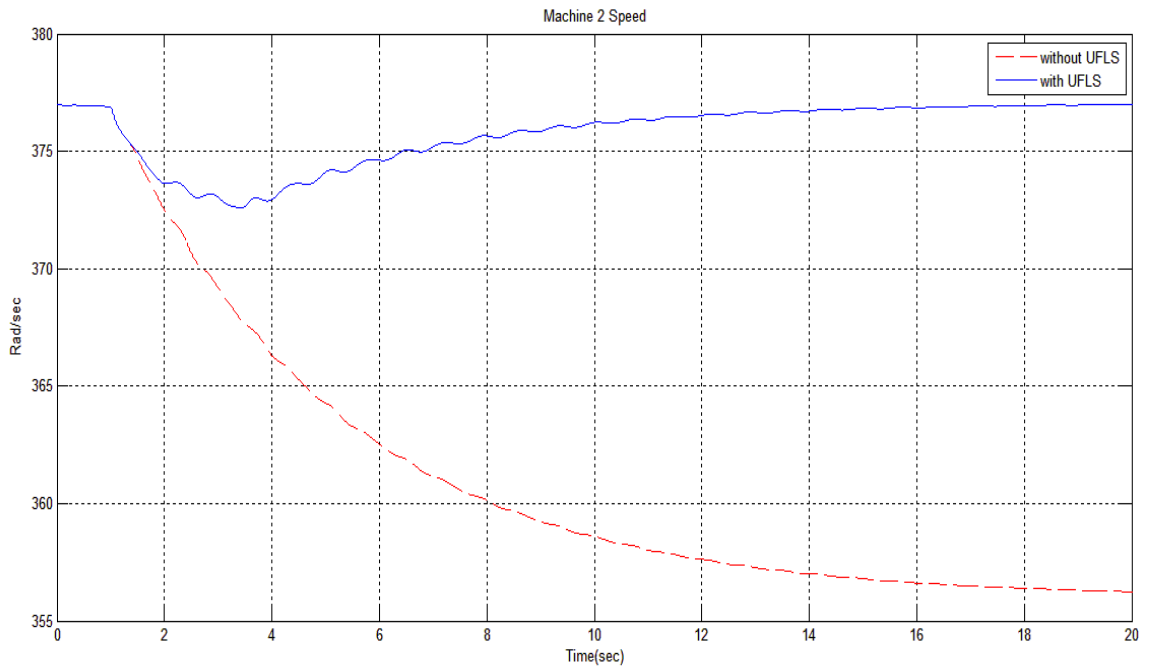
Figure 6.46:   Machine 2 Speed comparison for UFLS

172
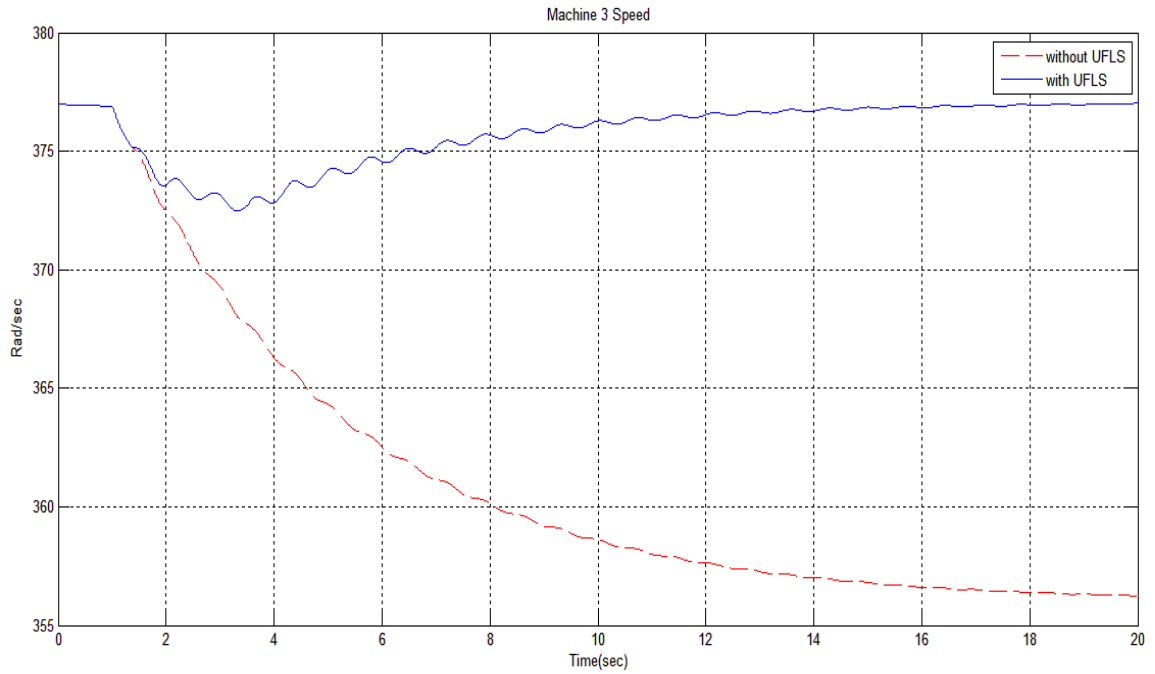
Figure 6.47:   Machine 3 Speed comparison for ULFS
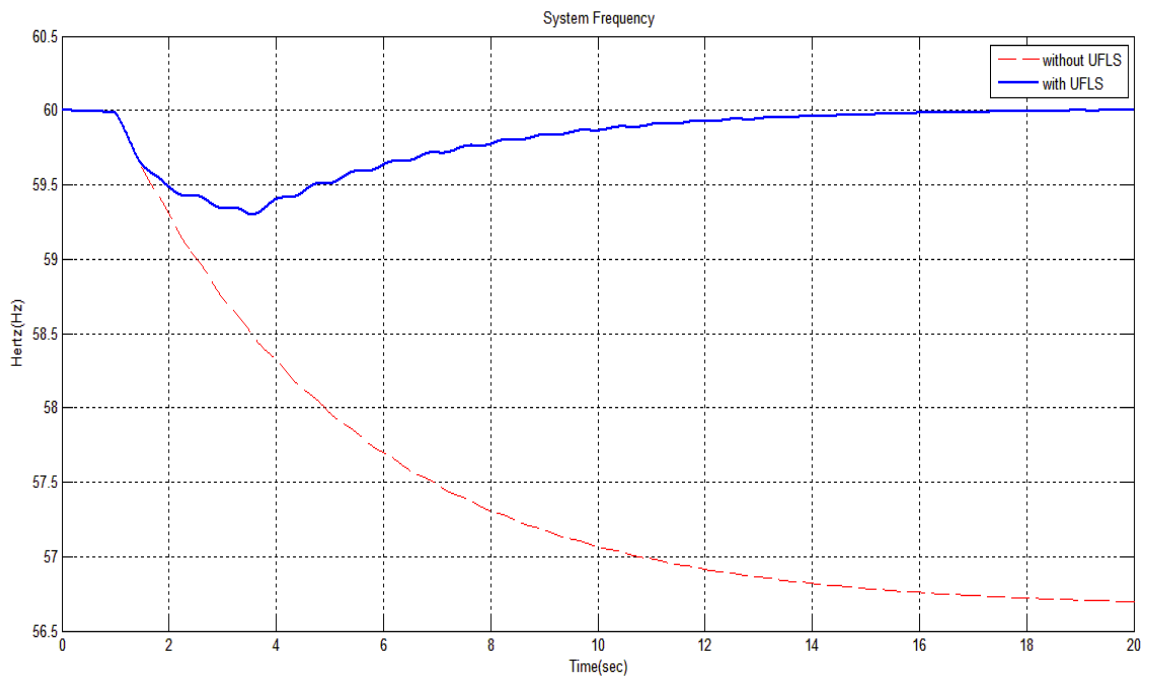
Figure 6.48:   Average System Frequency comparison

6.2.6 Experimental Validation of UFLS

The said UFLS is also experimentally verified by WSCC 3 machine 9 bus test system implemented on RTDS shown in Figure 6.49 and load shedding controller implemented on SVP shown in Figure 6.50. Figure 6.50 also shows the steps taken to maintain the frequency at 60 Hz. Figure 6.51 - Figure 6.53 shows the machine speed comparison with the system without UFLS and with UFLS. It can be seen that in the presence of governor and AVR the system recovers from the frequency dip faster than without the governor and AVR as in the case of SIMULINK.
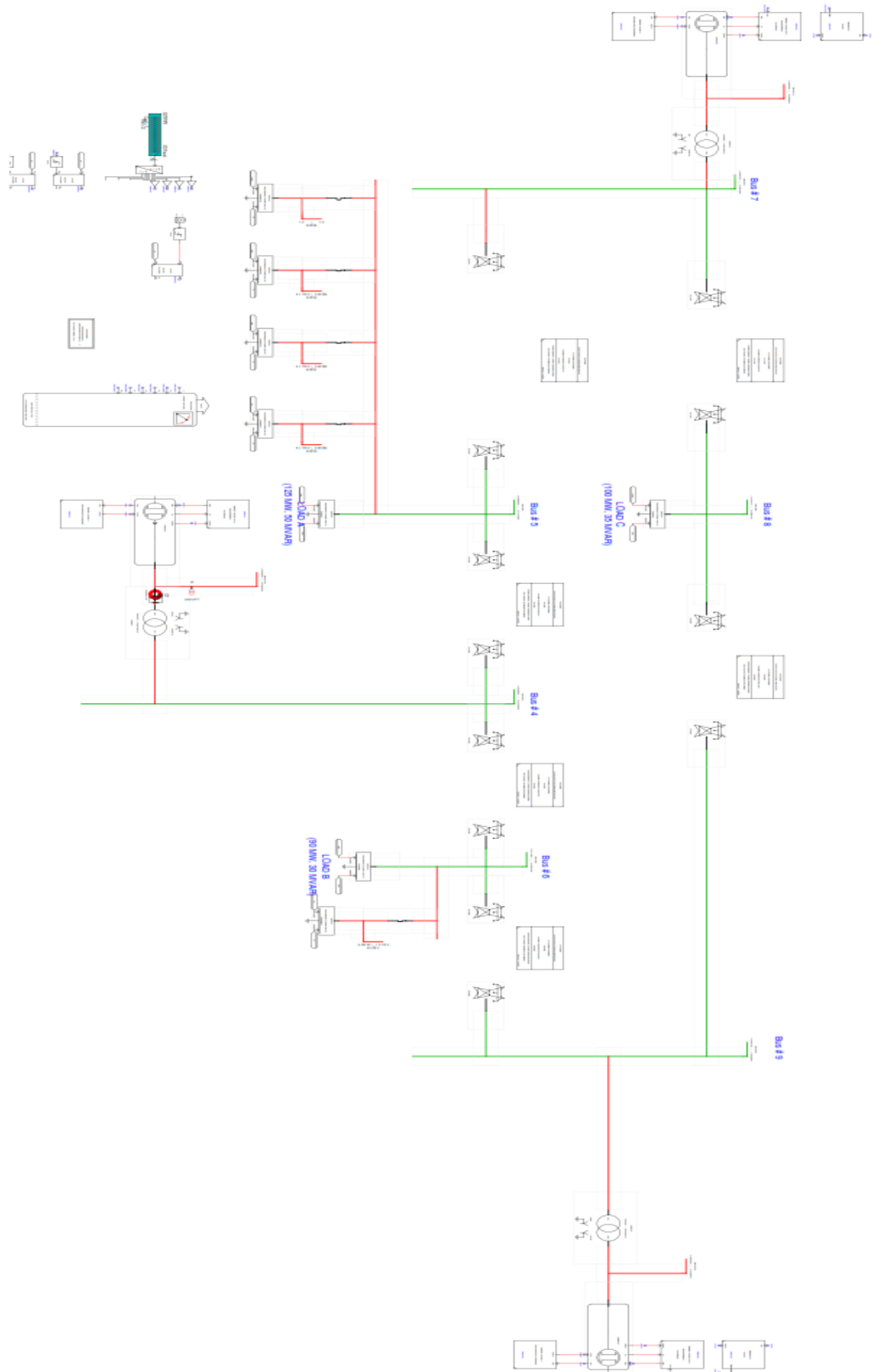
Figure 6.49:   RTDS Implementation of UFLS
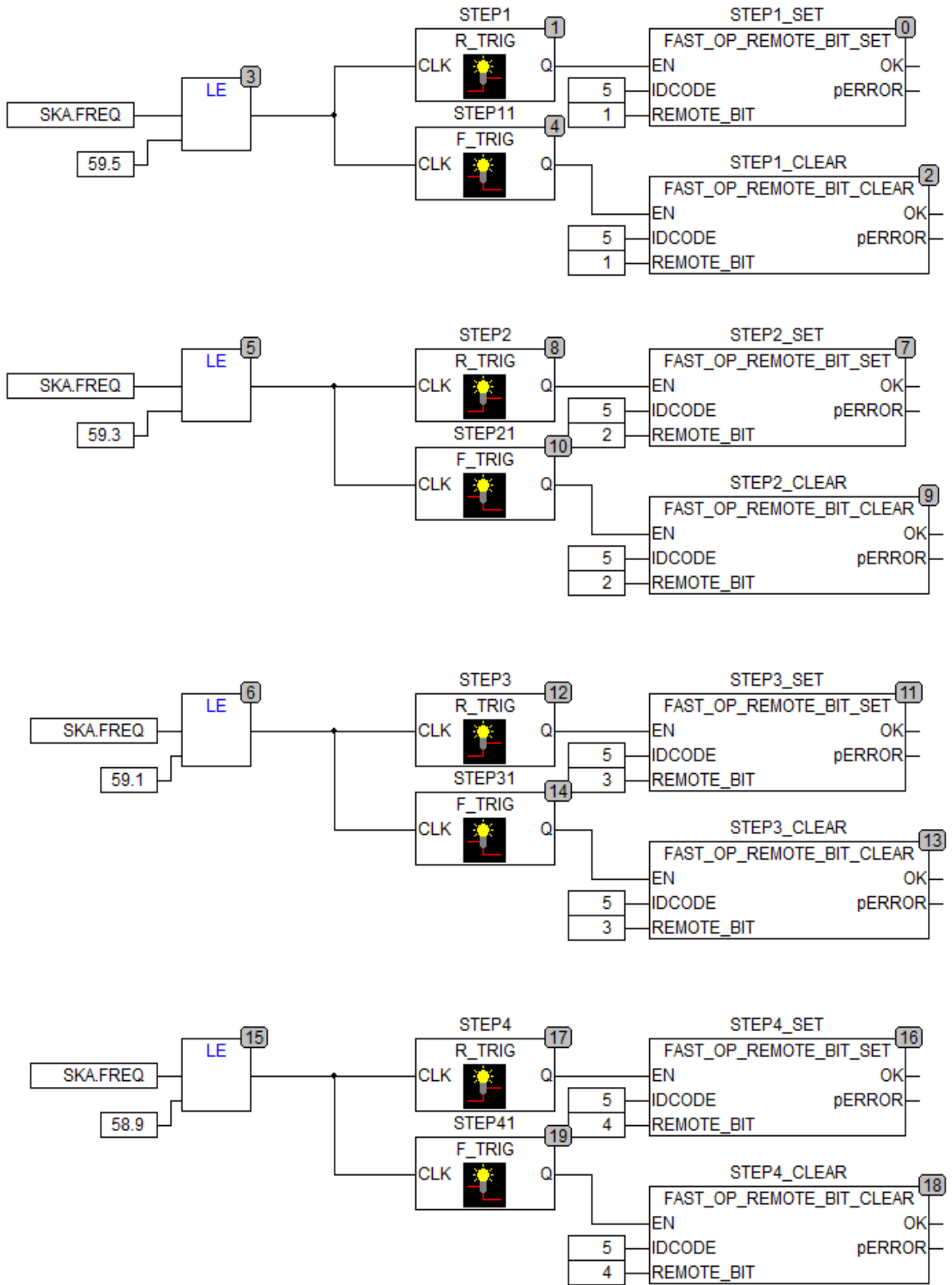
Figure 6.50: UFLS Controller implemented on SVP
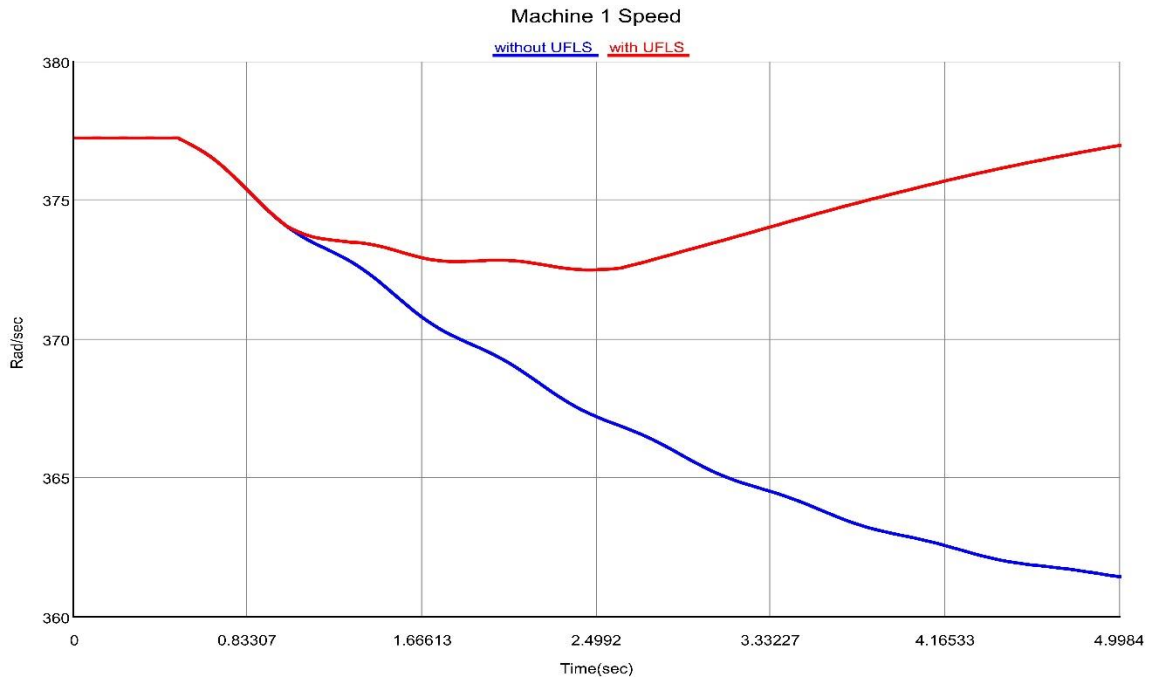
Figure 6.51:   Machine 1 Speed comparison for UFLS on RTDS and SYS-310
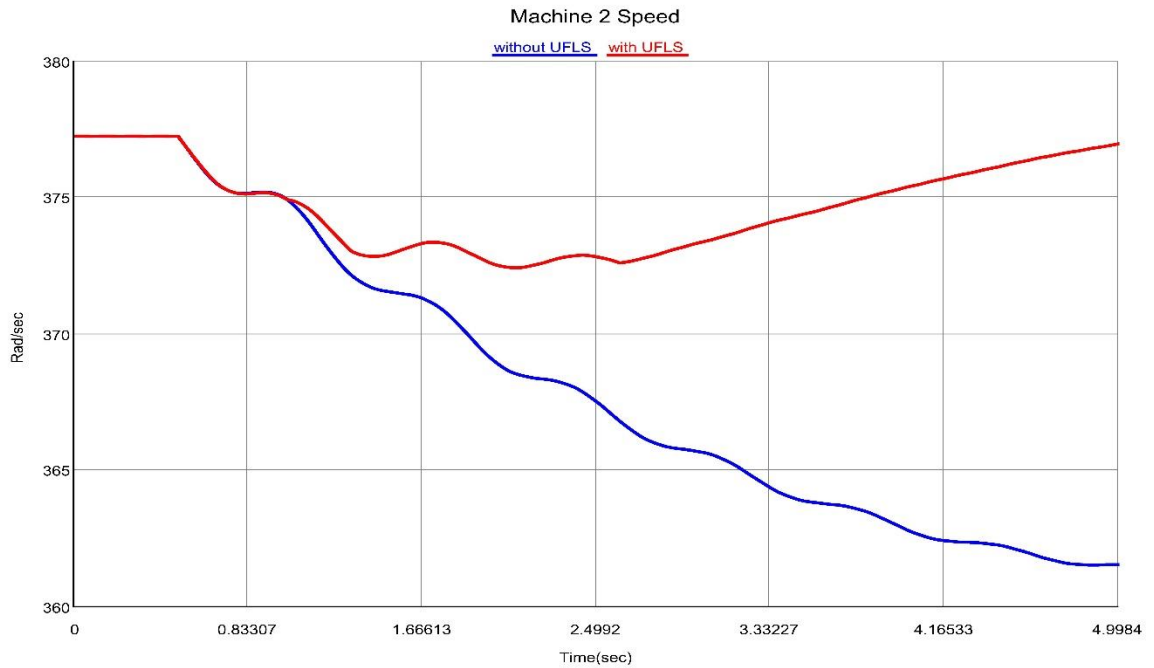
Figure 6.52:   Machine 2 Speed comparison for UFLS on RTDS and SYS-310

177
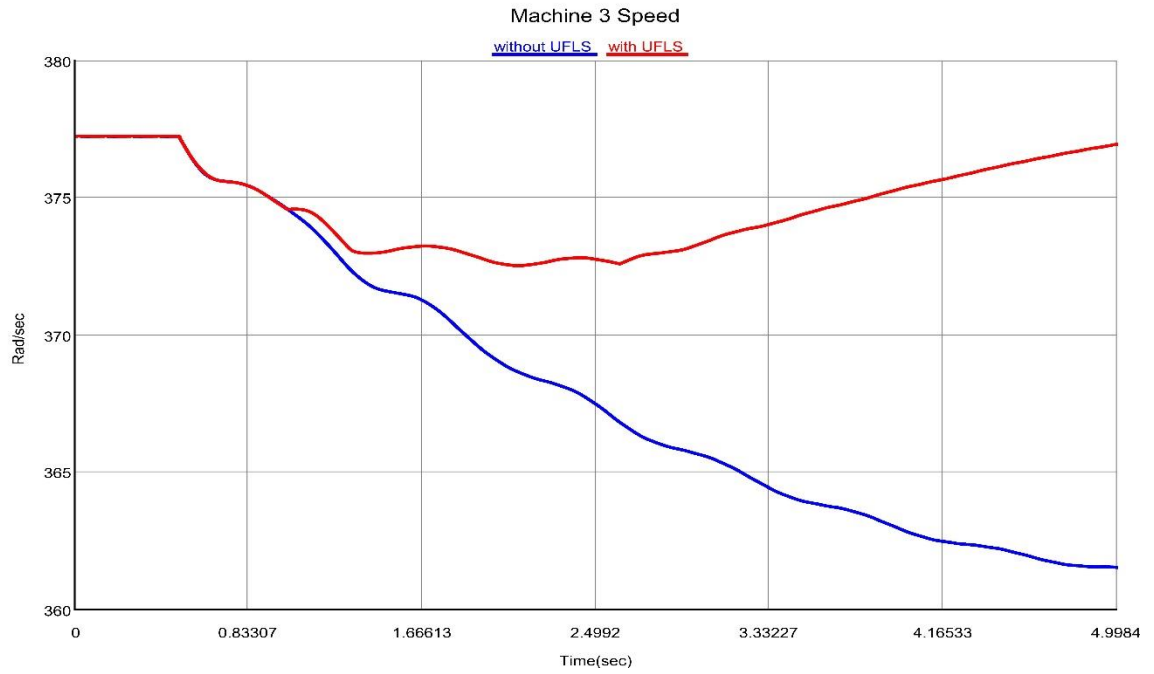
Figure 6.53:   Machine 3 Speed comparison for UFLS on RTDS and SYS-310

CHAPTER 7

CONCLUSIONS AND FUTURE WORK

In this chapter some conclusions are drawn and findings of this thesis work are summarized. Future research pathways are also enlightened in the area of transient stability improvement and detection.

7.1   Summary and Conclusions

A true multi objective formulation for OPP was first presented which takes into account the cost of the placement and to maximize the observability redundancy. The aim is to achieve full network observability with minimum number of PMUs while taking into account the physical constraints for the application and the system. One example of this constraint may be to place the PMUs at certain buses while another could be to avoid placement on certain buses. A solution based on Strength Pareto Evolutionary Algorithm (SPEA) is presented which presents three solutions namely, minimum cost solution, best compromise solution and maximum measurement redundancy solution. Each of the solution has its own importance. The highlighting fact of this kind of formulation being,

the decision maker is not bound to one solution as in the case of single objective optimization, but a variety of solutions are presented and decision maker is free to choose any solution he desire according to his requirement and application. The formulation is applied on different IEEE test systems and results are compared with different optimization algorithm. The proposed SPEA based formulation produces satisfactory results.

A novel formulation for the placement of the STATCOM in the power system in order to improve the transient stability is proposed. The formulation makes use of the system energy to find the optimal size and location of the STATCOMs in the system. The said formulation is solved through Differential Evolution (DE) Algorithm. The DE based solution is applied on WSCC 3 machine 9 bus test system and the placement is then tested through dynamic simulations.

A novel multi objective formulation for Optimal Power Flow is presented as another approach for improving the transient stability of the power system. The formulation makes use of the Kinetic energy of the system to reschedule the generators within the system physical bound in order to improve the transient stability of the power system. The said approach is solved using Strength Pareto Evolutionary Algorithm (SPEA) and is applied on standard test systems. The results of the approach are compared to state of the art published literature in the field of transient stability constrained optimal power flow. Through simulations and comparison it is found that the proposed approach tends to produce better result than the published literature.

Finally, the usage of the PMUs in real time transient instability prediction and mitigation is shown. A real time ANN based transient instability predictor is devised and

used in conjunction with PMU based remedial action schemes. The remedial action schemes are not only simulated but are tested through power hardware in loop (PHIL) simulations. Experimental validation of the said schemes is done on RTDS and real time hardware PMUs. It is shown that the computer simulation and hardware simulations complement each other in every case.

Generally speaking, the main findings and conclusions from this thesis can be drawn as follows

- The comprehensive literature survey on transient stability assessment reveals that, although being one of the oldest problem encountered in power system but it still poses questionable challenges in the modern days. There is a high interest of researcher towards the better usage of modern technology to effectively tackle the problem of transient instability. The usage of PMUs in this regards is also highlighted.

- It has been noted that a power system can be made observable by installing PMUs at approximately one third of its buses. The comparison of results produced by SPEA algorithm lies in conjunction with the published literature.

- The ability of the STATCOM in case of transient events is discovered. Even for the worst case scenarios the STATCOM was able to improve the transient stability of the power system.

- The ability within the power system to improve the transient stability is exposed in transient stable optimal power flow. Through simulations it was found that without any infrastructure investment transient stability can be improved by altering the available power system control parameters.

- The ability of PMUs to detect and mitigate with the instability is highlighted. The usage of the PMUs help in effective detection of instability and also to apply countermeasure against it. Real time hardware usage is shown in conjunction to the simulated PMUs.

7.2   Future Work

Following are some extensions that may be taken into consideration in future

- Inclusion of more physical constraints in OPP problem. Also inclusion of more objectives such as maximizing the observability with one or two lines lost.
- Formulating the optimal STATCOM placement as a multi objective problem may result in a better solution quality.
- Inclusion of constraints in the Transient Stable Optimal Power Flow Problem such as transformer taps can result in better solution. Inclusion of FACTS in this formulation can also be another problem worth researching.
- Hardware closing of the loop for ANN based predictor with closed loop PMU control can be an interesting research.

References

[1]   EPRI, "Phasor Measurement Unit (PMU) Implementation and Applications," Palo Alto, CA, 2007.

[2]   M. Bruch, "Power Blackout Risks," in *CRO Forum (Allianz)*, 2011, p. 32.

[3]   J. D. La Ree and V. Centeno, "Synchronized phasor measurement applications in power systems," *Smart Grid, IEEE …*, vol. 1, no. 1, pp. 20–27, 2010.

[4]   A. G. Phadke and J. S. Thorp, *Synchronized Phasor Measurements and Their Applications*. Springer; New York, 2008, p. 247.

[5]   J. Mutale and G. Strbac, "Transmission network reinforcement versus FACTS: an economic assessment," in *Proceedings of the 21st International Conference on Power Industry Computer Applications. Connecting Utilities. PICA 99. To the Millennium and Beyond (Cat. No.99CH36351)*, 1999, pp. 279–285.

[6]   C. Schaffner, "Value of controllable devices in a liberalized electricity market," in *Seventh International Conference on AC and DC Transmission*, 2001, vol. 2001, pp. 15–20.

[7]   G. Strbac and N. Jenkins, "Facts Devices In Uplift Control," in *Sixth International Conference on AC and DC Power Transmission*, 1996, pp. 214–219.

[8]   M. Huneault and F. D. D. Galiana, "A survey of the optimal power flow literature," *IEEE Trans. Power Syst.*, vol. 6, no. 2, pp. 762–770, May 1991.

[9]   S. C. Srivastava and R. K. Verma, "Impact of FACTS devices on transmission pricing in a de-regulated electricity market," in *DRPT2000. International Conference on Electric Utility Deregulation and Restructuring and Power Technologies. Proceedings (Cat. No.00EX382)*, 2000, pp. 642–648.

[10]   P. Kundur, J. Paserba, and S. Vitet, "Overview on definition and classification of power system stability," *IEEE Trans. Power Syst.*, vol. 19, no. 2, pp. 1387–1401, 2004.

[11]   L. L. Grigsby, *Power Systems, Third Edition (The Electric Power Engineering Handbook)*. CRC Press, 2012, p. 568.

[12]   Y. Xue, T. Van Custem, and M. Ribbens-Pavella, "Extended equal area criterion justifications, generalizations, applications," *IEEE Trans. Power Syst.*, vol. 4, no. 1, pp. 44–52, 1989.

[13] Y. Xue, T. Van Cutsem, and M. Pavella, "A Simple Direct Method for Fast Transient Stability Assesment of Large Power Systems," *IEEE Trans. Power Syst.*, vol. 3, no. 2, pp. 400–412, 1988.

[14] P. McNabb, J. Bialek, and A. Introduction, "A priori transient stability indicator of islanded power systems using Extended Equal Area Criterion," in *2012 IEEE Power and Energy Society General Meeting*, 2012, no. 1, pp. 1–7.

[15] W. Yang, Y. Xue, X. Song, D. Wu, F. Ge, and D. Xie, "Study on Stability Mechanism for a Typical Fault with EEAC Theory," in *2006 International Conference on Power System Technology*, 2006, pp. 1–4.

[16] Li Yi-qun, Tenglin, Liu Wang-shun, Liu Jian-fei, L. Y. Tenglin, and L. W. Liu, "The study on real-time transient stability emergency control in power system," *IEEE CCECE2002. Can. Conf. Electr. Comput. Eng. Conf. Proc. (Cat. No.02CH37373)*, vol. 1, pp. 138–143, 2002.

[17] K. W. Chan, Q. Zhou, and T. S. Chung, "Transient stability margin assessment for large power system using time domain simulation based hybrid extended equal area criterion method," in *APSCOM 2000 - 5th International Conference on Advances in Power System Control, Operation and Management*, 2000, vol. 2000, no. 2, pp. 405–409.

[18] C. M. Machado Ferreira, J. A. Dias Pinto, F. P. Maciel Barbosa, C. M. M. F. I, and F. P. M. Barbosaq, "Effect of the generators tripping in the transient stability of an electrical power system using the extended equal area criteria," in *POWERCON '98. 1998 International Conference on Power System Technology. Proceedings (Cat. No.98EX151)*, 1998, vol. 2, no. I, pp. 1295–1299.

[19] A. M. S. Tec and Y. Xue, "Fast analysis of stability using EEAC and simulation technologies," in *POWERCON '98. 1998 International Conference on Power System Technology. Proceedings (Cat. No.98EX151)*, 1998, vol. 1, pp. 12–16.

[20] P. Kundur, *Power system stability and control*. New York: McGraw-Hill, Inc., 1994, p. 1176.

[21] M. Pai, K. Padiyar, and C. Radhakrishna, "Transient Stability Analysis of Multi-Machine AC/DC Power Systems Via Energy-Function Method," *IEEE Trans. Power Appar. Syst.*, vol. PAS-100, no. 12, pp. 5027–5035, Dec. 1981.

[22] M. A. Pai, *Energy Function Analysis for Power System Stability*. Springer, 1989, p. 240.

[23] A.-A. A. Fouad and V. Vittal, *Power system transient stability analysis using the transient energy function method*. Englewood Cliffs, NJ: Prentice Hall, 1992.

[24]   T. Athay, R. Podmore, and S. Virmani, "A Practical Method for the Direct Analysis of Transient Stability," *IEEE Trans. Power Appar. Syst.*, vol. PAS-98, no. 2, pp. 573–584, Mar. 1979.

[25]   L. Chen, Y. Min, and W. Hu, "An Energy-Based Method for Location of Power System Oscillation Source," *IEEE Trans. Power Syst.*, vol. 28, no. 2, pp. 1–1, 2012.

[26]   M. A. AI-Taee, F. J. AI-Azzawi, A. A. Al-Taee, and T. Z. Al-Jumaily, "Real-time assessment of power system transient stability using rate of change of kinetic energy method," *IEE Proc. - Gener. Transm. Distrib.*, vol. 148, no. 6, p. 505, 2001.

[27]   T. Odun-Ayo and M. L. Crow, "Structure-Preserved Power System Transient Stability Using Stochastic Energy Functions," *IEEE Trans. Power Syst.*, vol. 27, no. 3, pp. 1450–1458, Aug. 2012.

[28]   N. Yorino, A. Priyadi, Y. Sasaki, Y. Zoka, and H. Sugihara, "A new method for direct computation of critical clearing time for transient stability analysis," in *2010 IREP Symposium Bulk Power System Dynamics and Control - VIII (IREP)*, 2010, pp. 1–9.

[29]   N. Fernandopulle and R. T. H. Alden, "Incorporation of Detailed HVDC Dynamics Into Transient Energy Functions," *IEEE Trans. Power Syst.*, vol. 20, no. 2, pp. 1043–1052, May 2005.

[30]   V. Azbe, U. Gabrijel, D. Povh, and R. Mihalic, "The Energy Function of a General Multimachine System With a Unified Power Flow Controller," *IEEE Trans. Power Syst.*, vol. 20, no. 3, pp. 1478–1485, Aug. 2005.

[31]   Jing Shi, Yuejin Tang, Yajun Xia, Li Ren, Jingdong Li, Fengshun Jiao, J. Shi, Y. Tang, Y. Xia, L. Ren, J. Li, and F. Jiao, "Energy Function Based SMES Controller for Transient Stability Enhancement," *IEEE Trans. Appl. Supercond.*, vol. 22, no. 3, pp. 5701304–5701304, Jun. 2012.

[32]   V. Azbe and R. Mihalic, "The Control Strategy for an IPFC Based on the Energy Function," *IEEE Trans. Power Syst.*, vol. 23, no. 4, pp. 1662–1669, Nov. 2008.

[33]   G. A. Maria, C. Tang, and J. Kim, "Hybrid transient stability analysis (power systems)," *IEEE Trans. Power Syst.*, vol. 5, no. 2, pp. 384–393, May 1990.

[34]   B. Bonvini, S. Massucco, A. Morini, and T. Siewierski, "A comparative analysis of power system transient stability assessment by direct and hybrid methods," in *Proceedings of 8th Mediterranean Electrotechnical Conference on Industrial Applications in Power Systems, Computer Science and Telecommunications (MELECON 96)*, 1996, vol. 3, pp. 1575–1579.

[35] C. K. Tang, C. E. Graham, M. El-Kady, and R. T. H. Alden, "Transient stability index from conventional time domain simulation," *IEEE Trans. Power Syst.*, vol. 9, no. 3, pp. 1524–1530, 1994.

[36] Y. Mansour, E. Vaahedi, A. Y. Chang, B. R. Corns, B. W. Garrett, K. Demaree, T. Athay, and K. Cheung, "BC Hydro's on-line transient stability assessment (TSA) model development, analysis and post-processing," *IEEE Trans. Power Syst.*, vol. 10, no. 1, pp. 241–253, 1995.

[37] H. H. Al Marhoon, S. M. Ieee, I. Leevongwat, M. Ieee, P. Rastgoufard, and H. H. Al Marhoon, "A practical method for power systems transient stability and security analysis," in *PES T&D 2012*, 2012, no. Student M, pp. 1–6.

[38] F. Lu and J.-L. Yu, "Using Critical Machine Couple Equal Area Criterion to Assess Multi-Machine System Stability," in *2009 Asia-Pacific Power and Energy Engineering Conference*, 2009, pp. 1–4.

[39] L. Le-Thanh, T. Tran-Quoc, O. Devaux, O. Chilard, C. Kieny, N. Hadjsaid, J. C. Sabonnadiere, S. Member, J. C. Sabonnadière, and F. Member, "Hybrid methods for transient stability assessment and preventive control for distributed generators," in *2008 IEEE Power and Energy Society General Meeting - Conversion and Delivery of Electrical Energy in the 21st Century*, 2008, pp. 1–6.

[40] A. Padilha and E. F. Denis, "Transient stability indices from a hybrid approach," in *2001 IEEE Porto Power Tech Proceedings (Cat. No.01EX502)*, 2001, vol. vol.2, p. 5.

[41] K. W. Chan, R. W. Dunn, and A. R. Daniels, "Transient and dynamic stability constraint assessment using hybrid TEF and clustering analysis," in *2000 IEEE Power Engineering Society Winter Meeting. Conference Proceedings (Cat. No.00CH37077)*, 2000, vol. 2, pp. 1383–1388.

[42] W. Kwok and K. W. Cheung, "An improved transient stability index for dynamic security assessment using a marginally unstable injection (MUI) approach," in *2000 IEEE Power Engineering Society Winter Meeting. Conference Proceedings (Cat. No.00CH37077)*, 2000, vol. 2, no. c, pp. 931–936.

[43] F. Hashiesh and H. Mostafa, "An intelligent wide area synchrophasor based system for predicting and mitigating transient instabilities," *IEEE Trans. Smart Grid*, vol. 3, no. 2, pp. 645–652, 2012.

[44] Y. Xu, Z. Y. Dong, K. Meng, R. Zhang, and K. P. Wong, "Real-time transient stability assessment model using extreme learning machine," *IET Gener. Transm. Distrib.*, vol. 5, no. 3, p. 314, 2011.

[45] F. R. Gomez, A. D. Rajapakse, U. D. Annakkage, and I. T. Fernando, "Support Vector Machine-Based Algorithm for Post-Fault Transient Stability Status Prediction Using Synchronized Measurements," *IEEE Trans. Power Syst.*, vol. 26, no. 3, pp. 1474–1483, Aug. 2011.

[46] A. M. a. Haidar, M. W. Mustafa, F. a. F. Ibrahim, and I. a. Ahmed, "Transient stability evaluation of electrical power system using generalized regression neural networks," *Appl. Soft Comput.*, vol. 11, no. 4, pp. 3558–3570, Jun. 2011.

[47] A. Karami, "Power system transient stability margin estimation using neural networks," *Int. J. Electr. Power Energy Syst.*, vol. 33, no. 4, pp. 983–991, May 2011.

[48] A. D. Rajapakse, F. Gomez, K. Nanayakkara, P. A. Crossley, and V. V. Terzija, "Rotor Angle Instability Prediction Using Post-Disturbance Voltage Trajectories," *IEEE Trans. Power Syst.*, vol. 25, no. 2, pp. 947–956, May 2010.

[49] N. Amjady and S. A. Banihashemi, "Transient stability prediction of power systems by a new synchronism status index and hybrid classifier," *IET Gener. Transm. Distrib.*, vol. 4, no. 4, p. 509, 2010.

[50] H. Sawhney and B. Jeyasurya, "A feed-forward artificial neural network with enhanced feature selection for power system transient stability assessment," *Electr. Power Syst. Res.*, vol. 76, no. 12, pp. 1047–1054, 2006.

[51] L. S. Moulin, A. P. A. daSilva, M. A. El-Sharkawi, and R. J. MarksII, "Support Vector Machines for Transient Stability Analysis of Large-Scale Power Systems," *IEEE Trans. Power Syst.*, vol. 19, no. 2, pp. 818–825, May 2004.

[52] K. . Sanyal, "Transient stability assessment using artificial neural network," in *2004 IEEE International Conference on Electric Utility Deregulation, Restructuring and Power Technologies. Proceedings*, 2004, vol. 2, no. April, pp. 633–637.

[53] D. J. Sobajic, Y.-H. Y. Pao, C. C. Time, M. L. Systems, A. P. Recognition, and R. Neural-net, "Artificial neural-net based dynamic security assessment for electric power systems," *IEEE Trans. Power Syst.*, vol. 4, no. 1, pp. 220–228, 1989.

[54] S. Yamashiro, K. Nara, and T. Koike, "Transient security enhancement of power systems using pattern recognition," *Electr. Eng. Japan*, vol. 105, no. 1, pp. 106–114, 1985.

[55] J. Zhu, *Optimization of Power System Operation (Google eBook)*. John Wiley & Sons, 2009, p. 624.

[56] G. Deconinck, R. Belmans, Z. Qiu, G. S. Member, and S. Member, "A literature survey of Optimal Power Flow problems in the electricity market context," in *2009 IEEE/PES Power Systems Conference and Exposition*, 2009, pp. 1–6.

[57] J. A. Momoh, R. J. Koessler, M. S. Bond, B. Stott, D. Sun, A. Papalexopoulos, and P. Ristanovic, "Challenges to optimal power flow," *IEEE Trans. Power Syst.*, vol. 12, no. 1, pp. 444–455, 1997.

[58] D. Gan, R. J. Thomas, and R. D. Zimmerman, "Stability-constrained optimal power flow," *IEEE Trans. Power Syst.*, vol. 15, no. 2, pp. 535–540, May 2000.

[59] H. Xin, D. Can, Y. Li, T. S. S. Chung, J. Qiu, and D. Gan, "Transient stability preventive control and optimization via power system stability region analysis," in *2006 IEEE Power Engineering Society General Meeting*, 2006, no. 1, p. 8 pp.

[60] L. Chen, S. Member, Y. Tada, H. Okamoto, R. Tanabe, A. Ono, and Y. Taka, "Optimal operation solutions of power systems with transient stability constraints," *IEEE Trans. Circuits Syst. I Fundam. Theory Appl.*, vol. 48, no. 3, pp. 327–339, Mar. 2001.

[61] Y. Sun, Y. Xinlin, and H. F. F. Wang, "Approach for optimal power flow with transient stability constraints," *IEE Proc. - Gener. Transm. Distrib.*, vol. 151, no. 1, p. 8, 2004.

[62] Y. Xia, K. W. W. Chan, and M. Liu, "Direct nonlinear primal–dual interior-point method for transient stability constrained optimal power flow," *IEE Proc. - Gener. Transm. Distrib.*, vol. 152, no. 1, p. 11, Jan. 2005.

[63] M. La Scala, M. Trovato, and C. Antonelli, "On-line dynamic preventive control: an algorithm for transient security dispatch," *IEEE Trans. Power Syst.*, vol. 13, no. 2, pp. 601–610, May 1998.

[64] Y. Yuan, J. Kubokawa, and H. Sasaki, "Optimal power flow solution with multi-contingency transient stability constraints," in *Proceedings. International Conference on Power System Technology*, 2002, vol. 4, pp. 2009–2013.

[65] D. Layden, B. Jeyasurya, and S. Member, "Integrating security constraints in optimal power flow studies," in *IEEE Power Engineering Society General Meeting, 2004.*, 2004, vol. 2, pp. 125–129.

[66] D. Z. Fang, Y. Xiaodong, S. Jingqiang, Y. Shiqiang, and Z. Yao, "An Optimal Generation Rescheduling Approach for Transient Stability Enhancement," *IEEE Trans. Power Syst.*, vol. 22, no. 1, pp. 386–394, Feb. 2007.

[67]   T. B. Nguyen and M. A. Pai, "Dynamic security-constrained rescheduling of power systems using trajectory sensitivities," *IEEE Trans. Power Syst.*, vol. 18, no. 2, pp. 848–854, May 2003.

[68]   D. Ruiz-Vega, A. Member, M. Pavella, and L. Fellow, "A comprehensive approach to transient stability control: part I-near optimal preventive control," *IEEE Trans. Power Syst.*, vol. 18, no. 4, pp. 1446–1453, Nov. 2003.

[69]   D. Chattopadhyay and D. Gan, "Market dispatch incorporating stability constraints," *Int. J. Electr. Power Energy Syst.*, vol. 23, no. 6, pp. 459–469, Aug. 2001.

[70]   D. Chattopadhyay and D. Gan, "Market dispatch incorporating stability constraints," *Int. J. Electr. Power Energy Syst.*, vol. 23, no. 6, pp. 459–469, 2001.

[71]   Z. Dong, P. Zhang, J. Ma, J. Zhao, M. Ali, K. Meng, and X. Yin, *Emerging Techniques in Power System Analysis*. New York: Springer, 2010, p. 202.

[72]   J. H. Chow, "Power system measurement data and their applications," *Eur. Trans. Electr. Power*, vol. 21, no. 4, pp. 1493–1495, May 2011.

[73]   R. Kavasseri and S. K. Srinivasan, "Joint optimal placement of PMU and conventional measurements in power systems," *Proc. 2010 IEEE Int. Symp. Circuits Syst.*, pp. 3449–3452, May 2010.

[74]   F. Aminifar, C. Lucas, A. Khodaei, and M. Fotuhi-Firuzabad, "Optimal Placement of Phasor Measurement Units Using Immunity Genetic Algorithm," *IEEE Trans. Power Deliv.*, vol. 24, no. 3, pp. 1014–1020, Jul. 2009.

[75]   R. Kavasseri and S. K. Srinivasan, "Joint placement of phasor and conventional power flow measurements for fault observability of power systems," *IET Gener. Transm. Distrib.*, vol. 5, no. 10, p. 1019, 2011.

[76]   D. Gyllstrom, E. Rosensweig, and J. Kurose, "On the impact of PMU placement on observability and cross-validation," in *2012 Third International Conference on Future Energy Systems: Where Energy, Computing and Communication Meet (e-Energy)*, 2012, pp. 1–10.

[77]   P. S. SrinivasaReddy, L. Ramesh, S. P. Chowdhury, and S. Chowdhury, "Power system PMU placement - a comparative survey report," in *International Conference on Information and Communication Technology in Electrical Sciences (ICTES 2007)*, 2007, pp. 249–255.

[78]   W. Yuill, A. Edwards, S. Chowdhury, and S. P. Chowdhury, "Optimal PMU placement: A comprehensive literature review," in *2011 IEEE Power and Energy Society General Meeting*, 2011, pp. 1–8.

[79] B. Gou, "Generalized Integer Linear Programming Formulation for Optimal PMU Placement," *IEEE Trans. Power Syst.*, vol. 23, no. 3, pp. 1099–1104, Aug. 2008.

[80] R. Sodhi, S. C. Srivastava, and S. N. Singh, "Optimal PMU placement to ensure system observability under contingencies," in *2009 IEEE Power & Energy Society General Meeting*, 2009, pp. 1–6.

[81] D. Dua and S. Dambhare, "Optimal multistage scheduling of PMU placement: An ILP approach," *IEEE Trans. Power Deliv.*, vol. 23, no. 4, pp. 1812–1820, 2008.

[82] B. Mohammadi-Ivatloo and S. H. Hosseini, "Optimal PMU placement for power system observability considering secondary voltage control," in *2008 Canadian Conference on Electrical and Computer Engineering*, 2008, pp. 000365–000368.

[83] S. Chakrabarti, G. K. Venayagamoorthy, and E. Kyriakides, "PMU placement for power system observability using binary particle swarm optimization," in *Australasian Universities Power Engineering Conference, 2008*, 2008, pp. 1–5.

[84] A. Sadu, R. Kumar, and R. G. Kavasseri, "Optimal placement of Phasor Measurement Units using Particle swarm Optimization," *2009 World Congr. Nat. Biol. Inspired Comput.*, pp. 1708–1713, 2009.

[85] S. Chakrabarti, E. Kyriakides, and D. G. Eliades, "Placement of Synchronized Measurements for Power System Observability," *IEEE Trans. Power Deliv.*, vol. 24, no. 1, pp. 12–19, Jan. 2009.

[86] S. Chakrabarti and E. Kyriakides, "Optimal Placement of Phasor Measurement Units for Power System Observability," *IEEE Trans. Power Syst.*, vol. 23, no. 3, pp. 1433–1440, Aug. 2008.

[87] A. Ketabi, S. M. Nosratabadi, and M. R. Sheibani, "Optimal PMU placement based on Mean Square Error using Differential Evolution algorithm," in *First Power Quality Conference (PQC), 2010*, 2010, pp. 1–6.

[88] V. Kekatos, G. B. Giannakis, and B. Wollenberg, "Optimal Placement of Phasor Measurement Units via Convex Relaxation," *IEEE Trans. Power Syst.*, vol. 27, no. 3, pp. 1521–1530, Aug. 2012.

[89] F. Aminifar, M. Fotuhi-Firuzabad, and A. Safdarian, "Optimal PMU Placement Based on Probabilistic Cost/Benefit Analysis," *IEEE Trans. Power Syst.*, vol. 28, no. 1, pp. 566–567, Feb. 2013.

[90] A. K. Zadeh, H. R. Mashhadi, and M. E. H. Abadi, "Optimal placement of a defined number of Phasor Measurement Units in power systems," in *2nd Iranian Conference on Smart Grids (ICSG), 2012*, 2012, pp. 1–9.

[91]   J. Liu, J. Tang, F. Ponci, A. Monti, C. Muscas, and P. A. Pegoraro, "Trade-Offs in PMU Deployment for State Estimation in Active Distribution Grids," *IEEE Trans. Smart Grid*, vol. 3, no. 2, pp. 915–924, Jun. 2012.

[92]   F. Aminifar, A. Khodaei, M. Fotuhi-Firuzabad, and M. Shahidehpour, "Contingency-Constrained PMU Placement in Power Networks," *IEEE Trans. Power Syst.*, vol. 25, no. 1, pp. 516–523, Feb. 2010.

[93]   Chunhua Peng and Xuesong Xu, "A hybrid algorithm based on BPSO and immune mechanism for PMU optimization placement," in *2008 7th World Congress on Intelligent Control and Automation*, 2008, pp. 7036–7040.

[94]   M. Hajian, A. M. Ranjbar, T. Amraee, and A. R. Shirani, "Optimal Placement of Phasor Measurement Units: Particle Swarm Optimization Approach," in *2007 International Conference on Intelligent Systems Applications to Power Systems*, 2007, pp. 1–6.

[95]   Peng Chunhua and Xu Xuesong, "A hybrid algorithm based on immune BPSO and N-1 principle for PMU multi-objective optimization placement," in *2008 Third International Conference on Electric Utility Deregulation and Restructuring and Power Technologies*, 2008, pp. 610–614.

[96]   M. a. Abido, "A niched Pareto genetic algorithm for multiobjective environmental/economic dispatch," *Int. J. Electr. Power Energy Syst.*, vol. 25, no. 2, pp. 97–105, Feb. 2003.

[97]   E. Zitzler and L. Thiele, "An Evolutionary Algorithm for Multiobjective Optimization : The Strength Pareto Approach," Zurich, 1998.

[98]   K. D. N. Srinivas, "Multiobjective Optimization Using Nondominated Sorting in Genetic Algorithms," *Evol. Comput.*, vol. 2, no. 3, pp. 221–248, 1994.

[99]   M. a. Abido, "Environmental/economic power dispatch using multiobjective evolutionary algorithms," *IEEE Trans. Power Syst.*, vol. 18, no. 4, pp. 1529–1537, Nov. 2003.

[100]   J. N. Morse, "Reducing the size of the nondominated set: Pruning by clustering," *Comput. Oper. Res.*, vol. 7, no. 1, pp. 55–66, 1980.

[101]   F. Herrera, M. Lozano, and J. L. Verdegay, "Tackling Real-Coded Genetic Algorithms: Operators and Tools for Behavioural Analysis," *Artif. Intell. Rev.*, vol. 12, no. 4, pp. 265–319, Aug. 1998.

[102]   A. Al-Mohammed, "Optimal PMU placement for power system observability using differential evolution," in *11th International Conference on Intelligent Systems Design and Applications*, 2011, pp. 277–282.

[103] D. Dua, S. Dambhare, R. K. Gajbhiye, and S. A. Soman, "Optimal Multistage Scheduling of PMU Placement: An ILP Approach," *IEEE Trans. Power Deliv.*, vol. 23, no. 4, pp. 1812–1820, Oct. 2008.

[104] S. Chakrabarti, "PMU placement for power system observability using binary particle swarm optimization," in *Power Engineering Conference, 2008. AUPEC '08. Australasian Universities*, 2008, pp. 1 – 5.

[105] B. Allagui, "Optimal placement of Phasor Measurement Units by genetic algorithm," in *First International Conference on Renewable Energies and Vehicular Technology (REVET)*, 2012, pp. 434–439.

[106] N. G. Hingorani and L. Gyugyi, *Understanding FACTS: Concepts and Technology of Flexible AC Transmission Systems*. Wiley-IEEE Press, 1999, p. 452.

[107] N. G. Hingorani, "FACTS-flexible AC transmission system," in *International Conference on AC and DC Power Transmission, 1991*, 1991, pp. 1–7.

[108] N. G. Hingorani, "High Power Electronics and flexible AC Transmission System," *IEEE Power Eng. Rev.*, vol. 8, no. 7, pp. 3–4, Jul. 1988.

[109] A. Edris, "Proposed terms and definitions for flexible AC transmission system (FACTS)," *IEEE Trans. Power Deliv.*, vol. 12, no. 4, pp. 1848–1853, 1997.

[110] Qingguang Yu, Pei Li, Wenhua Liu, and Xiaorong Xie, "Overview of STATCOM technologies," in *2004 IEEE International Conference on Electric Utility Deregulation, Restructuring and Power Technologies. Proceedings*, 2004, vol. 2, pp. 647–652.

[111] L. Gyugyi, "Dynamic compensation of AC transmission lines by solid-state synchronous voltage sources," *IEEE Trans. Power Deliv.*, vol. 9, no. 2, pp. 904–911, Apr. 1994.

[112] T. An, M. T. Powell, H. L. Thanawala, and N. Jenkins, "Assessment of two different STATCOM configurations for FACTS application in power systems," in *POWERCON '98. 1998 International Conference on Power System Technology. Proceedings (Cat. No.98EX151)*, 1998, vol. 1, pp. 307–312.

[113] I. A. Hamzah and J. A. Yasin, "Static var compensators (SVC) reouired to solve the problem of delayed voltage recovery following faults in the power system of the Saudi Electricity Company, Western Region (SEC-WR)," in *2003 IEEE Bologna Power Tech Conference Proceedings,*, 2003, vol. 4, pp. 487–494.

[114] N. Mithulananthan, C. A. Canizares, and J. Reeve, "Tuning, performance and interactions of PSS and FACTS controllers," in *IEEE Power Engineering Society Summer Meeting,*, 2002, vol. 2, pp. 981–987.

[115] C. Han, Z. Yang, B. Chen, W. Song, A. Q. Huang, A.-A. Edris, M. Ingram, and S. Atcitty, "System integration and demonstration of a 4.5 MVA STATCOM based on emitter turn-off (ETO) thyristor and cascade multilevel converter," in *31st Annual Conference of IEEE Industrial Electronics Society, 2005. IECON 2005.*, 2005, p. 6 pp.

[116] N. G. Hingorani, "Flexible AC transmission," *IEEE Spectr.*, vol. 30, no. 4, pp. 40–45, Apr. 1993.

[117] C. Schauder, M. Gernhardt, E. Stacey, T. Lemak, L. Gyugyi, T. W. Cease, and A. Edris, "Operation of ±100 MVAr TVA STATCON," *IEEE Trans. Power Deliv.*, vol. 12, no. 4, pp. 1805–1811, 1997.

[118] K. K. Sen, "STATCOM-STATic synchronous COMpensator: theory, modeling, and applications," in *IEEE Power Engineering Society. 1999 Winter Meeting (Cat. No.99CH36233)*, 1999, vol. 2, pp. 1177–1183 vol.2.

[119] Lai On Mak and Yixin Ni, "Design of fuzzy logic supplementary controller for STATCOM using polar coordinate variables," in *Proceedings of IEEE. IEEE Region 10 Conference. TENCON 99. "Multimedia Technology for Asia-Pacific Information Infrastructure" (Cat. No.99CH37030)*, 1999, vol. 2, pp. 891–894.

[120] F. F. Syed, A. H. M. A. Rahim, and J. M. Ba-Khashwain, "Robust STATCOM controller design using PSO based automatic loop-shaping procedure," in *Proceedings of 2005 IEEE Conference on Control Applications, 2005. CCA 2005.*, 2005, pp. 440–445.

[121] S. Panda and N. P. Padhy, "Optimal location and controller design of STATCOM for power system stability improvement using PSO," *J. Franklin Inst.*, vol. 345, no. 2, pp. 166–181, Mar. 2008.

[122] K. Y. Lee and M. A. El-Sharkawi, Eds., *Modern Heuristic Optimization Techniques*. Hoboken, NJ, USA: John Wiley & Sons, Inc., 2008, p. 616.

[123] A. A. Abou El Ela, M. A. Abido, and S. R. Spea, "Optimal power flow using differential evolution algorithm," *Electr. Power Syst. Res.*, vol. 80, no. 7, pp. 878–885, Jul. 2010.

[124] M. A. Abido and N. A. Al-Ali, "Multi-objective differential evolution for optimal power flow," in *2009 International Conference on Power Engineering, Energy and Electrical Drives*, 2009, pp. 101–106.

[125] A. H. Al-Mohammed, M. A. Abido, and M. M. Mansour, "Optimal PMU placement for power system observability using differential evolution," in *2011 11th International Conference on Intelligent Systems Design and Applications*, 2011, pp. 277–282.

[126] R. Storn, "System design by constraint adaptation and differential evolution," *IEEE Trans. Evol. Comput.*, vol. 3, no. 1, pp. 22–34, Apr. 1999.

[127] Q. Jiang and Z. Huang, "An Enhanced Numerical Discretization Method for Transient Stability Constrained Optimal Power Flow," *IEEE Trans. Power Syst.*, vol. 25, no. 4, pp. 1790–1797, Nov. 2010.

[128] D. Ernst, D. Ruiz-Vega, M. Pavella, P. M. Hirsch, and D. Sobajic, "A unified approach to transient stability contingency filtering, ranking and assessment," *IEEE Trans. Power Syst.*, vol. 16, no. 3, pp. 435–443, 2001.

[129] A. Pizano-Martianez, C. R. C. R. Fuerte-Esquivel, D. Ruiz-Vega, A. Pizano-martínez, and S. Member, "Global Transient Stability-Constrained Optimal Power Flow Using an OMIB Reference Trajectory," *IEEE Trans. Power Syst.*, vol. 25, no. 1, pp. 392–403, Feb. 2010.

[130] M. Yin, C. Y. Chung, K. P. Wong, Y. Xue, and Y. Zou, "An Improved Iterative Method for Assessment of Multi-Swing Transient Stability Limit," *IEEE Trans. Power Syst.*, vol. 26, no. 4, pp. 2023–2030, Nov. 2011.

[131] N. Mo, Z. Y. Zou, K. W. Chan, and T. Y. G. Pong, "Transient stability constrained optimal power flow using particle swarm optimisation," *IET Gener. Transm. Distrib.*, vol. 1, no. 3, pp. 476–483, 2007.

[132] K. Y. Chan, K. W. Chan, S. H. Ling, H. H. C. Iu, and G. T. Y. Pong, "Solving multi-contingency transient stability constrained optimal power flow problems with an improved GA," in *2007 IEEE Congress on Evolutionary Computation*, 2007, pp. 2901–2908.

[133] H. R. Cai, C. Y. Chung, and K. P. Wong, "Application of Differential Evolution Algorithm for Transient Stability Constrained Optimal Power Flow," *IEEE Trans. Power Syst.*, vol. 23, no. 2, pp. 719–728, May 2008.

[134] K. Tangpatiphan and A. Yokoyama, "Adaptive Evolutionary Programming with Neural Network for Transient Stability Constrained Optimal Power Flow," in *2009 15th International Conference on Intelligent System Applications to Power Systems*, 2009, pp. 1–6.

[135] M. a. Abido, "Multiobjective evolutionary algorithms for electric power dispatch problem," *IEEE Trans. Evol. Comput.*, vol. 10, no. 3, pp. 315–329, Jun. 2006.

[136] A.-A. Fouad and V. Vittal, *Power System Transient Stability Analysis Using the Transient Energy Function Method*. Prentice Hall, 1991, p. 384.

[137] P. W. Sauer and M. A. Pai, *Power System Dynamics and Stability*. Stipes Publishing Co., 2007, p. 349.

[138] R. D. Zimmerman, C. E. Murillo-Sanchez, and R. J. Thomas, "MATPOWER: Steady-State Operations, Planning, and Analysis Tools for Power Systems Research and Education," *IEEE Trans. Power Syst.*, vol. 26, no. 1, pp. 12–19, Feb. 2011.

[139] J. R. Altman, "A Practical Comprehensive Approach to PMU Placement for Full Observability," Virginia Polytechnic Institute and State University, 2008.

[140] A. G. Phadke, "The Wide World of Wide-area Measurement," *IEEE Power Energy Mag.*, vol. 6, no. 5, pp. 52–65, 2008.

[141] S. El Safty, M. M. Abo El Nasr, S. F. Mekhemer, and M. M. Mansour, "New technique for fault location in interconnected networks using phasor measurement unit," in *2008 12th International Middle-East Power System Conference*, 2008, pp. 6–10.

[142] K. Martin and J. Carroll, "Phasing in the Technology," *IEEE Power Energy Mag.*, vol. 6, no. 5, pp. 24–33, 2008.

[143] C. Borda, A. Olarte, and H. Diaz, "PMU-based line and transformer parameter estimation," in *2009 IEEE/PES Power Systems Conference and Exposition*, 2009, pp. 1–8.

[144] A. H. Al-Mohammed, M. M. Mansour, and M. A. Abido, "Application of Phasor Measurement Units (PMUs) for fault location in SEC-EOA interconnected network," in *2010 IEEE International Energy Conference*, 2010, pp. 435–439.

[145] C. D. Booth, "Protection and stability assessment in future distribution networks using PMUs," in *11th IET International Conference on Developments in Power Systems Protection (DPSP 2012)*, 2012, pp. P34–P34.

[146] F. Ding and C. D. Booth, "Applications of PMUs in Power Distribution Networks with Distributed Generation," in *46th International Universities' Power Engineering Conference*, 2011, pp. 1–5.

[147] N. Yorino, E. Popov, Y. Zoka, Y. Sasaki, and H. Sugihara, "An Application of Critical Trajectory Method to BCU Problem for Transient Stability Studies," *IEEE Trans. Power Syst.*, vol. PP, no. 99, pp. 1–8, 2013.

[148] M. Sanaye-Pasand and H. Seyedi, "New centralised adaptive load-shedding algorithms to mitigate power system blackouts," *IET Gener. Transm. Distrib.*, vol. 3, no. 1, pp. 99–114, Jan. 2009.

[149] N. Perumal, "Automatic load shedding in power system," in *Proceedings. National Power Engineering Conference, 2003. PECon 2003.*, 2003, pp. 211–216.

[150] N. I. Abdul Wahab and A. Mohamed, "Area-Based COI-Referred Rotor Angle Index for Transient Stability Assessment and Control of Power Systems," *Abstr. Appl. Anal.*, vol. 2012, pp. 1–23, 2012.

[151] A. A. M. Zin, H. M. Hafiz, and W. K. Wong, "Static and dynamic under-frequency load shedding: a comparison," in *2004 International Conference on Power System Technology, 2004. PowerCon 2004.*, 2004, vol. 1, pp. 941–945.

[152] J. Ostergaard and F. Mara, "A real-time simulation platform for power system operation," in *2010 Conference Proceedings IPEC*, 2010, pp. 909–914.

[153] R. Kuffel, J. Giesbrecht, T. Maguire, R. P. Wierckx, and P. McLaren, "RTDS - A Fully Digital Power System Simulator Operating in Real Time," in *ICDS '95. First International Conference on Digital Power System Simulators*, 1995, p. 19.

[154] R. Kuffel, J. Giesbrecht, T. Maguire, R. P. Wierckx, and P. McLaren, "RTDS-a fully digital power system simulator operating in real time," in *IEEE WESCANEX 95. Communications, Power, and Computing. Conference Proceedings*, 1995, vol. 2, pp. 300–305.

[155] D. Ouellette, M. Desjardine, R. Kuffel, Y. Zhang, and E. Xu, "Using a Real Time Digital Simulator with Phasor Measurement Unit technology," in *2011 International Conference on Advanced Power System Automation and Protection*, 2011, vol. 3, pp. 2472–2476.

[156] P. Tatcho, Y. Zhou, H. Li, and L. Liu, "A real time digital test bed for a smart grid using RTDS," in *The 2nd International Symposium on Power Electronics for Distributed Generation Systems*, 2010, pp. 658–661.

[157] Z. Q. Bo, A. Klimek, Y. L. Ren, and J. H. He, "A Real Time Digital Simulation System for Testing of Integrated Protection Schemes," in *2008 Joint International Conference on Power System Technology and IEEE Power India Conference*, 2008, pp. 1–5.

[158] S. Foo, "Real time simulation of power flow control strategies for fuel cell vehicle with energy storage by using Real Time Digital Simulator (RTDS)," in *2009 IEEE 6th International Power Electronics and Motion Control Conference*, 2009, pp. 2323–2327.

[159] H. Dommel, "Digital Computer Solution of Electromagnetic Transients in Single- and Multiphase Networks," *IEEE Trans. Power Appar. Syst.*, vol. PAS-88, no. 4, pp. 388–399, Apr. 1969.

Appendix A: Real Time Digital Simulator (RTDS) Overview

The RTDS solution algorithm represents power system in the basis of nodal analysis techniques. In order to calculate the instantaneous voltages at various nodes within the system, the inverse conductance matrix is multiplied by a column vector of current injections. The conductance matrix is generally a square, rather sparse matrix whose entries depend on the circuit components connected to the nodes. The ability to separate the conductance matrix into block diagonal pieces enables the simultaneous solution of the node voltages associated with each block. This so-called *subsystem* solution method is an important consideration in the parallel processing implemented in the RTDS. Each subsystem is simultaneously solved by different portions of the specialized hardware. The concept of mathematically isolated subsystems proved to be a significant consideration during the development of an interface to the analog simulator. [152]
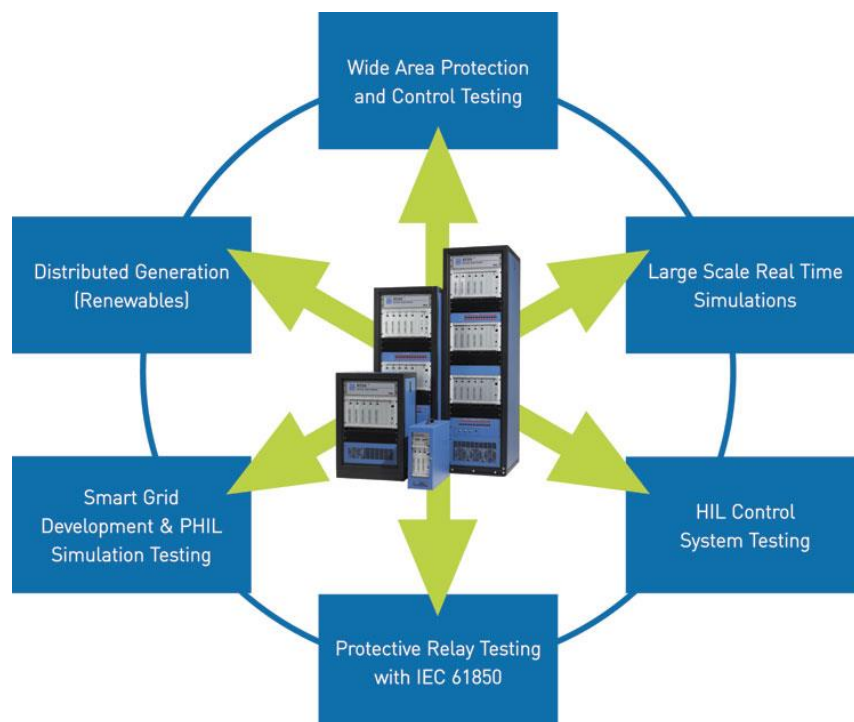

Figure A.1: RTDS Application areas

The RTDS simulator is a powerful computer that accomplishes the task of real-time simulation via parallel computation. Using trapezoidal integration and exploiting the delay in travelling waves on transmission lines, the system is capable of performing time domain simulation at real-time speed using time steps less than 50μs. Such small time steps enable the RTDS to accurately and reliably simulate power system phenomena in the range of 0 to 3 kHz. [152]

Appendix A.1:   RTDS Applications

The RTDS technology combines the real-time operating properties of analogue simulators with the flexibility and accuracy of digital simulation programs. Due to this, the RTDS simulator has found widespread applications in power systems. It is currently applied to many areas of development, testing and studying of power system planning, feasibility studies, system operation and behavior, integrated protection and control, etc. Furthermore, since the RTDS responds in real-time to events initiated through the user interface software (i.e. operator's console), it provides an excellent method for training operators and educating engineers in the principles of power system operation. In addition, because the RTDS is housed in one or more standard 19 inch cubicles, it can conveniently be taken to substation where equipment, such as protective relays, can be easily tested. [152]–[154]

When the RTDS is combined with suitable voltage and current amplification systems it can be used to perform closed-loop relay tests. A wide variety of tests can be performed, ranging from application of simple voltage and current waveforms through to complicated sequencing within a detailed power system model. Due to the availability of

an extensive power system component library, including measurement transducers, the relay can be tested under system conditions similar to those it will encounter in the real life. During all tests, the relay can be connected via analogue output channels to voltage and current amplifiers. Relay output contacts can in turn be connected back to circuit breaker models using the RTDS digital input ports. Closed-loop testing is unique to real-time simulation systems in that it provides a method of evaluating not only the performance of the relay, but also the response of the system to its reaction. [153], [154] Many of the wide area protection and control schemes proposed are based on or utilize PMU data. A PMU model has been developed for the RTDS simulator so new designs can be thoroughly tested under realistic network conditions. The PMU model allows eight PMU's to be represented per instance so an extensive WAMS can be simulated. A mechanism has been developed to synchronize the simulation time step to 1 pulse per second (PPS) timing signal so the RTDS simulator can be used for benchmark testing of PMU devices. The recent trend to adopt distributed generation schemes is another opportunity for the RTDS simulator. A number of manufacturers and utilities are now using the RTDS simulator to investigate the impact of distributed generation and smart grid concepts on their existing networks. With detailed models of wind, solar, fuel cell, etc. and implementation of required communication protocols, the RTDS is well suited for simulation of today's modern power systems. [155], [156]

In a manner similar to that described for protection system testing, the RTDS simulator can be applied to the evaluation and testing of physical control equipment. Required analogue and digital signals produced during simulation of the power system can be connected directly to the control equipment. The controller outputs are then

connected to input points on the particular power system component model being simulated. This again closes the test loop and allows evaluation of control equipment performance on the system to which the equipment is tested. [153], [154]

If appropriate interfacing points and methods are chosen, the RTDS can be used to expand and enhance the capabilities of traditional analogue simulators. A particular attention has been recently paid to expansion of HVDC analogue simulators to permit representation of larger ac networks at either end of the HVDC link. Because of the inherent difficulties associated with ac system modeling in analogue simulators, interfacing the RTDS to an analogue simulator offers a simple and relatively inexpensive alternative. [153], [154]

Appendix A.2:   RTDS Capabilities

The Real Time Digital Simulator which developed at the Manitoba HVDC Research Centre in the late 1980's is a fully digital electromagnetic transient power system simulator. The RTDS Simulator responsibility was transferred to RTDS Technologies in 1994 where it has since undergone numerous hardware and software developments. It can be used to conduct close-loop testing of physical devices such as protection equipment and control equipment; to perform analytical system studies and to educate operators, engineers and students [157]. It is a cost-effective replacement for transient network analyzers and analogue/hybrid simulators. RTDS allows the user to investigate the effects of disturbances on power system equipment and networks to prevent outages or complete failure. Moreover, RTDS added the capability to improve the simulation accuracy and

better capture the switching events [158]. The simulator is now widely used in the electric power industry by utilities, equipment manufacturers and research organizations.

RTDS is generally designed to simulate power systems in real time with time step-sizes on the order of 50µs. The system uses a number of digital signal processors (DSPs) which operated in parallel. It provides a number of digital and analog I/O ports for interfacing hardware to the simulation. It features a more powerful processor combined with FPGAs which allow the simulation of a limited number of power electronics devices with time step as small as 1.4-2.5 µs embedded in the 50µs time-step environment. Therefore, it allows the simulation of power electronics converter operating at higher switching frequency with sufficient accuracy. In addition, its real time capability allows the user to incorporate real devices into the simulation in a closed loop environment.

Appendix A.3:   RTDS Design

The beauty of the RTDS is that it works in continuous, sustained real time. This means that it can solve the power system equations fast enough to continuously produce output conditions that realistically represent conditions in the real network. Because the solution is real time, the simulator can be connected directly to power system control and protective relay equipment and adjust its calculations based on their operation [107]. RTDS is a combination of advanced computer hardware and comprehensive software. Real-time implementation setup using RTDS is shown in Figure A.2

Appendix A.3.1 Hardware

The RTDS Simulator hardware is based on a customized parallel processing architecture. It is designed specifically to solve the electromagnetic transient simulation algorithm developed by Dr. Hermann Dommel [159]. The design is modular so that different size power systems can be accommodated by adding units to the simulator. These units are called racks. Each rack of hardware includes both communication and processor cards linked through a common backplane. A large network is divided into separate subsystems. Each subsystem is solved by one rack. Each rack has an Inter-Rack Communication (IRC) card to share the information between the subsystems and contains a Giga Transceiver Workstation Interface (GTWIF) or Workstation Interface (WIF) card to synchronize the simulation calculations and to coordinate the communication between processor cards as well as the communication between racks.

RTDS Racks   RTDS Software

Computer Running RSCAD

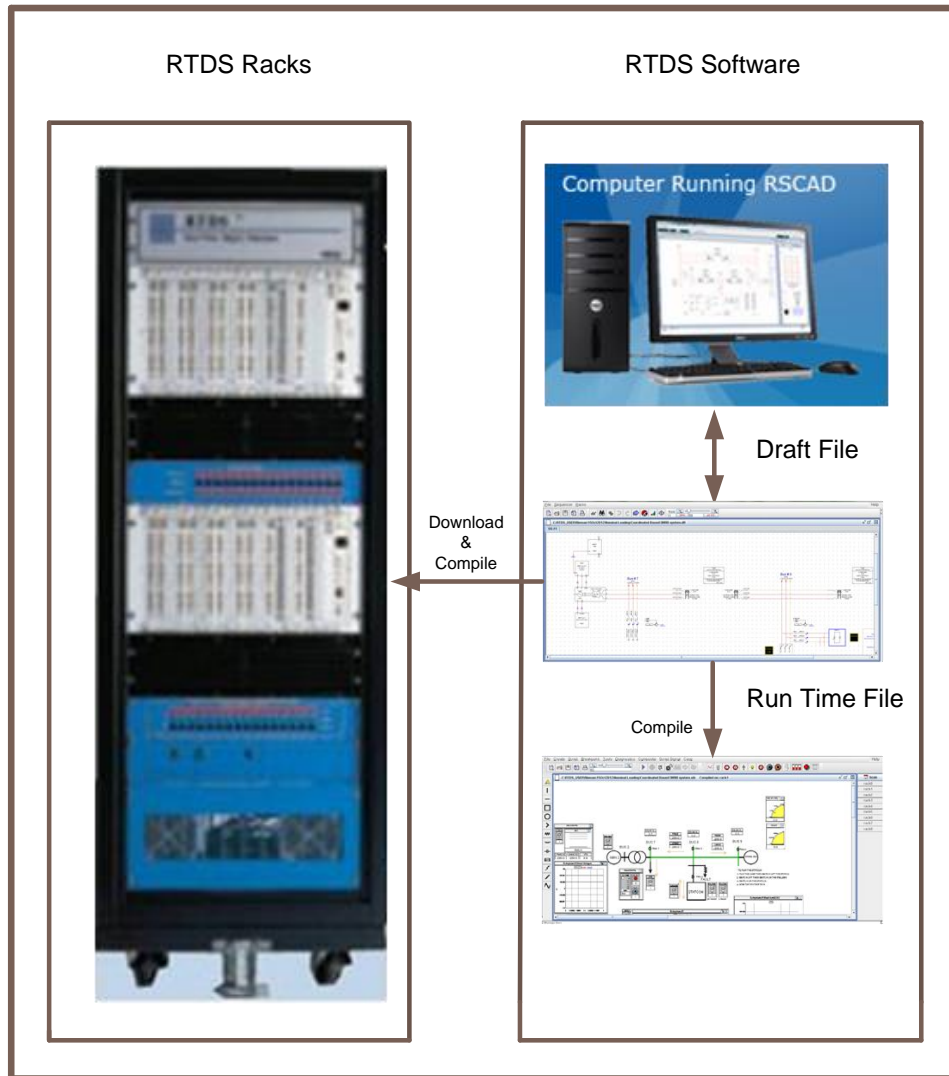Draft File

Download & Compile

Run Time File

Compile

Figure A.2:   RTDS Software and Hardware

Additionally the WIF provides Ethernet communication to and from the graphical user interface during real times simulations. The processor cards are responsible for calculating the overall network behavior. Different components are assigned to different processors so that their contribution to the subsystem response can be calculated in parallel. The current RTDS Simulator uses two different processor cards; the Triple Processor Card (3PC) and the Giga Processor Card (GPC) or PB5 Processor Card. Each 3PC card contains three floating point Digital Signal Processors (DSP) running at 40 MHz, a significant increase over the original Tandem Processor Card (TPC) which had only two DSP's running at 11 MHz The processors can communicate directly to another one at any time via shared memory, without having to access the backplane, and can therefore be used independently or together to solve more complex component models. The GPC is recently developed processor card which contains two RISC processors running at 1 GHz, whereas PB5 is the newest and powerful of them all having two parallel processor running at 1.7 GHz with cache memories.

Due to their computational power, the GPC and PB5 processors are often used to calculate more than one component model at the same time. Starting at the concept stage, the RTDS Simulator was intended for testing of physical protection and control equipment, thus making input/output (I/O) a primary design consideration. In some instances, hundreds of signals are passed to and from the simulator to external equipment. Great care was given to ensure that large amounts of I/O could be provided without significantly affecting the simulation time step. Instead of providing a central communication link, the processor cards and I/O were designed to communicate directly with another one to minimize the communication time. The Giga-Transceiver

Input/output (GT-I/O) cards are a family of I/O developed for the GPC card shown in Figure A.3 and Figure A.4
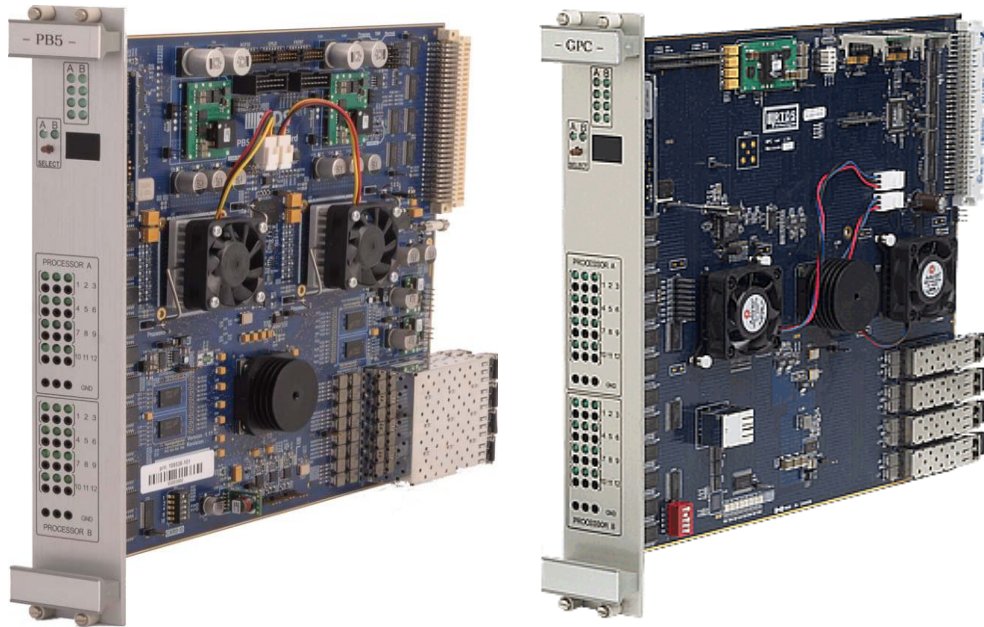

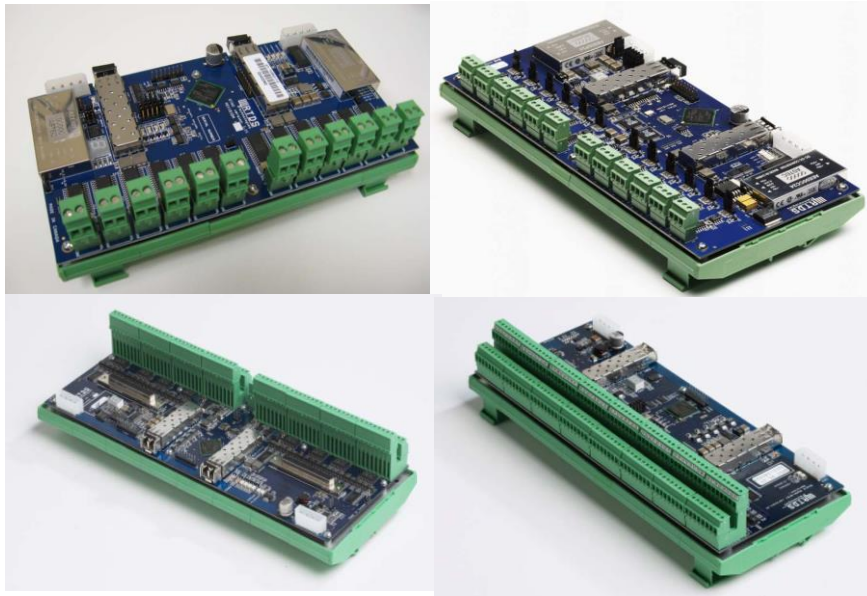Figure A.3:   GPC and PB5 Processor Cards

Figure A.4:   Different GTIO cards

The GT-I/O cards connect to the GPC via 2 GHz fiber optic links and provide complete optical isolation from the simulator. The GT-I/O cards include analogue input and output with 16-bit data converters as well as digital input and output. Typically the simulation time step for real time operation of the RTDS Simulator is in the order of 50 µs. Hard real time is ensured by the WIF card. If any processor cannot complete the calculations and I/O required within the given time step, the simulation is stopped and an error message issued. The largest simulation ever run in real time provided a full electromagnetic transient representation for a network with over 500 three-phase buses and 90 generators. Special hardware, algorithms and technique have been developed to provide a high degree of accuracy in representing high speed power electronics that typically require a response in the order of 1 µs.

Appendix A.3.2   Software

There are several levels of software involved with the RTDS Simulator. At the lower level are the component models (i.e. lines, transformers, generators, etc.) which have been optimized for real time operation. Over the years a comprehensive library of both power system and control components has been developed and refined. The highest level of software is the graphical user interface known as RSCAD. RSCAD allows simulation circuits to be constructed, run, operated and results to be recorded and documented. The RSCAD Draft module shown in Figure A.5 allows simulations to be constructed graphically by copying and connecting generic components from the library. The parameters of a particular component can be entered through a data menu. After the network has been constructed, it is compiled to create the simulation code required by the

simulator. Once the compile process has been executed, the simulation can be run using

RSCAD Run Time shown in Figure A.6
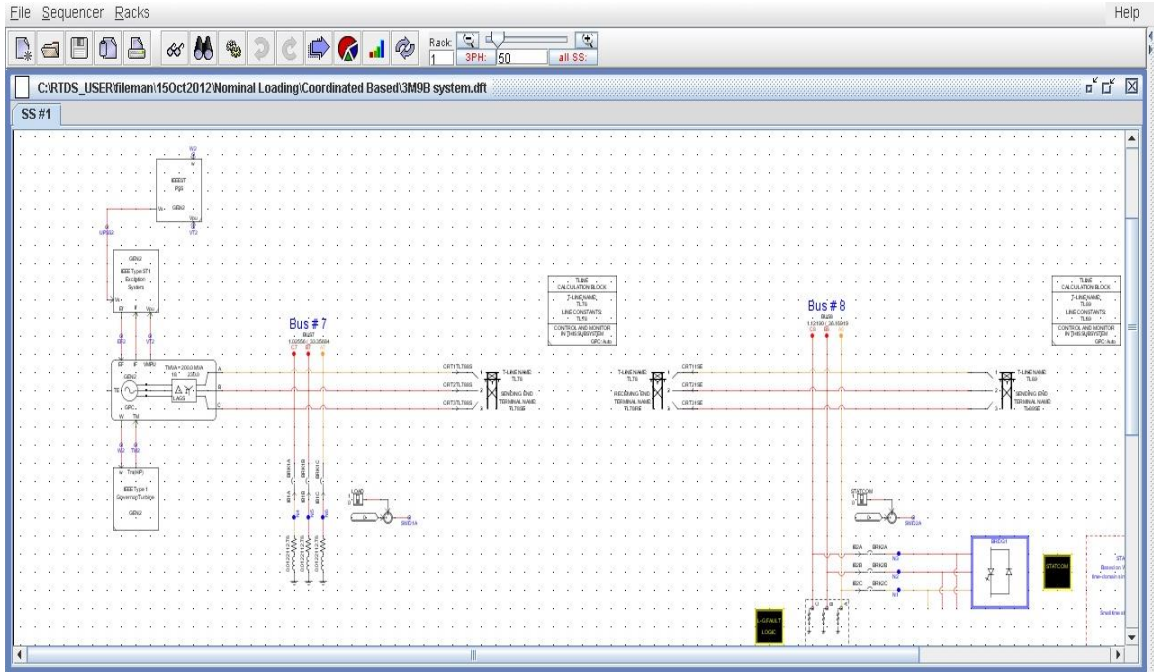
Figure A.5:   RTDS Draft File
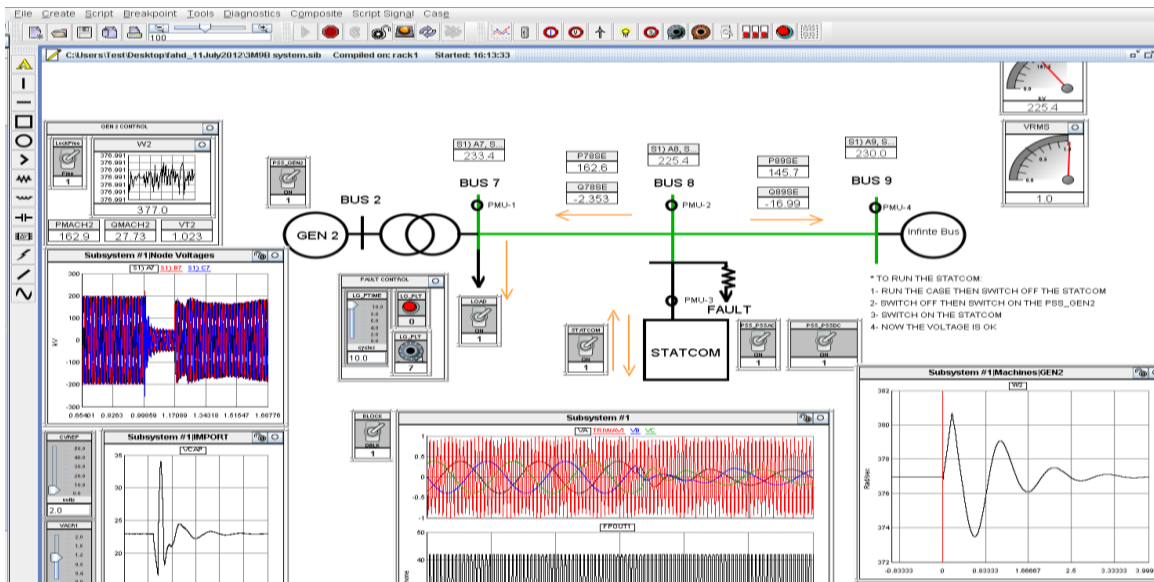
Figure A.6:   RTDS Run Time File

Runtime, which operates on a PC or workstation, communicates back and forth with the simulator WIF cards via Ethernet. The bidirectional communication allows simulations to be downloaded and run as well as for simulation results to be transferred to the Runtime screen. The network can be operated from Runtime by changing switching states or set points. Slow moving signals such as power, RMS bus voltage, machine speed, etc. can be monitored on a continuous basis to allow transient behavior and state of the network to be observed. Detailed plots of transient events, with a resolution as high as every time step, can also be recorded by the simulator WIF cards and displayed in Runtime plots.

Appendix B: SYS-310: SEL Synchro-Phasor Measurement Visualization, Analysis and Control System

Synchronized phasors (synchro-phasors) provide a real-time measurement of electrical quantities from across the power system. Applications include wide-area control, system model validation, determining stability margins, maximizing stable system loading, islanding detection, system-wide disturbance recording, and visualization of dynamic system response. Time-synchronized measurement can improve the system performance and reliability under consideration. Using time-synchronized measurements, we can improve local- and wide-area protection and control, state monitoring, power system modeling, and forensic event analysis. The SYS-310 at KFUPM is a complete synchro-phasor monitoring and control solution provided by Schweitzer Engineering Laboratories (SEL). The components of the system are as below

- SEL-2404 Satellite-Synchronized Clock (x 1).

- SEL-421 Protection, Automation, and Control System (x 2).

- SEL-3378 Synchrophasor Vector Processor (SVP) (x 1).

- SEL-3530 Real-Time Automation Controller (RTAC) (x 1).

- SEL-3354 Embedded Automation Computing Platform (x 1).

- SEL-5073 SYNCHROWAVE® Phasor Data Concentrator (PDC) Software.

- SEL-5078-2 SYNCHROWAVE® Central Software.

The basic architecture of the system is shown in Figure B.1.
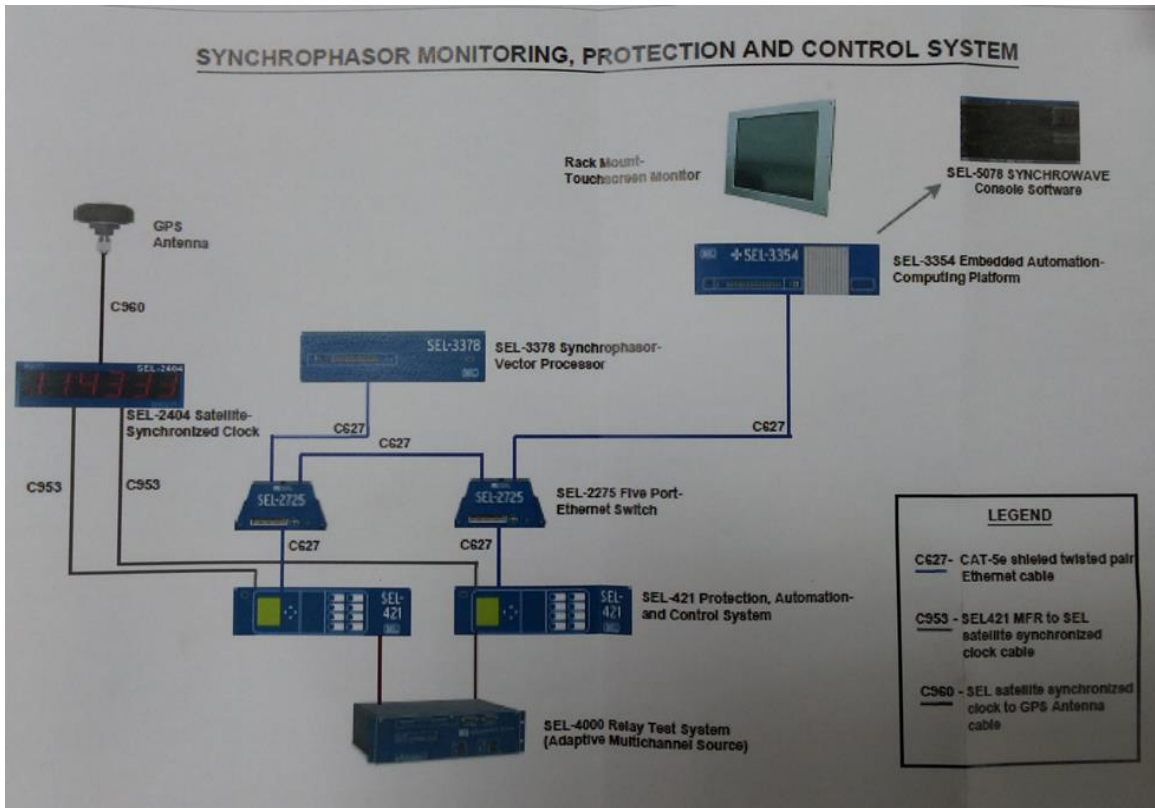
Figure B.1:   SYS-310 Basic Architecture and Connections

Each of the system's component details is provided below

Appendix B.1 :   SEL-2404 Satellite Synchronized Clock

Figure B.2:   SEL 2404 Satellite Synchronized Clock

The role of satellite-synchronized clocks has grown from basic sequence-of-event and fault recorder time referencing to mission-critical roles such as synchro-phasor measurement and detailed event analysis. These new applications require that satellite clocks meet the same environmental standards and be as reliable as the protective relays and other high-reliability devices with which these clocks are used. The SEL-2404 is a satellite-synchronized time source with a high-visibility display. Applicable for synchro-phasor, relay event correlation, and other high-accuracy timing needs. Demodulated IRIG-B outputs with ±100 ns accuracy meet requirements for existing and future timing applications. Can be installed in harsh environments. Exceeds IEEE C37.90 and IEC 60255 protective relay standards. Accurate operation from –40° to +80°C.

Appendix B.2 : **SEL-421 Protection, Automation and Control System**

Figure B.3:   SEL-421 Relay and Phasor Measurement and Control Unit (PMCU)

The SEL-421 is basically a state of the art multi-function protection relay. Embedded with in this relay is Phasor Measurement Unit (PMU), which can only be used for the

functionality of the relay but also can be user configured to meet their applications. This not only makes this relay versatile but also cheap as it can act both as a protective relay or a PMU. In SYS-310 the SEL-421 is used as a PMU to measure different electrical quantities with time synchronization. The time synchronization signal is provided by SEL-2404 Satellite Clock. Some basic features of SEL-421 are as below

- Compliance with IEEE 37.118 synchrophasor standards.

- Supports SEL FAST Messaging protocol.

- Variable synchrophasor message rate starting from 1 message per second (mps) to 60 mps.

- Each relay has effectively 2 PMUs built in it. The synchrophasor data elements consists of 6 x Current Transformer (CT) inputs, 6 x Voltage Transformer (VT) Input, 16 x analog channels and 64 x Digital channels.

- IEC-61850 substation automation can also be implemented.

Appendix B.3 :   SEL-3378 Synchrophasor Vector Processor (SVP)

Figure B.4:   SEL-3378 Synchrophasor Vector Processor (SVP)

The SEL-3378 Synchrophasor Vector Processor collects synchrophasor messages and processes them using the built-in programmable logic capability for wide-area protection and control applications. It combines the power of synchrophasor message processing with flexible programmable logic for wide-area protection and control applications. The Synchrophasor Vector Processor (SVP), the first real-time synchrophasor programmable logic controller, collects synchrophasor messages from relays and phasor measurement units (PMUs). The SVP time-aligns incoming messages, processes them with an internal logic engine, and sends control commands to external devices to perform user-defined actions. Additionally, the SVP can send calculated or derived data to devices such as other SVPs, phasor data concentrators (PDCs), and monitoring systems.

Appendix B.4 :   **SEL-3530 Real Time Automation Controller (RTAC)**

Figure B.5:   SEL-3530 Real Time Automation Controller (RTAC)

Suitable for use in utility substations or industrial control and automation systems, the SEL-3530 Real-Time Automation Controller (RTAC) provides complete and flexible

system control with integrated security, seamless configuration, unified logic, and reliability. The RTAC converts data between multiple protocols, communicates with any configured and connected device, and comes with an embedded IEC 61131 logic engine. The SEL-3530 Real-Time Automation Controllers (RTACs) are powerful automation platforms, designed to provide years of service in tough substation and plant environments. The RTAC combines an embedded microprocessor-based hardware platform, wide operating temperature range, real-time operating system, and secure communications with flexible, feature-rich IEC 61131-compliant programmability. The RTAC can provide any degree of functionality from that of a simple intelligent port switch to the sophisticated communication and data handling required for advanced substation integration projects.

Appendix B.5 :   SEL-5073 SynchroWave® Phasor Data Concentrator (PDC) Software

SynchroWAVe PDC Software connects to any IEEE C37.118-2005 compliant phasor measurement unit (PMU) or other client, such as the SEL-3378 Synchrophasor Vector Processor or SEL-5078-2 SynchroWAVe Central Software that adheres to the standard. Configure up to six different outputs, and send data to different locations or organizations, like an independent system operator or a regional coordinating council. Some key features are listed below.

- Concentrates synchrophasor measurements from more than 500 PMUs.

- Supports message rates from 1 message per second to 240 messages per second.

- Archives data using continuous and/or predefined triggers that provide both pre- and post-event PMU data.

- Sends selected concentrated PMU data to up to six different users/locations.

- Comes with PDC Assistant Software for easy setup and configuration.

- Includes individual and role-based account authentication, strong passwords, and access logs for a secure solution.

- Concentrates PMU or PDC inputs from multiple substations.

Appendix B.6 :   SEL-3354 Embedded Automation Computing Platform

Figure B.6:   SEL-3354 EACP

SEL-3354 is an industry grade PC preloaded with necessary softwares for SYS-310 functionality. It is used as a data concentrator in SYS-310 where data of 2 years with a message rate of 60mps for 4 PMUs can be archived. It has a windows based user interface makes it easy to use and interact.

Appendix B.7 :   SEL-5078-2 SYNCHROWAVE® Central Software

synchroWAVe Central Software allows, to quickly translate synchro-phasor data into visual information. Central Software completes the synchro-phasor system with a powerful yet easy-to-use solution for visualizing and analyzing real-time streaming data

or archived data, and provides a time-synchronized, wide-area view of the system. Some features are as follows:

- View real-time synchro-phasor measurements for improved situational awareness.

- Analyze and locate events of interest in historical data by utilizing "snapshot" event capture and zoom-and-pan features.

- Create and save customized displays to optimize power system analysis through user-configurable displays.

- Access Central Software simultaneously from one or more computers in your network.

Figure B.7:   SEL 5078-2 Software Graphical User Interface

Vitae

Name   : Muhammad Waqar Ahmed

Nationality   : Pakistani

Date of Birth   : 12/25/1988

Email   : waqarmuhammad88@hotmail.com

Address   : R-1031 Sector 16 A Buffer zone North Karachi, Pakistan.

Area of Interest   : Power system planning and operations, Wide area protection and control, PMU applications in power system, Artificial Intelligence application in power system

Background   : Bachelors in Engineering from NED University of Engineering and Technology, Karachi, Pakistan in 2010, degree with distinction; worked as Plant maintenance engineer in Dawlance Private Limited from Dec' 2010 till May 2011; worked as an Instrument and Control Engineer in GDF Suez Energy from Jun' 2011 till Aug'2012.